PhD degree in Systems Medicine (curriculum in Molecular Oncology)

European School of Molecular Medicine (SEMM),

University of Milan and University of Naples "Federico II"

Settore disciplinare: BIO/11

Identification of NCAM1/CD56 as a novel prognostic prostate cancer stem cell biomarker

Andrea Castiglioni,

European Institute of Oncology (IEO), Milan

Tutor: Prof. Pier Paolo Di Fiore

European Institute of Oncology (IEO), Milan

PhD Coordinator: Prof. Saverio Minucci

Anno accademico 2021-2022

“Sorridi perché fa bene all’anima,
perché nessuno merita che tu smetta di farlo.
Il tuo sorriso è gioia per chi ti ami,
rabbia per chi ti invidia.”

TABLE OF CONTENTS

Acknowledgments

I would like to first and foremost thank my supervisors, Prof. Pier Paolo Di Fiore and Prof. Salvatore Pece, who assisted me in the completion of my research project with their extraordinary support and mentorship. I will be grateful to you forever. I would also like to thank my internal and external advisors, Dr. Saverio Minucci and Dr. Riccardo Fodde, for their helpful scientific guidance.

A special thanks to the people who have helped me in this project: Davide DiSalvatore for the analysis of clinical data; Giovanna Jodice for the IHC staining; the Genomic Unit for the RNASeq and ScRNA-Seq data; Stefano Confalonieri and Francesco Tucci for the RNASeq analysis and Matteo Marzi for the fruitful discussions and analysis of ScRNA-Seq; the Cogentech staff for the RT-qPCR data and the valuable help in managing mice; Rosalind Gunby for all the time you spend correcting my applications and PhD thesis.

Thanks to Maria Grazia Malabarba, Bronia Matoskova and Emanuela Orlando for the interesting and light-hearted conversations in the relax-time and for solving with efficiency and with a smile any problem that arose.

My most heartfelt thanks for Blanca Alvarez, my mentor even if for a short time, the person who taught me everything there was to know about this project that she left me as a gift. I hope I did a good job and made you proud of me.

A heartfelt thanks to Dr. Giovanni Bertalot, for his infinite knowledge that helped me at every moment when I had doubts. A very special person.

A special thanks to Andrea Benvenuto, Martina Codibue, Giuseppe Ciossani, Alessandro D'Audino, with whom I shared science but also friendship, laughter, joys, thoughts, opinions, complaints, coffees, lunch breaks and several glasses of wine.

Last but first in importance a huge thank you to the people who have played a key role in my journey and whom I consider not just colleagues but friends. People I respect and who if they were not there my whole journey would not have tasted the same: Stefano Freddi, Francesca Montani, Federica Fruscitto, Deborah Salvi Mesa, Elisa Tonucci. You are really special.

Heartfelt thanks go to my family who has allowed me to get this far and has always supported me, and to Sara, a fundamental presence in my life who has put up with me every day for years and supports me in everything.

List of Abbreviations

A: acetylation
aa: amino acid
AA: arachidonic acid
AATT: androgen-receptor axis-targeted therapies
ABC: ATP-binding cassette
ABI: abiraterone
ACK: Ammonium-Chloride-Potassium
ADAM: A-disintegrin and metalloprotease
ADT: androgen deprivation therapy
AF-1/2: activation function-1/2
AG: ampullary gland
AJCC: American joint committee on cancer
ALCAM/CD166: activated leukocyte cell adhesion molecule
ALDH: aldehyde dehydrogenase
ALL: acute lymphoblastic leukemia
AML: acute myeloid leukemia
AP: anterior prostatic lobes
APA: apalutamide
APC: antigen presenting cell
APC: adenomatous polyposis coli
AR: androgen receptor
AR-V: androgen receptor splicing variant
ARE: androgen response elements
ARID5B: AT-rich interactive domain-containing protein 5B
ARSI: androgen receptor signalling inhibitor
AS: active surveillance
ASI: alpha-secretase inhibitor
ASN: asparagine
AUA: American urologist association
AURKA: Aurora A cell cycle kinase
BCA: Bicinchoninic acid
BCL-2: B-cell lymphoma 2
BCR: biochemical recurrence
BLL: acute B lymphoblastic leukemia
BMP: bone morphogenetic protein
BPE: Bovine Pituitary Extract
BPH: benign prostatic hyperplasia
BRCA1/2: breast cancer type 1/2
BRIP1: BRCA1 interacting helicase 1
BTG1: BTG Anti-Proliferation Factor 1
CAM: cell adhesion molecules
CAMKK2: calcium/calmodulin dependent protein kinase kinase 2
cAMP: cyclin-AMP
CAR: chimeric antigen receptor
CARN: castrate-resistant Nkx3-1 expressing cell
CASP3: caspase-3
CBP: p300/CREB binding protein
CCL2: chemokine ligand 2
CCL20: chemokine ligand 20
CCL22: chemokine ligand 22
CCNB1: cyclin-B1
CCND1: cyclin-D1
CCNG2: cyclin G2
$CD44^{high}$: high levels of CD44
$CD44^{low}$: lower levels of CD44
CDC20: cell division cycle protein 20
CDK-1/9: cyclin-dependent kinase-1/9
CDKN1A/P21: Cyclin Dependent Kinase Inhibitor 1A
CDKN1B/P27: Cyclin dependent kinase inhibitor 1B

CDKN1C/P57: cyclin-dependent kinase inhibitor 1C

CDKN2A: cyclin-dependent kinase inhibitor 2A

CDKN2A/P16: cyclin dependent kinase inhibitor 2A

CHEK2: checkpoint kinase 2

CHGA: Chromogranin A

CI: interval of confidence

CIS: carcinoma in situ

CK14: Cytokeratin 14

CK18 Cytokeratin 18

CK5: cytokeratin 5

CK8: Cytokeratin 8

cM0: clincally non-metastatic

cM1: clinically metastatic

CMV: cytomegalovirus

CAN: copy number aberration

CO: controlled cells

co-IP: co-immunoprecipitation

COX2: cyclooxygenase 2

cPSA: complexes PSA

CREB: cyclin-AMP response-element binding protein

CRPC: castration-resistant prostate cancer

CSC: cancer stem cell

cT: clinical T category

CTC: circulating tumor cells

CTLA-4: cytotoxic T-lymphocyte antigen 4

Ctr: Control

CXCL10: C-C motif chemokine ligand 10

CYP11A1: cytochrome P450 11A1

CYP17A1: cytochrome P450 17A1

DAG: diacylglycerol

DAPI: 4′,6-diamidino-2-phenylindole

DAPT: N-[N-(3,5-Difluorophenacetyl)-l-alanyl]-S-phenylglycine t-butyl ester

DAR: darolutamide

DBD: DNA-binding domain

$DD3^{PCA3}$: prostate cancer antigen 3

DDIT4: DNA Damage Inducible Transcript 4

DEX: dexamethasone

DHEA: dehydroepiandrosterone

DHT: Dihydrotestosterone

DLL4: delta-like-4

DM: distant metastasis

DMEM: Dulbecco's Modified Eagle Medium

DNER: Delta/Notch-like EGF-related receptor

DP: dorsal prostatic lobes

DRE: digital rectal exam

DTC: disseminated tumor cells

DU145: androgen-independent prostatic carcinoma cells

DUA: dutch urological association

EAU: European association of urology

EBRT: external beam radiation

EC: endothelial cell

ECAD: E-cadherin

ECM: extracellular matrix

EGF: epithelial growth factor

ELDA: Extreme Limiting Dilution Analysis

ELISA: Enzyme-linked immunosorbent assay

EMT: epithelial–mesenchymal transition

ENZ: enzalutamide

EpCAM: Epithelial Cell Adhesion Molecule

EPI: ExoDX prostate intelliscore

ERG: ETS transcription factor

ERK: Extracellular signal-regulated kinases
ERSPC: European randomized screening for PCa
ESC: embryonic stem cells
ETV1-4: ETS variant transcription factor 1-4
EV: empty vector
EZH2: enhancer of zeste homologue 2
F3: fibronectin-type III related homology
FACS: Fluorescence activated cell sorting
FAM175A: abraxas BRCA1 A complex subunit
FBS: Fetal Bovine Serum
NA: North American
SA: South American
Fc: fold change
FCCG: Finnish Medical Society Duodecim
FCH: fluorocholine
FDA: food and drug administration
FDR: False discovery rate
FGF: fibroblast growth factor
FGF18: Fibroblast Growth Factor 18
FGFR: fibroblast growth factor receptor
FISH: fluorescence in situ hybridization
FOXA1: Forkhead box A1
FOXA2: forkhead box protein A2
fPSA: free PSA
G: Gleason grade
GA: gallium
GAPDH: glyceraldehyde-3-phosphate dehydrogenase
GD2: disialogangloside2
GDNF: glial derived neutrophic factor
GEN1: GEN1 Halliday junction 5' flap endonuclease
GFL: GDNF family ligands
GFR-α: GPI-linked GDNF family receptor alpha
GGG: Gleason grade group
GLB1: β-galactosidase
GLI-1: glioma-associated oncogene transcription factors 1
GLI-2: glioma-associated oncogene transcription factors 2
GLI-3: glioma-associated oncogene transcription factors 3
GM-CSF: granulocyte-macrophage colony-stimulating factor
GP: Gleason pattern
GS: Gleason score
GSI: γ-secretase inhibitor
GWAS: genome wide association study
H3K27: histone H3 lysine 27 methylation
HDR: high dose rate
HES1: hairy and enhancer of split-1 (Hes Family BHLH Transcription Factor 1)
HEY1: Hes Related Family BHLH Transcription Factor with YRPW Motif 1
HFD: high fat diet
HG: High Gleason
HGF: hepatocyte growth facto
HHV8: herpes virus type 8
HIF1α: hypoxia-inducible factor 1-alpha
HOXB13: homeobox 13
HPCa: human prostate cancer
HPV: papillomavirus
HR: hazard ratio
HR: hinge region
HR: homologous recombination

HSC: hematopoietic stem cells
HSD17B: 17beta-hydroxysteroid dehydrogenase
HSD3B: 3beta- hydroxysteroid dehydrogenase
HSV2: herpes simplex virus type 2
IB: Immunoblot
IDH1: isocytrate dehydrogenase
IFNα: interferon alpha
IFNγ: interferon gamma
IGF: insulin-like growth factor
IgG: Immunoglobulin-G
IHC: Immunohistochemical
IL1β: interleukin 1 beta
IL23: interleukin 23
IL6: interleukin 6
IL8: interleukin 8
IMGN901: Lorvotuzumab mertansine
IP3: inositol triphosphate
iPS: induced pluripotent stem cells
iso-PSA: isoform PSA
ITH: intratumoral heterogeneity
JAG-1: Jagged Canonical Notch Ligand 1
K: lysine
KDM5B: Lysine Demethylase 5B
KIT/CD117: Stem Cell Factor Receptor
KLK2: kallikrein 2
KLK3: kallikrein 3
KO: knock-out
KRT5: cytokeratin 5
KRT15: cytokeratin 15
KRT14: cytokeratin 14
KRT8: cytokeratin 8
KRT18: cytokeratin 18
KRT19: cytokeratin 19
KRT7: cytokeratin 7
KSFM: Keratinocyte serum-free medium
LBD: ligand-binding domain
LDA: limiting dilution assay
LDR: low dose rate
LEN: lenaminolide
LG: Low Gleason
LHRH: luteinizing hormone releasing hormone
LP: lateral prostatic lobes
M metastasis
MALAT1: Long-Chain Non-Coding RNA Metastasis-Related Lung Adenocarcinoma Transcript 1
MAML2: Mastermind Like Transcriptional Coactivator 2
MAPK: Mitogen-activated protein kinase
mCRPC: metastatic castration resistant prostate cancer
MCSC: metastatic cancer stem cell
mCSPC: metastatic castration-sensitive prostate cancer
MDO: mouse-derived organoid
MDT: moderately differentiated
Me: methylation
MET: mesenchymal to epithelial transition
MHC I: major histocompatibility complex class 1
MICA/B: MHC class I polypeptide-related sequence
MM: multiple myeloma
MMP: matrix metalloproteinase
MMR: mismatch repair

mpMRI: multi-parametric magnetic resonance imaging
MRE1: homolog double strand break repair nuclease
MSH2: muts homolog 2
MSH6: muts homolog 6
MUC1: Mucin-1
$MUC1^{high}$: Mucin-1 high expression
MXD4: MAX Dimerization Protein 4
Myr-AKT: myristoylated-AKT
N: lymph node
N: number
NBN: nibrin
NCAD: n-cadherin
NCAM: Neural cell adhesion molecule
NCCN: national comprehensive cancer network
NCCS: national cancer centre Singapore
NCNN: clinical practice guidelines in oncology
NDRG1: N-Myc Downstream Regulated 1
NE: neuroendocrine
NEAT1: Nuclear Paraspeckle Assembly Transcript 1
NEPC: neuroendocrine prostate cancer
NFkB: Nuclear Factor kappa B
ng/ml: nanogrammi/millilitre
NGF: nerve growth factor
NGS: next generation sequencing
NICE: National Institute for Health and Clinical Excellence
NK: natural killer
NLS: nuclear localization signalnmCRPC: non-metastatic castration-resistant prostate cancer
NOS: nitric oxide synthase
NRP1: neuropilin-1
Ns: not significant
NSCLC: non-small-cell lung cancer
NSE: neuron-specific enolase
NSG: NOD/SCID gamma mouse (NOD/SCID $IL2R\gamma^{null}$)
NTD: N-terminal domain
OE: overexpressing
OFE: organoid forming efficiency
OPN: osteopontin
OS: overall survival
OXPHOS: oxidative phosphorylation
P: phosphorylation
p: p-value
PALB2: PMS2 partner and localizer of BRCA2
PAP: prostatic acid phosphatase
PARPi: poly (ADP-ribose) polymerase inhibitors
PBS: phosphate buffered saline
PCa: Prostate cancer
PCFA: Prostate Cancer foundation of Australia
PCPT: prostate cancer prevention trial
PCSC: prostate cancer stem cell
PCT: prostate cancer taskforce
PD-1: programme cell-death 1
PDGF: platelet-derived growth factor

PDGFR: platelet-derived growth factor receptor
PDL-1: programme death ligand 1
PDO: patient-derived organoid
PDT: poorly differentiated
PECM: Prostate Epithelial Culture Medium
PEN-STREP: Penicillin-Streptomycin
PET: positron-emission tomography
PFA: paraformaldehyde
pFGFR2: phospho-FGFR2
PFS: progression free survival
PGE2: prostaglandin E2
PhIP: 2-amino-1-methyl-6-phenylimidazo(4,5-b)pyridine
PIA: proliferative inflammatory atrophy
PIN: preneoplastic intraepithelial neoplasia
PIP_2: phosphatidylinositol 4,5-biphosphate
PIVOT: prostate cancer intervention versus observation trial
PKA: protein kinase A
PKC: protein kinase C
PLCO: prostate, lung, colorectal, ovarian cancer
PLCγ: phospholipase C-gamma
PMS2: PMS1 homolog 2 mismatch repair system component
PMSF: Phenylmethylsulfonyl fluoride
pN: lymph node status
PNI: Perineural invasion
PPAT: periprostatic adipose tissue
pro-PSA: precursor PSA
PROM1: Prominin-1
PSA: prostate specific antigen
PSA-NCAM1 N-glycosylated with polysialic acid NCAM1
PSA/KLK3: Prostate-Specific Antigen/Kallikrein Related Peptidase 3
PSMA: prostate specific membrane antigen
pT: tumor size
PTCH-1: Patched-1
PTHrP: parathyroid hormone-related protein
R: arginine
R0: negative surgical margins
R1: positive surgical margins
RANKL: receptor activator of nuclear factor kappa-B ligand
RB: retinoblastoma
RBPJk: Recombination signal binding protein for immunoglobulin kappa J region
rhFGF18: recombinant human FGF18
RNA-Seq: RNA-Sequencing
ROS: reactive oxygen species
RP: Radical Prostatectomy
rPB: rat probasin
RR: relative risk
RT: radiotherapy
RT: room temperature
RT-qPCR: real time-quantitative polymerase chain reaction
S: SUMOylation
SABR: stereotactic ablative radiotherapy
SASP: senescent-associated secretory function
SC: stem cell
SCAN: south east Scotland taskforce
SCLC: small cell lung cancer

Scr: scramble vector
ScRNA-Seq: single cell-RNA sequencing
SD: Standard Deviation
SDF-1: stromal cell-derived factor
SEMG1/2: semenogelin 1/2
SESN3: Sestrin 3
SEUG: south European uroncological group
ShNCAM1 Short hairpin-NCAM1
ShRNA short-hairpin RNA
siDNER: Short interfering RNA for DNER
siFGF18: Short interfering RNA for FGF18
siFGFR2: Short interfering RNA for FGFR2
siRBPJk: Short interfering RNA for Notch-1 co-factor RBPJk
siRNA: Short interfering RNA
siSOX4: Short interfering RNA for SOX4
siZEB1: short interfering RNA for ZEB1
SMO: Smoothened
SNAI1/SNAIL: Snail Family Transcriptional Repressor 1
SNAI2/SLUG: Snail Family Transcriptional Repressor 2
SNP: single nucleotide polymorphism
SNV: single nucleotide variant
SOX4: SRY-Box Transcription Factor 4
SPINK1: serine peptidase inhibitor Kazat type I
SPOP: speckle type BTB/POZ
SRD5A: 5alpha-reductase
SRT: salvage radiotherapy
SSTR1-5: somatostatin receptors 1-5
SUMO: small ubiquitin-like modifiers
SV40: simian virus 40
SYN: synaptophysin
T: tumor size
T-C1: TRAMP-C1
T-C2: TRAMP-C2
TA: transit-amplifying compartment
TACC2: transforming acidic coiled-coil-containing protein 2
Tag: large T-antigen
TAM: tumor-associated macrophages
TCGA: The cancer genome atlas
TGFβ: transforming growth factor beta
TIC: tumor-initiating cells
TKI: tyrosine kinase inhibitor
TMB: 3,3',5,5'-Tetramethylbenzidine
TME: Tumor microenvironment
TMPRSS2: transmembrane protease serine 2
TNFα: Tumor necrosis factor alpha
TNM: tumor node metastasis
TOB1: Transducer of ERBB2, 1
TP53: Tumor Protein P53
TP53INP1: Tumor Protein P53 Inducible Nuclear Protein 1
TP63: Tumor Protein P63
TPM: transcript per million
TRAMP: transgenic adenocarcinoma mouse prostate
Treg: immune regulatory T cells
TRUS: transrectal ultrasound scan
TSC22D1: TSC22 Domain Family Member 1
TSP-1: thrombospondin-1
TURP: transurethral resection of the prostate
TWIST1: Twist Family BHLH Transcription Factor 1
TX: therapy
U: ubiquitination

UGM: urogenital sinus mesenchyme
UGS: urogenital sinus
UGSM: urogenital sinus of mouse embryos
UMAP: Uniform manifold approximation and projection
VEGFA: vascular endothelial growth factor A
VEGFR 1-3: vascular endothelial growth factor receptor 1-3
VI: vascular invasion
VIM: vimentin
VS: vas deferens
WDT: well-differentiated tumor
WHO: world health organization
WT: wild type
Xn1: xenograft first generation
Xn2: xenograft second generation
ZEB1: Zinc Finger E-Box Binding Homeobox 1
β-GAL: beta-galactosidase
μM: micromolare
μm: micrometro
pg/ml: picogrammi/millilitro

Figures and Tables Index

Introduction

Results

1. Abstract

Serum prostate-specific antigen and Gleason grade are parameters routinely used for risk stratification in prostate cancer (PCa), but they present some limitations in the prediction of disease progression and in their use to guide clinical decision making. Prostate cancer stem cells (PCSCs) are widely considered to be responsible for tumorigenesis, disease progression and therapy failure. Their identification and characterization are mandatory for understanding the intricate intratumoral heterogeneity (spatial and molecular) of PCa and for developing relevant clinical tools to effectively manage patients and tailor therapy.

Here, we proposed the surface glycoprotein neural cell adhesion molecule (NCAM1/CD56), a known marker of neuroendocrine (NE) cells, as a novel PCSC marker that provides prognostic information and molecular insights into the process of tumorigenesis. NCAM1 defines clusters of cells enriched in proliferative inflammatory atrophy (PIA) regions, without NE traits (hereafter referred as $NCAM1^{+}$). In a retrospective cohort of 406 PCa patients treated with radical prostatectomy (RP), we uncovered that NCAM1 is an independent prognostic marker for predicting distant metastasis and biochemical recurrence and its expression in radical prostatectomy biopsies concurred with diagnostic biopsies (concordance 87.6%).

Using the human cell lines, LNCaP (androgen-sensitive) and DU145 (androgen-insensitive), we found that NCAM1, but not other candidate PCSC markers, allowed FACS-based prospective purification of PCa cells displaying *i)* unique self-renewal ability *in vitro*, in a serial 3D-Matrigel organoid propagation assay, *ii)* tumorigenic potential upon limiting dilution transplantation *in vivo.* Relevant to real-life human PCa, we found that the ability to generate primary-derived organoids (PDOs) from dissociated high Gleason PCa biopsies exclusively resided in the purified $NCAM1^{+}$ cell fraction, a property that was efficiently inhibited by treatment with an anti-NCAM1 blocking monoclonal antibody. We also found that the progressive development of adenocarcinoma in transgenic TRAMP mice crossed with $NCAM1^{-/-}$ mice was blocked at very early stages of tumorigenesis, indicating that genetic NCAM1 ablation prevents premalignant lesions to expand and progress to advanced stages.

PCa is a paradigm tumor model for clinical, spatial and molecular heterogeneity and this heterogeneity is reflected in the $NCAM1^{+}$ cell population. Single cell-RNA sequencing (sc-RNASeq) of purified $NCAM1^{+}$ cells (cell lines and primary human PCa biopsies) uncovered heterogenous cellular states reflected in several distinct clusters. Phylogenetic tree reconstruction of the evolutionary relationship among the different clusters along with single cell trajectory analysis revealed the existence of a cell fraction with basal traits ($p63^{+}/AR^{-}/CD117^{+}$ cells) and a quiescent

phenotype, sitting at the apex of the hierarchical structure of the NCAM1$^+$ population. These cells were functionally characterized by Hedgehog signaling which drives NCAM1$^+$/CD117$^+$ -PCSC self-renewal ability. Moreover, they were molecularly characterized by a transcriptional signature called "Stem Score" which could have potential as a prognostic tool for identifying patients at risk of biochemical recurrence (BCR) and distant metastasis.

Androgen deprivation therapy (ADT) is the standard management for advanced PCa. Despite its initial effectiveness, the majority of patients relapse and develop castration resistant prostate cancer (CRPC), which is thought to be mediated by resistant PCSCs. ADT-treated NCAM1$^+$ cells isolated from both dissociated human PCa biopsies and the LNCaP cell line enter into a quiescent state and retained the ability to generate organoids *in vitro* and tumors *in vivo,* escaping the ADT-induced senescence observed in NCAM1$^-$ cells. By global transcriptional profiling RNASeq analysis of NCAM1-overexpressing LNCaP cells, followed up by high-resolution studies, we uncovered an NCAM1-FGFR2-FGF18 molecular circuitry and an NCAM1-DNER-Notch1 molecular circuitry that mediate resistance to ADT-induced senescence. Thus, targeting these pathways with FGFR or Notch pathway inhibitors could represent a promising strategy to eradicate ADT-resistant NCAM1$^+$ cells and prevent CRPC.

Taken together, these data highlight NCAM1 as a novel predictive-prognostic biomarker in PCa, which could significantly improve the clinical management of PCa patients and pointed out druggable molecular pathways that could be targeted to eradicate "true" NCAM1$^+$-PCSCs (self-renewal) and stem-like NCAM1$^+$ progenitors (ADT-resistance).

2. Introduction

2.1 Prostate Gland

The prostate is a gland of the male reproductive apparatus (it includes also the seminal vesicles, the penis and the testicles) that is essential for the secretion of semen and sperm welfare. It is located under the bladder, in front of the rectum, and the urethra runs through its center. The gland is anatomically divided into five regions: the central zone, the periurethral region, the transition zone, the peripheral zone from which most tumors originate, and the fibromuscular region or stroma. Internally, prostate tissue is enriched in ducts defined by a columnar luminal inner epithelium and a basal outer layer, and acini surrounded by stroma. The stroma contains mainly fibroblasts and smooth muscle, both responsible respectively of prostate development and physiological contractility. Neuroendocrine cells are also distributed within the ducts but their role in prostate physiology is still unclear (see section 2.2.9) (McNeal, 1981; Timms, 2008; Verze, Cai and Lorenzetti, 2016).

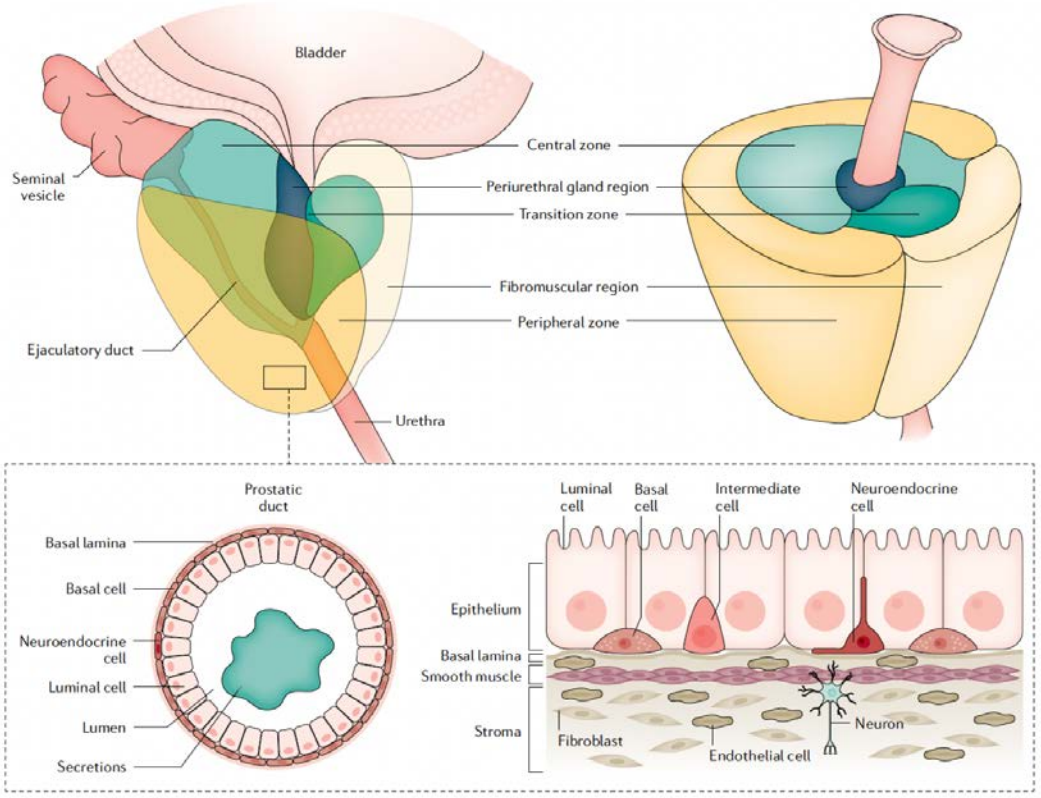

Figure 1. Anatomy and histology of human prostate gland. *Prostate gland division in five regions: central zone, periurethral region, transit zone, peripheral zone, and fibromuscular region (stroma). Boxed area referred to epithelial distribution of ducts and acini (Rebello RJ et al, Nat Rev Dis Prim 2021).*

2.2 Prostate Cancer

2.2.1 Epidemiology

Prostate cancer (PCa) is the second most diagnosed cancer in men, after lung cancer, with ~1 million new cases per year and more than 350,000 annual related deaths worldwide making it as one of the leading causes of cancer-associated death in men (Foreman *et al.*, 2018). Due to the increase in life expectancy in developed countries, the number of new PCa cases and related deaths is predicted to increase in the next years with a great impact on national health services. Therefore, investigating in PCa research is crucial to define novel predictive biomarkers and target therapies.

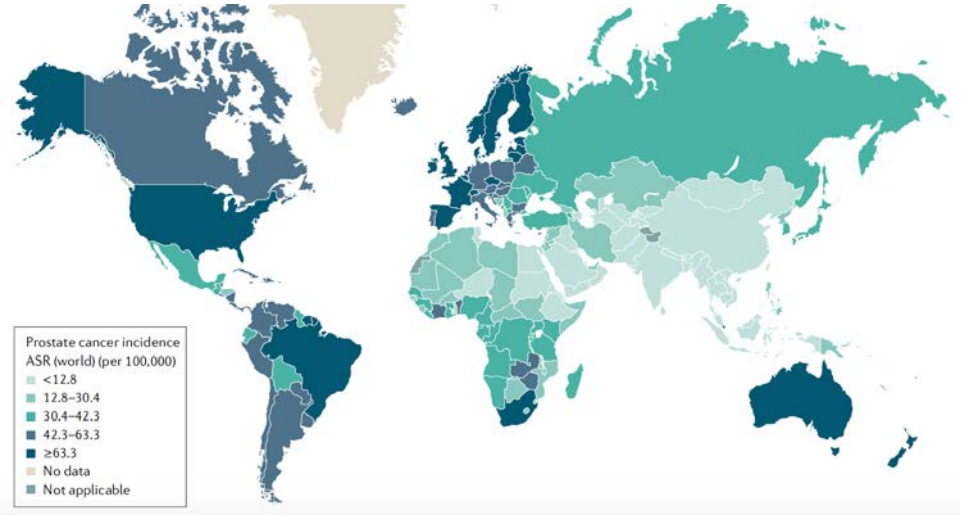

Figure 2. Worldwide incidence of PCa. *Global incidence of PCa in 2018. Colors refer to number of cases per 100,000 people (Rebello et al., 2021).*

2.2.2. Risk factors in PCa

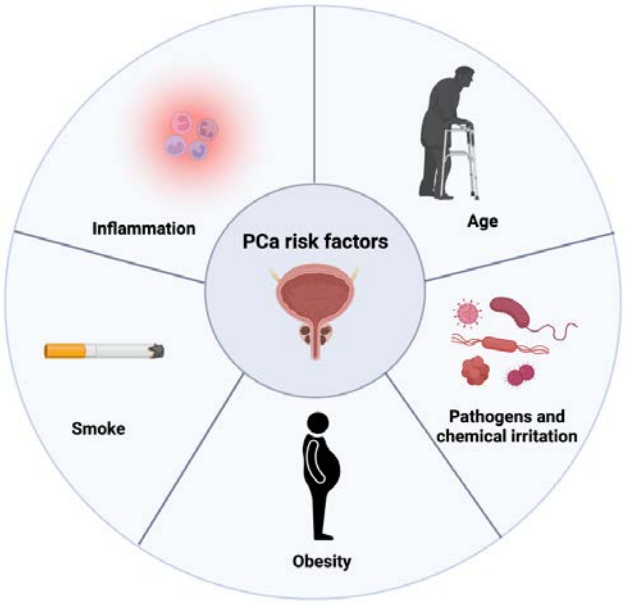

Figure 3. Summary of risk factors in PCa. *Pie chart reporting the common risk factors predisposing to PCa: age, inflammation, pathogens, diet and obesity, smoke and lifestyle, genetic factors. Graph was edit by Biorender software.*

2.2.2.1 Age

Old age is the most relevant risk factor in PCa (Crawford, 2003; Bray *et al.*, 2018) with more than 85% of PCa cases being newly diagnosed in men with > 60 years of age. Nonetheless, autopsy series revealed in a fraction (29%) of men between 30 to 40 years of age (Sakr *et al.*, 1994) with traits typical of aberrant prostate tissue growth (hyperplasia) or low-grade cancer suggesting paradoxically that a relevant percentage of men die with PCa and not by it (Jahn, Giovannucci and Stampfer, 2015).

2.2.2.2 Pathogens and chemical irritation

The prostate microbiome has a pivotal role in controlling tumor development and progression and several epidemiological studies have correlated bacterial and viral infection with prostatic inflammation (Liss *et al.*, 2018; Sfanos *et al.*, 2018; Shrestha *et al.*, 2018). Viruses such as papillomavirus (HPV), herpes simplex virus type 2 (HSV2), cytomegalovirus (CMV) and herpes virus type 8 (HHV8) have been detected in the prostate (Strickler and Goedert, 2001; Zambrano *et al.*, 2002; Samanta *et al.*, 2003). In addition, sexually transmitted organisms such as *Chlamydia trachomatis, Trichomonas vaginalis* and *Treponema pallidum* (Poletti *et al.*, 1985; Gardner, Culberson and Bennett, 1986; Caini *et al.*, 2014) and non-sexually transmitted bacteria such as *Propionibacterium acnes* and *Escherichia Coli* have been detected. Interestingly, an experiment conducted in C57 mouse model demonstrated that the transurethral injection of human-derived *E. Coli 1677* stimulates acute and chronic inflammation in prostate tissue that lead to hyperplasia with basal-to-luminal differentiation (Boehm *et al.*, 2012; Kwon *et al.*, 2014), correlating the bacterial infection with the risk to cancer initiation.

The presence of E. Coli in the urinary tract, derived from urinary reflux, is the cause of prostatitis (Kirby *et al.*, 1982; Mitsumori *et al.*, 1999; De Marzo *et al.*, 2007). Prostatitis can be classified into 4 categories (Palapattu *et al.*, 2005):

I. acute that results from an *E. Coli*-mediated acute bacterial infection;
II. chronic that results from the persistent localization of bacteria in prostate tissue;
III. chronic non-bacterial that is the most diagnosed (> 90% of cases);
IV. asymptomatic that is diagnosed in men without symptoms but showing histological inflammatory traits.

At the molecular level, bacterial prostatitis negatively impacts transcription of the tumor suppressor *NKX3.1* favoring DNA damage without efficient repair (Khalili *et al.*, 2010). Moreover, urine reflux does not transport only bacteria into the prostate but also chemicals excreted by the urine, such as uric acid, which can precipitate and form crystals in tissues and provoke a very strong inflammatory

response (Ghaemi-Oskouie and Shi, 2011). This response boosts the innate immunity through the activation of the caspase-1-activating NALP3 inflammasome that in turn sustains chronic inflammation by the continuous release of cytokines in the prostatic tissue (Martinon *et al.*, 2006).

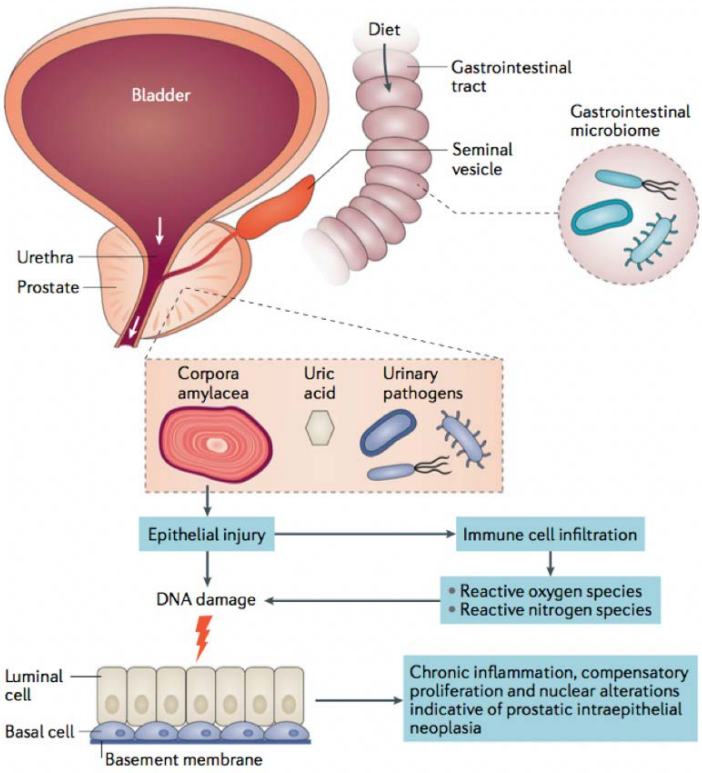

Figure 4. Prostate transformation mediated by pathogens. *Pathogens derived from gastrointestinal microbiome or from urinary reflux, uric acid on luminal secretion (corpora amylacea) are responsible of DNA damage and epithelial injury that enhance compensatory epithelial proliferation indicative of PIN (preneoplastic intraepithelial neoplasia) (de Bono et al., 2020).*

2.2.2.3 Obesity

Preclinical and clinical studies revealed that obese patients have a higher risk of developing PCa (Wilson *et al.*, 2022). Mice fed with a high fat diet (HFD) in the presence of oncogenic lesions, such as Myc amplification or PTEN loss, or with a diet enriched in 2-amino-1-methyl-6-phenylimidazo(4,5-b)pyridine (PhIP), a chemical compound released by overcooked red meat, have an increased probability of developing prostatic adenocarcinoma (Cross *et al.*, 2005; Sinha *et al.*, 2009; Alexander *et al.*, 2010; Nouri-Majd *et al.*, 2022). This increase occurs due to a strong inflammatory microenvironment created by peri-prostatic adipose tissue (PPAT) through the transcriptional regulation of pro-inflammatory cytokines (e.g., interleukin-6 (IL-6), interferon-γ (IFN-γ) and interferon-α (IFN-α)) and chemokines (e.g., C-C motif chemokine ligand 10 (CXCL10)) (Mangiola *et al.*, 2019) that act in a paracrine manner. Moreover, adipocytes can crosstalk with neighboring cells through the release of specific cytokines (adipokines such as leptin), which

stimulate proliferation, androgen-independent cell migration and angiogenesis in PCa (Sierra-Honigmann *et al.*, 1998; Somasundar *et al.*, 2004; Huang *et al.*, 2011).

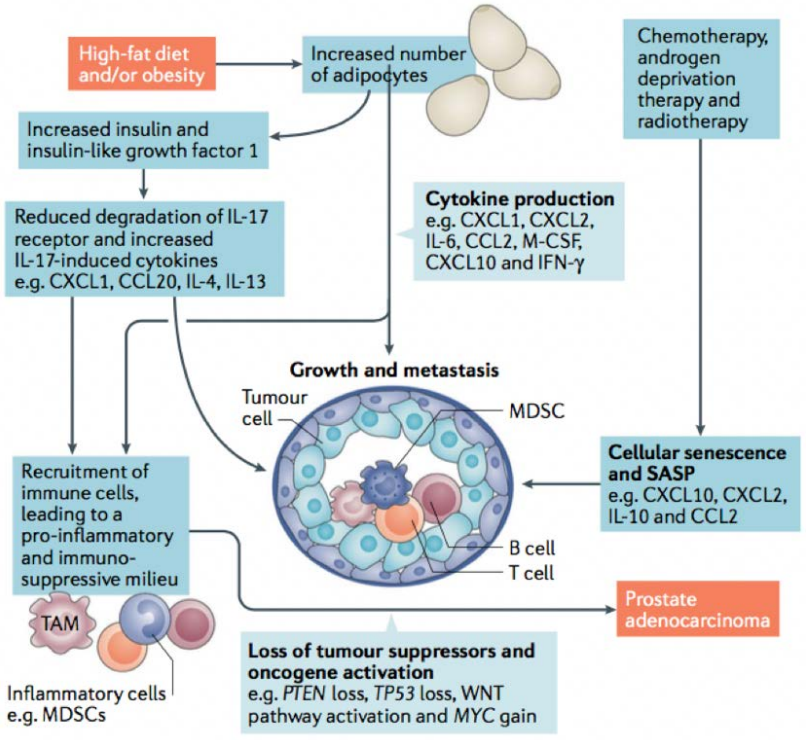

Figure 5. Obesity-related inflammatory factors in PCa initiation and progression. *Endocrine function of adipocytes that through the releasing of several cytokines/chemokines sustain prostatic inflammation by modulating immune cells and senescence with secretory function (SASP) (de Bono et al., 2020).*

2.2.2.4 Smoke and lifestyle

In the literature, the correlation between the large intake of red meat and animal fat with the risk of developing PCa is widely accepted. A clinical trial with 51,259 enrolled men correlated the intake of animal products and PCa risk, basing the evidence on questionnaires completed by patients, before and during the follow-up (Michaud *et al.*, 2001). Mechanistically, the release of heterocyclic aromatic amines and polycyclic aromatic hydrocarbons from high temperature-cooked meat was found to promote DNA damage and chronic inflammation, which was suggested underly the increased risk of PCa (Giovannucci *et al.*, 1993).

Tobacco smoking is widely considered to be a cause of various cancers, included PCa. Although a meta-analysis of prospective cohort studies revealed a modest but significant involvement of smoke in fatal PCa (Islami *et al.*, 2014), the relationship between smoking and PCa adenocarcinoma was tested in 24 cohort studies enrolling 21,579 patients. Data revealed that former smokers demonstrated increased risk (RR = 1.09) and current smokers had increased risk of fatal PCa (RR = 1.14). Moreover, the number of cigarettes smoked per year impacts on PCa associated death, with the heaviest smokers having ~30% greater risk than nonsmokers (Huncharek *et al.*, 2010).

2.2.2.5 Inflammation

Inflammation is defined as a highly evolutionary conserved mechanism central to the adaptive response following tissue damage or infections, modulating the recruitment of innate and adaptive immune cells to restore tissue homeostasis (Meizlish *et al.*, 2021). When the stimuli causing the inflammation are present in a tissue for a prolonged time, they promote chronic inflammation in that tissue. Intraprostatic inflammation is one of the most important risk factors for PCa development and progression. Chronic inflammation of the prostate gland was detected at autopsy in at least 50% of men who had not been diagnosed with prostatic disease, suggesting that inflammation is a common age-related event (Delongchamps *et al.*, 2008; J. de Bono *et al.*, 2020).

Chronic inflammation is widely accepted as one of the main causes of tumorigenesis in several types of cancer with a prominent role in tumor initiation (Ames, Gold and Willett, 1995; Coussens and Werb, 2002). Indeed, chronic inflammation contributes significantly to both tumor initiation and progression steps:

i. accumulation of mutations or genetic alterations in genes and/or signaling pathways that confer advantages to the cell over neighboring normal cells. In detail, many mutations or genetic alterations can be caused directly by reactive oxygen species (ROS) that leads to the inactivation of enzymes involved in mismatch repair, thus provoking genomic instability and DNA damage (Hussain, Hofseth and Harris, 2003; Colotta *et al.*, 2009; Grivennikov, Greten and Karin, 2010) or cancer genes, such as *TP53, MYC* and *BCL6* with DNA breaks, by cytosine deamination, and chromosome translocation (Robbiani *et al.*, 2009).
ii. amplification and establishment of malignant clones and outgrowth into the surrounding healthy tissue.

The continuous crosstalk between cancer cells and tumor microenvironment (TME) by the release of mediators such as cytokines and chemokines [IL-6, interleukin-8 (IL-8), interleukin-1β (IL1β), C-C motif chemokine ligand 2 (CCL2) and C-C motif chemokine ligand 20 (CCL20)], which can act in an autocrine and/or in a paracrine manner, is essential for mediating antitumor or protumoral immune responses, thus creating an inflammatory microenvironment that sustains cancer progression and contributes to cellular plasticity (Mantovani *et al.*, 2008; Dougan and Dranoff, 2009). Plasticity is defined as genetic and phenotypic alterations that change cells during cancer progression (Yuan, Norgard and Stanger, 2019). The best-characterized change is the epithelial-to-mesenchymal transition (EMT) (see section 2.2.7.1.1) and the reverse process of mesenchymal-to-epithelial transition (MET) that are highly determined by extracellular factors, such as cytokines and growth factors. In detail, cytokines, for example, tumor-necrosis factor-α (TNFα) and IL-1β, modulate the transcription of EMT-related genes including TWIST and SLUG (Suarez-Carmona *et al.*, 2017;

Francart *et al.*, 2018), while interleukin-11 (IL-11) and interleukin-17 (IL-17) have been shown to support tumor invasion in the colon and breast due to the promotion of immune escape (Calon *et al.*, 2012; Marusyk *et al.*, 2014; Coffelt *et al.*, 2015). Although the link between chronic inflammation and PCa is well established, the initial cause of prostatic chronic inflammation remains unclear. Several potential contributing factors have been investigated including local infection, urine reflux, exposure to chemical agents and dietary factors or obesity which are described below.

Overall process	Putative factor	Key mechanism
Chronic inflammation	Urinary microorganisms	These microbes drive prostatic inflammation, epithelial injury and hyperplasia
	Gut microbes	These microbes stimulate the production of metabolites and androgens that can potentially affect prostate cancer development
	High dietary fat intake and obesity[a]	A diet high in saturated fat leads to a form of obesity that enhances the oncogenic *MYC* transcriptional programme through epigenetic mechanisms
		A diet high in saturated and monounsaturated fats leads to a form of obesity that may activate the SREBP pro-metastatic transcriptional regulator of lipid homeostasis in prostate cancer
		Adipocytes can release growth hormones, sex hormones, steroids and inflammatory cytokines that promote prostate cancer progression and metastases
		Hyperinsulinaemia prevents the degradation of the receptor for the inflammatory cytokine IL-17
	Chemical injury	Urinary reflux exposes prostatic epithelium to chemicals, such as uric acid, that can directly activate innate immune responses
	Corpora amylacea[b] (physical trauma)	These are frequently found within the lumen of prostatic ducts and are often associated with damaged epithelium and areas of inflammation in benign areas of the prostate

Figure 6. Summary of factors stimulating chronic inflammation in prostate. *(de Bono et al., 2020).*

2.2.2.5.1 Proliferative inflammatory atrophy (PIA)

Inflammation promotes atrophy in prostate glands, accompanied by an increase in the proliferation marker Ki-67, hyperplasia in prostate tissue and the release of inflammatory factors such as IL-6, interleukin-1 (IL-1) family members and COX2. The atrophic tissue is commonly detected in focal lesions in the peripheral zone of the prostate and are defined as PIA lesions. PIA regions are proposed to be precursor lesions of prostatic adenocarcinoma that may develop into high-grade PIN or perhaps directly into cancer (De Marzo *et al.*, 2016). PIA originate because of a continuous regeneration of the prostate epithelium in response to damage (De Marzo *et al.*, 1999) with an expansion of cells with an intermediate phenotype that express both basal and luminal markers, such as cytokeratin (CK)-8 and -18 (luminal) and CK-5 (basal) (van Leenders *et al.*, 2001). Thus, they are considered to be enriched in cells with stem potential (De Marzo *et al.*, 1999). Alterations in several pivotal components of cancer pathways have also been detected in PIA, including the downregulation of

tumor suppressors (e.g., NKX3.1, p27, PTEN and p53) in addition to the increase in oncogenic proteins such as Myc, ETS transcription factor (ERG), ETS variant transcription factor 1-4 (ETV1-4), AR and BCL2 (De Marzo *et al.*, 1999; Bethel *et al.*, 2006).

Moreover, the chronic inflammation associated with PIA alters the immunobiology of the prostate. PIA displays an increase in $CD45^+$ leukocyte infiltration, of which 70-80% are $CD3^+$ T lymphocytes, while 10-15% are $CD19^+$ or $CD20^+$ B lymphocytes. Furthermore, the cytotoxic $CD8^+$ T cells, usually present in the prostate gland are replaced by $CD4^+$ T cells that can influence drug response and patient's outcome (Mercader *et al.*, 2001; Steiner *et al.*, 2003; Davidsson *et al.*, 2013; Leibowitz-Amit *et al.*, 2014; Lorente *et al.*, 2015). Inflammation also sustains the recruitment not only of lymphocytes but also subtypes of leukocytes such as myeloid cells and macrophages in PIA regions (Ammirante *et al.*, 2010; Escamilla *et al.*, 2016; Calcinotto *et al.*, 2018). MDSCs also produce ROS which are responsible for DNA damage and breaks that in turn activate SASP. Senescence is defined as a permanent block of cell cycle with the appearance of β-galactosidase in combination with other hallmarks, such as loss of laminin B1, overexpression of p16 and elevation of p21 and p53 transcription (Gorgoulis *et al.*, 2019). Moreover, SASP is characterized by the release of pro-inflammatory cytokines, growth factors and MMPs that have a role in cell dissemination (Coppé *et al.*, 2010), and results in the activation of several pathways, including NFkB, Notch-1, IL-6 and JAK-STAT, which drive prostate carcinogenesis creating an immunosuppressive microenvironment by recruiting MDSCs (Wang, Lankhorst and Bernards, 2022).

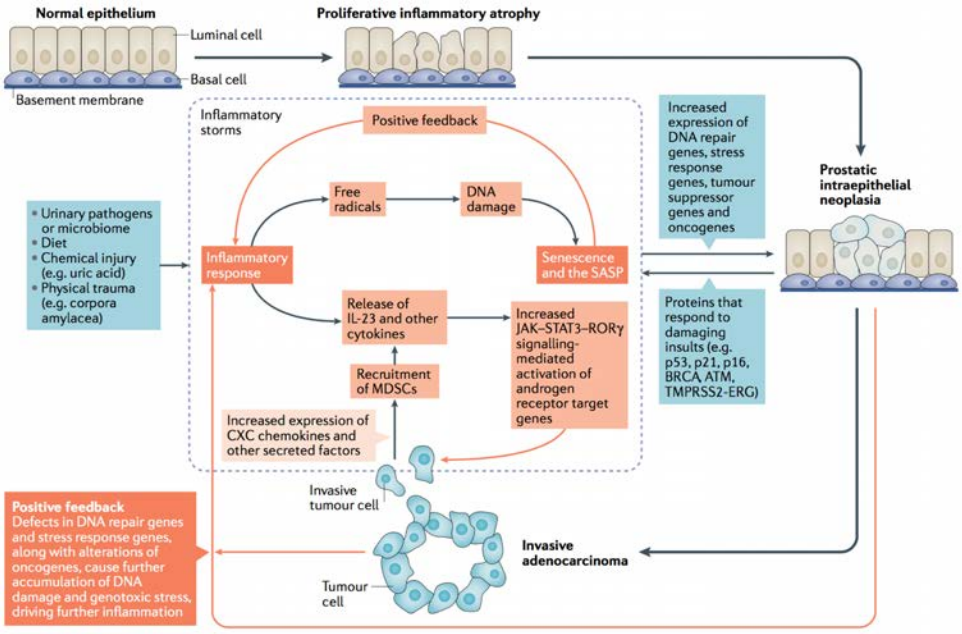

Figure 7. From PIA to cancer: the "inflammatory storm". *Endogenous and exogenous insults (microorganism, chemicals, physical trauma, diet) are responsible for triggering inflammation, which leads to proliferative inflammatory atrophy (PIA) and then PIN. Then, inflammation sustains invasive adenocarcinoma with immune-mediated cytokines/chemokines releasing (de Bono et al., 2020). SASP: senescent-associated secretory phenotype; MDSC: myeloid-derived suppressor cells.*

2.2.2.6 Genetic predisposition

Prostate tumorigenesis derives in 5-10% of cases from genetic predisposition linked to inherited germline mutations that affect key cancer-related genes. Familial studies of PCa patients with more than two relatives with the disease, have revealed mutations linked to hereditary PCa. For example, a recurrent mutation (G48E) in the transcription factor Homeobox-13 (HOXB13*)* located on chromosome 17q21-22 increases the relative risk in early-appearing PCa by 3-fold (onset at <60 years of age) (Kote-Jarai *et al.*, 2011; Ewing *et al.*, 2012; Karlsson *et al.*, 2014). Other germline mutations that predispose patients to PCa include those involved in DNA damage repair (DDR), such as BRCA DNA repair associated (BRCA1 and BRCA2), ATM Serine/Threonine kinase (ATM), ATR Serine/Threonine kinase (ATR), and mismatch repair (MMR)-related genes [e.g., MLH-1 and PMS2 partner and localizer of BRCA2 (PALB2)], RAD51 paralog D (RAD51D) and checkpoint kinase 2 (CHEK2). In particular, BRCA1/2 mutations, which are linked to an increased risk of developing breast and ovarian cancer in younger age (De Talhouet *et al.*, 2020), have been shown to increase the risk of early onset PCa. BRCA2 mutations were detected in at least 2% of younger PCa patients (< 65 years old) and increased the risk of developing PCa by 5 to 7-fold. Instead, in the same set of patients, BRCA1 mutations carry up to an 8.6% cumulative risk of developing PCa (Attard *et al.*, 2016; Fraser *et al.*, 2017; Armenia *et al.*, 2018; Sandhu *et al.*, 2021).

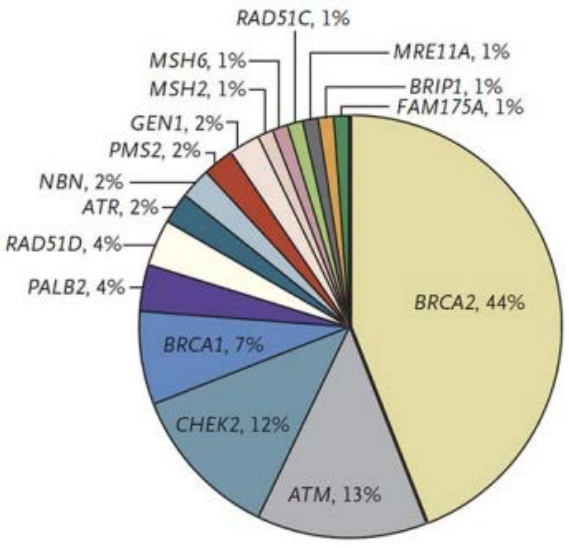

Figure 8. Germline mutations distribution in PCa patients. *Pie chart reporting the distribution (%) of DNA-repair genes reported to predispose prostate cancer. Breast cancer gene A 1-2 (BRCA-1, -2); ATM serine/threonine kinase (ATM); checkpoint kinase 2 (CHEK2); partner and localizer of BRCA1 (PALB2); RAD51 recombinase parolog D (RAD51D) and C (RAD51C); ATR serine/threonine kinase (ATR); nibrin (NBN); PMS1 homolog 2 mistmatch repair system component (PMS2); GEN1 Halliday junction 5' flap endonuclease (GEN1); muts homolog 2 (MSH2) and homolog (MSH6); MRE11 homolog double strand break repair nuclease (MRE11); BRCA1 interacting helicase 1 (BRIP1); abraxas1 BRCA1 A complex subunit (FAM175A) (Pritchard et al., 2016).*

2.2.3 Genetic alterations in PCa progression

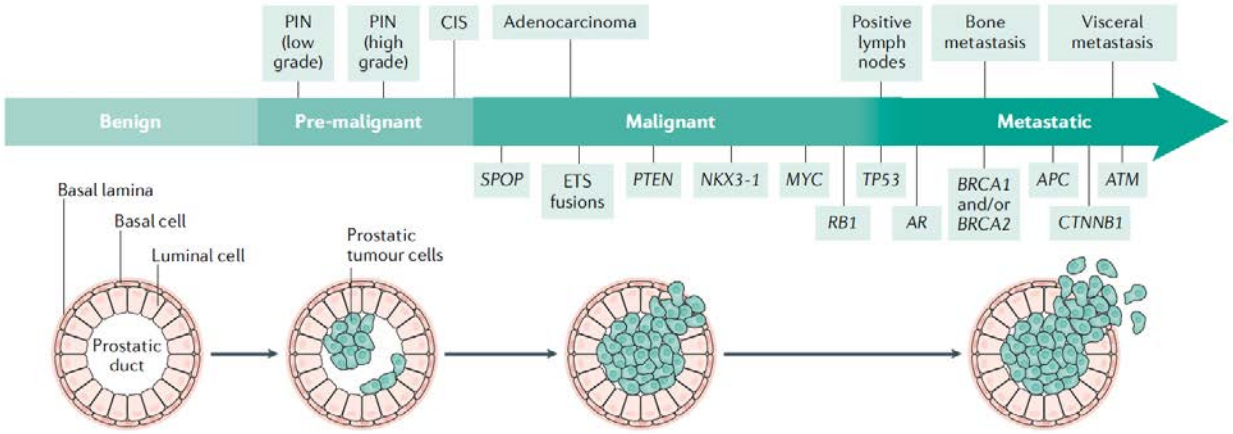

Figure 9. Genetic alterations reported in PCa progression. *The line of PCa progression stages, from benign to metastatic, report common mutations in each phase of the disease. CIS: carcinoma in situ; PIN: prostatic intraepithelial neoplasia (Rebello et al., 2021).*

The development of high-throughput sequencing analyses, such as whole genome or transcription sequencing such as whole exome and whole transcriptome, has allowed the identification of novel molecular alterations and aberrations that enhance PCa development and support progression to aggressive forms (Berger *et al.*, 2011; Baca *et al.*, 2013; Robinson *et al.*, 2015). Genome-wide association studies (GWAS) reported >170 single nucleotide polymorphisms (SNPs) predisposing patients to PCa onset (Rebello *et al.*, 2021), notably in proximity to the oncogene *c-MYC* (Ahmadiyeh *et al.*, 2010), located at chromosome 8q24, and to the kallikrein (KLK) genes *KLK2* and *KLK3* (encodes for prostate specific antigen (PSA); see section 2.2.5.1) located at chromosome 19q13 (Kote-Jarai *et al.*, 2011). Moreover, next-generation sequencing (NGS) highlighted somatic genetic lesions linked to PCa. The most common lesion (present in almost 50% of PCa) is the fusion between the androgen-responsive promoter of the transmembrane protease serine 2 (*TMPRSS2*) gene and ERG, both located at chromosome 21q22 (Tomlins *et al.*, 2005, 2008; Carver *et al.*, 2009). *TMPRSS2* is an androgen-target gene in prostate that encodes for a serine-protease family member, while ERG is an oncogene that transcribes for a transcription factor controlling pivotal biological cell functions, such as proliferation, differentiation and apoptosis (Gasi Tandefelt *et al.*, 2014)

Point mutations in key genes involved in prostate carcinogenesis have also been described, such as speckle type BTB/POZ (*SPOP)* (5-15% of cases), which encodes a substrate adaptor of Cullin-based E3 ubiquitin ligases (Clark and Burleson, 2020); Forkhead Box A1 (*FOXA1)* (3-5% of cases), which encodes a DNA-binding protein involved in AR transcription (Sahu *et al.*, 2011); and serine peptidase inhibitor Kazat type I (*SPINK1*) (5-10% of cases), which encodes a secreted serine protease inhibitor (Flavin *et al.*, 2014) involved in the early phase of the disease.

Analysis of "The Cancer Genome Atlas" (TCGA) dataset revealed that homozygous deletion of the *PTEN* gene is frequently observed in primary PCa (~15% of cases) and even more so in metastatic disease (~ 40% of cases), demonstrating its relevance to PCa progression (Taylor *et al.*, 2010; Grasso *et al.*, 2012). Metastatic lesions (~18%) harboring alterations in key modulators of this pathway, such as *CTNNB1* which encodes for β-Catenin (4% of cases) and *APC* (9% of cases) that controls β-Catenin stability and nuclear translocation (Grasso *et al.*, 2012; Hovelson *et al.*, 2015; Robinson *et al.*, 2015). BRAF is the most common member of the MAPK pathway to be mutated in PCa (2-3% of cases), while 1% of PCa display a point mutation (Arg132His) in *IDH1* gene (Grasso *et al.*, 2012; Robinson *et al.*, 2015). *IDH1* encodes for isocitrate dehydrogenase, and this mutation alters its enzymatic function leading to overproduction of 2-hydroxyglutarate (2-HG) that alters tissue metabolism (Turkalp, Karamchandani and Das, 2014) .

Moreover, AR is involved in PCa progression. In detail, amplification or mutation was found only in 1% of localized PCa and 4% in metastatic disease but interested up to 70% of castration-resistant PCa with metastatic traits (mCRPC) (Wang *et al.*, 2020). Due to the relevance of AR in prostate, it is discussed in depth in the next paragraph (see section 2.2.4).

2.2.4. Androgen receptor

2.2.4.1 Structure and function

Androgen receptor (AR) is a steroid receptor transcription factor that has a key role in prostate development and growth (Fujita and Nonomura, 2019). The gene is located on chromosome X (Xq11-12) with a coding region consisting in 2757 nucleotides that encodes for the protein with 919 amino acids (110 kDa) (Gelmann, 2002). Structurally, AR is composed of 4 functional regions: the N-terminal domain (NTD) (1-555 aa); a DNA-binding domain (DBD) (555-623 aa); a ligand-binding domain (LBD) (665-919 aa) linked to DBD with a flexible hinge region (623-665 aa) and the nuclear localization signal (NLS) (617-633 aa) (Mangelsdorf *et al.*, 1995). The NTD is enriched in polyglutamine and polyglycine repeats that are highly variable in men and they affect the structure and the assembly of this domain (Hsing *et al.*, 2000; Sasaki *et al.*, 2003; Werner *et al.*, 2006; Davies *et al.*, 2008) and the NTD residue was also demonstrated to be determinant for complete transcriptional activity (Simental *et al.*, 1991). The DBD is composed of two zinc fingers each comprising four cysteine residues conjugated to a zinc ion. The NLS region allows the entering of AR as active dimer into the nucleus. The LBD is made up of eleven α-helices and four β-strands (Matias *et al.*, 2000) that form a pocket for binding androgens; the presence of the docking site activation function 2 (AF2) domain is required to stabilize this interaction and to recruit cofactors

(Nadal *et al.*, 2017). The α-helix of the LBD can bind specifically to androgen-response elements (AREs) 5'-GGTTCT-3' in the promoter region of target genes such as secreted proteins (KLK2 and KLK3), fusion genes (TMPRSS22/ERG), growth stimulator [Insulin like growth factor 1 receptor (IGF1R)], transcription factors [NK3 homeobox 1 (NKX3.1) and Forkhead Box P1 (FOXP1)], metabolic enzyme [Calcium/Calmodulin dependent protein kinase kinase 2 (CAMKK2)] and cell cycle regulator [Transforming acidic coiled-coil-containing protein 2 (TACC2)] (Claessens *et al.*, 1996; Shaffer *et al.*, 2004; Fujita and Nonomura, 2019), in cooperation with coregulatory proteins, such as SRC family members of tyrosine kinases (i.e., FYN, SRC and FGR) and p300/CREB binding protein (CBP) (Boggon and Eck, 2004; Takayama and Inoue, 2013).

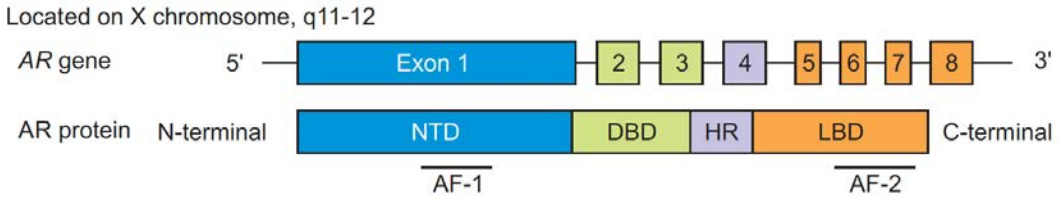

Figure 10. Androgen receptor (AR) gene and protein structure. *Graphical representation of AR gene and protein domains. NTD: N-terminal domain; DBD: DNA-binding domain; HR: hinge region; LBD: ligand-binding domain; AF: activation function-1 (AF-1) and -2 (AF-2) (Fujita and Nonomura, 2019).*

Functionally, AR drives the hormonal-mediated prostate development and proliferation through the binding with androgens. Androgens are produced in and released by the testes as testosterone or by adrenal glands as androgen precursors: androstenedione and dehydroepiandrosterone (DHEA). In the prostate, testosterone is converted into dihydrotestosterone (DHT) by 5-alpha-reductase and can bind the AR, while the precursors are converted into testosterone by 17-beta-hydroxysteroid dehydrogenase (El-Alfy *et al.*, 1999; Hsing, 2001). AR is mainly expressed by luminal prostate epithelial cells, in which also control secretory functions such as the releasing of PSA, while is weakly expressed or absent in the basal epithelium.

Moreover, in normal prostate epithelium AR is expressed also by stromal cells such as fibroblasts and smooth muscle cells (Singh *et al.*, 2014). Here, it exerts a critical role in prostate development through the releasing of paracrine factors such as epithelial growth factor (EGF), fibroblast growth factor (FGF), nerve growth factors (NGF) and insulin-like growth factor (IGF). The pivotal role of stromal AR was evidenced also *in vivo* C57 mouse model AR knockout in both fibroblasts and smooth muscle cells (Yu *et al.*, 2012). Indeed, these mice displayed aberrant prostate development and reduction in cell growth, mediated by IGF-1.

2.2.4.2 AR genetic alterations

Several alterations involving the AR gene or protein, such as gene amplification, mutations, expression of splice variants and post-translational modifications occur in PCa.

Point mutations

These mutations, usually amino acids substitutions, typically enhance the ability of AR to bind ligands leading to receptor transactivation (Taplin *et al.*, 1999; Buchanan *et al.*, 2001) and are observed in 20-40% of untreated metastatic PCa, while they are not present in less aggressive tumors (Tilley *et al.*, 1996; Marcelli *et al.*, 2000). As previously described, the AR is activated by hormones which bind directly to the LBD. Several AF2 domain point mutations have been annotated (Heinlein and Chang, 2004) but the most frequent is the T876A occurring in at least 30% of metastatic patients (Taplin *et al.*, 1999). This substitution allows the activation of AR by DHEA, estradiol and progesterone and it is determinant for AR agonists resistance (Veldscholte *et al.*, 1990; Miyamoto *et al.*, 1998; Yeh *et al.*, 1998; Shi *et al.*, 2002). Instead, the T877A mutation, which displaces helix 12 and changes the co-activator binding, enhances the affinity for estrogen and progesterone binding, while the F877L, a missense mutation that promotes agonist activity from AR antagonists compounds such as enzalutamide (Gaddipati *et al.*, 1994; Joseph *et al.*, 2013). Further, some mutations enhance affinity not only for low levels of testosterone but also for non-androgen ligands such as glucocorticoids, progestins, estrogens and dehydroepiandrosterone (Suzuki *et al.*, 1993; Tan *et al.*, 1997; Watson, Arora and Sawyers, 2015) such as the AR L107H and AR L107H/T877A that both enhance sensitivity of AR to glucocorticoids cortisone and cortisol (van de Wijngaart *et al.*, 2010). Then, the NH2 domain of AR, which is relevant for the interaction with co-regulators, is interested by point mutations. Mutational analysis of xenografts derived from the LNCaP PCa cell line identified the sequence ^{435}WHTLF^{439} in the NH2 domain involved in androgen-independent AR activation (Dehm *et al.*, 2008; Imamura and Sadar, 2016).

Table 1. Summary of previously indicated AR point mutations and their function

Point mutation	Function	Reference
T876A	AR agonist	(Taplin *et al.*, 1999)
T877A	Estrogen/Progesterone binding	(Gaddipati *et al.*, 1994)
F877L	Enzalutamide resistance	(Balbas *et al.*, 2013)
L107H	Cortisone/cortisol sensitivity	(van de Wijngaart *et al.*, 2010)
^{435}WHTLF^{439}	Androgen-independent activation	(Dehm *et al.*, 2008)

Amplification

The term amplification refers to the increase in gene copy number compared to a normal diploid state and these alterations are revealed by the fluorescence *in situ* hybridization (FISH). The AR gene was found to be amplified in at least 20% of patients who received ADT, with a two-fold increase in mRNA levels (Visakorpi *et al.*, 1995; Bubendorf *et al.*, 1999; Linja *et al.*, 2001; Wadosky and Koochekpour, 2016) and results in higher levels of AR protein. Several studies revealed that AR amplification allows the growth of prostate cells even in very low levels of circulating androgens as occurring during endocrine treatments. In fact, AR amplification was estimated, by genomic hybridization, in at least 30% of human prostate tumors that did not respond to hormonal treatments and progress to androgens insensitive tumors (Visakorpi *et al.*, 1995).

Splice variants

AR splice variants (AR-Vs) are expressed as truncated forms of AR, lacking the C-terminal LBD but with an intact N-terminal domain. Despite the absence of the canonical hormone binding domain, AR-Vs are active as transcription factors and function independently of ligand (Hu *et al.*, 2009). There are several proposed mechanisms of AR-V expression in PCa which consider both cell context and splicing factors. In the LuCAP 86.2 cell line, an androgen-insensitive xenograft-derived cell line, FISH analysis revealed an intragenic rearrangement that produced an AR-V lacking exons 5-7 (AR^{v567es}) in at least 50% of detected cells, which contributes to PCa with androgen-independent behavior (Nyquist *et al.*, 2013).

AR-V7 is one of the most expressed AR variants in anti-androgens drug resistant PCa (Hu *et al.*, 2009) and several studies have provided evidence of its relevance to PCa progression and poor clinical outcome. AR-V7 lack the end of exon 3 (truncation) and the detection of this variant by immunohistochemistry (IHC) (Guo *et al.*, 2009) or semi-quantitative RT-qPCR in the nucleus is often associated with androgen-resistant PCa and not indolent disease compared to full-length AR (Hu *et al.*, 2009; Sun *et al.*, 2010). AR-V7 protein expression in a cohort of 358 primary was rarely identified by IHC in primary PCa (< 1%), while 75% of 293 metastatic PCa result positive to the staining suggesting that this variant is enhanced during PCa progression, also due to the selective pressure of AR-inhibitors and worsening the overall survival (OS) compared to AR-V7 negative patients (25 *vs.* 74 months) (Sharp *et al.*, 2019). AR-V7 can be detected also in circulating tumor cells (CTCs) at mRNA and protein levels, facilitating the clinical employment of AR-V7 detection in clinics (Armstrong *et al.*, 2020). In a clinical study enrolling 62 patients with metastatic disease with resistance to androgen-receptor axis-targeted therapies (AATTs) demonstrated to have AR-V7-

positive CTCs. These patients, compared to AR-V7-negative CTCs, have worse prognosis confirming the potential role as predictive biomarker in clinics (Zhang *et al.*, 2020).

Post-translational modifications

Many AR post-translational modifications have been characterized commonly in androgen-independent PCa such as acetylation, methylation, phosphorylation, ubiquitination and SUMOylation (Coffey and Robson, 2012), which control protein stability, transcriptional activity and target gene modulation (Wen, Niu and Huang, 2020). AR is phosphorylated by several kinases at different residues. For example, i) SRC phosphorylates Tyr534 resulting in the sensitization of the AR to low levels of androgens (Guo *et al.*, 2006); ii) ETK phosphorylates Tyr551/552 which confers AR activity also in presence of very low levels of androgens (Dai *et al.*, 2010); iii) ACK1 phosphorylates Tyr267 which correlates with disease progression and decreased survival in PCa (Mahajan *et al.*, 2017); iv) cyclin-dependent kinase-1 and -9 (CDK1 and CDK9) phosphorylate Ser81, a determinant for AR protein stability (Gao *et al.*, 2021); v) the phosphorylation of residues Ser308 and Ser791 has been shown to inhibit the transcriptional activity of the AR and is associated with poor clinical outcome (McCall *et al.*, 2013). AR is acetylated on lysine (K) 630-633 by p300 that augments the interaction with androgens, and on K618, which is mediated by ARD1 and increase its transcriptional activity and translocation into the nucleus (Fu *et al.*, 2006; DePaolo *et al.*, 2016). Instead, AR is methylated on K630-632 by Set9 (H3K4 histone monomethyltransferase) that enhances AR transcriptional activity; on Arginine (R) 761 by PRMT5 that attenuated the transcriptional activity (Mounir *et al.*, 2016). AR is ubiquitinated by the E3 ubiquitin ligase Siah2 which promotes transcriptional activity (Qi *et al.*, 2013) and SUMOylation, a modification that requires the addition of small ubiquitin-like modifiers (SUMO) by the protease SENP1, enhances transcriptional activity of AR .

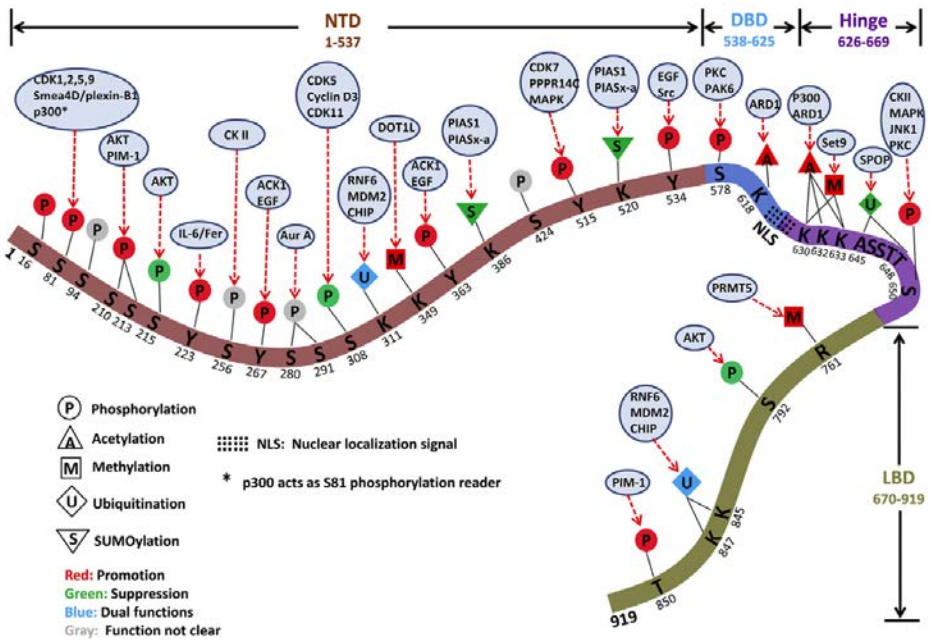

Figure 11. AR post-translational modifications. *AR residues are modulated by several modifications: phosphorylation (P), acetylation (A), methylation (Me), ubiquitination (U) and SUMOylation (S). Modifications with positive effect on AR transcriptional activity are in red, while the negatives are in green. In blue and in grey are indicated respectively the modifications with double or unknown function. NTD: N-terminal domain; DBD: DNA-binding domain; LBD: ligand-binding domain (Wen, Niu and Huang, 2020).*

2.2.5 Screening and diagnosis

Screening is widely recognized as an important tool in cancer prevention (Gates, 2001). The main goal of screening is detected early-stage asymptomatic cancers and giving the opportunity to have many curative therapeutic options available for curing patients. In colon cancer the gold standard is colonscopy in patients with > 50 years (US Preventive Services Task Force *et al.*, 2021); in breast cancer mammography every 2 years in women between ages 50-74 (Nattinger and Mitchell, 2016); in cervical uterine PAP-test every 3 years in women > 25 years (US Preventive Services Task Force *et al.*, 2018). In PCa the clinical valid screening is the PSA test, described in detail in the next paragraph (2.2.5.1).

2.2.5.1 PSA screening test

The PSA test was first approved by the Food and Drug Administration (FDA) and became routinely used as a diagnostic marker in 1994 (Ung *et al.*, 2002; Lilja, Ulmert and Vickers, 2008). PSA is a serine protease belonging to the *KLK*-related peptidase family. It is encoded by the *KLK3* gene (Lilja, Ulmert and Vickers, 2008). The physiological function of PSA in the prostate is still under debate. It

has been demonstrated to proteolyze semenogelins (SEMG1 and SEMG2) and fibronectin to liquefy the seminal fluid (Lilja *et al.*, 1987). Other biological studies reported that PSA could have a role in the mechanism of seminal fluid release. Indeed, the proteolytic cleavage of glycoproteins in the seminal fluid by PSA produces a kinin-like substance that promotes smooth muscle contraction before ejaculation (Fichtner *et al.*, 1996).

PSA is physiologically expressed in normal prostate and altered PCa. In healthy men, less than 50 years old, the amount of detectable PSA in the blood is 0.6 ng/ml while it is 0.3 to 3 mg/ml in the seminal fluid (Schieferstein, 1999). Current guidelines recommend the screening of the majority of men between the ages of 50 and 70, while for men with a history of familial PCa the screening is recommended from 45 years of age. When the circulating detectable PSA levels exceed 4 ng/ml, patients are referred for a biopsy. This is based on evidence indicating (Carlsson and Vickers, 2020):

- PSA <4 ng/ml: very low or null probability of having cancer;
- $4 \leq PSA \geq 10$ ng/ml: 25% probability of having a positive biopsy for PCa;
- PSA >10 ng/ml: 50% probability of having a positive biopsy for PCa.

Nevertheless, this 4 ng/ml threshold is under debate; the Prostate Cancer Prevention Trial (PCPT), which studied 5119 men, demonstrated that 15% of men with PSA levels < 4 ng/ml had a PCa-positive biopsy (Thompson *et al.*, 2006). This finding was confirmed in a large multicentric European study involving 182 160 men with PCa recruited in 9 centers (Netherlands, Belgium, Italy. Spain, Switzerland, Sweden, Finland and French with two centers) in which 21-25% of men with PSA levels between 2 – 2.99 ng/ml, and 33% of men with PSA levels between 3 – 3.99 ng/ml, had PCa (Otto *et al.*, 2003).

Interestingly, several other randomized clinical trials were carried out to establish the relevance of PSA as a diagnostic marker. The Prostate, Lung, Colorectal and Ovarian (PLCO) Cancer Screening trial showed that annual PSA tests improved PCa incidence and affected the rate of mortality (Gohagan *et al.*, 2000), as observed in the European Randomized study of screening for PCa (ERSPC) (Hugosson *et al.*, 2019). In contrast, the Cluster Randomized Trial of PSA testing for PCa, involving 1,244 men in Denmark, revealed that overall PCa mortality was not affected by PSA screening, and that more low-risk PCa were detected as a result of screening (Kirkegaard *et al.*, 2013). These findings, in combination with further evidence that several other factors can cause serum PSA levels to be elevated, such as prostate enlargement dependent on benign prostatic hyperplasia (BPH), age, inflammation of the urinary tract, ejaculation, physical activities (cycling), urological procedures or certain medications (e.g., testosterone) (Catalona *et al.*, 1991), raises the possibility of overdiagnosis linked to the PSA test.

Overdiagnosis is a well-known clinical problem that leads to overtreatment of patients. The PSA test, in addition to indicating the presence of PCa, also uncovers indolent cancer or benign hyperplasia without progression. After receiving a positive PSA test, these individuals are subjected to unnecessary clinical exams, biopsies and invasive therapies. Interestingly, only 25% of men that undergo biopsy due to high levels of PSA have PCa, suggesting that in most cases the PSA test gives false-positive results (Fenton *et al.*, 2018).

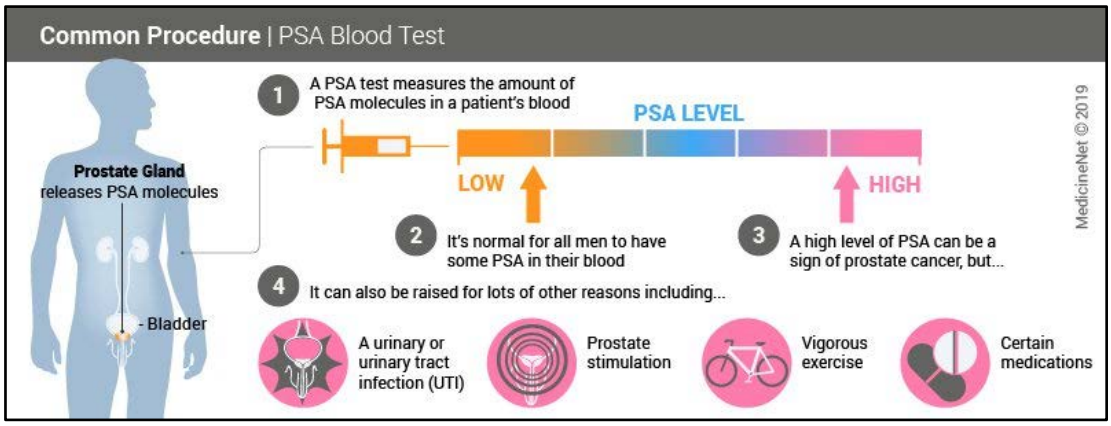

Figure 12. Prostate-specific antigen (PSA) blood test. *Pitfalls of PSA blood test as biomarker for PCa detection (Medicinet, 2019).*

2.2.5.2 Alternative PCa biomarkers

In addition to PSA, other biomarkers have been used for PCa diagnosis, in particular the enhanced level of the prostate cancer antigen 3 ($DD3^{PCA3}$) mRNA in the urine (Tinzl *et al.*, 2004). This is a noncoding RNA expressed specifically in the prostate and overexpressed in 95% of primary tumors (Bussemakers *et al.*, 1999). As a biomarker, $DD3^{PCA3}$ demonstrated higher specificity than PSA alone (n=201) in PCa diagnosis and has been used to reduce the number of unnecessary biopsies (Tinzl *et al.*, 2004). Additionally, several gene signatures have been developed and clinically validated for PCa. The 4Kscore Test is used to improve the specificity of PSA screening in early detection of PCa risk (Punnen, Pavan and Parekh, 2015). This test combines data obtained from total PSA, free PSA, intact PSA and human KLK2 (hK2) with clinical factors such as age and prior history of biopsy. The ExoDx Prostate Intelliscore (EPI) is another test used in the clinic to identify patients that require biopsy due to an estimated high probability to develop cancer. This test is based on the expression of biomarkers in the urine detected with the exosome gene expression assay. It is used for men with PSA serum levels between 2 and 10 ng/ml and ≥ 50 years old and has a 92% sensitivity in identifying men that require a biopsy (Tutrone *et al.*, 2020). Instead, ConfirmMDx is a molecular test that detects epigenetic alterations, such as methylation of the *GSTP1, APC* and *RASSF1* genes, and is applied to

patients with a PCa-negative biopsy but with PSA levels > 6 ng/ml and an enlarged prostate (Yonover *et al.*, 2019). Finally, the SelectMDx detects *HOXC6* and *DLX1* mRNA in the urine to identify patients with a high or low risk of PCa (Hendriks *et al.*, 2021).

Table 2. Signatures for prostate cancer screening *PSA= prostate specific antigen; fPSA= free-PSA; proPSA= PSA truncated variant; PCA3= prostate cancer antigen 3. (Carroll and Mohler, 2018)*

Test	Source	Components
PHI	Serum	PSA, fPSA, -2proPSA
4Kscore	Serum	PSA, fPSA, intact PSA, kallikrein-related peptidase 2
ExoDx Prostate	Urine	ETS transcription factor, ERG, PCA3
Michigan Prostate Score	Urine	PCA3, PSA, TMPSS2:ERG
SelectMDx	Urine	mRNA DLX1, HOXC6
ConfirmMdx	Tissue	DNA methylation, GSTP1, APC, RASSF1

2.2.5.3 PCa diagnostic techniques

Although the PSA and biomarker tests are routinely employed in the clinic to indicate the probability of having prostate tumors, physical exam results are necessary for a certain diagnosis.

Digital rectal exam (DRE)

DRE is a routinely performed exam, usually in combination with the PSA test, where the urologist uses the rectal route to investigate the back of the prostate gland. It can be used to detect the presence of hard masses or nodules in the prostate, however 17% of men with a normal DRE have a diagnosis of PCa at biopsy (Izawa *et al.*, 2006).

TRUS and MRI-TRUS

Upon detection of high PSA levels, patients typically undergo a transrectal ultrasound scan (TRUS) biopsy as indicated by current guidelines (Mottet *et al.*, 2017). This technique involves taking 12 needle biopsies from the prostate gland by ultrasound guidance through the rectum (Guo, Xu and Zhang, 2017). Since 1980, it has been considered the standard procedure for PCa diagnosis, however this technique has disadvantages. Due to technical limitations, not all of the gland can be sampled, and the anterior and caudal prostate are omitted even though the anterior region frequently harbors the disease (Moussa *et al.*, 2010). Thus, this procedure can yield false-negative results as revealed by the PROMIS study (n= 714) where 26% of men with a negative TRUS-biopsy had cancer, diagnosed with targeted biopsies (Ahmed *et al.*, 2017).

Multi-parametric magnetic resonance imaging (mpMRI) is the alternative approach to the TRUS-guided biopsy and provides information not only on the tissue anatomy and histology, but also on the

volume, cellularity and vascularity of the prostate (Ahmed *et al.*, 2017). In general, each mpMRI technique displays greater efficiency in detecting clinically relevant PCa compared to systematic TRUS biopsy. Indeed, for the majority of cases (90%) with a mpMRI positive result, the biopsy sampling is correctly guided to the area where tumor is present, while a negative mpMRI result avoids the need for a follow-up biopsy thus reducing the risk of diagnosing clinically indolent small cancer (Valerio *et al.*, 2015; Moldovan *et al.*, 2017; Drost *et al.*, 2019; Parker *et al.*, 2020).

Positron-emission tomography (PET)

PET scan is widely used in clinics to reveal biochemical or metabolic alterations in tissues using radioactive drugs (Unterrainer *et al.*, 2020). PSMA is a transmembrane glutamate carboxypeptidase strongly expressed in PCa (Israeli *et al.*, 1993). Pro ıte specific membrane antigen (PSMA)-PET is employed to improve PCa detection and to obtain a better indication of the stage of the disease, with a particular focus on intermediate and high-risk patients, while metastatic burden cannot be detected with this technology. The PSMA-PET diagnostic technology relies on an antibody against PSMA conjugated with α or β-emitting radioisotopes to detect tumors (Sandhu *et al.*, 2021). Since it provides a measurement of tumor volume, this technology is also used to monitor drug response and disease relapse (Unterrainer *et al.*, 2020). Interestingly, in a small prospective study (n= 17), PMSA-PET was shown to better define tumor volume compared with mpMRI, thus becoming a decisive tool for PCa diagnosis and patient management (Bettermann *et al.*, 2019; Unterrainer *et al.*, 2020). In a retrospective study of 116 patients with intermediate or high-risk PCa analyzed with the PMSA-PET scan [using PSMA-11 conjugated with 68-Gallium (Ga)], only 3 cases were found to have no pathological PSMA expression in the tumor (2.6%) (Ferraro *et al.*, 2020; Tsechelidis and Vrachimis, 2022). Finally, other radioactive molecules can be used as a sensor to detect tumors by PET, such as ^{11}C-choline, ^{18}F-fluorocholine (FCH) and ^{18}-fluoride, which all display increased sensitivity compared with routinely used MRI-imaging techniques. The European Association of Urology (EAU) has recommended both ^{68}Ga-PSMA-PET and ^{11}C-choline-PET for patients treated with radiotherapy and showing a PSA increment (Mottet *et al.*, 2017).

2.2.6 Staging and risk assessment

Tumor classification is an important step in the clinical management of patients because it allows prognosis prediction and guides therapeutic decision making. Several parameters are evaluated in PCa to categorize patients, including clinical (OS, disease free-survival, metastasis free-survival), surgical (disease encapsulation, involvement of seminal vesicles, positive margins and lymph node positivity), and biochemical (PSA) parameters and the Gleason score (Rodrigues *et al.*, 2012).

2.2.6.1 Grading system

Gleason scoring was established by Donald Gleason in 1966 based on the microscopic assessment of histological alterations present in prostate glands, such as degree of glandular differentiation and stromal invasion. A grade is assigned to tumors cells on a scale from 1 to 5 where 1-2 defines well-differentiated cells, 3 defines moderately differentiated cells, and 4-5 defines poorly-differentiated cells (Gleason, 1966; Kweldam, van Leenders and van der Kwast, 2019). The sum of the grades for the first and the second most prominent lesions in the tissue gives the Gleason Score (GS).

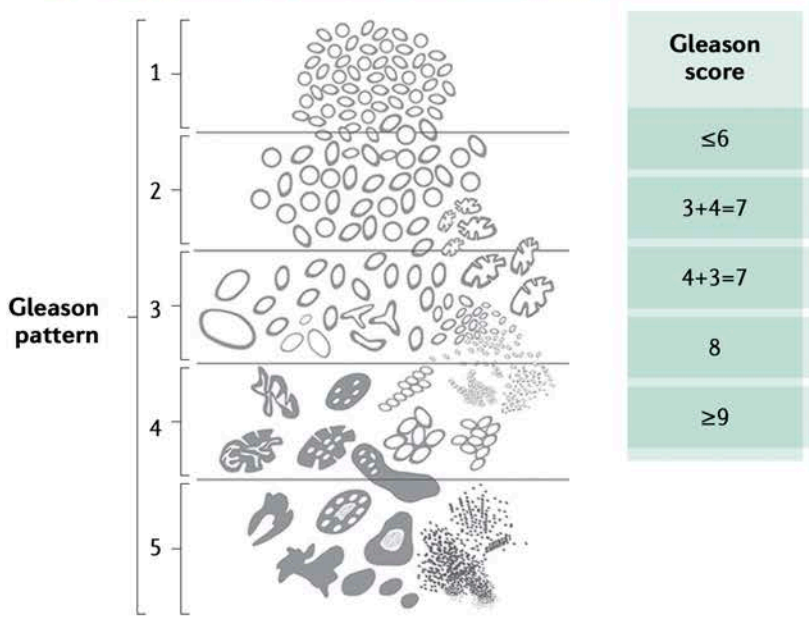

Figure 13. Definition of Gleason pattern and Gleason score. *Gleason score (GS) is defined as the sum of the most prominent and second most prominent Gleason pattern (GP) number. Each indicated number referred to histological appearance of prostate gland architecture (Rebello et al., 2021).*

A summary of the grading systems is reported in Table 3.

Table 3. Grading system and prostate histological traits

Gleason Score	Grade Group	Histology
6 (3+3)	1	Cells appear as healthy normal PCa cells, and the tumor grows very slowly.
7 (3+4)	2	Most cells are like the healthy normal one and cancer is likely to grow slowly.
7 (4+3)	3	Cells are less similar to healthy normal prostate cells. Cancer is likely to grow at a moderate rate.
8 (4+4)	4	Some cells appear as morphologically aberrant, and cancer grows quickly or at a moderate rate.
9-10 (4+5; 5+4; 5+5)	5	Cells are strongly morphologically aberrant, and cancer grow very quickly.

2.2.6.2 TNM staging

PCa can also be classified based on the tumor-node-metastasis (TNM) staging system that defines the size of cancer and how far it has spread. The parameters are defined as described below.

Table 4. Definition of prostate tumor size (T)

T1: cancer too small for diagnosis	a: cancer in less than 5% of the removed tissue
	b: cancer in less than 5% or more of the removed tissue
	c: cancer is founded by biopsy.
T2: cancer is completely limited to the organ	a: unilateral one-half of one lobe or less
	b: unilateral greater than one-half of one lobe
	c: bilateral disease
T3: cancer with extracapsular invasion	a: cancer breaks through the capsule of the organ
	b: cancer spread in seminal vesicles
T4: cancer has spread to the bladder or pelvic wall	

Table 5. Node (N) defines the lymph node invasion by tumoral cells

N0	Nearby lymph nodes are free from cancer cells.
N1	Lymph nodes are infiltrated by malignant cells.

Table 6. Metastasis (M) refers to spread of cancer in the body.

M0	No spreading out of cancer cells in the body.
M1	a: cancer cells in lymph nodes outside pelvis.
	b: cancer cells detected in bone.
	c: cancer cells far from the site of origin such as in the lungs.

2.2.6.3 Risk of recurrence stratification

2.2.6.3.1 D'Amico risk stratification

D'Amico and colleagues in 1998 developed a system to estimate the risk of PCa recurrence (low, intermediate or high) after curative treatments (D'Amico *et al.*, 1998) based on several parameters: PSA levels, Gleason Score and tumor size (T). More recently, the Clinical Practice Guidelines in Oncology (NCCN) added two more categories to this risk classification system: "very low" and "very high" to ameliorate patients' stratification and management that respectively include PSA density parameter and T3-T4 tumor size (Mohler *et al.*, 2010). The risk classification system is summarized in Table 7.

Table 7. D'Amico risk classification for localized PCa

Risk classification	PSA (ng/ml)	Gleason Score	Tumor (T)
Very Low	≤ 10 density < 0.15 ng/ml/g	< 6	T1c
Low	≤ 10	≤ 6	T1 or T2a
Intermediate	10.1 – 20	7	T2b
High	> 20	≥ 10	≥ T2c
Very High	> 20	> 10	T3b-T4

2.2.7 Metastatic PCa

In PCa, 17% of patients experience metastatic disease with a limited OS (3.5 years) an increased in mortality (Scosyrev *et al.*, 2012; James *et al.*, 2015). At genetic and epigenetic levels, metastatic cells acquire advantageous alterations that contribute to metastatic dissemination and colonization (Turajlic and Swanton, 2016). Clonal evolution analysis in metastatic disease highlights a phylogenetic mutational tree from primary to distant metastasis that revealed mutations in *PTEN, TP53* and *SPOP* compared to lesion of origin (Haffner *et al.*, 2013; Hong *et al.*, 2015). Moreover, other frequent alterations in metastasis are on *AR*, *RB*, lysine N-methyltransferase *KMT2C* and *KMT2D* and DNA repair genes (Dan R et al, 2015). A multicenter study (n= 692 men) revealed that germline mutations are extensively characterized in metastatic PCa patients (11.8%), in particular in *BRCA1/2, ATM, CHEK2, RAD51D* and *PALB2* gene, compared to localized disease (4.6%) (Pritchard *et al.*, 2016). A large autopsy study on 1,600 PCa patients revealed that 90% of metastases occur in bone, followed by lungs, liver, pleura, and adrenals. In detail, bone metastases affect spine (90%), ribs (18%), long bones (15%) and skull (8%) (Bubendorf *et al.*, 2000).

2.2.7.1 The metastatic process

Metastatic cancer derives from cancer cells from the primary tumor that break away from the site of origin and migrate through the bloodstream in secondary organs (i.e., brain, lung, bone) in which they can originate tumor. Since 90% of all cancer deaths are associated with metastasis it is important to understand the underlying mechanisms that sustain this process and develop target therapies (Seyfried and Huysentruyt, 2013). The metastatic process involves at least five different stages (Massagué and Obenauf, 2016):

1) loss of adhesion with adjacent cells and consequent invasion of neighboring tissue.
2) intravasation into bloodstream or lymphatic system.
3) activation of pathways that confer survival in blood flow.
4) extravasation at the secondary sites.
5) colonization and formation of distant metastasis.

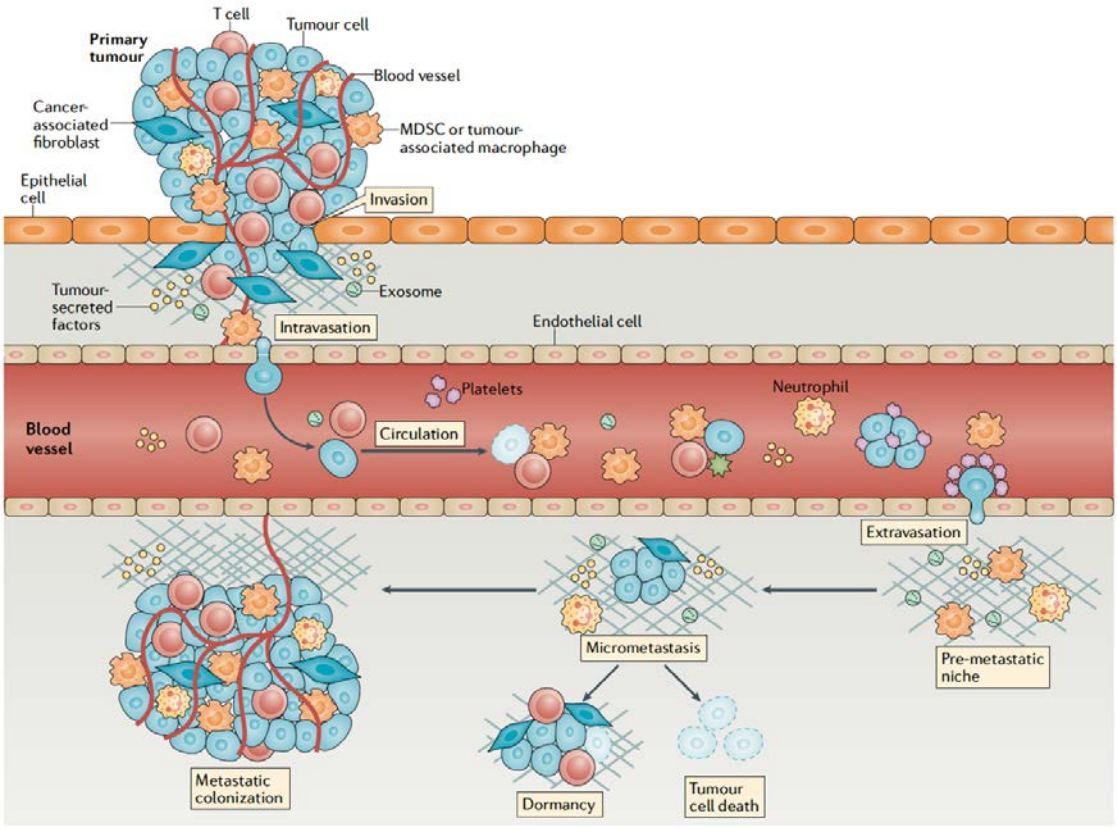

Figure 14. Overview of metastatic cascade. *Endothelial cells and fibroblasts remodel tissue through angiogenic factors and transforming growth factor- β (TGF-β) to promote tumor cell invasion. In the bloodstream platelets bind and protect circulating tumor cells (CTCs) up to their implantation in secondary sites, characterized by a specific pre-metastatic niche, in which cells remain dormient. MDSC: Myeloid-derived suppressor cells. (Anderson et al., 2019)*

2.2.7.1.1 Epithelial-to-mesenchymal transition (EMT)

EMT is characterized by the loss of epithelial traits in cancer cells (i.e., E-cadherin, EpCAM, laminins) with acquisition of mesenchymal phenotype (i.e., N-cadherin, vimentin, fibronectin), cytoskeletal rearrangement (Hall, 2009) and release of MMPs, enzymes required for extracellular matrix degradation (Kessenbrock, Plaks and Werb, 2010). EMT is a physiological process that occurs in normal cells to repair tissue damage, while in cancer it is deregulated and sustained cells invasion and migration by paracrine stimulation, derived from the "reactive" tumor stroma (i.e., fibroblast, endothelial and immune cells), that enhance invasiveness through cytokines, interleukins, TGFβ and growth factors (Thiery *et al.*, 2009). The main transcription factors involved in EMT are the members of the SNAIL family (SNAIL-1, -2 and -3), the snail family transcription repressor 2 (SLUG), the twist family BHLH transcription factors (TWIST-1 and -2) and the zinc finger E-box binding homeobox 1 (ZEB1), all integrating several molecular pathways (i.e., TGFβ, WNT-β-catenin, IL-6 and TNFα) and enhancing the transcription of target genes including not only those necessary for

EMT (E/N-cadherin, vimentin, MMPs), but also for proliferation (cyclins, P21) or survival (BCL2, BID, caspases) (Barrallo-Gimeno and Nieto, 2005; Seo *et al.*, 2021). EMT is a reversible process. The mesenchymal-to-epithelial transition (MET) is fundamental for metastatic establishment and growth through the reacquisition of epithelial traits.

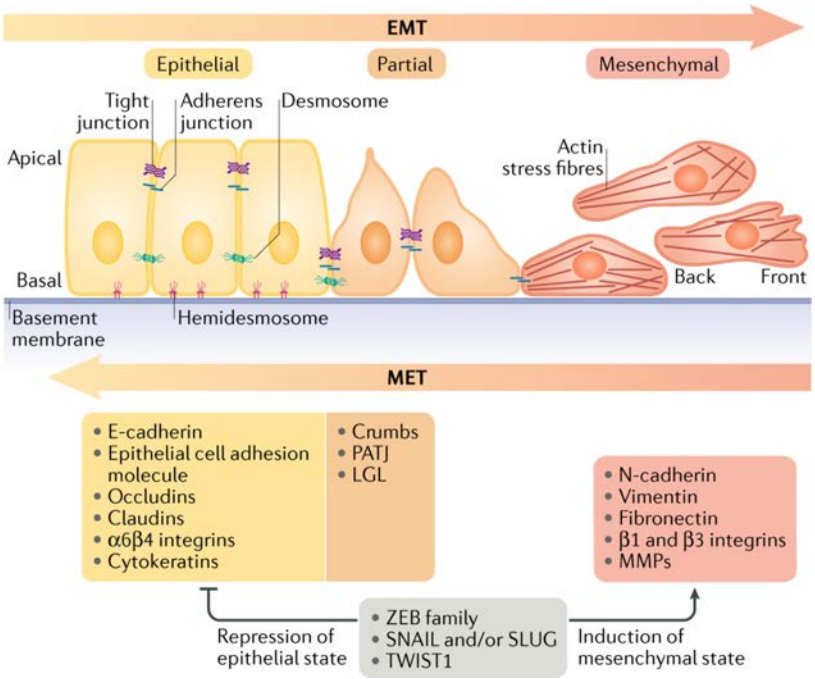

Figure 15. Epithelial-to-mesenchymal transition (EMT). *Epithelial cells are jointed together with tight junctions, adherens junctions and desmosomes. EMT induction leads to the expression of EMT-related transcription factors ZEB1, SNAIL/SLUG and TWIST, which inhibits (yellow box) or activates (orange box) transcription of target genes. EMT is plastic and mesenchymal cells reverted their state to epithelial cells through the mesenchymal-epithelial transition (MET) (Dongre and Weinberg, 2019). PATJ: Crumb cell polarity complex component; LGL: Scribble cell polarity complex component.*

2.2.7.1.2 Circulating tumor cells (CTCs)

Some cancer cells, as individual cells or in clusters, can enter in the bloodstream through blood or lymphatic vessels, the springboard for the intravasation process, and disseminate becoming CTCs (Chiang, Cabrera and Segall, 2016). These cells face several obstacles and harsh environments in the bloodstream such as hemodynamic forces or the direct exposure to immune system response, in particular natural killer (NK) cells that exert an anti-metastatic role in several cancers by attacking and killing CTCs . However, CTCs evade the immune system by masking themselves taking advantage of the interaction with platelets. Platelets surround the CTCs protecting them firstly from the fluid sheer stress, and then hiding them from immunity. Moreover, platelets have an active functional role crosstalking directly with CTCs. In fact, platelets release functional mediators such as platelet-derived growth factor (PDGF), VEGFA and transforming growth factor (TGFβ), required

for cell survival and proliferation as observed in ovarian cancer and osteosarcoma (Cho *et al.*, 2012; Takagi *et al.*, 2014). Furthermore, these released molecules promote evasion from apoptosis induced by chemotherapeutic agents by maintaining cells quiescent, activating anti-apoptotic pathway (Radziwon-Balicka *et al.*, 2012), or inhibiting anoikis, a program cell death induced by loss of cellular attachment (Aceto *et al.*, 2014).

2.2.7.1.3 Metastatic colonization

The ultimate step of the metastatic cascade is the invasion of distant tissue and the onset of metastatic lesions. The peculiarity of the stage is the presence of active dormant tumor cells (DTCs) in the secondary tissue. In 1889, Paget theorized organotropism with the "seed and soil" theory in breast cancer (Paget, 1989). Cancer cells are the seeds and are attracted to the compatible microenvironment, the soil, where they implant and grow (Gao *et al.*, 2019). These cells are very difficult to detect due to very low abundance: 1 tumor cell/10^6 bone marrow cells and 1-2 tumor cells/20 ml of blood but they are crucial in cancer progression to metastatic phenotype (Meng *et al.*, 2004; Lacroix, 2006). In PCa, the detection of DTCs is relevant for prognosis or to predict therapy response (Köllermann *et al.*, 2008). In a clinical trial enrolling 100 patients with non-metastatic PCa (T1-3, N0, M0), the detection of DTCs in bone marrow predicts poor survival in 15 years of follow-up (Lilleby *et al.*, 2013). Similarly, detection of $CK18^+$ PCa cells in bone marrow established prognostic factors after radical prostatectomy (RP) (n=82) estimated as BCR (Weckermann *et al.*, 2001). The hallmarks of DTCs are cell cycle arrest (G0/G1 phase), niche dependence, drug resistance, immune evasion, and metastatic relapse (reviewed in Phan TG and Croucher PI, 2020).

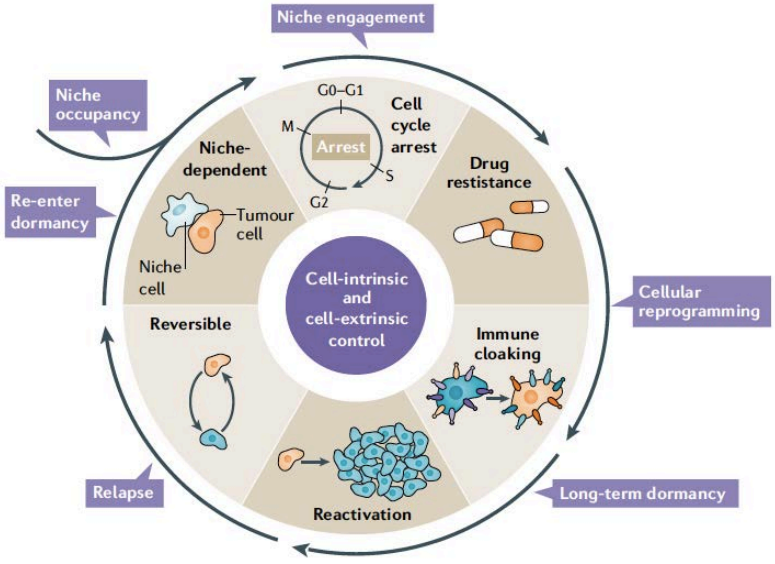

Figure 16. DTCs hallmarks and cell life cycle. *Graphical representation of cell life cycles of DTCs including: niche occupancy and engagement with cell cycle arrest; cellular reprogramming for drug resistance; long-term dormancy and immune cloaking; relapse with reversible phenotype; re-enter in dormant state in presence of harsh conditions (Phan and Croucher, 2020).*

2.2.8 Management of PCa

The management of PCa should take into account several factors including stage of the disease, histopathological and molecular features, and patient characteristics. Moreover, the choice of treatment options should weigh up efficacy versus toxicity for the patient, and the side effects of each treatment, such as infertility, sexual dysfunction and urinary problems, should be clearly communicated. The main treatment options that are currently available for PCa include active surveillance (AS), watchful waiting, conventional therapies such as surgery, radiotherapy and chemotherapy, immunotherapies, and androgen-deprivation therapies (ADT), such as surgical castration, luteinizing hormone releasing hormone (LHRH) agonist and antagonist, androgen synthesis inhibitors, and AR-inhibitors.

2.2.8.1 Active surveillance

AS is one management option that clinicians use for patients who have been diagnosed with slow growing low-grade PCa to avoid unnecessary and potentially harmful treatments (R. C. Chen *et al.*, 2016). The protocol includes a period of observation with stringent monitoring of changes in clinical parameters (i.e., PSA levels), which in the case of relevant variations allows a reclassification of PCa grade and this justifies the administration of radical treatments (Parker, 2004; Bul *et al.*, 2013). AS differs from watchful waiting in that AS involves monitoring of PCa growth using clinical tests (e.g., biopsies) whereas watchful waiting refers simply to monitoring symptoms and patients referred any occurring changes to the doctor. Watchful waiting is recommended for frail older patients with complex medical conditions, limited life expectancy (< 10 years), and who wouldn't be eligible for standard treatments (radical prostatectomy or radiotherapy/chemotherapy) (Albertsen, Hanley and Fine, 2005). The aim of watchful waiting is to monitor the progression of PCa until the appearance of metastatic dissemination or severe symptoms that obstruct critical physiological processes (e.g., urination).

The criteria of inclusion in AS are in general: stage T1c/T2 tumors, a Gleason score <6, core biopsy samples and serum PSA levels strictly < 10 ng/ml (Bruinsma *et al.*, 2016). Once patients have been included in AS they should be adequately monitored with routine clinical exams to assess PCa progression or metastatic dissemination, thereby allowing timely interventions with proper therapies. The least invasive exam is the detection of PSA blood levels, for at least 5 years, with a frequency of every 6 months or no more than 3 months if the situation risks to rapidly evolve. Moreover, the DRE is indicated for monitoring tumor volume. Patients are subjected to this approach every 3 months in the first 2 years after diagnosis, and then every 6-12 months from the third year. Instead, to assess

pathological evolution in terms of tumor grade, repeated biopsies are necessary. The interval of this clinical exam is at least 12 months unless there are negative observations from PSA levels or DRE. Finally, MRI should be considered routinely in AS and is strongly encouraged for patients with rising PSA levels but negative biopsy exams for tumor detection (Bruinsma *et al.*, 2016).

The efficacy of AS in patients with localized PCa was tested in the Prostate Testing for Cancer and Treatment trial (ProtecT) involving 1643 men randomly distributed to receive AS, surgery or radiotherapy (Hamdy *et al.*, 2016). AS was associated with an increased risk of developing metastasis (6.3 events per 1000 person-years; 95% CI 4.5-8.8) compared with surgery (2.4 events per 1000 person-year; 95% CI 1.4-4.2) or radiotherapy (3 events per 1000 person-year; 95% CI 1.9-4.9). However, mortality remained unchanged regardless the treatment assigned in 10-year observational period (Hamdy *et al.*, 2016)

2.2.8.2 Conventional therapies (surgery, radiotherapy and chemotherapy)

When PCa patients are no more eligible for AS, if displayed localized non-metastatic disease, are treated with conventional therapies. Localized non-metastatic disease is defined by cTn1-cTn2, cN0 and M0, and typically display a slow rate of tumor growth, low metastatic potential and favorable prognosis, with 1% risk of death at 10 years of follow-up, independent of primary management (Klotz and Emberton, 2014). For these patients, the established clinical protocols propose different options:

- Surgery in the form of RP (open retropubic or perineal, laparoscopic or robotic) with or without pelvic lymph node dissection.
- Primary ablative radiotherapy or intestinal low-dose brachytherapy (Trewartha and Carter, 2013; Vanneste *et al.*, 2016; Rebello *et al.*, 2021).

Despite undergoing RP, 27-53% of patients display PSA levels > 0.2 ng/ml and this is defined as biochemical recurrence (BCR) (Zaffuto *et al.*, 2017; Van den Broeck *et al.*, 2019; Parker *et al.*, 2020; Vale *et al.*, 2020). BCR is a well-established oncological endpoint for treatment failure. A summary of the clinical parameters used to define whether patients who experience BCR after RP are at low-risk or high-risk of death is shown in Table 8 (Van den Broeck *et al.*, 2020).

Table 8. Risk stratification in PCa patients with BCR after RP

Risk group	Clinical Parameters
BCR after radical prostatectomy (RP)	
Low-risk BCR	PSA-doubling time >1 yr and Gleason Score <8 (ISUP grade <4).
High-risk BCR	PSA-doubling time ≤1 yr and Gleason Score 8-10 (ISUP grade 4-5).

Salvage radiotherapy (SRT) is recommended for high-risk BCR patients to reduce the risk of local relapse (Rans *et al.*, 2020; Mottet *et al.,*2017). This treatment achieves a 75% reduction in the risk of cancer progression and an 88% increase in the probability of being disease-free after 5 years (Boorjian *et al.*, 2009; Kneebone *et al.*, 2020). Furthermore, if the level of PSA is persistently higher than 0.2 ng/ml, patients should undergo a PET/CT scan (e.g., PSMA-based PET) to detect possible hidden metastases which, if present, would indicate the need to change therapeutic approach (Roach *et al.*, 2018). In a recent study, patients with BCR who were PET-positive for a metastatic pelvic lymph node were given SRT in the absence of hormone therapies; 90% of treated men did not display BCR anymore (Shmidt-Hegemann *et al.*, 2018).

In PCa, chemotherapy is indicated for the treatment of aggressive tumors usually in combination with hormonal therapies. Chemotherapy drugs that are commonly used for PCa include docetaxel, cabazitaxel, mitoxantrone and estramustine. Docetaxel belongs to the taxoid antineoplastic drug family which have an anti-mitotic function. In the clinical trial TAX327, a three-week infusion with docetaxel increased the OS of men with advanced PCa (n=1,006) more than mitoxantrone (HR 0.88) (Berthold *et al.*, 2008). The latter is a type II topoisomerase inhibitor that is commonly used in palliative treatments. Similarly, the phase 3 study SWOG 9916 showed that docetaxel improves survival in advanced PCa compared to mitoxantrone or estramustine – an antimicrotubule agent (Tannock *et al.*, 2004; Franke *et al.*, 2010). Cabazitaxel is a second-generation semisynthetic taxane that was developed for PCa patients who were refractory to docetaxel. The TROPIC trial randomly treated 755 ADT-refractory metastatic patients, already treated with docetaxel, with mitoxantrone or cabazitaxel every three weeks. Only cabazitaxel improved OS with a median survival of 15 versus 12.7 months in the Mitoxantrone treated group. However, all chemotherapy agents have severe side effects including hair loss, increased risk of infection and fatigue.

2.2.8.3 Immunotherapy

Immunotherapy has become a standard treatment for several cancers. Its aim is to activate or suppress the immune system of patients to modulate the progression of cancer. In PCa, several immunotherapy agents have been developed, including the FDA approved cancer vaccine, sipuleucel-T (Provenge). This therapeutic vaccine consists of autologous antigen presenting cells (APC), including dendritic cells, macrophages and B cells, that have been activated *ex vivo* with a recombinant fusion protein antigen, which contains prostatic acid phosphatase (PAP) and GM-CSF, and present PAP to T-cells that are activated and ready to kill PCa cells (Anassi and Ndefo, 2011). This approach is indicated for men with disease progression upon ADT, have testosterone levels < 50 ng/ml or metastatic disseminated disease. A clinical trial (phase III) including 512 patients showed that this vaccine prolonged the survival (4.1 months) of men with metastatic castration resistant PCa (Kantoff *et al.*, 2010).

In addition to vaccines, immune checkpoint inhibitors could be effective immunotherapy agents for PCa. Ipilimumab is a monoclonal antibody that selectively targets the cytotoxic T-lymphocyte antigen 4 (CTLA-4), thus depleting intratumoral T regulatory cells and enhancing anti-tumor activity (Ribas, 2015; Tang and Zheng, 2018). Ongoing studies are now investigating the basis of this long-term response and also the efficacy of Ipilimumab at an earlier stage of PCa. Instead, when ipilimumab is combined with nivolumab (Opdivo), a human IgG4 monoclonal antibody directed against PD-1, as demonstrated in the phase 2 NEPTUNES trial, displays anti-tumor activity in 36 metastatic castration-resistant patients with prolonged OS (18 months) and PFS (5 months) (Wong *et al.*, 2019).

The programme cell death protein-1 (PD-1) and programme death ligand (PDL-1) are other well-characterized targets for immune checkpoint inhibitors. Pembrolizumab, approved by FDA in 2017, is a monoclonal antibody that targets PD-1 on cytotoxic T-lymphocytes and boosts the anti-tumoral response. Despite being well tolerated in metastatic PCa patients who had already been treated with chemotherapy (E. D. Kwon *et al.*, 2014; Beer *et al.*, 2017), Pembrolizumab failed to prolong OS in KEYNOTE-122 Phase 3 studies, in comparison with chemotherapy (docetaxel) (HR: 0.9) in 233 metastatic castration-resistant patients (Petrylak *et al.*, 2021).

2.2.8.4 Androgen-deprivation therapies (ADT)

Several therapeutic options for PCa have been developed to target the hormones responsible for promoting tumor growth. These therapies are collectively known as ADT which includes surgical castration, LHRH agonists and antagonists, and AR antagonists.

Surgical castration. Bilateral orchiectomy is an extremely invasive and irreversible procedure that involves the ablation of both testicles. Although it is considered the most effective anti-androgen therapy, this technique is no longer employed.

LHRH agonists and antagonists. This set of drugs affect the LHRH receptor in the anterior pituitary gland counteracting the release of testosterone by the testicles, thus mimicking surgical castration. Clinically employed LHRH agonist drugs include leuprolide, goserelin, triptorelin and leuprolide mesylate and they are administered every 3 to 6 months via subcutaneous implants. These ADT agents have proved to be very effective at ameliorating clinical outcomes in the majority (89-98%) of patients by reducing the circulating testosterone levels to under 20 ng/dL. Clinical studies have shown that just one-month of treatment with leuprolide alone is sufficient to reduce testosterone to this level, while triptorelin treatment required three months and goserelin was only effective in 25-55% of patients after one month of treatment (McLeod *et al.*, 2001; Dias Silva *et al.*, 2012; Kao *et al.*, 2012; Spitz *et al.*, 2016; Shore *et al.*, 2017; Crawford *et al.*, 2019). Leuprolide is under investigation in phase 3 EMBARK clinical trial (NCT02319837) in combination with enzalutamide in high-risk non metastatic patients (n= 1,050). The efficacy of Leuprolide was compared to goserelin in combination with androgen blockade therapy. Data revealed that progression events and deaths were similar for goserelin plus antiandrogen and leuprolide plus antiandrogen, thus these approaches are equivalent to manage PCa patients (Sarosdy *et al.*, 1998). Similar observations derived from a clinical trial involving 284 men with advanced PCa that were treated with leuprolide and triptorelin. Even if triptorelin reduce the levels of circulating testosterone more rapidly than leuprolide, both maintained castration for the same time (Heyns *et al.*, 2003). Finally, a recent clinical trial compared goserelin *vs.* triptorelin *vs.* leuprolide in 125 PCa patients. All three drugs displayed the same efficacy in achieving castration (Shim *et al.*, 2019).

LHRH antagonists competitively bind to and inhibit the LHRH receptor. Degarelix and relugolix (ORGOVYX) are the LHRH antagonist approved for advanced PCa management. A randomized, open-label trial, tested the efficacy and the safety of degarelix compared to leuprolide, involving 610 patients with adenocarcinoma. Degarelix suppressed testosterone as effective as leuprolide (< 0.5 ng/ml) over a one-year treatment but degarelix achieved these levels in 3 days while at this time point none of leuprolide treated patients reached this level (Klotz *et al.*, 2008). Degarelix is under investigation in the clinical trial CS37 (NCT00928434) in US in comparison with leuprolide, in patients that displayed BCR after localized therapy, and in the clinical trial CS30 (NCT00833248) compared to goserelin/bicalutamide in prostate size reduction, in high-risk PCa as neoadjuvant treatment before radiotherapy.

Relugolix demonstrated to have the same efficacy and safety of degarelix in men with advanced PCa (n= 2,059) (Sari Motlagh *et al.*, 2022). Moreover, relugolix was tested in a phase III clinical trial (HERO) that enrolled 1,327 patients with advanced PCa compared to leuprolide. Data collected pointed out that this compound efficiently reduced and maintain suppression of testosterone levels. 56% of patients treated with relugolix have castrate levels of testosterone compared to 0% with leuprolide (Shore *et al.*, 2020).

Androgen synthesis inhibitors. Androgens are not only released by the testicles. Indeed, patients treated with LHRH agonists or antagonists still maintain some circulating testosterone which is released by adrenal glands and by the tumor itself. In the adrenal glands, the androgen precursor dehydroepiandrosterone (DHEA) needs to be converted into testosterone or dihydrotestosterone (DHT). DHEA is biochemically transformed into testosterone by 17β-hydroxysteroid dehydrogenase (HSD17B) and 3β-hydroxysteroid dehydrogenase (HSD3B) in the prostatic gland. Testosterone is then further converted into DHT by the steroid 5α-reductase (SRD5A). Instead, PCa respond to lack of androgens by synthesizing testosterone from adrenal androgens. PCa cells enhance the capacity to recruit weak levels of adrenal androgens DHEA and androstenedione, after ADT, and metabolize them to produce DHT. Enzymes such as cytochrome P450 11A1 (CYP11A1) and cytochrome P450 17A1 (CYP17A1), which are increased intratumorally, are necessary for *de novo* steroid synthesis (Cai *et al.*, 2011).

Thus, pharmacological approaches have been developed to counteract the production of testosterone, such as abiraterone acetate that blocks the CYP17A1 enzyme that is specifically required for the conversion of steroid precursors (i.e., progesterone and pregnenolone) into androgens in cancer cells, and thus blocks testosterone-sustained tumor growth. The efficacy of abiraterone was tested in high-risk metastatic castration-sensitive PCa (LATITUDE trial) and high-risk locally advanced or metastatic disease (STAMPEDE trial). The LATITUDE trial is a double-blind trial where 1,199 patients randomly received ADT with abiraterone and prednisone, a glucocorticoid medication, or with placebo. The administration of abiraterone decreases the tumor burden thus prolonging the OS of patients (HR 0.62; 95% CI 0.51-0.76; $p < 0.0001$) (Fizazi K et al, 2017). Similar data were obtained in the multigroup, multistage trial STAMPEDE (20% node positive, 27% high-risk, locally advance disease, 5% BCR), where the addition of abiraterone and prednisolone to ADT (LHRH agents or surgical castration) prolonged the OS and decreased the mortality (HR 0.63; 95% CI 0.52-0.76; $p < 0.001$) compared to ADT alone (James ND et al, NEJM 2017).

Androgen receptor inhibitors. Several drugs have been developed to specifically compete with androgens for the binding of the AR, such as the first-generation inhibitors, flutamide, bicalutamide and nilutamide and the next-generation inhibitors enzalutamide, apalutamide and darolutamide. The ENZAMET randomized trial (phase III study) tested the efficacy of enzalutamide in comparison to first-generation inhibitors (bicalutamide, nilutamide and flutamide) in 1,125 men with metastatic hormone-sensitive disease. Enzalutamide significantly prolonged PFS and OS compared to standard inhibitors (HR 0.67; 95% CI 0.53-0.86). The benefit of enzalutamide in arresting PCa progression was also demonstrated in the ARCHE phase III clinical trial where patients treated with ADT and enzalutamide displayed prolonged PFS compared with patients treated with ADT and placebo (HR 0.39; 95% CI 0.3-0.5; $p < 0.001$) (Armstrong *et al.*, 2019). Enzalutamide has also been evaluated in patients with high-risk ADT-resistant disease without metastasis (PROSPER trial) or with metastasis (PREVAIL trial). Enzalutamide conferred prolonged metastasis-free survival (36.6 *vs.* 14.7 months; HR 0.29) and OS (HR 0.71) compared with placebo, respectively (Beer *et al.*, 2014; Hussain *et al.*, 2018). Apalutamide and darolutamide have also been tested in ADT-resistant patients without metastasis. In the SPARTAN trial, apalutamide increased metastasis-free survival (40.5 *vs.* 16.2 months; HR 0.28) compared to placebo (Smith *et al.*, 2018), while darolutamide was tested in the ARAMIS trial and also resulted in prolonged metastasis-free survival (40.4 *vs.* 18.4 months; HR 0.41) compared with placebo (Fizazi K *et al.*, 2019).

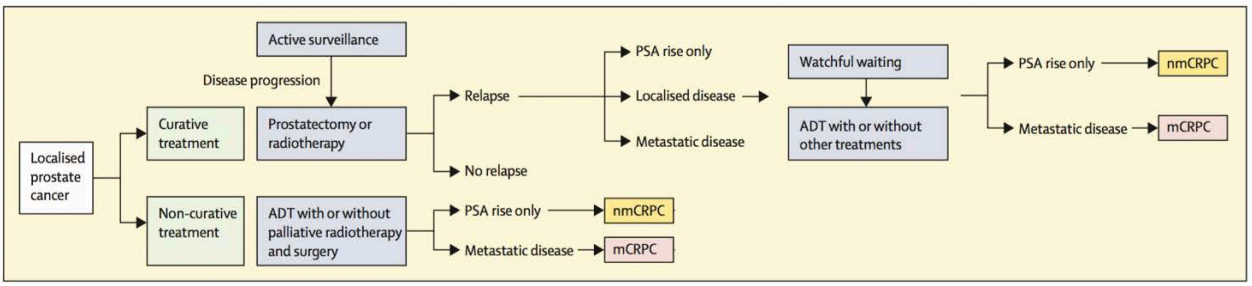

Figure 17. Schematic representation of therapeutic approaches for localized PCa. *ADT: androgen deprivation therapy; APIs: androgen pathway inhibitors; mCRPC: metastatic castration-prostate cancer; mCSPC: metastatic castration-sensitive prostate cancer; nmCRPC: non-metastatic castration-resistant prostate cancer; PARPi: poly(ADP-ribose) polymerase inhibitors (adjusted from Sandhu et al., 2021).*

2.2.8.5 Metastatic disease management

Metastatic disease is usually detected by imaging techniques, such as ^{68}Ga-PSMA or ^{11}C/^{18}F-choline PET/CT and MRI, which improve the early detection of metastatic lesions and permit the selection of the most appropriate treatments (Francini *et al.*, 2018; Gravis *et al.*, 2018). Once metastatic disease has been diagnosed, it is classified into two main categories, hormone-sensitive and castration-resistant, which define the treatment options.

Hormone-sensitive metastasis. The gold standard for hormone-sensitive metastasis is ADT, mainly with LHRH agonists; however, prolonged exposure (18-24 months) can enhance the appearance of castration-resistance. After first-line ADT, several other treatments can be administered such as palliative radiotherapy, transurethral resection of the prostate (TURP), ureteric stenting and suprapubic catheter insertion (Karantanos, Corn and Thompson, 2013; Patrikidou *et al.*, 2015).

Bone-targeting treatments. Treatments targeting the metastatic burden, mainly in the bone, have been shown to improve clinical outcome (Kim, Karam and Wood, 2014). These bone-targeting therapies include drugs (i.e., zoledronic acid and denosumab), radiotherapy (e.g., radium-223 and stereotactic ablative radiotherapy "SABR"), and PARP inhibitors.

Metastatic castration-resistant prostate cancer (mCRPC)

The most relevant clinical problem in PCa is that the majority of patients treated with anti-androgens and LHRH analogs developed CRPC within 2-3 years (Harris *et al.*, 2009). Castration resistance is commonly diagnosed through two separate measurements of PSA, no more than one week apart, showing an increase of 2 ng/ml over initial measurements in patients with serum testosterone < 50 ng/ml (Arlen *et al.*, 2008; Saad and Hotte, 2010; Cookson *et al.*, 2013; Morote *et al.*, 2022). Despite the effectiveness of AR-blocking agents or inhibitors of AR signaling, tumors that acquire resistance appear to reactivate the AR or maintain active AR signaling as demonstrated by the increase of PSA levels, which is one of the functional readouts of AR activity in tumors (Attard, Cooper and de Bono, 2009).

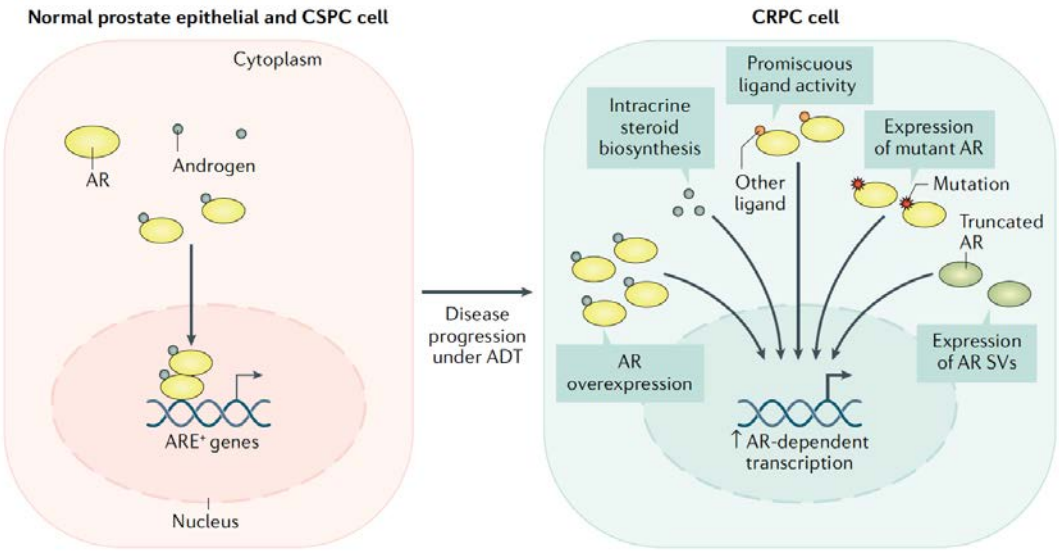

Figure 18. Role of androgen receptor in castration-resistant PCa (CRPC). *In normal prostate epithelial cells AR enter the nucleus and bind to androgen-response elements (AREs). Abnormal AR occurring in CRPC is mainly due to gene amplification, overexpression, point mutations result in truncated AR (splice variants). These variants can be constitutively active or sustained AR signaling by binding non-specific ligands (promiscuous activity) or synthesizes steroids intracellularly (Rebello et al., 2021).*

For many years the standard of care for mCRPC patients was docetaxel, but nowadays several other therapeutic approaches are proposed to prolong life expectancy, such as combined docetaxel plus prednisone treatment (Tannock *et al.*, 2004), cabazitaxel in combination with prednisone (de Bono *et al.*, 2010; Oudard *et al.*, 2017; Rebello *et al.*, 2021), the vaccine sipuleucel-T (Kantoff *et al.*, 2010) and the PARP inhibitor olaparib (J. S. de Bono *et al.*, 2020).

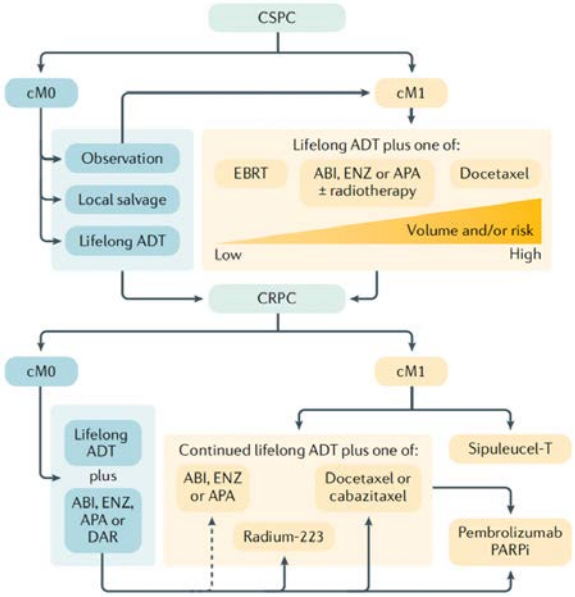

Figure 19. Summary of advanced PCa management. *Schematic representation of clinical protocols for advanced PCa management. CSPC: castration-sensitive PCa; cM0: clinically non-metastatic; cM1: metastatic; ARSI: AR signaling inhibitor; ABI: Abiraterone; ENZ: Enzalutamide; APA: Apalutamide; EBRT: external beam radiotherapy; DAR: darolutamide; CRPC: castration resistant PCa; PARPi: PARP inhibitors Olaparib or rucaparib (Rebello et al., 2021),*

2.2.9 Neuroendocrine differentiation

A subfraction of CRPC (~10%) patients display neuroendocrine differentiation (NED) (Hirano *et al.*, 2004). Neuroendocrine (NE) cells are rare scattered single cells (~1%) present normally in the prostate gland and interspersed among luminal and basal cells (Marker *et al.*, 2003; Terry and Beltran, 2014). NE cells are completely negative for AR expression and therefore are intrinsically resistant to castration (Bonkhoff, 2003; Zong and Goldstein, 2013). Thus, NE cells have been proposed to be pivotal in explaining CRPC (Beltran *et al.*, 2014; Butler and Huang, 2021). In support of this notion, NE cells are enriched in tumors upon exposure to ADT, becoming 5-10% of the entire prostate cell population (Jiborn, Bjartell and Abrahamsson, 1998; Huang *et al.*, 2005). Similar findings were also obtained in the human established androgen-sensitive PCa cell line LNCaP, which when treated with ADT express NE markers (Shen *et al.*, 1997).

The precise function of NE cells in the prostate gland is not fully understood. They have a secretory capacity, releasing neuropeptidases (e.g., bombasin, calcitonin, parathyroid-like hormone, serotonin, adrenomedullin) and growth factors (i.e., VEGFA) (Abrahamsson, 1999). NE prostate tumors are characterized by negative immunostaining for both AR and PSA and a high Ki67 proliferative index (Beltran *et al.*, 2014). Furthermore, they express CK-18 and CK-8 but not basal markers, such as CK-5 and P63 (Huang *et al.*, 2006). Histologically, NE cells are characterized by lateral spreading of dendritic processes (Parimi *et al.*, 2014) and by IHC for NE markers they can easily detected.

The common markers used in clinics are chromogranin-A (CHG-A), synaptophysin (SYN), neuron-specific enolase (NSE) and NCAM1/CD56 (Helpap, Köllermann and Oehler, 1999; Wang and Epstein, 2008; Komiya *et al.*, 2009). CHG-A is a member of granin protein family. The gene is located on chromosome 14q32.12 and transcribes a 439 amino acid protein. Its physiological role is the biogenesis of secretory granules and it facilitates the exchange of calcium to control calcium homeostasis (D'amico *et al.*, 2014). SYN is an integral membrane protein with four transmembrane domains, initially isolated from neuronal presynaptic vesicles, with a role in calcium binding and vesicle content releasing (Wiedenmann *et al.*, 1986). NSE is an isoenzyme that was specifically detected in neurons where it acts with the enolase enzyme in glycolysis (Haque *et al.*, 2016). NCAM1/CD56 is the neural adhesion molecule with a role in signal transduction (Walmod *et al.*, 2004) (see section 2.2.10).

2.2.9.1 The origin of NE cells

The cell of origin of NE tumors is still under debate. The Selection Model proposes the existence in the tumor of a rare subfraction of cells heterogeneously dependent on androgens that overwhelm the others under the selective pressure of hormone availability. In contrast, the Adaptation Model considers the genetic or epigenetic changes that allow the survival of rare tumor cells in the absence of androgens (Zong and Goldstein, 2013).

The Selection Model was proposed based on experimental observations performed by Isaacs and Coffey in 1980s in the Dunning R-3327-H rat prostate adenocarcinoma model. Here, they determined that PCa cells were heterogenous in their sensitivity to androgens, with some being sensitive while others were insensitive to castration and could drive clonal outgrowths (Isaacs and Coffey, 1981). Some years later, in 1997, Gingrich and colleagues made the same observations in the TRAMP (transgenic adenocarcinoma of the mouse prostate) murine model that spontaneously develop PCa (Gingrich *et al.*, 1999) (see section 2.2.11.3). In this engineered mouse model, castration at 12 weeks of life slowed down PCa growth but the progression from poorly differentiated to metastatic disease was not delayed compared to control mice suggesting that in the normal prostate gland androgen-independent cells exist (Gingrich *et al.*, 1997; Zong and Goldstein, 2013).

The Adaptive Model is based on the concept that cancer cells are able to switch from one state to another in response to precise stimuli; this is known as “plasticity” (Yuan, Norgard and Stanger, 2019). As previously described, adenocarcinoma can be invaded by NE-like cells that are not necessarily the same as normal NE cells (Nakada *et al.*, 1993). Genetic analysis of NE-like cells isolated from primary tumors revealed that they are not genetically different from the neighboring adenocarcinoma cells. *In vitro* lineage tracking, a well-established assay for cell fate specification, suggested that some luminal adenocarcinoma cells, exposed to ADT, acquired NE traits changing their steady state into an intermediate meta-state called transdifferentiation. Re-exposure of these cells to normal culture conditions resulted in the restoration of an AR-dependent state revealing a reversible plasticity (Nouri *et al.*, 2017).

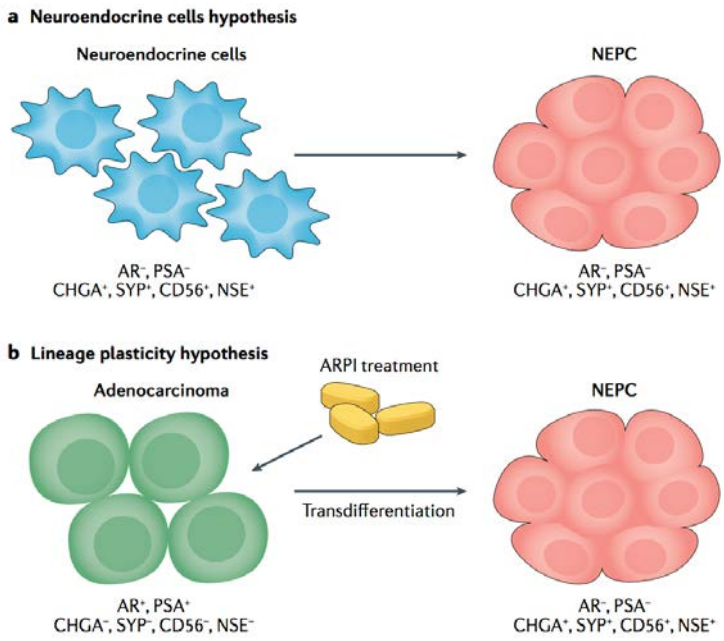

Figure 20. Models of neuroendocrine (NE) PCa tumor origin. *a) Neuroendocrine PCa (NEPC) originates from NE cells via neoplastic transformation and maintain NE markers Chromogranin-A (CHGA), Synaptophysin (SYP), CD56 and neuron-specific enolase (NSE). b) AR^+PSA^+ cells due to exposure to AR pathway inhibitor (ARPI) undergo transdifferentiation and develop AR^-PSA^+ NE^+ NEPC cells with genetic/epigenetic rearrangements (Wang et al., 2021).*

2.2.10 NCAM1/CD56 in PCa

2.2.10.1 NCAM1 structure

NCAM1/CD56 is a member of the surface glycoprotein family. The gene is located on chromosome 11 and contains 19 exons (Walmod *et al.*, 2004). This protein exists in three main isoforms derived from alternative splicing, NCAM-180, NCAM-140 and NCAM-120, variously expressed in primary tumors and cancer cell lines (Walmod *et al.*, 2004). They are immunoglobulin-like cell adhesion molecules (Ig CAMs). Structurally, NCAM1 is comprised of an extracellular domain containing five Ig-homology modules and two fibronectin-type III related homology (F3) modules, a transmembrane domain, and an intracellular domain which differs in length depending on the isoform (Campbell and Spitzfaden, 1994; Chothia and Jones, 1997; Spitz *et al.*, 2016).

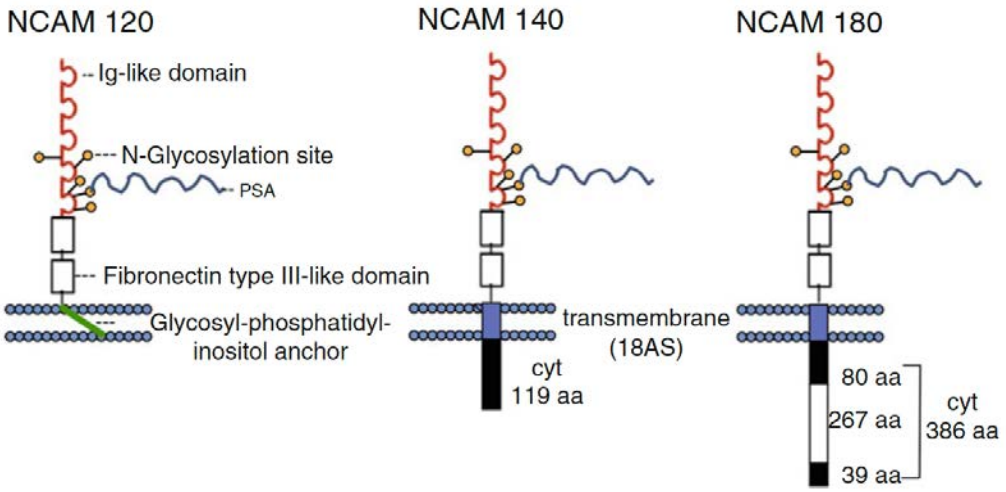

Figure 21. NCAM1/CD56 structure and isoforms. *Schematic representation of NCAM1-120/-140/-180 isoforms (Horstkorte et al., 2012).*

NCAM1 is anchored to plasma membrane by palmitoylations, the covalent binding of fatty acids on cysteine residues (C11, C16 and C22) in the cytoplasmic region (Little, Edelman and Cunningham, 1998). Moreover, NCAM1 in nervous system is N-glycosylated with polysialic acid (PSA). Polysialylation is specified by the addition of 150 monomers of sialic acid in the N-glycans of the fifth immunoglobulin-like domain, in close proximity to plasma membrane with a determinant role in development of neuronal systems (Kiss and Rougon, 1997).

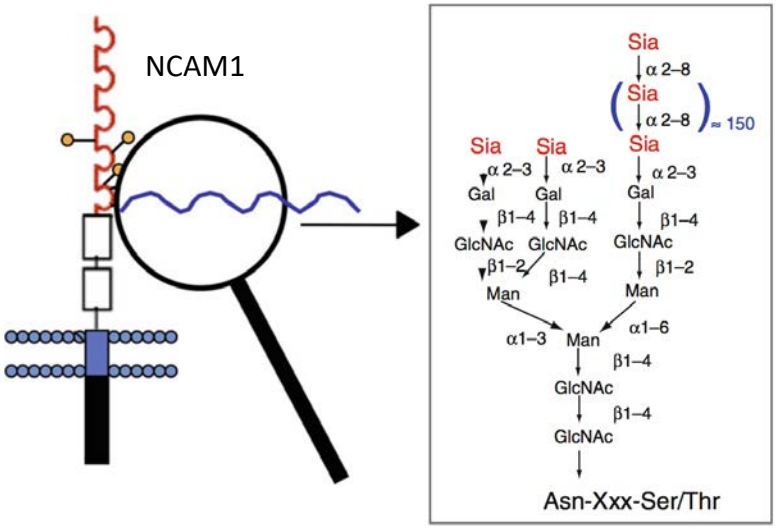

Figure 22. NCAM1 polysialylation. *Chemical structure of polysialylation on Asparagine (ASN)-linked glycan structure (Horstkorte et al., 2012).*

2.2.10.2 Physiological role of NCAM1

NCAM1 is physiologically expressed in several normal tissues and cells such as neurons, astrocytes, cerebellum, nerves, gastric parietal cells, follicular cells of thyroid, T lymphocytes, pancreatic islet cells, a subsets of T lymphocyte ($\alpha\beta$), NK, monocytes, dendritic cells as well as NE cells (Rutishauser *et al.*, 1978; Moretta *et al.*, 1989). NCAM1 exerts cell adhesion upon homophilic or heterophilic interactions with other molecules that activated intracellular signaling (see section 2.2.10.4). In brain mediates several functions including neuronal migration, axonal branching, synaptogenesis (Vukojevic *et al.*, 2020). NCAM1 functions are well characterized also in immune systems (Van Acker *et al.*, 2017). In NK cells, it is not only a marker to isolate these cells ($CD56^{+}CD3^{-}$) but it has a pivotal role in mediating anti-cancer response against tumor cells $CD56^{+}$, as demonstrated in breast cancer (Taouk *et al.*, 2019) and hematopoietic cells (Valgardsdottir *et al.*, 2014) *in vitro*. In T lymphocytes-$\alpha\beta$ expressing NCAM1 have a killing role and release inflammatory factors such as IFN-γ, upon stimulation with interleukin-12 (IL-12) and interleukin-15 (IL-15) (Guia *et al.*, 2008). In dendritic cells (DC) NCAM1 enhances antigen presentation mechanism to immune system and induce innate lymphocyte activation, upon stimulation with interleukins (Gruenbacher *et al.*, 2009; Anguille *et al.*, 2012).

2.2.10.3 Role of NCAM1 in cancer

NCAM1 expression has been linked to tumorigenesis, metastatic dissemination and poor clinical outcome in a range of human cancers. In medulloblastoma, released PSA-NCAM1 in cerebrospinal fluid (n=145 patients), measured by ELISA test, is a suitable marker for monitoring response to therapies identifying refractory patients at risk of relapse (Figarella-Branger *et al.*, 1996). In glioblastoma (GBM), the detection by ELISA of PSA-NCAM1 (>10 pg/μg) in GBM-derived human samples was shown to have prognostic value (n= 56) predicting shorter OS (12 months *vs.* 21 months for patients with PSA-NCAM1 < 10 pg/μg) and PFS (6 months *vs.* 11 months for patients with PSA-NCAM1 < 10 pg/μg) (Amoureux *et al.*, 2010). NCAM1 was found to be associated with a subgroup of patients with lymphomas displaying aggressive disease course (Kern *et al.*, 1993). More recently, NCAM1 displayed a crucial role in acute myeloid leukemia (AML). Here, it demonstrated to be essential in leukemic progenitors for cell survival, tumorigenicity, and confer chemotherapy resistance investigated with *in vivo* and *in vitro* assay (Sasca *et al.*, 2019). Similarly, in ovarian cancer NCAM1 is associated with high tumor grade and cancer aggressiveness. In epithelial ovarian carcinoma cell lines, the expression of NCAM1 confers migratory and invasive potential, and metastatic dissemination *in vivo* (Zecchini *et al.*, 2011). In multiple myeloma (MM), NCAM1 is expressed in 94% of cases while it is not expressed in normal plasma cells from which MM is derived (Bataille *et al.*, 2006). Similarly, NCAM1 is undetectable in normal exocrine cells but its expression in pancreatic cancer correlates with tumor appearance and predicts poor prognosis (n=25) (Kameda *et al.*, 1999; Tezel *et al.*, 2001; Naito *et al.*, 2006). NCAM1 was also identified in a population of CSCs in Wilms' tumor, a pediatric renal disease with intrinsic drug resistance and relapse potential (Markovsky *et al.*, Mol Canc Ther 2017). In PCa, NCAM1 is commonly used as biomarker to define NE cells, but its functional role in tumorigenesis has never been investigated.

2.2.10.4 NCAM1-mediated interactions and signal transduction

NCAM1 can dimerize with several molecules such as the glial cell-line derived neutrophic factor (GDNF) (Paratcha, Ledda and Ibáñez, 2003); members of extracellular matrix including phosphacan (Milev *et al.*, 1994), neurocan (Friedlander *et al.*, 1994), collagens (Probstmeier, Kühn and Schachner, 1989; Kiselyov *et al.*, 1997), heparin (Cole and Glaser, 1986); spectrin (Pollerberg *et al.*, 1987); the focal adhesion kinase $p125^{fak}$ and tyrosine kinase $p59^{fyn}$ (Beggs *et al.*, 1997); fibroblast growth factor receptors (FGFRs) (Kiselyov *et al.*, 2003; Christensen *et al.*, 2006).

2.2.10.4.1 Role of NCAM1 in GDNF signaling

NCAM1 interacts with GDNF that belongs to the transforming growth factor-β (TGFβ) superfamily and has a role in neuronal survival and differentiation. GDNF family ligands (GFLs) act usually through the receptor tyrosine kinase, RET that complexes with the GPI-linked GDNF family receptor α (GFR-α) but the presence of NCAM1 has been shown to be sufficient to integrate GDNF signaling through a direct interaction with GFR-α and the NCAM-GFR α-GDNF interaction mediates neurite outgrowth and cell migration (Airaksinen, Titievsky and Saarma, 1999; Baloh *et al.*, 2000; Paratcha, Ledda and Ibáñez, 2003).

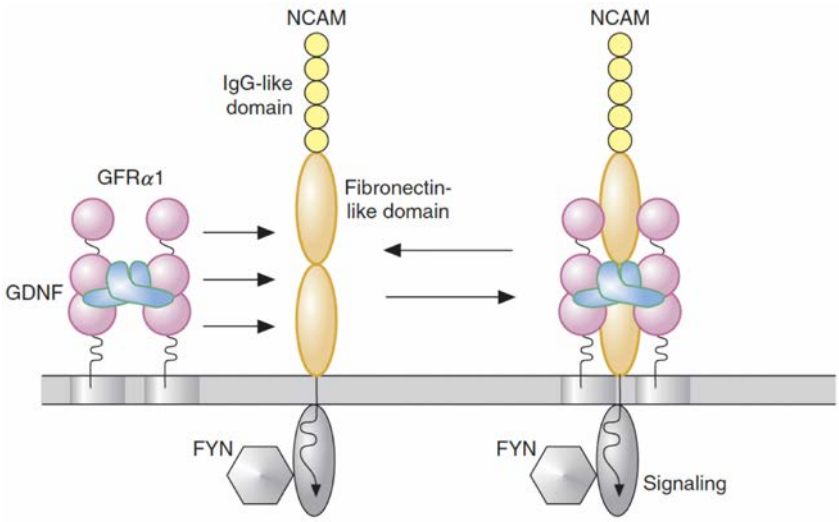

Figure 23. NCAM1 and GDNF interaction. *NCAM-140 dimerizes with GDNF-GFRα-1 and activates Fyn signaling (Saarma, 2009).*

2.2.10.4.2 NCAM1 and the extracellular matrix (ECM)

NCAM1 binds components of ECM such as the glycosaminoglycan heparin through the "heparin-binding domain" in the Ig-II module (Cole and Glaser, 1986; Herndon, Stipp and Lander, 1999) .It also binds chondroitin sulfate proteoglycans (CSPG), such as phosphacan or neurocan, and heparan sulfate proteoglycans (HSPGs) (Kröger and Schröder, 2002). The interactions with ECM members are fundamental for cell adhesion and to modulate cytoskeleton dynamics. Alterations in this pathway are involved in the process of carcinogenesis and metastatic dissemination (Jinka *et al.*, 2012)

2.2.10.4.3 NCAM1 and FGFR signaling

NCAM1 is known to interact FGFR family members that contain CAM-homology domains required for the interaction with NCAM1 (Williams *et al.*, Neuron 1994; Saffell *et al.*, Neuron 1997). NCAM1 was demonstrated to interact with FGFRs in different cellular contexts: i) in neural tissue NCAM1 has been shown to bind FGFR1 and FGFR2 and this interaction is involved in cellular matrix adhesion

and neurite outgrowth (Williams *et al.*, 1994; Kiselyov *et al.*, 2003; Christensen *et al.*, 2006); ii) in pancreatic cancer the interaction of NCAM1 with FGFR4 has been shown to have a key role in cell adhesion (Cavallaro *et al.*, 2001); iii) in immune cells NCAM1 binding to FGFR1 contributes to the relationship between NK and T cells (Kos and Chin, 2002); iv) in ovarian cancer in which orchestrate cell growth, motility and metastatic dissemination (Francavilla *et al.*, 2007; Zecchini *et al.*, 2011).

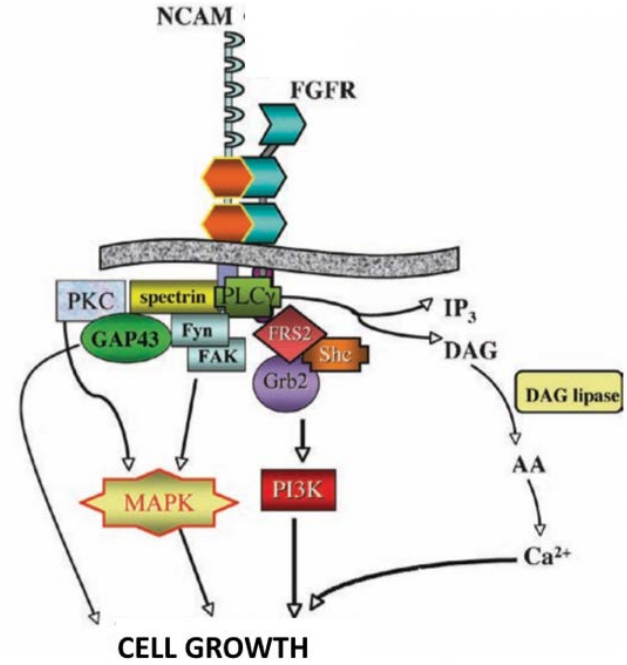

Figure 24. NCAM1 and FGFRs interaction. *NCAM1-FGFRs interaction regulates mainly cell growth through several co-factors that activate three downstream pathways: DAG lipase, MAPK and PI3K-AKT. DAG: diacylglycerol; AA: arachidonic acid; IP3: inositol triphosphate (Zecchini and Cavallaro, 2010).*

.

2.2.10.4.3.1 FGFRs in clinical oncology

The FGFR family members are FGFR1, FGFR2, FGFR3 and FGFR4. They are receptor tyrosine kinase (RTKs) that structurally present an extracellular ligand-binding and an intracellular tyrosine-kinase domain. Upon binding with FGF ligands, the receptor dimerizes and activates downstream pathways such as phospholipase Cγ (PLCγ), RAS-MAPK and PI3K-AKT.

FGFR signaling is commonly activated in several cancers and sustains proliferation, survival and in many cases drug resistance (Katoh, 2019a). Due to their clinical relevance, several therapeutic strategies have been developed to efficiently target FGFRs, and some of them are being tested in clinical trials in several types of cancer, in particular small molecule kinase inhibitors (Babina and Turner, 2017). For example, Dovitinib, Ponatinib, Anlotinib and Nintedanib that target other RTKs (e.g., PDGFR, VEGFR, MET) as well as FGFRs and AZD4547, a more specific FGFR inhibitor (Gavine *et al.*, 2012). AZD4547 has been tested in squamous cell lung carcinoma in the S1440D phase II clinical trial (n= 43), where it demonstrated a modest effect on PFS and OS and an acceptable

safety profile (Aggarwal *et al.*, 2019). No evaluation has been conducted in PCa. In contrast, Dovitinib has been tested in several tumors including PCa. In CRPC (KCSG-GU11-05; n=44) Dovitinib had modest effects on PFS and OS. 23% of treated patients with Dovitinib as a monotherapy experienced improvement with resolution or partial reduction of metastases, 57% of patients had stable disease at 8 weeks and 17% experienced disease progression (Wan *et al.*, 2014a) .

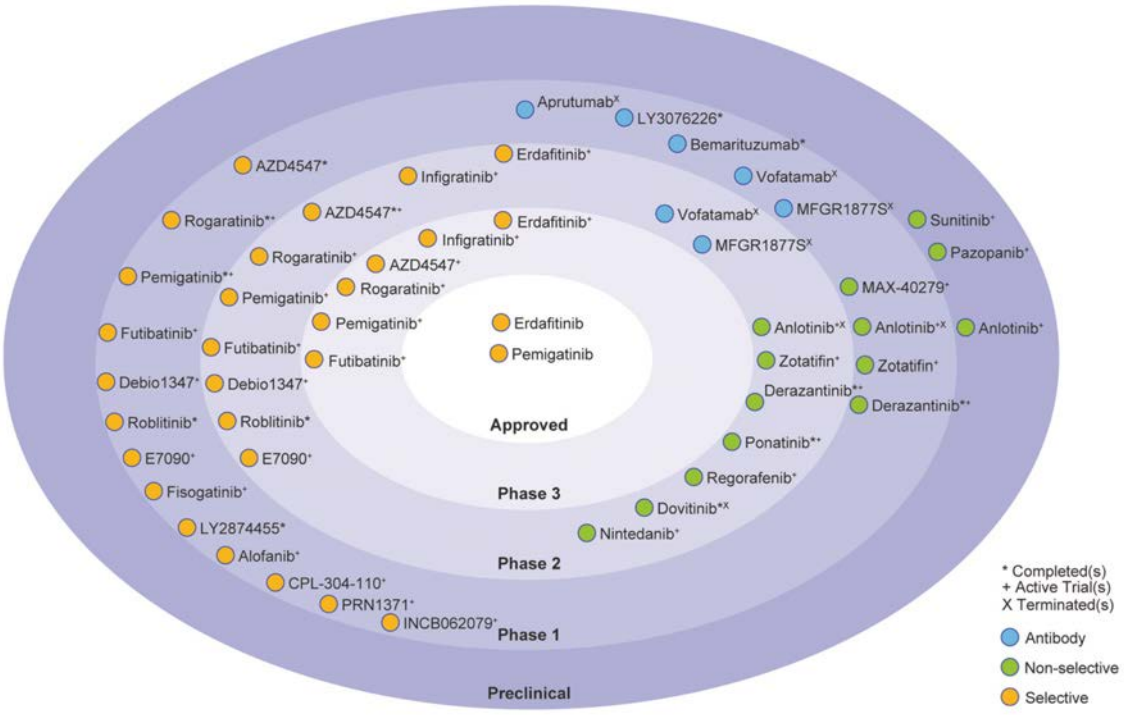

Figure 25. Landscape of FGFRs inhibitors in clinics. *α-FGFRs drugs are currently being assessed in preclinical, phase 1, phase 2, phase 3 and FDA-approved. Color code referred to the type of compound: antibody (blue); non-selective (green); selective (orange).*

2.2.10.5 NCAM1 and metastasis

Due to the role of NCAM1 in cell adhesion and cell motility, it is clearly implicated in tumor metastasis as previously highlighted in ovarian cancer and melanoma (Shi *et al.*, 2011; Zecchini *et al.*, 2011). Moreover, it was also described to be regulated at transcriptional levels by the downregulation ECAD, in murine mammary gland epithelial cells, and the loss of ECAD is the hallmark of EMT (Lehembre *et al.*, 2008).

2.2.10.6 Anti-NCAM1 therapies

2.2.10.6.1 Monoclonal antibodies

Due to the role of NCAM1 in cancer progression and metastatic dissemination it became an attractive target for developing therapies. The conjugated IMGN901 (Lorvotuzumab mertansine) compound is a humanized monoclonal antibody developed against CD56 and covalently linked with the tubulin-binding maytansinoid DM1.

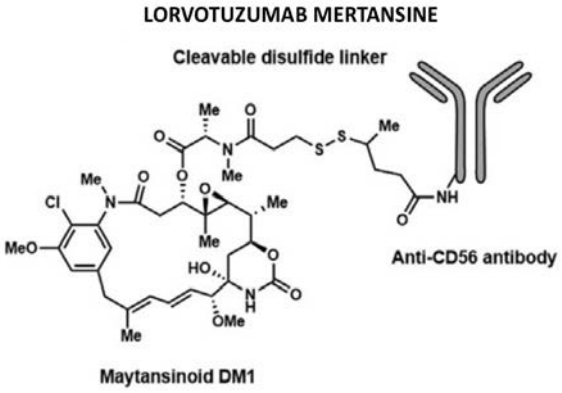

Figure 26. Lorvotuzumab Mertansine chemical structure. *(Xie et al., 2018).*

IMGN901 efficacy and safety were tested in several multicancer clinical trials and preclinical models. In small cell lung cancer, it displayed efficacy in counteracting tumorigenesis in cell lines xenograft models also in combination with platinum therapies to prevent relapse (Whiteman *et al.*, 2014). In NK cells (established cell line and primary derived from patient with malignant lymphoma), IMGN901 exerts suppressive cell growth and viability (Ishitsuka and Tamura, 2008). In patients, with relapsed and/or refractory CD56-positive small cell carcinoma, IMGN901 was tested in combination with carboplatin-etoposide. In a cohort of 96 patients, the combinatory approach (IMGN901 + carboplatin/etoposide) significatively improved the OS compared to patients treated with carboplatin/etoposide alone, however the combinatory approach increased the toxicity (Socinski *et al.*, 2021). Lorvotuzumab mertansine was also tested in relapsed/refractory CD56-positive MM. In 35 patients it demonstrated clinical benefit with good pharmacokinetics and safety profiles (Chanan-Khan *et al.*, 2016).

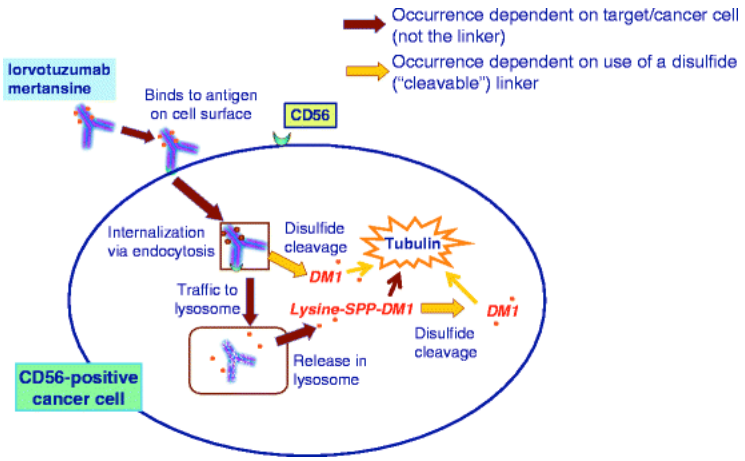

Figure 27. Lorvotuzumab mertansine mechanism of action. *(Lambert et al., 2012).*

Other therapeutic approaches to target NCAM1 have been developed. The monoclonal antibody 123C3 was developed to target specifically the FNIII domains of NCAM1. It was shown to block neuritogenesis and neurite cell survival by interfering with the binding of NCAM1 with FGFR1 (Anderson *et al.*, 2005). The same efficacy was demonstrated in ovarian cancer, where *in vivo* administration prevented ovarian cancer cell dissemination and metastasis appearance (Zecchini *et al.*, 2011). Similarly to 123C3, the Eric1 monoclonal antibody was developed against FNIII domains of NCAM1 and it inhibits the interaction with FGFR1 opposing migration in ovarian cancer cells (Gerardy-Schahn and Eckhardt, 1994; Zecchini *et al.*, 2011). In PCa, none of these α-NCAM1 compounds have been tested.

2.2.11 *In vitro* and *in vivo* models for studying PCa

2.2.11.1 Cell lines

Established cell lines are the most used preclinical models for studying pathophysiological mechanism and drug discovery. In PCa several models of human established cell lines were developed and are widely used to study this pathology, and the most employed are summarized in Table 9 (Namekawa *et al.*, 2019).

Table 9. Summary of the most commonly used established human cell lines for studying PCa.

NAME	PATHOLOGY	ORIGIN	AR
1013L	Adenocarcinoma	Primary	-
E006AA	Adenocarcinoma	Primary	+
RC-77T/E	Adenocarcinoma	Primary	+
DU145	Adenocarcinoma	Metastasis	-
PC-3	Adenocarcinoma	Metastasis	-
LNCaP	Adenocarcinoma	Metastasis	+
ARCaP	Adenocarcinoma	Metastasis	Low
MDA PCA 2a/b	Adenocarcinoma	Metastasis	Low
LuCap 23	Adenocarcinoma	Xenograft	+
LAPC-4	Adenocarcinoma	Xenograft	+
22Rv1	Adenocarcinoma	Xenograft	+
VCaP	Adenocarcinoma	Xenograft	+
KUCaP	Adenocarcinoma	Xenograft	+
PC346	Adenocarcinoma	Xenograft	+

2.2.11.2 3D organoid models

From their introduction, 3D *in vitro* culture techniques to generate organoid cultures have been instrumental in revolutionizing our understanding of cancer heterogeneity and its relevance to drug sensitivity. 3D organoids are easily manipulated miniature *in vitro* models of organs (LeSavage *et al.*, 2022) that have been employed for studying SC traits, such as proliferation, self-renewal and differentiation potential. In fact, pluripotent SCs or early progenitors with stem traits have the capacity to grow in harsh conditions, such as in suspension in Matrigel, which is a basement membrane matrix secreted by the Engelbreth-Holm-Swarm mouse sarcoma resembling the laminin/collagen-IV enriched basement membrane extracellular microenvironment (Hughes, Postovit and Lajoie, 2010).

Several protocols have been developed to generate organoid cultures from PCa cells. In particular, for generating organoids from primary mouse prostate glands, epithelial cells are grown in Matrigel supplemented with stromal cells obtained from the urogenital sinus mesenchyme (UGM), derived from the embryonic day 16 (E16) mouse urogenital sinus (UGS). This co-culturing approach improves not only the survival rate and organoid-formation efficiency but also enhances the tissue characteristics (Richards *et al.*, 2019).

At the phenotypical level, mouse-derived organoids (MDO) and patient-derived organoids (PDO) display the histological traits of the corresponding parental tissue. Specifically, they display $P63^{+}CK5^{+}$ basal cells surrounding $CK8^{+}$ luminal cells which are positive also for AR and Nkx3.1 (Chua *et al.*, 2014; Karthaus *et al.*, 2014; Servant *et al.*, 2021).

Furthermore, organoids are also a useful tool to verify self-renewal ability through the serial propagation assay. CSCs or early progenitors with a prolonged lifespan, have the unique ability to retain organogenetic or tumorigenic potential even after the derived organoids are disaggregated a re-passed to generate subsequent generations (Hofer and Lutolf, 2021).

Nevertheless, organoid models have several limitations (Zhou, Cong and Cong, 2021):

1. Very low success rate.
2. Difficulties in establishing organoids derived from PCa patients.
3. Difficulties in maintaining organoids in culture for a prolonged time.
4. Very simple system lacking fundamental TME players, such as immune cells and the vascular compartment.

2.2.11.3 TRAMP mouse

The transgenic adenocarcinoma of mouse prostate (TRAMP) mouse model is a genetically engineered model for the spontaneous development of PCa (Hurwitz *et al.*, 2001). The TRAMP mouse is usually generated in a C57BL/6 background with a transgene comprising the rat probasin (rPB) gene promoter region (-426 to +28 bp fragment), which directs the tissue-specific expression of simian virus 40 (SV40) early genes (Large T-antigen) in the prostate epithelium. Transgenic male mice are routinely obtained by breeding the C57BL/6 TRAMP female with C57BL/6 non-transgenic males (Gingrich *et al.*, 1999). The *rPB* gene encodes for an androgen regulated protein in the dorsolateral epithelium though a direct stimulation in its 5' flanking region, while the SV40 Large T-antigen (TAg) has oncogenic activity through the interaction with the tumor suppressor proteins Rb and P53 (Greenberg *et al.*, 1995). TRAMP mice develop progressively aggressive tumors that become invasive over time with dissemination to the lungs and lymph nodes (Gingrich *et al.*, 1996). PCa development and progression occurs with the following timeline:

i. 4-6 weeks of age: low-grade PIN.
ii. 6-10 weeks of age: traits of high-grade PIN.
iii. 10-18 weeks of age: high-grade PIN with local epithelial invasion.
iv. 18-28 weeks of age: well/moderately-differentiated carcinoma (WDT/MDT).
v. 28-38 weeks of age: poorly-differentiated carcinoma (PDT) and metastasis.

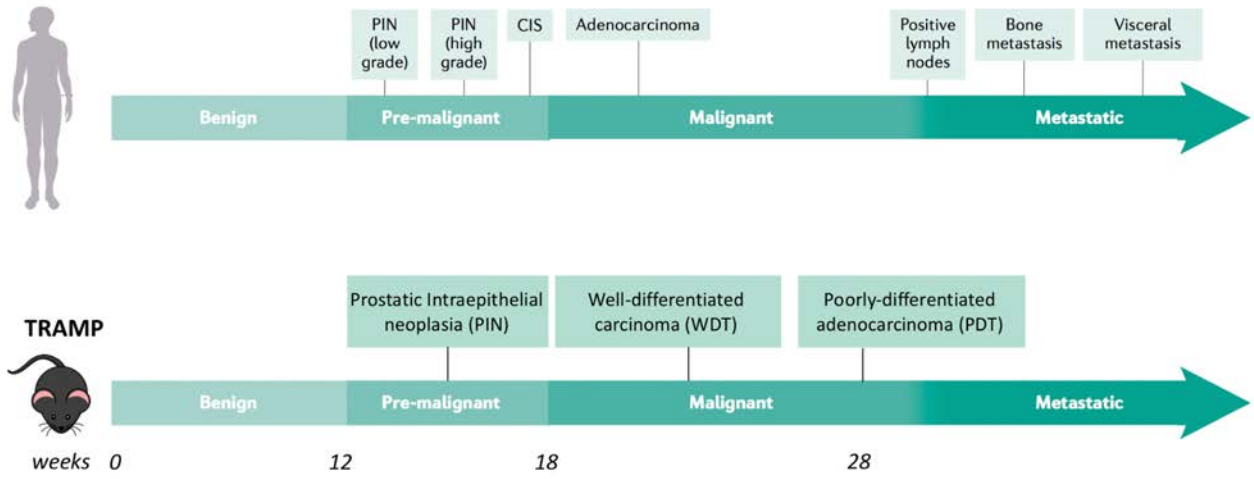

Figure 28. Comparison between human and TRAMP PCa progression. *(Adjusted from Rebello et al., 2021). PIN: prostate intraepithelial neoplasia; CIN: carcinoma in situ.*

The histological traits in each phase of the disease allow the definition of a mouse PCa grading system summarized in Table 10 (taken from Gingrich *et al.*, 1999)

Table 10. Histological features of each stage of TRAMP PCa. *PIN: preneoplastic intraepithelial neoplasia; WDT: well-differentiated tumors; MDT: moderately-differentiated tumors; PDT: poorly-differentiated tumors.*

Grade	Histological features
Normal	Single layer of columnar secretory epithelium with round, basal nuclei, 3 ± 4 cell layers of fibromuscular stroma.
Low-grade PIN	Variably elongated nuclei with condensed chromatin.
High-grade PIN	Increasing variability in nuclear shape, very condensed chromatin, appearance of mitotic figures and apoptotic bodies; epithelial stratification and tufting with micropapillary and cribriform structures.
WDT	Epithelial cells obviously invading through fibromuscular stroma layer and/or the presence of rounded nuclei with condensed chromatin within the fibromuscular stroma which is increased to more than 3 ± 4 cells layers.
MDT	Numerous apoptotic bodies and mitotic figures in compacted, irregularly shaped glands with maintenance of some secretory function.
PDT	Widely variable nuclear shape, clumped chromatin; sheets of cells with little to no glandular formation.

However, this model has some limitations:

1. PCa is sustained by a viral protein not involved in human carcinogenesis.
2. TRAMP mice spontaneously develop NE tumors that instead are rare in human.
3. The TAg is weakly expressed in the first week of life in the mouse and it can affect the development of the prostate gland.
4. TAg expression is downregulated by androgens at adulthood which can introduce bias in ADT experiments.

2.3 Heterogeneity in cancer: Cancer Stem Cells

Cancer is a dynamic disease that evolves over time becoming a heterogenous disease. Heterogeneity is observed both at the intertumoral and intratumoral level. Intertumoral heterogeneity refers to the differences observed between tumors of the same type in different patients while the intratumoral heterogeneity (ITH) refers to subclones of cells with different phenotypes present in the same tumor. This section will be focused on ITH and the link to CSCs.

2.3.1 Definition of ITH in cancer

2.3.1.1 Spatial and Temporal ITH

ITH is divided into spatial or temporal heterogeneity. Spatial heterogeneity refers to subclones of cells harboring distinct genetic traits distributed across the entire tumor, while temporal heterogeneity refers to the appearance of more adaptive clones during the evolution of the tumor, following the acquisition of advantageous genetic and epigenetic alterations (DNA methylation, histone modification, chromatin openness, microRNA and noncoding RNA) or clonal selection due to drug exposure (Nowell, 1976; Baylin and Jones, 2011; Magee, Piskounova and Morrison, 2012; Meacham and Morrison, 2013).

Spatial ITH was demonstrated in an elegant study that performed exome sequencing, chromosome aberration analysis and ploidy profiling of spatially separated primary biopsies derived from a renal carcinoma and its matched metastatic lesion (Gerlinger *et al.*, 2012). Data analysis demonstrated ITH in every tumor with spatial distribution of heterogeneous somatic mutations and chromosomal imbalance. Phenotypic intratumoral diversity could be linked to mutations within the inhibitory domain of the mammalian target of rapamycin (mTOR) kinase leading to constitutive activation of this pathway, or uniformity of loss-of-function mutations in tumor suppressor genes

such as *SETD2*, *PTEN* and *KDMC5*. Thus, ITH is associated with heterogeneity in protein function that could foster tumor progression and drug resistance through clonal selection.

2.3.1.2 Models of ITH

The cellular origin of ITH can be explained by two models: the clonal evolution model and the CSC model.

2.3.1.2.1 Clonal evolution model

Clonal dynamics

The cancer evolution model explains the ITH as derived from a natural selection or adaptation of fittest clones in the tumors. This was proposed by Nowell in 1976 that theorized cancer as an evolutionary dynamic disease based on somatic-cell mutation and subclone selection, similarly to what was theorized by Darwin for the origin of the species. The Darwin's principle proposed that individuals have a common descent, but the evolution occurs through genetic variations in the progeny and environmental pressures with a natural selection of the fittest species. Similarly, in cancer, clonal evolution derived from the combination of 'driver' lesions, passenger lesions and deleterious lesions that contribute to selective advantage, and the microenvironment contribute to clonal selection (Nowell, 1976; Merlo *et al.*, 2006; Greaves and Maley, 2012).

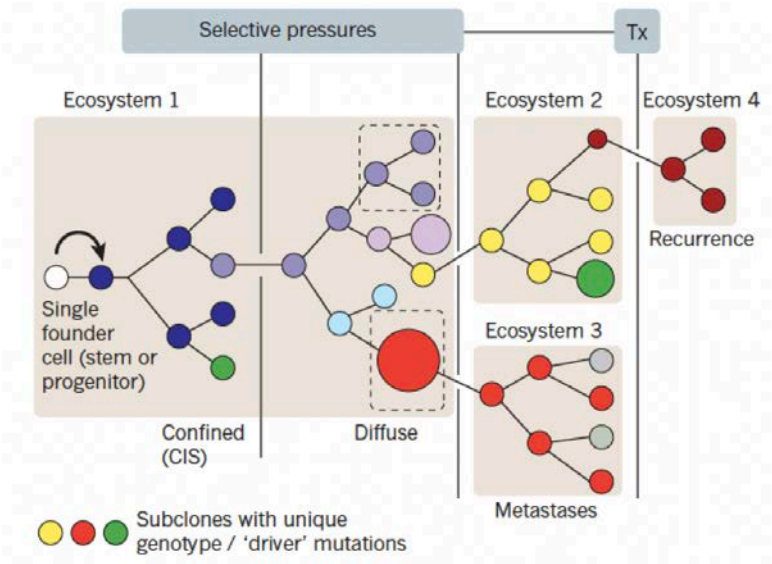

Figure 29. Darwinian principle in cancer evolution. *The destiny of mutant subclones (expansion vs. extinction/permanent dormancy) is controlled by selective pressured from microenvironment. Ecosystem 1-4 referred to localized habits or niches. Each colored dot is genetically distinct subclone. Each subclones branch off into different minor or major clones in primary tumor. TX: therapy; CIS: carcinoma in situ (Greaves and Maley, 2012).*

Whole-genome sequencing is one of the techniques to reveal the genetic complexity in the evolution of cancer cells. Each tumor harbors hundreds to thousands of mutations and chromosomal alterations, but not all of them are necessary for cancer initiation and progression. In fact, cancers can require just a few phenotypic traits that however can derive from thousands of evolutionary trajectories and different assortments of driver mutations (Hanahan and Weinberg, 2011). In PCa, spatial genomic heterogeneity was interrogated in Gleason score 7 patients (n=74) by copy number aberration (CNA) profiles and whole-genome sequencing. These patients displayed high heterogeneity for single-nucleotide variants (SNVs), CNAs and genomic rearrangements, and a recurrent amplification of MYCL gene that was found to contribute to the divergent tumor evolution. Similarly, recurrent and heterogenous CNAs were detected also in *MYC*, *NKX3-1* and *PTEN* genes in low- and intermediate-risk PCa with prognostic value after surgery or radiotherapy management (Locke *et al.*, 2012; Zafarana *et al.*, 2012) .

Cancer ecosystem

Microenvironment heterogeneity is a determinant for clonal selection. A computational model demonstrated that spatial microenvironments with specific resources (oxygen levels or nutrients) sustained cell migration and dissemination determining selection of metastatic clones (Chen *et al.*, 2011). However, the tumor ecosystem is dynamic and is changed by systemic factors (nutrients, hormones) and inflammatory cells, also through external factors such as genotoxic agents (cigarettes, UV), infection and diet. Furthermore, several clinical approaches such as radiotherapy and chemotherapy contribute to modulate the cancer landscape exerting a selective pressure, despite their fundamental action of killing most of the cancer cells. In this way, these drugs allow pre-existing resistant cancer cells to emerge and become predominant in the relapsed tumor with severe clinical implications (Greaves and Maley, 2012).

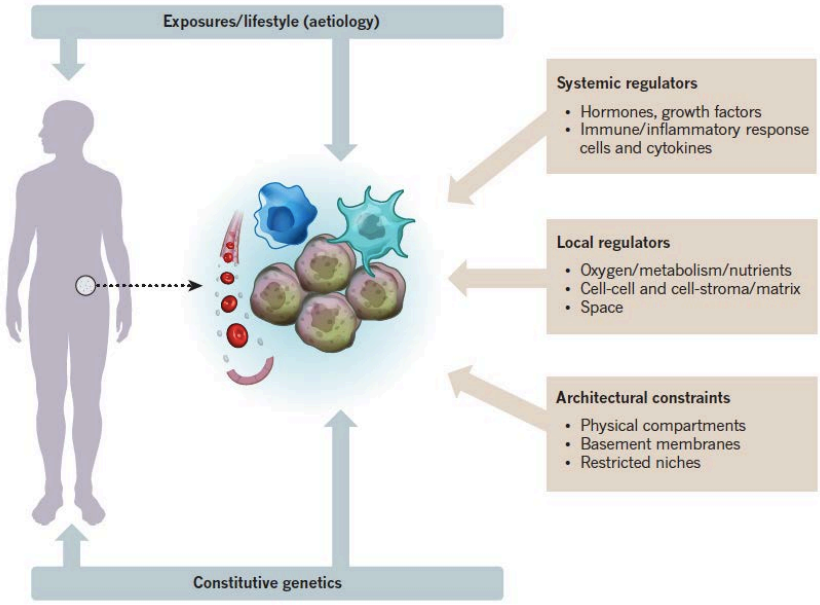

Figure 30. Role of tissue ecosystems and tumor evolution. *External cues reported as systemic regulators, local regulators or architectural constraints, are fundamental for tumor evolution through exerting selective pressures (Greaves and Maley, 2012).*

2.3.1.2.2 CSC model

The CSC model proposes that tumor population is hierarchically organized and contains a subfraction of cells that have stem traits (the CSCs) including the ability to regenerate the tumor. These CSCs give rise to the other cells that make up the bulk of the tumor mass (the progenitors) which are characterized by a high proliferative capacity and a more differentiated state compared with the CSCs but have a limited capacity to contribute to tumor maintenance and progression (Hamburger and Salmon, 1977).

Evidence supporting the CSC model has been obtained in various human cancers, such as leukemia, brain and intestinal tumor mouse models (Lapidot *et al.*, 1994; Chen *et al.*, 2012; Schepers *et al.*, 2012) , with relevance in tumor regrowth upon treatments. In glioblastoma cells treated with chemotherapy only a subfraction of quiescent cells with stem traits maintain the ability to reconstitute tumor, and in intestinal cancer, the subfraction of $LGR5^{+}$ CSCs is necessary for tumorigenesis (Chen *et al.*, 2012; Junttila *et al.*, 2015) .

Three models of stem cell (SC) differentiation were proposed: linear, bidirectional, and independent.

1. The *linear lineage model* proposes that SCs divide by asymmetric cell division resulting in one daughter SC (self-renewal ability) and one multipotent progenitor (transit-amplifying cells).

2. *The bi-directional lineage model* proposes that the SC differentiates into a common bi-potent progenitor which in turn can give rise to each lineage of differentiation.
3. *The independent lineage model* proposes that different tumor-initiating cells (TICs) can exist in cancer that are responsible for heterogeneous tumor growth.

Considering ITH alongside the CSC model it suggests that phenotypic differences exist among the CSC pool, for example, differences in their growth potential, metastatic potential, and resistance to therapies (Clevers, 2011). These phenotypic differences in the CSC content of tumors could underly differences in tumor aggressiveness, therapy response and patient outcome. This implies that all cancer cells share the same probability of surviving and to regenerate tumors, thus the resistance can derive from epigenetic and genetic differences among tumorigenic cancer cells, as proposed by clonal evolution. Indeed, these two models are not mutually exclusive and clonal evolution occurs in CSCs as revealed in a study led in chronic myeloid leukemia in which CSCs were shown to be initially sensitive to imatinib until they developed resistance and were clonally selected (Barabé *et al.*, 2007; Shah *et al.*, 2007).

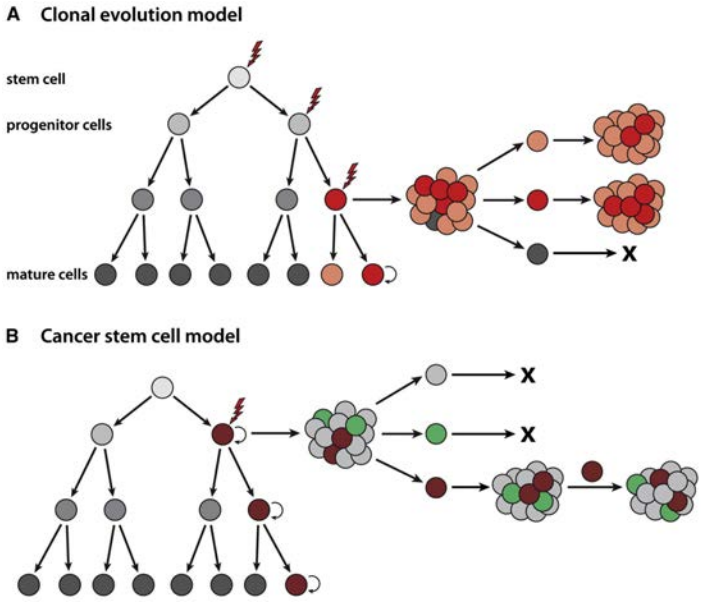

Figure 31. Clonal evolution and CSC model. *A) In clonal evolution model mutations arise in tumor cells for conferring selective advantages. Red dot is the mutated cell that produces a dominant clone. Cells (red and orange) originating from this cell have similar tumorigenic capacity. B) In the CSC model a small subset of cells sustain tumorigenesis and generate tumor heterogeneity. As depicted, mutations in the progenitors (brown) can lead to the acquisition of stem properties such as self-renewal ability and give rise to a range of tumor cells (gray and green)* (Visvader and Lindeman, 2012).

2.3.1.3 Single cell RNA-sequencing (scRNA-seq)

Tumor heterogeneity can be interrogated with scRNA-seq to understand tumor complexity in detail, which could not be done with a bulk analysis, and contributes not only to understanding the hierarchy of individual cancer cells but also allows the identification of rare cell populations implicated in cancer resistance and progression (Navin *et al.*, 2011; Hwang, Lee and Bang, 2018). ScRNA-seq assesses differences in gene expression and the resulting molecular profiles are required to reconstruct dynamic cellular trajectories. This technique in melanoma cells revealed a subfraction of cells, expressing high levels of the RTK AXL, which are resistant to RAF/MEK inhibitors (Tirosh *et al.*, 2016). Instead, in PCa, scRNA-seq revealed the existence in cell lines of a subpopulation of quiescent androgen-insensitive cells, suggesting these cells as clones selected upon exposure to ADT (Horning *et al.*, 2018). The heterogeneity in TME can also be investigated by single-cell analysis. In melanoma, this approach revealed different microenvironments related with distinct malignant cells and a subset of them controlled the proportion of T cells in tumor area highlighting spatial heterogeneity in the communication between cancer cells and the TME (Tirosh *et al.*, 2016).

2.3.2 Role of stem cells in normal and cancer tissues

Cancer versus normal SCs

The cellular hierarchy proposed in the CSC theory reflects the normal tissue hierarchical organization. Normal SCs are somatic cells, essential for tissue regeneration and homeostasis, whose expansion is strictly regulated (Morrison and Kimble, 2006). They are characterized by extensive cell division, self-renewal ability and intrinsic potential to differentiate into more specialized cells as demonstrated in hematopoietic cells in which a single cell undergoes multilineage differentiation (Till and McCULLOCH, 1961; Lobo *et al.*, 2007). Self-renewal is one of the key features of SCs and defines the mechanism by which these cells divide to originate one (asymmetric division) or two (symmetric division) daughters to control the long-term growth of SCs. Due to the prolonged lifespan of normal SCs, it has been hypothesized that they can accumulate more genetic alterations that are passed to progenitors and thus be the origin of cancer. The frequency of CSCs is highly heterogenous in tumors and is typically between 1-2% of total cancer cells but can be > 80% for example in acute lymphoblastic leukemia (ALL) (Singh *et al.*, 2003; Kelly *et al.*, 2007; Ricci-Vitiani *et al.*, 2007; Eramo *et al.*, 2008; Enderling and Rejniak, 2013). This heterogeneity derives from the observation that in tumors not only CSCs are present but also transit-amplifying cells which are characterized by long-term repopulation and self-renewal ability and cellular plasticity known as TICs that refer to

cells with tumorigenic ability when transplanted in mice models but not necessarily possessing all the CSCs traits (Ishizawa *et al.*, 2010; Nguyen *et al.*, 2012).

2.3.2.1 Cells of origin for cancer

The CSC model does not explain whether the normal SCs are responsible for tumor initiation. Indeed, the origin of CSCs is still under debate. Two main hypotheses have been proposed. 1) Genetic alterations in normal SCs result in the uncontrolled proliferation of this pool of cells that can sustain tumor growth (Lapidot *et al.*, 1994). 2) Progenitors which acquire self-renewal ability might have a role in originating the tumor. This hypothesis is based on evidence in hematopoietic cells where progenitor cells can differentiate into mature blood cells (Cozzio *et al.*, 2003; Huntly *et al.*, 2004; Clarke and Fuller, 2006). This dedifferentiation process involves the acquisition of EMT and plasticity traits.

Genetic and epigenetic predisposition factors

The mechanism of cell transformation and tumorigenesis is a stochastic event that can happen in both SCs and progenitors. However, normal SCs share with CSCs the self-renewal ability and tissue regeneration potential thus they are plausible as the origin of cancer. A mathematical model supports this hypothesis identifying a correlation between rate of SC division and risk to develop cancers (Hanahan and Weinberg, 2011). The proof that mutations in normal SCs increase the risk to develop cancers was obtained with an elegant lineage tracing experiment following the $CD133^+$ cells in several organs in mice. This study demonstrated that mutations in $CD133^+$ cells are not enough to induce tumors but, in combination with external stress such as inflammation it leads to transformation and tumor initiation (Zhou *et al.*, 2022). Similarly, in PCa a castration assay revealed the existence of very rare castration-resistant cells in the prostate luminal compartment, expressing the Nkx3-1 marker; these cells are known as CARNs (castrate-resistant Nkx3-1-expressing cells). These cells display bipotent differentiation in a lineage tracing assay in the absence of androgens and maintained self-renewal ability but if CARNs are deleted for the oncosuppressive protein PTEN, they acquired CSC traits including enhanced tumorigenic potential (Lawson *et al.*, 2007; Wang *et al.*, 2009)

Epigenetic changes enhance SC plasticity and non-CSCs can dedifferentiate to acquired CSCs traits. Indeed, genetic alterations alone are not enough to induce all the CSC phenotypes, thus genetic changes are accompanied with epigenetic modifications including methylation, CpG islands promoter hypermethylation, histone modifications and nucleosome remodeling (Dawson and Kouzarides, 2012). Methylation in the promoter of genes involved in DNA repair (e.g., DNA mismatch protein MHL1) predisposes colorectal normal cells to mutations (Hitchins *et al.*, 2011).

2.3.3 The hallmarks of CSCs

Figure 32. CSCs hallmarks. *Graphical representation of CSCs hallmarks including self-renewal/multilineage differentiation; survival; EMT; metabolism; quiescence; immune suppression (Turdo et al., 2019).*

CSCs are characterized by six hallmarks: quiescence, self-renewal ability, drug resistance, metabolism, EMT and immune evasion.

1. CSC quiescence refers to the reversible non-proliferative G0 phase. This feature is responsible for dormancy in primary and secondary tumors with a key role in metastasis, and for conferring drug resistance to chemotherapy. At the molecular level, quiescence is controlled by p21, p27, p53 and Rb and also members of the Notch-pathway such as Forkhead Box O (FoxO) transcription factor that regulates vascular growth and metabolic reprogramming in several cancers (Charitou *et al.*, 2015; W. Chen *et al.*, 2016).
2. Self-renewal ability is the capacity of CSCs to continuously sustain tumor growth. Several molecular pathways are known to regulate this feature, including Hedgehog pathway and the polycomb complex protein B (BMI-1) in hematopoietic SCs as well as glioma and ovarian cancer. Self-renewal is also sustained by crosstalk with TME such hypoxia, acidity, extracellular matrix remodeling, nutrient availability and immune cells (Godlewski *et al.*, 2008; Bhattacharya *et al.*, 2009)

3. Therapy resistance of CSCs is the most relevant clinical problem for tumor relapse and metastasis. CSCs resist genotoxic stress by upregulating the DNA damage response by activating the checkpoint kinases. Moreover, CSCs upregulate anti-apoptotic proteins such as Survivin, BCL2, BAX and c-FLIP, downregulate pro-apoptotic proteins such as caspases, or upregulate metabolic-related genes such as aldehyde dehydrogenase (ALDH) (Bartucci *et al.*, 2012; Safa, 2016; Vitale *et al.*, 2017; Vassalli, 2019).
4. CSC metabolism is heterogenous in cancers. In breast, liver and nasopharyingeal CSCs, glycolysis is the preferred metabolic pathway (Dong *et al.*, 2013; Shen *et al.*, 2015), instead other studies in lung, glioblastoma and leukemia demonstrated enriched oxidative phosphorylation (OXPHOS) (Ye *et al.*, 2011; Janiszewska *et al.*, 2012; Lagadinou *et al.*, 2013).
5. TME is the major source of factors that control EMT in CSCs. Fibroblasts secrete hepatocyte growth factor (HGF), osteopontin (OPN) and stromal cell-derived factor (SDF-1) which positively control the WNT/β-Catenin signaling, pivotal for the induction of EMT in colorectal cancer (Todaro *et al.*, 2014). TGFβ is commonly associated with EMT in cancer cells, as observed in colorectal cancer in which it modulates TWIST1 in the $CD44^+$ subfraction of cells or in non-small-cell lung cancer (NSCLC) in which the chronic stimulation of the $CD133^+$ cells with TGFβ upregulates the transcription of vimentin and Slug (Tirino *et al.*, 2013; Nakano *et al.*, 2019).
6. CSC immune microenvironment is usually compromised, and CSCs have a key role in releasing immunosuppressive factors, which in turn sustain stemness. CSCs efficiently degrade the major histocompatibility complex class I (MHC-I), fundamental for T-cell receptor interaction on CTLs that failed to recognize and kill CSCs, as shown in glioblastoma and head and neck squamous cell carcinoma (Di Tomaso *et al.*, 2010; Iovino *et al.*, 2011; Chikamatsu *et al.*, 2012; Liao *et al.*, 2013). Moreover, CSCs negatively modulate the NK cells that in coculture experiments were shown to lyse CSCs in cell lines and primary tumors (Jewett *et al.*, 2012; Ames *et al.*, 2015).

2.3.3.1 Role of CSCs in metastasis

EMT (see section 2.2.7.1.1) is a characterizing feature of CSCs that is considered to be responsible of metastatic dissemination and outgrowth in a distant organ, and moreover it is implied in drug resistance such as chemotherapy and radiotherapy, in several types of cancers (Shibue and Weinberg, 2017). The relationship between EMT and CSCs has been proved discovering that induction of mesenchymal factors, including transcription factors (ZEB, TWIST, SNAIL) gives rise to the transcription of genes associated with stemness such as CD44 and the downregulation of CD24. As proof of concept, the molecular profiling of DTCs founded in the bone marrow of breast cancer

patients revealed that they are characterized by the expression of the CSC markers $CD44^{+}/CD24^{-}$ and displayed tumor growth potential when transplanted into immunodeficient mice (Balic *et al.*, 2006; Theodoropoulos *et al.*, 2010).

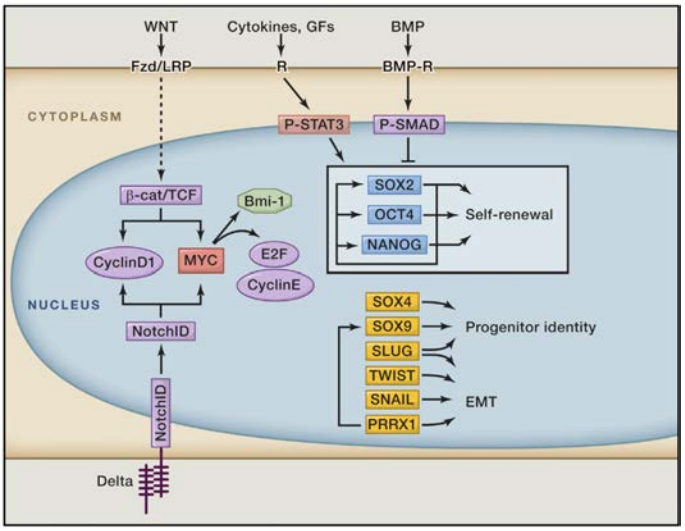

Figure 33. CSCs signaling pathways involved in metastasis. *In CSCs, WNT/β-Catenin, Notch pathway promote cell cycle progression via Cyclin D1 and Myc, which control BMI-1. Together with STAT3 these pathways control self-renewal associated genes such as SOX2, OCT4 and NANOG. Additional transcription factors, as reported in the yellow boxes, control progenitor differentiation of EMT. Rectangle: transcription factors; ovals: cell-cycle components; octagon: epigenetic regulation. Functional groups are color coded (Giancotti et al., 2013).*

However, not all the CSCs have metastatic potential. As observed in PCa, bone metastases can arise from a subpopulation of $CD133^{+}/CD44^{+}$ cells that have the ability to disseminate and form metastases when injected into the bone marrow of NSG mice. These data support that in the CSC population there exists a subfraction of CSCs, named metastatic cancer stem cells (MCSCs), which is uniquely capable of invasion and metastatic growth. MCSCs rapidly disseminate in the bloodstream and through asymmetric division originate a metastatic tumor in another tissue (Brabletz *et al.*, 2005; Kaplan *et al.*, 2005; Baccelli and Trumpp, 2012; Sceneay, Smyth and Möller, 2013).

2.3.3.2 CSCs and TME

CSCs are pivotal in controlling the TME, crucial for tumor evolution, and contribute to cancer heterogeneity. CSCs engage with several adverse conditions in tumor such as hypoxia or low nutrient availability, which in turn control stem traits. Hypoxic areas are distributed in the tumor mass and CSCs have the ability to survive and maintain the stemness program and quiescence (Kim *et al.*, 2018). The hypoxic response is mediated by hypoxia-inducible factors (HIFs). HIF-2 was found to be upregulated in chronic hypoxia and to control stemness by upregulating transcription factors such as KLF4, SOX2 and OCT4, in human embryonic SCs (Mathieu *et al.*, 2011). In PCa, hypoxia keeps

CSCs, derived from the mouse cell line TRAMP-C1, quiescent by attenuating cell metabolism through the downregulation of the PI3K-mTOR axis (Marhold *et al.*, 2015).

In turn, CSCs in hypoxic areas reconstitute the TME; by stimulating the perivascular niche they release VEGFA and induce angiogenesis needed to supply cancer cells with oxygen, nutrients and factors that sustain dormancy and self-renewal ability. In PCa, it has been demonstrated that an autocrine stimulation with VEGFA is required to sustain CSCs. In particular, an axis was described involving VEGFA and neuropilin-2, an alternative VEGF receptor that controls the transcription of Bmi-1 which in turn controls self-renewal in PCa (Goel and Mercurio, 2013).

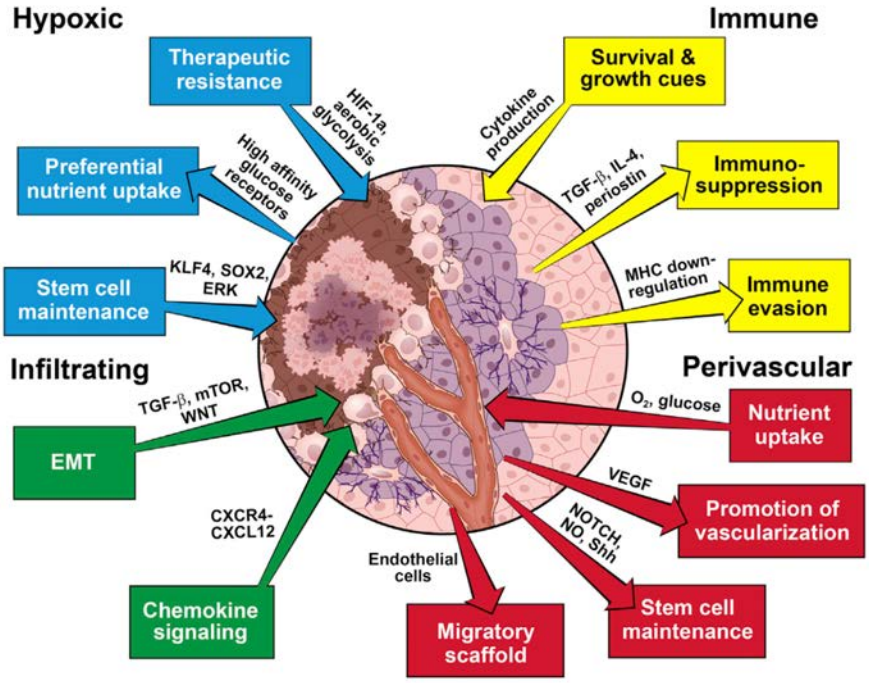

Figure 34. Reciprocal crosstalk between CSCs and tumor niche. *Through specific mechanisms, CSCs promote immunosuppression, therapeutic resistance, and EMT, receiving in turn supportive factors that sustain stemness. Supportive niche is detailed: hypoxic niche (blue), the immune niche (yellow), the perivascular niche (red) and the infiltrating region (green) (Prager et al., 2019).*

2.3.3.3 CSCs and drug resistance

One of the hallmarks of CSCs is the intrinsic resistance to the conventional anticancer drugs and the conserved ability to reconstitute tumor with more aggressive features. Moreover, clinical observations revealed that patients treated with conventional chemotherapies or radiotherapies are enriched in CSCs upon drugs exposure. In lung cancer cells, the treatment with the tyrosine kinase inhibitor gefitinib enhances the transcription of ALDH1A1 and stem potential (Shien *et al.*, 2013). CSCs have alterations also in the DNA damage repaired mechanisms. In $CD90^{+}$ breast CSCs even if

radiated with UV they still maintain the ability to survive and grow thanks to the ROS scavenger machinery that decreased amount of free ROS in the cells (Diehn *et al.*, 2009). Furtherly, CSCs are responsible of multidrug resistance due to the regulation of drugs transporter on the plasma membrane. ATP-binding cassette (ABC) transporters are the main regulators of this process due to their ability to pump drugs out of the cells though ATP hydrolysis and are usually overexpressed in CSCs isolated from several tumors (Karthikeyan and Hoti, 2015). Finally, quiescence is a feature of several CSCs that allow escaping from chemotherapies, which affect proliferating cells. Moreover, it is widely assumed as notion that chemotherapy-responsive cancer cells released cytokines and mitogenic molecules that sustain quiescence (Chan, 2016).

2.3.4 CSC biomarker heterogeneity in cancers

The expression of biomarkers demonstrated to isolate CSCs are not uniform among cancers. CD133, CD44, CD166, CD24 and ALDH1 are proven to isolate cells with stem potential from solid tumors (Medema, 2013). CD133 is a well-recognized CSC marker in glioblastoma (Singh *et al.*, 2004) and colon-rectal cancer (Ricci-Vitiani *et al.*, 2007) but it is not functional in breast cancer. Interestingly, in small cell lung cancer, CD166, but not CD133 and CD44, emerged as a CSC biomarker (W. C. Zhang *et al.*, 2012). Moreover, combinations of biomarkers have been shown to be efficient in the isolation of CSCs. $CD44^{+}/EpCAM^{+}/CD166^{+}$ recognize a fraction of CSCs in colon rectal cancer more robustly than CD133 alone (Dalerba *et al.*, 2007). $CD34^{+}/CD38^{-}/IL3R\alpha^{+}$ recognize leukemia CSCs (Du *et al.*, 2011). $CD44^{high}/CD24^{low}/ALDH^{high}$ recognize a further subfraction of CSCs in breast cancer with enhanced tumorigenic potential compared to the $CD44^{high}/CD24^{low}$ (Ginestier *et al.*, 2007).

2.3.4.1 Identification of prostate cancer stem cells

PCSCs are usually prospectively isolated from bulk tumoral cells through flow cytometry that employs antibodies to recognize surface biomarkers expressed uniquely on prostate SCs. Several markers have been tested and proposed to isolate cells with SC potential, but their clinical relevance is still unproven.

1. $CD117^{+}$ cells in mouse models are detected in the proximal region of the prostate and this pool of cells expands upon castration and the regeneration assay, and exhibits stem potential *in vivo* (Leong *et al.*, 2008). Moreover, CD117 was found expressed in PCa-associated CTCs, suggesting an intrinsic intravasation potential (Kerr *et al.*, 2015), and in the PCSC-like subpopulation with enhanced stem traits and prognostic value (Harris *et al.*, 2021).

2. CD44 was used alone to isolate cells with stem traits from the established cell lines LNCaP and DU145. These $CD44^{+}$ cells displayed engrafting potential *in vivo*, sphere-forming ability *in vitro*, and the enrichment in stem genes (OCT3/4, BMI1, SOX2 and β-Catenin) (Patrawala *et al.*, 2006).
3. PSA was used to isolate cells with stem potential. In particular, $PSA^{low/-}$ cells were shown to be quiescent and refractory to androgen ablation, to exhibit prolonged tumor-propagating capacity and to differentiate through asymmetric division in the PSA^{+} cells (Qin *et al.*, 2012).
4. Recently, Liu and colleagues demonstrated that luminal $CD38^{low}$-expressing cells displayed enhanced activity in the colony-formation assay in 2D and in the organoid-formation assay in 3D. Moreover, these cells are characterized by low dependence on androgens and increased expression of an inflammatory gene signature. In fact, $CD38^{low}$ cells are located close to inflamed areas surrounding of normal prostate gland tissue and, if transformed by the co-expression of oncogenic proteins, such as Myc and the constitutively active myristoylated-AKT (Myr-AKT), they are able to promote carcinogenesis *in vivo*. The IHC staining for CD38 in a TMA cohort of PCa patients (n=281) revealed that the low intensity of the staining for this protein predicted risk for PCa progression (Liu *et al.*, 2016).
5. $CD44^{+}/\alpha 2\beta 1^{high}/CD133^{+}$ cells isolated from primary human-derived samples and the established human-derived PCa cell line DU145 displayed enhanced proliferative potential and multilineage differentiation *in vitro*, but they have never been tested for tumorigenic potential in the mouse model (Birnie *et al.*, 2008).
6. The combination of $Lin^{-}/Sca\text{-}1^{+}/CD49f^{high}$ allowed the isolation of TICs from the *Pten* null mouse model. This cell population is characterized by the expression of basal markers, such as CK5 and CK14, and low levels of AR (Lawson *et al.*, 2007). Functionally, they displayed organogenetic ability *in vitro* and tumorigenic capacity in renal grafting *in vivo* (Mulholland *et al.*, 2009). Moreover, the enforced expression of AKT in $Lin^{-}/Sca\text{-}1^{+}/CD49f^{high}$ cells, in combination with PTEN deletion, induced poorly differentiated cells showing tumorigenicity (Mulholland *et al.*, 2009). The subfraction of the $Lin^{-}/Sca\text{-}1^{+}/CD49f^{high}$ normal cells that also express CD133/CD44/CD117 were able to reconstitute the prostate in kidney transplantation experiments, but, while in mouse these cells are both luminal and basal, in human this cell population is exclusively basal (Leong *et al.*, 2008).
7. The combination of $Trop2^{high}/CD166\ (ALCAM1)^{+}/PSA^{-/low}$ and ALDH1A1 led to the isolation of PCSCs in primary PCa with enhanced organoid formation, self-renewal and castration resistance (Goldstein *et al.*, 2008; Jiao *et al.*, 2012; Qin *et al.*, 2012).

A summary of all these PCSCs markers is shown in Table 11.

Table 11. List of published prostate cancer stem cells (PCSCs) biomarkers

Markers	References
CD44/$\alpha2\beta1^{high}$/$CD133^{+}$	Collins et al., 2005
$CD44^{+}$/ $\alpha2\beta1^{high}$	Patrawala et al., 2006
$CD44^{+}$/$CD133^{+}$	Hurt et al., 2008
$CD133^{+}$	Vander Griend et al., 2008
$CD49f^{high}$/$Trop^{high}$/ $CD166^{+}$	Goldstein et al., 2008
LSC^{high}/$CD166^{high}$	Jiao J et al., 2012
$CD44^{+}$/$ALDH^{high}$/ $\alpha2\beta1$	van den Hoogen et al., 2010
$CD38^{low}$	Liu et al., 2016
$CD44^{+}$/$CD133^{+}$/$CD117^{+}$	Leong et al., 2008

2.3.4.1.1 Therapeutic approaches targeting PCSCs

The development of pharmacological strategies to eradicate PCSCs is crucial for tumor eradication. The signaling pathways relevant for stem traits are candidate targets for such therapies and drugs targeting many of these pathways are already in clinical development and we focused our attention of Hedgehog pathway and Notch signaling.

Hedgehog pathway. The first FDA approved drug was vismodegib (GDC-0449) that is an oral compound that selectively inhibits the Hedgehog pathway receptor Smoothened (SMO). The NTC01163084 clinical trial is still evaluating the role of this drug as a neoadjuvant treatment for PCa with the anti-androgen therapies leuprolide acetate or goreselin in locally advanced PCa patients. Promising results have also been derived from erismodegib (LDE-225), another selective antagonist of the SMO receptor. In $CD44^{+}$/$CD133^{+}$ cells, erismodegib inhibits spheroid-formation *in vitro* and controls self-renewal ability at the transcriptional level by decreasing the *NANOG, OCT4, SOX2* and *C-MYC* mRNA levels. Asa neoadjuvant therapy, erismodegib is effective in abrogating Hedgehog signaling in prostate tissue before surgery, however the benefit of this approach to oncology is still unknown (Nanta *et al.*, 2013; Ross *et al.*, 2017). GANT61 is a hexahydropyrimidine selective inhibitor of the GLI1 and GLI2 transcription factors that are activated by the Hh pathway. GANT61 was tested in PCa cell line 22Rv1 in which strongly diminished cell proliferation, impaired stemness traits and promoted apoptosis (Lauth *et al.*, 2007).

Notch signaling pathway. γ-secretase inhibitors (GSIs), such as DAPT (N-[N-(3,5-Difluorophenacetyl)-l-alanyl]-S-phenylglycine t-butyl ester), are compounds that affect the enzymatic activity of the intramembrane cleaving protease (γ-secretase) responsible for the cleavage and activation of Notch-1 (cleaved-Notch-1). GSIs have been shown to enhance docetaxel efficacy in CRPC men and to revert androgen-resistance mediated by Notch-1 activation in enzalutamide-resistant PCa cells (Cui *et al.*, 2015; Stoyanova *et al.*, 2016; Farah *et al.*, 2019). Other strategies for inhibiting Notch signaling are being developed including alpha-secretase inhibitors (ASIs) that interfere with the Notch cleavage mediated by ADAM (A-disintegrin and metalloprotease)-10 and -17 and antibody inhibitors of Notch or its ligand, such as Delta-like-4 (DLL4) (Noguera-Troise *et al.*, 2006; Zhou *et al.*, 2006; Wu *et al.*, 2010).

2.3.5 *In vivo* assay for CSC detection

Xenotransplantation in immunocompromised mouse models is the gold standard to evaluate the presence and quantify the number of CSCs/TICs into a fraction of cells, usually through serial dilutions. Obtained xenografts can be digested and re-transplanted several times, however with several limitations such as the digestion of tumors (both enzymatically or mechanical) destroy the cell contacts and extrapolate cancer cells out the original microenvironment (Batlle and Clevers, 2017). To overcome these difficulties genetic-lineage tracing has been proposed as an alternative method. This technique labels a subfraction of cells expressing the candidate gene with a recombinase (e.g., Cre) that activates the promoter. Several studies have used this approach. In skin tumors, mice labelled with the CK14-Cre allowed the identification of a small fraction of CSCs that generate the transit-amplifying cells through asymmetric division (Driessens *et al.*, 2012). Instead, in PCa, the constructs K14rtTA/TetOCRE/RosaYFP and K5CREER/RosaYFP in basal cells revealed the existence of multipotent subfraction of cells in this compartment of the prostate gland with the potential to originate all the prostate epithelial lineages (basal, luminal and NE) (Ousset *et al.*, 2012). On the other hand, luminal and basal lineage tracing experiments in healthy mice revealed that both epithelium lineages are able to sustain prostate regeneration suggesting the presence of CSCs resistant to lack of androgens in both the compartments and susceptible to oncogenic transformation as the cancer cell of origin (Xin *et al.*, 2007; Goldstein *et al.*, 2010; Choi *et al.*, 2012).

3. CLINICAL DATA

In our lab, we focused the line of research on identifying the role of NCAM1 in PCa considering that its role in this context is still unknown and it has never been tested as a clinical marker in a cohort of PCa patients. We have obtained evidence of the prognostic value of NCAM1 expression in PCa, which formed the basis for my thesis. These data are summarized below and were kindly provided by Blanca Alvarez, Dr. Giovanni Bertalot, Stefano Freddi and Davide DiSalvatore (unpublished data).

3.1 NCAM1 is an independent prognostic marker in PCa patients

A retrospective consecutive cohort of 406 PCa patients, who underwent RP at IEO between 2000 and 2009 IEO(00-09) and who were associated with complete follow-up data (see characteristics of patients, Table 1), were interrogated for NCAM1 expression by IHC in entire prostate sections.

Table 1. Clinicopathological data of the IEO prostate cancer patient cohort IEO(00-09)

Characteristics	Entire PCa cohort
Age	n = 406
<65 yr	236 (58.13%)
>=65 yr	170 (41.87%)
Gleason Group (GG)	n = 406
1-2	258 (63.55%)
3	69 (17%)
4-5	77 (18.97%)
NA	2 (0.49%)
pN	n = 406
pN0	196 (48.28%)
pN+	26 (6.4%)
pNx	184 (45.32%)
pT	n = 406
pT2	225 (55.42%)
pT3	180 (44.33%)
pT4	1 (0.25%)
PNI	n = 406
Absent	82 (20.20%)
Present	310 (76.35%)
NA	14 (3.45%)
VI	n = 406
Absent	318 (78.33%)
Present	73 (17.98%)
NA	15 (3.69%)
Margins	n = 406
Negative	301 (74.14%)
Positive	100 (24.63%)
NA	5 (1.23%)
PSA	n = 406
<10 ng/mL	316 (77.83%)
>=10 ng/mL	90 (22-17%)

NCAM1 displayed two distinct expression patterns in tumors and we noted that these different patterns of distribution correlated with differences in the expression of the NE markers CHGA and SYN. $NCAM1^+$ cells co-expressing the other NE markers, as revealed by the IF staining, were detected as rare scattered single cells in areas of normal tissue (surrounding the tumoral areas) and in tumoral tissue, consistent with an NE phenotype **(Fig. 1A,B)**. In a minority of PCa cases (~2%), triple-positive $NCAM1^+/CHGA^+/SYN^+$ cells appeared as foci of variable size spread into the tumoral areas indicating focal NED in these tumors **(Fig. 1A,B)**. However, another subset of $NCAM1^+$ cells lacking the expression of both CHGA and SYN, was detectable in ~40% of PCa. These $NCAM1^+$ only cells appeared typically arranged in "threads" of 3 to 10 (or sometimes more) cells delimiting the border of prostate glandular structures, as shown by IF staining (referred to hereafter as $NCAM1^+/NE^-$) **(Fig. 1C,D)**. Of note, NCAM1 was undetectable in ~14% of cases.

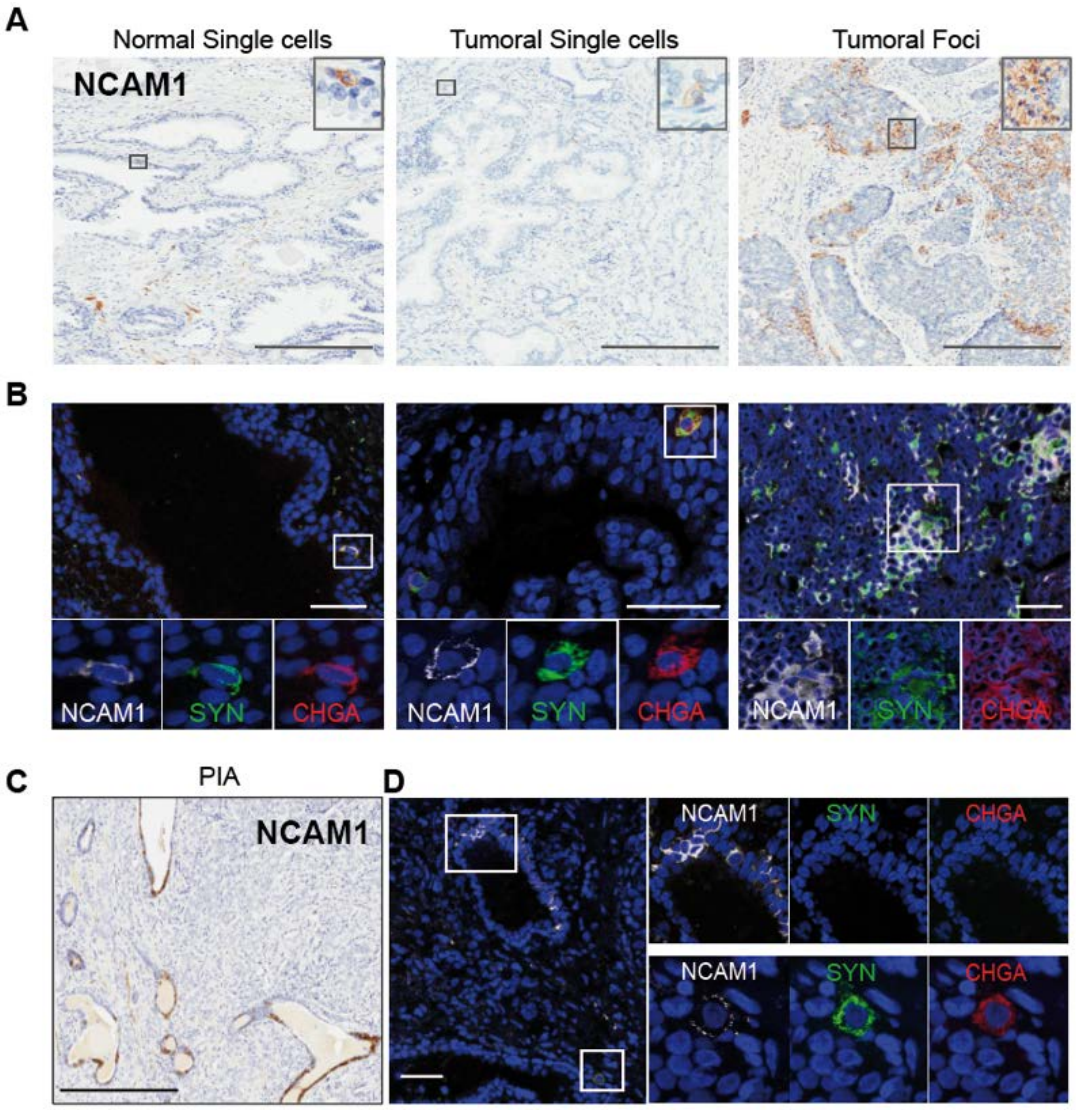

Figure 1. Co-expression of NCAM1 and other NE markers in human PCa. *The expression of NCAM1 and the NE markers SYN and CHGA was analyzed in entire tumor prostate sections obtained from the IEO(00-09) cohort.* ***A)*** *Representative immunohistochemical analysis of NCAM1 expression in areas of normal and tumor tissue (n= 406) showing different distributions of NCAM1-expressing cells as single cells or foci. Boxed region is magnified in the top right corner. Scale bars = 100 µm.* ***B)*** *Representative immunofluorescence (IF) images of samples as in "A" with single cells and foci of NCAM1$^+$ cells (white) co-expressing the NE markers SYN (green) and CHGA (red). DAPI nuclear counterstain (blue). Scale bars = 50 µm.* ***C)*** *Representative immunohistochemical analysis of NCAM1 expression in proliferative inflammatory atrophy (PIA) regions showing distribution of NCAM1-expressing cells as "threads" of cells. Scale bars = 100 µm* ***D)*** *Representative IF images of a human tumoral prostate gland stained for NCAM1 (white), CHGA (red) and SYN (green). Boxed regions show an NCAM1$^+$/CHGA$^-$/SYN$^-$ cell thread bordering a prostate gland (top) and a triple-positive NCAM1$^+$/CHGA$^+$/SYN$^+$ single cell (bottom). Scale bar = 100 µm.*

The NCAM1^{+}/NE^{-} cell threads are expressed in atypical histological regions called PIA, a precursor lesion associated with the development of high-grade PIN and PCa (DeMarzo *et al*., 2016) Indeed, we revealed that NCAM1^{+} cell threads express very low levels of AR as evidenced by IF **(Fig. 2A)**, and are located in highly proliferating glands, estimated by the presence of Ki-67-positive cells **(Fig. 2B)**, which are also characterized by high levels of the anti-apoptotic marker BCL-2 **(Fig. 2C)**. Further IF analysis of the PIA structures containing NCAM1^{+} cell threads revealed the typical luminal (CK8^{+})/basal (CK5^{+}) bilayer structure with NCAM1 expression appearing mainly in the luminal layer **(Fig. 2D)**.

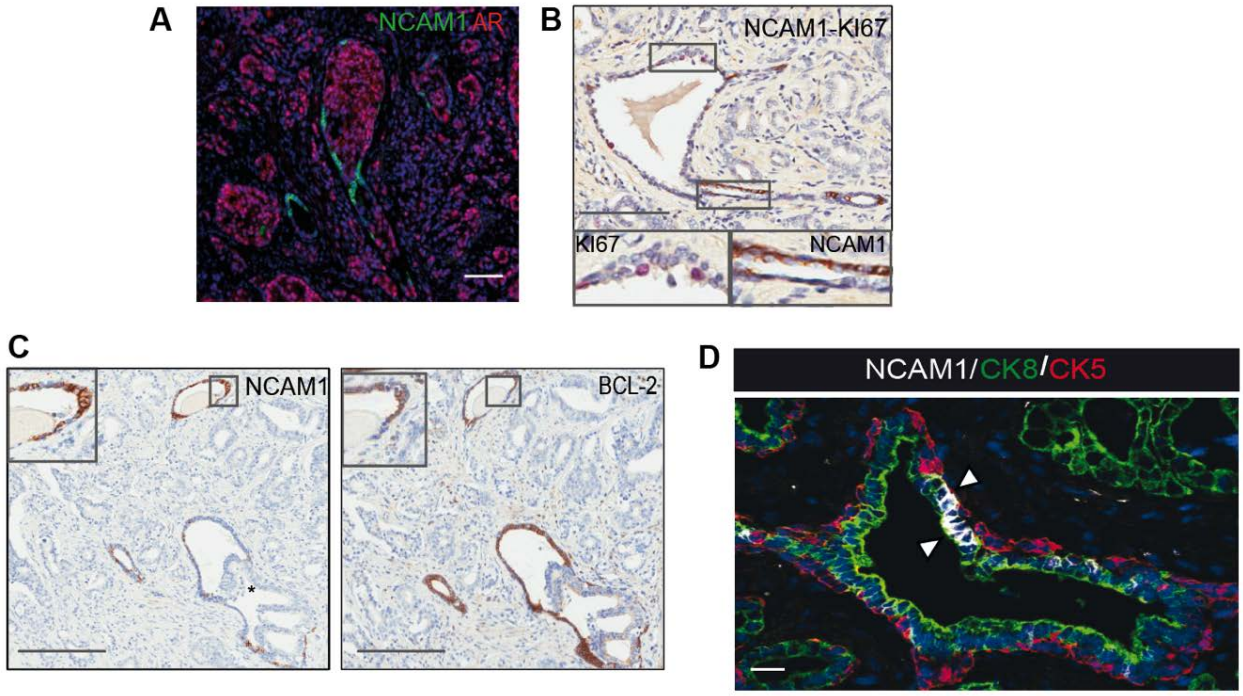

Figure 2. Characterization of NCAM1^{+} cell threads lacking NE marker expression in PIA areas in human PCa. A) *Immunofluorescence (IF) for androgen receptor (AR, red) and NCAM1 (green) expression in a human prostate gland structure. Scale bar = 100 µm.* ***B)*** *Double IHC with NCAM1 (brown) and Ki-67 (red) showing the presence of actively proliferating cells in proliferative inflammatory atrophy (PIA)-structures also containing NCAM1^{+} cell threads. Scale bar = 100 µm. Boxed regions are magnified below.* ***C)*** *Serial IHC analysis of NCAM1-clusters with BCL-2, displaying co-expression of NCAM1 (left) and BCL-2 (right) in the same human prostate gland structures. Scale bar = 200 µm. Boxed regions are magnified on the upper left in each panel.* ***D)*** *IF of human prostate tissue section for NCAM (white), CK5 (red) and CK8 (green). The NCAM1^{+} cell thread is indicated with white arrows. Scale bar= 100 µm.*

The clinical relevance of different NCAM1 patterns was investigated in the entire cohort: negative, single cells (SCs), positive with < 9 clusters or with ≥ 9 clusters of at least four NCAM1^{+} cells. The presence of single NCAM1^{+} cells did not provide any prognostic information, as witnessed by the

similar rate of BCR between patients with tumors displaying only isolated NCAM1$^+$ cells and patients with tumors with no NCAM1$^+$ cells (Hazard Ratio (HR) = 0.84; p-value = 0.73) **(Fig. 3)**. In contrast, PCa patients whose tumors displayed PIA-associated clusters of at least four NCAM1$^+$ cells/cluster had a shorter BCR-free survival compared to patients with tumors showing only scattered NCAM1$^+$ single cells or no NCAM1$^+$ cells, regardless the number of NCAM1$^+$ clusters **(Fig. 3)**.

The sum of these results clearly showed that only NCAM1$^+$ cell clusters associated with PIA-structures are prognostically relevant to PCa, in contrast to NCAM1$^+$ single cells scattered in the tumor area. Thus, for the purpose of this study, we categorized tumors with PIA-associated NCAM1$^+$ cell clusters as NCAM1-positive (NCAM1^{POS}), while tumors with complete absence of NCAM1$^+$ cells or the presence of only single scattered NCAM1$^+$ cells were classified as NCAM1-negative (NCAM1^{NEG}) **(Fig. 3)**.

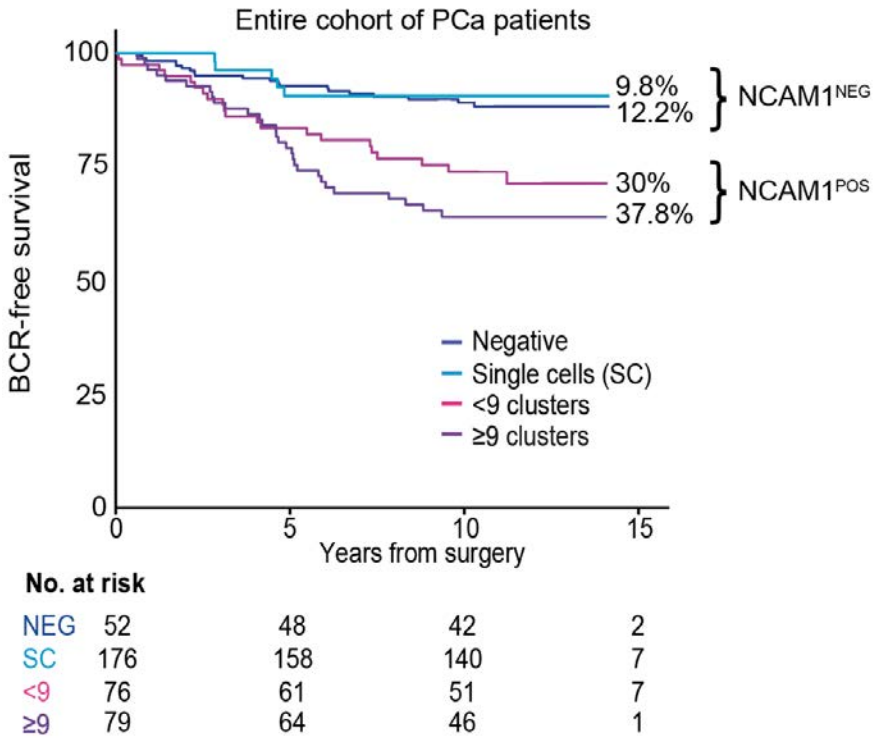

Figure 3. NCAM1 predicts BCR regardless of the number of NCAM1$^+$ clusters in the tumor.

The IEO(00-09) PCa cohort (N= 406) was screened for NCAM1 expression by IHC analysis using the NCAM1 antibody on FFPE samples. PCa patients were divided into 4 categories established according to the presence of NCAM1$^+$ cells and their respective distribution pattern in the tumors: 1) no NCAM1$^+$ cells (negative); ii) tumors containing only single NCAM1$^+$ cells; iii) tumors with less than 9 NCAM1$^+$ PIA-associated clusters; iv), tumors with 9 or more NCAM1$^+$ PIA-associated clusters. Kaplan-Meier curves of biochemical recurrence (BCR)-free survival for the PCa patients stratified by the 4 NCAM1 expression patterns for the entire follow-up period are shown. No. at risk, number of patients at risk at the indicated time points. Patients with tumors with no NCAM1 expression or with only single NCAM1$^+$ cells had a similar prognosis and were classified as NCAM1-negative (NCAM1^{NEG}). Patients with any number of NCAM1$^+$ PIA-associated clusters had a worse prognosis and were classified as NCAM1-positive (NCAM1^{POS}).

We used the Cox proportional hazard regression model to evaluate whether the presence of PIA-associated NCAM1^{+} clusters is prognostic in the prediction of BCR or distant metastasis (DM) in individual PCa patients. Patients with PIA-related NCAM1^{+} clusters had an increased probability of developing BCR and DM (34.7% and 13%, respectively) compared with NCAM1^{NEG} patients (11.1% and 2.5%, respectively), in the 15-year follow up period. The HR in a multivariate analysis for BCR was HR*=3.05 (p-value < 0.0001), while for DM it was HR*=3.55 (p-value = 0.014) **(Fig. 4A,B)**. The prognostic value of NCAM1^{+} PIA clusters was maintained in low/intermediate and in high/very-high risk groups defined by clinicopathological features (pT, Gleason grade, PSA levels). In the low-intermediate group, NCAM1^{POS} patients were more prone (15.6%) to undergo BCR than NCAM1^{NEG} (2.6%) at 15 years post-surgery. Similarly, in the high/very-high group, BCR was higher in NCAM1^{POS} (42.1%) than in NCAM1^{NEG} patients (21.9%) **(Fig. 4C,D)**.

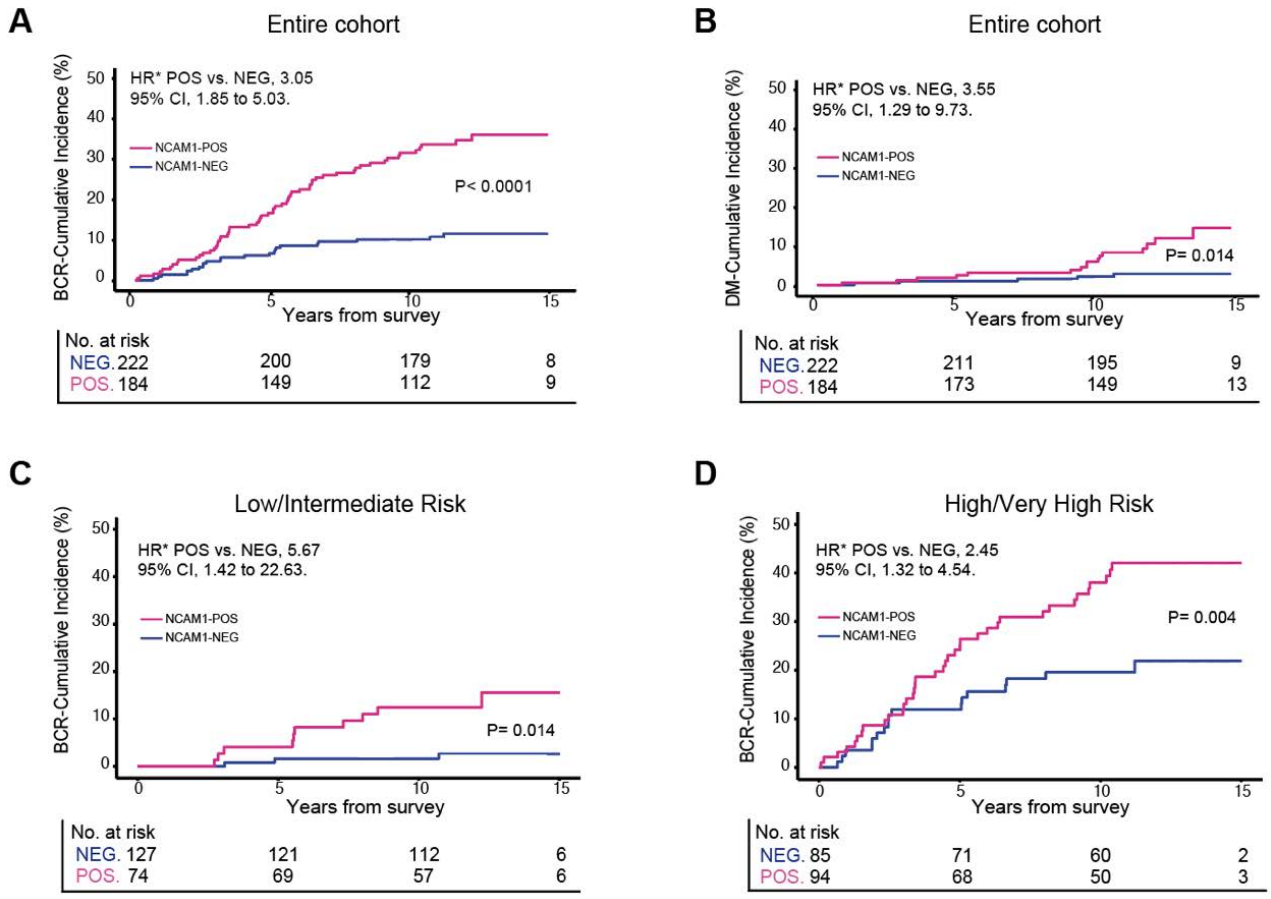

Figure 4. Stratification of PCa patients by NCAM1 status. A-D) *Kaplan-Meier analysis of biochemical recurrence (BCR) or distant metastasis (DM) cumulative incidence (%) in the IEO(00-09) PCa cohort (n=406) stratified by NCAM1 status. Neg: NCAM1^{-}; Pos: NCAM1^{+} (i.e., PIA-related clusters); HR*: hazard ratio from multivariable analysis adjusted for Gleason grade, pathological tumor stage (pT), lymph node metastasis (pN), preoperative PSA levels, perineural invasion (PNI), vascular invasion (VI), age and surgical margins; No. at risk: number of patients at risk*

In defining clinical risk groups, surgical margins are not typically considered despite the strong association between positive margins and loco-regional relapse. However, we found that patients with positive surgical margins (R1) and NCAM1^{+} PIA clusters had a 63.2% risk of BCR over 15 years, while NCAM1^{NEG} R1 patients had a much lower risk (14.8%) **(Fig. 5A)**. Interestingly, comparing patients with negative surgical margins (R0) and those with positive surgical margins (R1), we noted that NCAM1^{NEG} R0 patients had the same risk to develop BCR as NCAM1^{NEG} R1 patients (HR* = 1.01) suggesting that the latter patients could be safely followed by AS without proceeding to standard cancer therapies **(Fig. 5B)**.

Moreover, currently pT2-3 tumors with positive margins but without lymph nodes invasion (pT2+pT3, R1, N0) are suitable candidates for adjuvant radiotherapy (RT) after RP. Within this subgroup, NCAM1^{NEG} patients exhibited lower rates of BCR (~12%) 15 years post-surgery in comparison to NCAM1^{POS} patients (~59%) (HR = 6.32; p-value = 0.0002) **(Fig. 5C)**, suggesting that NCAM1^{NEG} patients could avoid RT exposure.

Furthermore, in a mini-cohort of 75 PCa patients, contained in the original cohort, we uncovered a strong overall concordance between NCAM1 status (87.6%; Cohen's kappa = 0.732, p-value<0.0001) in the primary tumor after RP and in the original diagnostic biopsy **(Fig. 5D)**, indicating that NCAM1 can be used for risk stratification at the initial diagnosis.

Thus, NCAM1 status is a valuable prognostic-predictive biomarker and is an informative marker in the decision-making process of adjuvant therapies after RP for the individualized management of PCa patients.

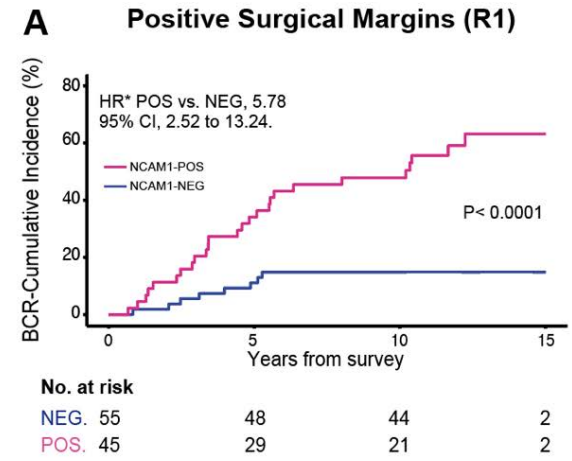

B

		R1			
		NCAM1+		NCAM1-	
		HR multivariable (95% CI)	*P*-value	HR multivariable (95% CI)	*P*-value
R0	NCAM1+	2.38 (1.38;4.11)	0.0018	0.46 (0.21;1.00)	0.05
	NCAM1-	5.25 (2.62;10.52)	<.0001	1.01 (0.41;2.47)	0.98

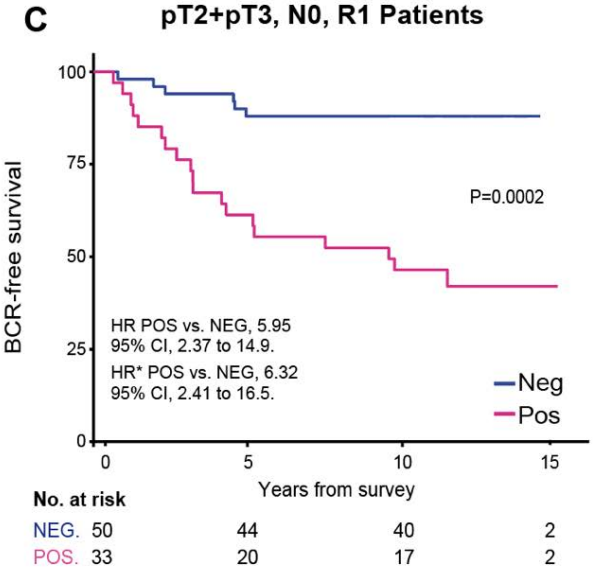

D

		BIOPSIES		
		NCAM1+	NCAM1-	TOTAL
RP	NCAM1+	36	7	43
	NCAM1-	3	29	32
TOTAL		39	36	75
		Concordance = 87.6% Kappa di Cohen = 0.732		P<.0001

Figure 5. Stratification of PCa patients with positive margins (R1) by NCAM1 status. ***A)*** *Kaplan-Meier analysis of biochemical recurrence (BCR) cumulative incidence (%) in a subcohort of patients from the IEO(00-09) PCa cohort with positive surgical margins, R1 (n=100) stratified by NCAM1 status. Neg: NCAM1; Pos: NCAM1^{+} (i.e., PIA-related clusters); HR*: hazard ratio from multivariable analysis adjusted for Gleason grade, pT, pN, preoperative PSA levels, PNI, VI and age; No. at risk: number of patients at risk.* ***B)*** *Table comparing patients with negative (R0) and positive (R1) surgical margins, with both groups stratified by NCAM1 status. HR multivariable: hazard ratio from multivariable analysis adjusted for Gleason grade, pT, pN, preoperative PSA levels, PNI, VI and age. 95% CI (confidence interval).* ***C)*** *BCR-free survival of pT2+pT3 patients without lymph node invasion (N0) and positive surgical margins (R1) stratified by NCAM1 status. HR*: hazard ratio from multivariable analysis adjusted for Gleason grade, pT, pN, preoperative PSA levels, PNI, VI and age; No. at risk: number of patients at risk.* ***D)*** *Table reporting the agreement between NCAM1 expression in diagnostic biopsies and in radical prostatectomy (RP) samples in the PCa mini-cohort (n=75).*

4. HYPOTHESIS AND AIMS

4.1 Hypothesis

An urgent unmet clinical need in PCa is the identification of novel biomarkers with prognostic and therapeutic implications. In particular, biomarkers that can discriminate potentially indolent *vs.* aggressive tumors are necessary to guide clinical decisions on therapeutic options for PCa patients. CSCs endowed with potential for self-renewal, tumorigenicity and multidrug resistance, are the putative mediators of cancer therapy failure and tumor progression. In PCa, the definition of the PCSC subpopulation is still unclear. Therefore, the identification of biomarkers of PCSCs and the definition of the molecular mechanisms responsible for self-renewal and drug resistance are critical for the identification of prognostic biomarkers and the development of targeted therapies aimed at eradicating PCSCs and preventing tumor progression and relapse. Despite a growing number of proposed PCSC biomarkers in the literature (e.g., CD44, CD113, CD117. See section 2.3.4.1), none of them have proved to be clinically relevant so far. Our preliminary data shows that NCAM1 expression in cell clusters associated with areas of PIA behaves as independent biomarker that predicts PCa aggressiveness. Given our previous observation in breast cancer, showing that the CSC content of a tumor correlates with biological aggressiveness (Pece *et al.*, 2010), we hypothesized that NCAM1, which is currently accepted as a marker of the NE lineage in PCa, could be a potential PCSC biomarker with relevance to the clinical management of PCa patients.

4.2 Aims

The overall goal of this thesis was to test our hypothesis that NCAM1 is a clinically relevant PCSC biomarker. Specifically, we aimed to:

1. Characterize the biological function of NCAM1 in PCa using established PCa cell lines, mouse/human primary samples, and the transgenic PCa mouse model, TRAMP.
2. Deconvolute, by scRNA-Seq, the heterogeneity of the NCAM1$^+$ PCa cell population, which potentially includes *bona fide* PCSCs, progenitor cells and NE cells, to establish the hierarchy in the tumor cell population and to identify the PCSC-of-origin with self-renewal potential.
3. Determine the molecular mechanism sustaining the self-renewal ability of PCSCs to propose therapeutic strategies to block expansion of these cells.
4. Uncover the relevance of NCAM1 in therapy resistance focusing on ADT.
5. Characterize the molecular mechanisms that sustain drug resistance in NCAM1$^+$ cells in order to identify candidate targets for rationally designed therapies.

5. MATERIAL AND METHODS

5.1 Cell culture

The human androgen-sensitive PCa cell line LNCaP was cultured in Roswell Park Memorial Institute (RPMI)-1640 medium completed with 10% fetal bovine serum (FBS)-North American (NA), while the human androgen-insensitive PCa DU145 was cultured in Dulbecco's Modified Eagle Medium (DMEM) supplemented with 10% FBS-NA. Both media contained 1% stable glutamine and 1% Penicillin (PEN)-Streptomycin (STREP) (100 U/ml). To mimic ADT, LNCaP cells were cultured in RPMI-1640 supplemented with 15% charcoal-stripped serum, while DU145 cells were used as a negative control and cultured in DMEM with 10% charcoal-stripped serum. The established mouse TRAMP-derived cell lines, TRAMP-C1 and TRAMP-C2, were cultured in DMEM supplemented with 10% FBS-South American (SA), 5% please Nu-serum IV (BD Bioscience, #355104), 0.005 ng/ml recombinant human Insulin (Roche, #11376497001) and 10 nM dehydroisoandrosterone 3-acetate (DHEA, Sigma-Aldrich, #390089). All cells were cultured in a humidified atmosphere at 37°C and 5% CO_2.

5.2 Genetic manipulation

Lentiviral pGFP-C-Lenti vectors containing a construct for human *NCAM1* (OriGene) or a scrambled negative control were used to overexpress NCAM1 in the LNCaP cell line. Lentiviral pGFP-C-shLenti vectors containing a 29mer shRNA construct against mouse *NCAM1* (OriGene, #TL501438A) or a scrambled negative control (OriGene, #TR30021) were used to silence NCAM1 in TRAMP-C1 and TRAMP-C2 cell lines. In brief, $12x10^6$ 293T cells were plated in a 15 cm dish and transfected with PMDL (15 µg), REV (15 µg) and Vesicular stomatitis virus G (VSVG) protein (15 µg), along with the lentiviral vector (45 µg) using the calcium phosphate protocol. Culture medium of 293T cells was replaced by TRAMP-C1/C2 culture medium 6-8 h post-transfection and virus was harvested 24 h and 48 h later. Harvested medium was centrifuged at 500g for 5', filtered through a 0.45 µm Polyethersulfone (PES) filter and stored in aliquots at -80°C. TRAMP cell lines were plated at 100,000 cells in a 6-well plate 24 h before infection. Cells were subjected to 2 rounds of infection with 4 ml of virus-enriched medium containing 8 µg/µl polybrene (Sigma-Aldrich, #TR1003) and 2 nM DHT (Sigma-Aldrich, #D-073) over 8 h and, after 2 days of recovery, infected cells were selected with 2 mg/ml puromycin for 7 days. TRAMP-derived cell lines were always maintained with 1 mg/ml puromycin.

The LNCaP cell line overexpressing NCAM1, in the absence of GFP expression, was obtained by stable transfection with a pcDNA 3.1 vector containing a construct for human *NCAM1* by Lipofectamine 3000 (Invitrogen, #L3000015), following the manufacturer's instructions. Cells positively transfected were selected by puromycin and then sorted by Fluorescence-activated cell sorting (FACS) based on the expression of NCAM1. Clones were then amplified and the more stable clone expressing NCAM1 were routinely cultured in RPMI supplemented with 15% FBS-NA. The control LNCaP empty vector (EV) cell line was established in parallel by transfection with an empty plasmid following the same procedure.

The *NCAM1* gene was knocked out (KO) in LNCaP and DU145 cells using the NCAM1-CRISPR/CAS9-KO plasmid (SantaCruz, #sc-400302-KO-2). Cells were double transiently transfected (the second transfection was performed 24 h after the first transfection) using Lipofectamine 3000, following the manufacturer's instructions, and then used for experiments.

siRNAs were transiently transfected using the Lipofectamine RNAiMAX transfection reagent (Thermofisher, #13778075) and were provided by Origene. siFGF18 (#SR305815); siFGFR2 (#SR320162); siFGFR1 (#SR320159); siDNER (#SR314218); siRBPJK (#SR320629).

5.3 Flow cytometry and FACS analysis

LNCaP and DU145 cells were detached from culture plates using trypsin-EDTA (Lonza, #BE17-161E) while TRAMP-derived PCa were digested as reported in the section 5.7. Obtained single cells were resuspended in FACS blocking solution (Leibovitz's L-15 medium, Gibco, #31415-029, containing 1.5% BSA). Cells were stained for 15' at 4°C with the following antibodies, at the manufacturer's suggested concentration: NCAM1/CD56-APC (BD, #341027); NCAM1/CD56-PE-Cy7(BD, #335826); CD117-APC (BD, #553356); c-KIT/CD117-PE (Beckman Coulter, #104D2D1); PROM1/CD133-PE (MACS Miltenyi Biotec, #AC141); CD44-APC (BD, #17712); CD44-PE (BD, #555479); CD38-PE (BD, #555460); CD166-FITC (ThermoFisher, #MA5-23565). Cells were washed and resuspended in Leibovitz's L-15 medium with EDTA (2 mM) and processed with the BD Influx™ cell sorter and BD FACS™ software (BD Biosciences).

5.4 3D organoids and the serial propagation assay

Cells isolated by FACS were resuspendend in 1 ml of cell culture medium supplemented with Matrigel 8% (BD Matrigel Matrix Growth Factor Reduced, #354230) and plated in 6-well plates. Each well had previously been covered with 450 μl of Matrigel (100%) that had been let to become stiff at 37°C, for 5'. After 24 h, cell culture medium was added in each well. At 8-10 days, the number

of obtained organoids was determined using an EVOS M5000 microscope, counting only organoids with a minimum diameter of 70 μm. The organoid-forming efficiency (OFE) was determined as the ratio between number of obtained organoids and the number of plated cells. For the serial propagation assay, medium was removed from each well and organoids embedded in the Matrigel were scrapered and resuspended in 700 μl of Cell Recovery Solution (Corning, #354253) and left at 4°C, until the Matrigel had been dissolved. Then, the organoids were isolated by centrifugation at 1800 rpm for 5', resuspended in Phosphate-buffered saline (PBS) ph 7.4 and filtered with a 70 μm cell strainer. The unfiltered organoids were reduced to single cells with 1ml trypsin-EDTA, then counted and re-plated at the same number as the first generation, with the same procedure as before. Each serial passage was performed with the same protocol.

5.5 Patient-derived organoids

RP tissues, collected by the IEO biobank with the patients' informed consent, were digested in DMEM/F-12 (1:1) culture medium (Lonza, #BE12-614F/Invitrogen, #31765-027) containing 100 U/ml penicillin-100 µg/ml streptomycin (P/S) (Lonza, #17-602E), amphotericin B (Sigma, #A2942), 2 mM L-glutamine (Lonza, #BE17-605E), 100 U/ml collagenase IV (Life Technologies, #17104-019), and 100 U/ml hyaluronidase (Sigma-Aldrich, #H3884) for 5 h at 37°C. Samples were centrifuged at 2300 rpm for 5' and the pellet was resuspended in trypsin-EDTA (Lonza, # BE17-161E), syringed with an 18G needle (BD Medical) and filtered through a nylon mesh filter with 70 µm pore size (Millipore). Filtered aggregates were syringed with a 21G needle and filtered with 40 µm mesh filter. Trypsin-EDTA was inactivated with DMEM supplemented with 10% FBS, 1% L-glutamine and PEN/STREP and the samples were filtered through a 20 µm filter to obtain a single cell suspension. Single cells were subsequently stained with mouse conjugated antibodies: EpCAM-APC (BD Biosciences, #34720) and NCAM1/CD56-PE-Cy7(BD Biosciences, #335826) were employed to isolate cells from a tumor bulk population. That cells were plated in a drop with 4-parts of Matrigel and 1-part keratinocyte serum-free medium (KSFM) supplemented with 5 ng/ml Epidermal growth factor (EGF) (Sigma Aldrich, #E5036), 2 nM DHT (Sigma-Aldrich, #D-073) and 10 µM Y-27632 (ROCK-inhibitor, Sigma–Aldrich, #Y0503). Drops were left to become stiff at 37°C and then covered with KSFM complete medium. After 48 h, medium was removed and drops were covered with DMEM medium with 10% FBS-NA, 5 ng/ml EGF, 2 nM DHT and 10 µM Y-27632. The patient-derived organoids (PDOs) were left to grow for 10 days and then all counted using the EVOS M5000 microscope. For each biopsy, associated clinicopathological information, including tumor size, tumor stage T (pT), and Gleason score (primary and secondary), was available.

5.6 TRAMP mouse model and tissue collection

TRAMP containing the PB-Tag Line 8247 transgene, were kindly gifted by Dr. Matteo Bellone (San Raffaele Hospital, Milan, Italy). The strain was maintained by breeding TRAMP hemizygous females with C57BL/6 males obtained from the Charles River Laboratories (Italy). For transplantation experiments, TRAMP female breeders in pure C57BL/6 background were mated with non-transgenic FVB male mice (Envigo Rms Srl, Italy) to generate a hybrid background F1 (C57BL/6xFVB). Mice were sacrificed by CO_2 inhalation between 25 and 35 weeks of age. All animal procedures described in this thesis were performed at the IEO animal facility in compliance with the Italian Law (Legislative Decree 26/2014), which enforces EU Directive 2010/63 ruled by the European Parliament and the Council on 22 September 2010 for the protection of animals used for scientific purposes (IACUCs Nº 761/2015).

For histological and immunofluorescence (IF) studies, prostates were fixed during 4-6 h in 4% formalin and stored in 70% ethanol until they were processed and embedded in paraffin. Hematoxylin & Eosine (H&E) of entire prostate tissue was performed and using Aperio Image scope, a pathologist demarcated the tumor area using a pattern recognition software tool (Genie, Leica Biosystems) that was trained to segment the tumor area to precisely determine the total tumor area (μm^2).

5.7 TRAMP mouse-derived 3D organoids and *in vivo* outgrowths

TRAMP tumors were digested in DMEM/F-12 (1:1) (Lonza, #BE12-614F/Invitrogen, #31765-027) containing 100 U/ml penicillin-100 µg/ml streptomycin (P/S) (Lonza, #17-602E), 2 mM L-glutamine (Lonza, #BE17-605E), 100 U/ml collagenase IV (Life Technologies, #17104-019), 100 U/ml hyaluronidase (Sigma-Aldrich, H3884) and 10 µM Y-27632 (ROCK-inhibitor, Sigma–Aldrich, #Y0503) for 4-5 h at 37°C. After digestion, tumors were centrifuged at 700 g for 5' and red blood cells were removed with ACK Lysing Buffer (Lonza, #10-548E) for 1' at room temperature (RT). Then, the pellet was resuspended in trypsin-EDTA (Lonza, #BE17-161E), syringed with an 18G needle (BD Medical) and filtered through a nylon mesh filter with 70 µm pore size (Millipore). Filtered aggregates were syringed with a 21G needle and filtered with 40 µm mesh filter. Trypsin-EDTA was inactivated with DMEM supplemented with 10% FBS, 1% L-glutamine and PEN/STREP and filtered through a 20 µm filter to obtain a single cell suspension. Single cells were subsequently stained with mouse conjugated antibodies: EpCAM-PE (cl. G8.8, #4303743, eBioscience) and NCAM1-APC (#FAB7820A, R&D systems).

For organoid culture, cells isolated by FACS were mixed with the same number of mouse urogenital sinus mesenchymal (UGSM, see section 5.8) cells and resuspended in Matrigel (BD 354234) and Prostate Epithelial Culture Medium (PECM) in a 3:1 ratio. The mixture of cells and Matrigel:PECM was pipetted in drops in a culture dish and the plate was placed at 37ºC for 10' to allow the Matrigel to solidify. Subsequently, the drops were covered with DMEM, supplemented with 10% FBS and 10 μM Y-27632 for 48 h to increase cell viability. Finally, organoids were grown for 15 days in PECM and medium was refreshed every 4-5 days. PECM medium contains 1% L-glutamine, 1% P/S, 5 ng/ml EGF (Tebu-Bio 100-15), 50 μg/ml Bovine Pituitary Extract (BPE) (Life Technologies, #13028014), 30 ng/ml Cholera toxin (Sigma-Aldrich, #C8052), 10 μM Y-27632 and 2 nM DHT (Sigma-Aldrich, #D-073) in keratinocyte serum-free medium (Gibco, #17055-034).

For *in vivo* transplantation, FACS sorted tumor cells derived from TRAMP tumors were combined with same number of UGSM cells (~50,000-100,000 total cells), resuspended in 30 μl of Matrigel:PECM (3:1) and pipetted in drops in a culture dish. Drops were placed in a 37°C incubator for 15-20' to allow solidification and incubated with pre-warmed DMEM medium containing 10% FBS-NA, 1% PEN/STREP, 1% L-Glutamine, 10 μM Y-27632 and 2 nM DHT until subcutaneous transplantation in NOD SCID IL-2R-γnull (NSG) mice. Recipient mice were supplemented with midscapular implantation of Azalet osmotic minipumps (model 2004, 0.25 μl/h, Charles River Laboratories, #0010197657) filled with 200 μl of testosterone propionate (Sigma-Aldrich, #86541-5G). Testosterone powder was dissolved at 75 mg/ml in pure ethanol and stored in aliquots at -80°C. Prior to pump implantation, testosterone was diluted in PEG-400 (Sigma-Aldrich, #202398) to a final concentration of 23.2 mg/ml. Osmotic pumps were replaced every 28 days. The TRAMP-C1/2 cell lines were embedded in 100 μl of Matrigel and Prostate Epithelial Culture Medium (PECM) and transplanted in the two flanks of NSG mice. All outgrowths were monitored by routine palpation and tumor volumes were determined by external caliper. Mice were sacrificed by carbon dioxide (CO_2) inhalation when tumors reached 0.8 cm of diameter and sacrifice time was considered the time of the event.

5.8 Urogenital sinus mesenchymal cell preparation

Mouse UGSM were cultured in DMEM 10% Nu serum IV (BD Biosciences, #355104), 1% L-glutamine, 1% PEN/STREP and 2 nM DHT (Sigma-Aldrich, #D-073) and passaged for no more than 5 times.

5.9 TRAMP-NCAM1$^{-/-}$ genetic mouse model

The TRAMP-NCAM1$^{-/-}$ mouse colony was obtained by crossing a TRAMP transgene (TG) female breeder in a pure C57BL/6 background with a male NCAM1$^{-/-}$ (B6.129P2-Ncam^{tm1Cgn}) mouse provided by Charles River Laboratories. The colony was maintained by breeding a male NCAM1-heterozygous (HE) with a female NCAM1 (HE)-TRAMP (TG). The genotype for NCAM1 and the large-T-antigen (employed as control of TRAMP colony) was checked for each progeny obtained by PCR, with these assays:

NCAM1 (GATGGTTGGAGGCAGGGAGCTGACC; TGCAATCCATCTTGTTCAATGGCCG; CCTGGAGCTGAAATCCAGGCATCAGAG),

*T-antigen (*GCGCTGCTGACTTTCTAAACATAAG; GAGCTCACGTTAAGTTTTGATGTGT; CTAGGCCACAGAATTGAAAGATCT; GTAGGTGGAAATTCTAGCATCATCC).

5.10 NOD-SCID mouse xenografts

NCAM1^{+} Sorted cells form PCa cells lines (LNCaP and DU145) and LNCaP-EV or LNCaP-NCAM1-OE cells were pelleted and resuspended in 10 µl of collagen type I solution prepared as follows: 250 µl of collagen type I rat tail 4 mg/ml (Corning, #354236) mixed with 28.4 µl of 10x PBS and 5.8 µl of 1N NaOH. Collagen I solution was left on ice for at least 10' before use and it was prepared fresh each time. The mixture of cells and collagen was pipetted in drops in a culture dish and the plate was placed at 37ºC for 15-20' to allow the collagen to solidify. Subcutaneous transplantation of collagen drops was performed in 8-12-week-old NSG male mice, bred in-house and previously anesthetized with isoflurane. Outgrowths were monitored by routine palpation and tumor volumes were determined by external caliper. Mice were sacrificed by carbon dioxide (CO_2) inhalation when tumors reached 0.8 cm of diameter and sacrifice time was considered the time of the event. For the limiting dilution assay (LDA), the tumor initiating cells (TICs) frequency was calculated using the ELDA linear regression method (http://bioinf.wehi.edu.au/software/elda/). The accuracy of this test was determined by the correlation coefficients (R^2 values) and provides 99% confidence intervals to compare TIC numbers between samples.

5.11 Immunofluorescence and immunohistochemistry

Prostate tissue and tumors were fixed with 4% formalin for 4-6 h and embedded in paraffin for histological and IHC analysis. IHC was performed on 3-µm-thick sections using a Bond Max Automated Immunohistochemistry Vision Biosystem (Leica Microsystems GmbH, Wetzlar, Germany). First, tissues were deparaffinized and pre-treated with the Epitope Retrieval Solution

(Leica Biosystems, #AR9961) (ER1 pH6 for human NCAM1 and murine Ki-67; and ER2 pH9 for SYN, BCL-2, SV40 Large T-antigen and human Ki-67) at 100°C for 20'. After washing steps, peroxidase blocking was carried out for 10' using the Bond Polymer Refine Detection Kit DC9800 (Leica Microsystems GmbH). Then, tissues were washed and incubated for 15' with the primary antibody diluted in Bond Primary Antibody Diluent (Leica Biosystems, #AR9352). Subsequently, tissues were incubated with DAB-Chromogen for 10' and counterstained with Hematoxylin for 5'. For image acquisition and analysis, eSlide Manager (Aperio Technologies, Vista, CA) was used. The antibodies used for IHC staining were: NCAM1 (Novocastra, #NCL-L-CD56-504; SantaCruz, #sc-7326), Bcl-2 (Cell Signaling Technology, #15071), Ki-67 (DAKO, #M7240; Abcam, #ab16667), Large T-Ag (BD Biosciences #554149), Androgen Receptor (DAKO, #M3562), CD38 (SantaCruz, #sc-374650), CD133 (Thermofisher, #PA5-82184), CD117 (c-kit) (DAKO, #A4502), CD44 (Abcam, #ab157107), CD166 (Abcam, #ab109215), CHGA (R&D, #MAB90981).

For immunofluorescence (IF) staining of cells, cells were cyto-spinned on SuperFrost Plus adhesion slides (ThermoFisher) at 1000g for 4'. Then cells were surrounded by DAKO Pen and fixed in paraformaldehyde (PFA) for 10'. Cells were permeabilized with 0.2% Triton X-100 for 2' and blocked with 5% BSA + 10% Normal Donkey Serum (Li-Starfish, 017-000-121) for 1 h. Cells were incubated overnight at 4°C with primary antibodies in blocking solution, then washed 2 times with PBS and incubated with Alexa-labeled secondary antibody (Cy3 Donkey anti-rabbit or anti-mouse 1:400). They primary antibodies used for the staining were: NCAM1 (SantaCruz, #sc-7326; R&D systems, #MAB7820), Ki-67 (Abcam, #ab833), Cleaved-caspase-3 (Cell Signaling Technology, #9661), β-galactosidase (Cell Signaling Technology, #27198).

For IF staining of tissue sections, samples were deparaffinized, permeabilized with 0.1% Triton X-100 for 2' and blocked with 5% BSA + 1% Normal Donkey Serum (Li-Starfish, #017-000-121) for 1 h. Sections were incubated overnight with primary antibodies in blocking solution at 4°C, then washed with cold PBS three times for 3' each, and incubated with Alexa-labeled secondary antibody (Alexa488 Donkey anti-mouse 1:100, Invitrogen A-21202; Cy3 Donkey anti-rabbit 1:400, Li-Starfish 711-165-152; Alexa647 Donkey anti-rat 1:100, Li-Starfish J712-605-153 and Alexa647 Donkey anti-goat 1:100, Invitrogen #A-21447) at room temperature for 45'. They primary antibodies used for the staining were: NCAM1 (SantaCruz, #sc-7326; R&D systems, #MAB7820); Synaptophysin (Abcam, #ab16659); Chromogranin-A (SantaCruz, #sc-1488); Androgen Receptor (SantaCruz, #sc-816); Cytokeratin-8 (CK8, Produced in our facility); Cytokeratin-5 (CK5, Abcam, #ab53121); p63 (DAKO, #M7317); Vimentin (Abcam, #ab8069); Cytokeratin-14 (CK14, Covance, #PRB-155P-100); E-Cadherin (Abcam, #ab76055); Cytokeratin-18 (CK18, Cell Signaling Technology, #4548); Ki-67 (Abcam, #ab833).

For IF of cryopreserved tissue, samples were fixed with 4% PFA, permeabilized with 0.1% Triton X-100 for 2' and blocked with 3% BSA plus 1% Normal Donkey Serum (Li-Starfish, #017-000-121) for 1 h, and then processed as described above.
IF was detected by confocal microscopy (Leica TCS SP5 microscope system) using oil-immersion objectives under the control of LSA AF Software (Leica) and with a Leica DM6 Fluorescence Microscope. Image processing was performed using ImageJ software.

5.12 Senescence β-galactosidase staining

The Senescence β-galactosidase staining kit (Cell Signaling Technology, #9860) were employed to detect β-galactosidase enzyme activity at pH 6. Briefly, ADT-treated and untreated LNCaP and DU145 cells were washed on time with PBS, then fix for 10-15' with Fixative Solution. The β-galactosidase staining solution was added and cells where incubated at 37°C overnight in a dry incubator without CO_2. Blue-positive cells were acquired by microscope at magnification 200X.

5.13 Whole-cell lysis and western blot

Cells were harvested by scraping, washed twice in ice-cold PBS, resuspended in lysis buffer Tris-HCl ph 8.00 (NaCl 150 μM, 1% NP-40, Tris-HCl 50 mM) supplemented with phosphatase inhibitors (20 mM sodium pyrophosphate, 2 mM PMSF, 10 mM sodium orthovanadate, 50 mM sodium fluoride) and complete Mini EDTA-free Protease Inhibitor Cocktail (Roche, #0469315900) for 30' on ice, then centrifuged at 10,000g for 10' at 4°C. Protein concentration in supernatants was quantified with the BCA protein assay (Pierce BCA, ThermoFisher). Protein (at least 30 µg) was prepared in Laemmli 1x buffer (2% SDS, 62.5 mM Tris-HCl, pH 6.8, 10% glycerol, 0.1% bromophenol blue, 5% β-Mercaptoethanol) and resolved on polyacrylamide gel with an acrylamide:bis ratio of 30:0.8 and transferred to a nitrocellulose transfer membrane (Bio-Rad) at 25V and 1.3A for 11' in a Trans-Blot Turbo Transfer System (Trans-Blot® Turbo Bio-Rad). Membranes were blocked, for at least 1 h in agitation, with 5% non-fat dry milk (PanReac Applichem, #8V015284), dissolved in TBS-Tween 0,1% and incubated overnight at 4ºC with primary antibodies for: NCAM1 (SantaCruz, #123C3); β-Tubulin (ThermoFisher Scientific, #MA5-16308); GAPDH (Cell Signaling Technology, #5174,); pMAPK p44/p42 (Cell Signaling Technology, #4370); MAPK p44/p42 (Cell Signaling Technology, #4695), Cleaved-Notch1(Val1744, Cell Signaling Technology, #4147); Notch1 (Cell Signaling Technology, #3608); pFGFR1 (Tyr653/654, Cell Signaling Technology, #3471), FGFR1 (ThermoFisher, #13-3100); Nicastrin (Cell Signaling Technology, #5665); FGFR2 (GeneTex, #GTX25476); pFGFR2 (Ser782, ThermoFisher, #PA-64796); Vinculin

(Sigma, #05-386); Androgen Receptor (SantaCruz, #sc-816); Vimentin (Abcam, #ab8069); E-Cadherin (Abcam, #ab76055); N-Cadherin (Abcam, #76011). Horseradish peroxidase conjugated-secondary antibodies were used with standard procedures. Membrane images were acquired with Chemidoc and analyzed with ImageLab software.

5.14 Co-immunoprecipitation

Seeded cells in 100 mm-plates were harvested and lysed as described above (Section 5.12). Cleared lysate (800 μg total protein) was used for co-immunoprecipitation (co-IP) assay. Sepharose-A beads (100 μl) were washed twice with 1 ml of Tris-HCl buffer ph 8.00 (NaCl 150 μM, 1% NP-40, Tris-HCl 50 mM) on a rocking wheel for 5' at 4°C. Antibody (2 μg) against the protein being immunoprecipitated was added to the lysate and the sample was left rocking for 1 h, at 4°C. Fresh washed beads were added to the lysate and the sample was incubated on the rocking wheel overnight at 4°C. The protein-antibody complexes linked to the beads were precipitated at 1000g for 5' and eluted by adding 40 μl of Laemmli SDS sample buffer (1X) and incubating at 95°C for 10'. Twenty μl of each sample was analyzed by western blot. As controls, a parallel co-IP was performed with a non-specific IgG antibody and without adding antibody to the lysate (indicated as "Beads"). The primary antibodies used for the co-IP were: NCAM1 (Sino Biological, #10673-T52); FGFR2 (GeneTex, #GTX25476); pFGFR2 (Ser782, ThermoFisher, #PA-64796); Nicastrin (Cell Signaling Technology, #5665); Notch1 (Cell Signaling Technology, #3608).

5.15 RT-qPCR

Total RNA was extracted from cells and retro-transcribed into cDNA with a TaqMan Fast Advanced Cells-to-Ct kit (Thermofisher). After 10 cycles of pre-amplification, RT-qPCR reactions were performed with Taqman Assays and TaqMan Fast Advanced MasterMix (Thermofisher). The assays employed were the following: *MKI67* (hs00606991)*; P21/CDKN1A* (hs00355782); *P27/CDKN1B* (hs00153277)*; TP53* (hs00153349)*; GLB1* (hs01035168)*; P16/CDKN2A* (hs00233365)*; NCAM1* (hs00941830; mm00456815); *FGFR2* (hs01552926; mm01269930)*; NOTCH1* (hs00473187; mm00435245); *FGF18* (hs00826077; mm00433286); *DNER* (hs01039911; mm00548872); *SNAI2* (hs00161904); *AR* (hs00171172); *TP63* (hs00978340); *KRT5* (hs00361185); *KRT8* (hs01670053); *KRT18* (; *KRT19* (hs00761767); *NKX3-1* (hs00171834); *BCL2* (hs04986394); *CHGA* (hs00900370); *SYP* (hs00300531); *HES1* (hs00172878); *RBPJK* (hs00794653); *MAML2* (hs00418423); *JAG1* (hs01070032). C*t* values were obtained for each gene in technical triplicate in each biological

replicate (n≥3). The mean of each replicate was calculated and the the 2^-ΔC*t*. *GUSB*, *ACTB* and *TBP* were used as internal controls and for the normalization of the expression of each gene.

5.16 RNA extraction and sequencing

Total cellular RNA was extracted with the miRNeasy Kit (Qiagen) following the manufacturer's instructions, and the quality was assessed using the BioAnalyzer 2100. For each sample, the total RNA was depleted of ribosomal RNA with the Ribo-Zero rRNA Removal Kit (Illumina). The efficiency of ribosomal RNA removal was checked with the BioAnalyzer 2100. RNASeq libraries were prepared with the Illumina TruSeq Stranded Total RNA Kit, following the manufacturer's protocol. Briefly, after the fragmentation of RNA, cDNA is synthesized, 5'-end repaired and 3'-end adenylated. Following adapter ligation, libraries were amplified by PCR. Amplified libraries were checked by the BioAnalyzer and quantified with picogreen reagent. Libraries with distinct TruSeq adapter indexes were multiplexed. Sequenced raw reads were processed with the NF-CORE RNASeq pipeline (github.com/nf-core/rnaseq, version 3.1), using the human GRCh38 as reference genome. Transcript abundances were quantified using the Salmon pseudo-aligner. Differential expression of genes was tested with two-tailed Quasi-Likelihood F Test as implemented in the "edgeR" R package (version 3.34). P-values were FDR adjusted. Genes with an absolute log2(Fold Change) > 0.5 and an FDR adjusted p-value < 0.05 were considered as differentially expressed. Pathway analysis was performed by assessing the overrepresentation of upregulated genes annotated in each pathway with the hypergeometric test. Given the untargeted nature of RNAseq experiments, we defined all the genes annotated in the GRCh38 reference genome as background for the test. Gene annotations for the MSigDB Hallmark pathways (gsea-msigdb.org/gsea/msigdb/index.jsp) were retrieved with the "msigdbr" R package (version 7.5.1). Significantly enriched pathways (FDR adjusted p-value < 0.05) were ranked by their enrichment ratio (number of upregulated genes in the pathway/number of genes annotated in the pathway).

5.17 Receptor-Ligand interaction analysis

Autocrine signaling induced or upregulated by NCAM1 overexpression were identified by matching the list of upregulated ligands (Log_2(Fold Change) > 0.05 and adj p-value < 0.05) with the list of expressed receptors (mean Log_2(Transcripts Per Million (TPM)+1) > 0.1). Ligand-receptor pairs were obtained from the Fantom5 database (Ramilowski *et al.*, 2015). The most relevant interactions were ranked with a score accounting both the upregulation of the receptor and of the ligand (Interaction strength = Log_2(Ligand Fold Change) + Log_2(Receptor Fold Change).

5.18 Drug treatments

Organoids from NCAM1^{+} and NCAM1^{-} cells isolated from LNCaP and DU145 were treated with inhibitor when they reached 30 μm of diameter, measured by the EVOS M5000 microscope through a scale bar. Then, the growth of treated organoids was monitored for up to 10 days to determine the OFE and serially propagated, as previously described (Section 5.4), without any more treatment. The same protocol was used for pharmacological pathway inhibitors: DAPT [30 μM] (Notch-1 inhibitor; #S2215); dovitinib [6 μM] (TKI-258, CHIR-258; Class III, IV,V RTK-inhibitor; #S10118); AZD4547 [5 μM] (FGFR inhibitor; #S2801); bicalutamide [5 μM](AR inhibitor; #B9061); Cyclopamine [5 μM] (Smo inhibitor; #ab120392); GANT61 [20 μM] (GLI1/2 inhibitor; #G9048) all provided by Selleckchem, while bicalutamide was provided by Sigma Aldrich. As a control, organoids were treated with vehicle DMSO.

The isolated NCAM1^{+} and NCAM1^{-} cells from untreated and ADT-treated (for 5 days) LNCaP, DU145 and human primary PCa cells were treated with a purified anti-NCAM1 (#123C3) antibody [1.4 μg/μl], kindly provided by Dr. Ugo Cavallaro (IEO, Milan, Italy), for 1 h, at 4°C, in L15 medium + 1.5% BSA. Then, cells were cultured in Matrigel for organoid formation, following the previously protocols (Section 5.4). OFE was determined by counting organoids with the EVOS microscope. LNCaP NCAM1-OE and -EV cells were treated *in vitro* with recombinant human FGF18 (rhFGF18) [500x] (Peprotech, #100-28).

5.19 ELISA assay

An ELISA test specific for FGF18 (Mybiosource; #MBS912811) was performed following manufacturer's instructions. Briefly, cell culture supernatants were clarified from debris by centrifugation 15' at 1000g. Samples (100 μl) were added to each well of the ELISA plate, already pre-coated with antibody recognizing FGF18, and incubated for 2 h at 37°C. Then, 100 μl of biotinylated antibody was added in each well for 1 h at 37°C. After five washes with Wash-buffer, 100 μl of HRP-avidin was incubated for 1 h. After the addition of 90 μl TMB substrate and 50 μl of stop solution, the optical density was determined using a microplate reader with a wavelength set to 540 – 570 nm. Then, we averaged standard curve and sample data and subtracted the average zero standard optical density to establish the picogram (pg) of detected protein levels. Standard curve was generated by following manufacturer's instructions.

5.20 Single cell RNA-Sequencing

Libraries were generated through Chromium Next Single Cell 3' Reagent Kits v3.1 (Dual Index) (#PN-1000268). Gel-beads in emulsion (GEMs) (#PN-2000164) are conjugated with poly(dT) primer that enables the production of barcoded, full-length cDNA from poly-adenylated mRNA. GEMs were generated by combining barcoded Single Cell 3' v3.1 Gel beads, a Mater Mix containing cells and Partitioning Oil onto Next GEM Chip G. Following GEM generation, the Gel Bead was dissolved, primers were released, and any cell was lysed. Each primer contains an Illumina TruSeq Read 1, 16 nt 10x Barcode, 12 nt unique molecular identifier (UMI), 30 nt poly(dT) sequence. Primers were mixed with cell lysate and a Master Mix containing reverse transcription (RT) reagents. Incubation of the GEMs produces full-length cDNA from polyadenylated mRNA. After incubation, GEMs were broken, and pooled fractions were recovered. Silane magnetic beads were used to purify the first-strand cDNA from the post GEM-RT reaction mixture, which includes leftover biochemical reagents and primers. Full-length cDNA was amplified via PCR to generate sufficient mass for library construction. Enzymatic fragmentation and size selection were used to optimize the cDNA amplicon size. P5, P7, i7 and i5 sample indexes, TruSeq Read 2 are added via End Repair, A-tailing, Adaptor Ligation, and PCR. The final libraries contain P5 and P7 primers used in Illumina amplification. A Chromium Single Cell 3' Gene Expression Dual Index library comprises standard Illumina paired-end constructs which begin and end with P5 and P7. The 16 bp 10x Barcode and 12 bp UMI are encoded in Read 1, while Read 2 is used to sequence the cDNA fragment. NCAM1+ cells were isolated by FACS from DU145, LNCaP or a pool of primary prostate cancers and then immediately subjected to the 10X Single Cell Protocol for transcriptome determination through droplet-based single-cell RNA-seq methodology (10X Genomics Chromium, Macosko E., 2017). Cells were separated into droplet emulsion using the Chromium Single Cell 3' Solution (V3.1) and Single-cell RNA-seq libraries were prepared according to the Single Cell 3' Reagent Kits User Guide (V3.1). Libraries were sequenced on a Novaseq 6000 flowcell (Illumina), with a minimum depth of 50K reads/cell. FASTQ reads were aligned, filtered and counted through the Cell Ranger pipeline (v3.1). using standard parameters. Subsequently, 10X data matrix were imported into Seurat (v3) (Stuart *et al.*, 2019) and subjected to quality control and normalization. Specifically, we filtered out cells with less than 2000 detected features and more than 30% mitochondrial reads. Then, the standard Seurat pipeline was followed to log normalize the data, find the variable features, scale the dataset and perform PCA on scaled data. Cells were clustered and visualized according to a non-linear dimensional reduction approach (UMAP; dims 1:30). We calculated cell cycle phase scores based on canonical markers Seurat3. Finally, data were imported in the Cerebro application (v1.1) (Hillje, Pelicci and Luzi, 2020) for interactive visualization and including the optional trajectory analysis

(pseudo-timing) performed with Monocle (v2) (Trapnell *et al.*, 2014) . The assessment of pathway activity and the calculation of the STEM_SCORE was performed using the *AddModuleScore* module of Seurat3.

5.21 Patient selection

We used the retrospective-prospective cohort described in the Preliminary data. This cohort was comprised of 406 PCa patients (including the 75 patients used in the mini-cohort) that underwent RP at IEO between 2000 and 2009, who were metastasis-free at diagnosis and who did not receive neoadjuvant therapy. The analyses were truncated at 15 years from surgery. The clinicopathological characteristics of the patients are summarized in Table 17.

5.22 Statistical Analysis

The two-sided unpaired t-test and the one-way or two-way ANOVA tests were employed for comparisons, as indicated in the figure legends, and performed using the GraphPad software (v.6). Differences in the distribution of clinicopathological features between patient groups ($NCAM1^{POS/+}$ and $NCAM1^{NEG/-}$) were evaluated using univariate and multivariable logistic regression models. BCR-free survival and DM-free survival were estimated using the Kaplan–Meier method. Hazard ratios were estimated for the entire follow-up period using the Cox proportional hazards model. Multivariable models were adjusted for Gleason group, tumor size (pT), lymph node status (pN), PSA at surgery, margins, perineural invasion (PNI), vascular invasion (VI) and age at surgery. Subgroup analysis was performed to investigate possible differences in the prognostic power of NCAM1 status in the different subpopulations. Cohen's kappa and chi-square tests were performed to determine the correlation between NCAM1 status in primary tumors and in biopsies. All analyses were carried out with the R software (http://cran.r-project.org/). All reported p-values are two-sided.

6. RESULTS

6.1 NCAM1 is a novel biomarker of cells with stem cell traits in PCa

6.1.1 NCAM1 is expressed early in PCa development in TRAMP PCa

To investigate the biological function of NCAM1 and its role in PCa initiation and progression, we took advantage of the TRAMP PCa mouse model. TRAMP mice spontaneously develop prostate tumors with stages similar to human PCa progression (see section 2.2.11.3). Hematoxylin/Eosin (H&E) staining of TRAMP mouse prostate glands collected at each stage of disease progression starting from normal tissue and then going on to well-differentiated tumors (WDT), moderately-differentiated tumors (MDT) and poorly-differentiated tumors (PDT), revealed progressive modifications in the histological architecture of the glands, which appears progressively aberrant up to the PDT stage when it is completely altered **(Fig. 6A)**. At the molecular level, glands in WDTs express AR in luminal cells that are positive for CK8 (known luminal markers) **(Fig. 6B)**. These cells are surrounded by a few basal cells marked with the known basal markers p63 and CK14, without displaying the NE marker SYN **(Fig. 6B)**. Instead, PDTs have completely lost the expression of AR, and there was no detectable expression of luminal markers CK8 and the basal marker CK14, while only rare p63-positive cells were visible; however, there was a striking upregulation of the SYN NE marker indicative of NED in these tumors **(Fig. 6B)**. Furthermore, during tumor progression from WDT to PDT, epithelial traits (E-cadherin) are lost while mesenchymal traits (vimentin) and more basal traits are acquired **(Fig. 6C)**.

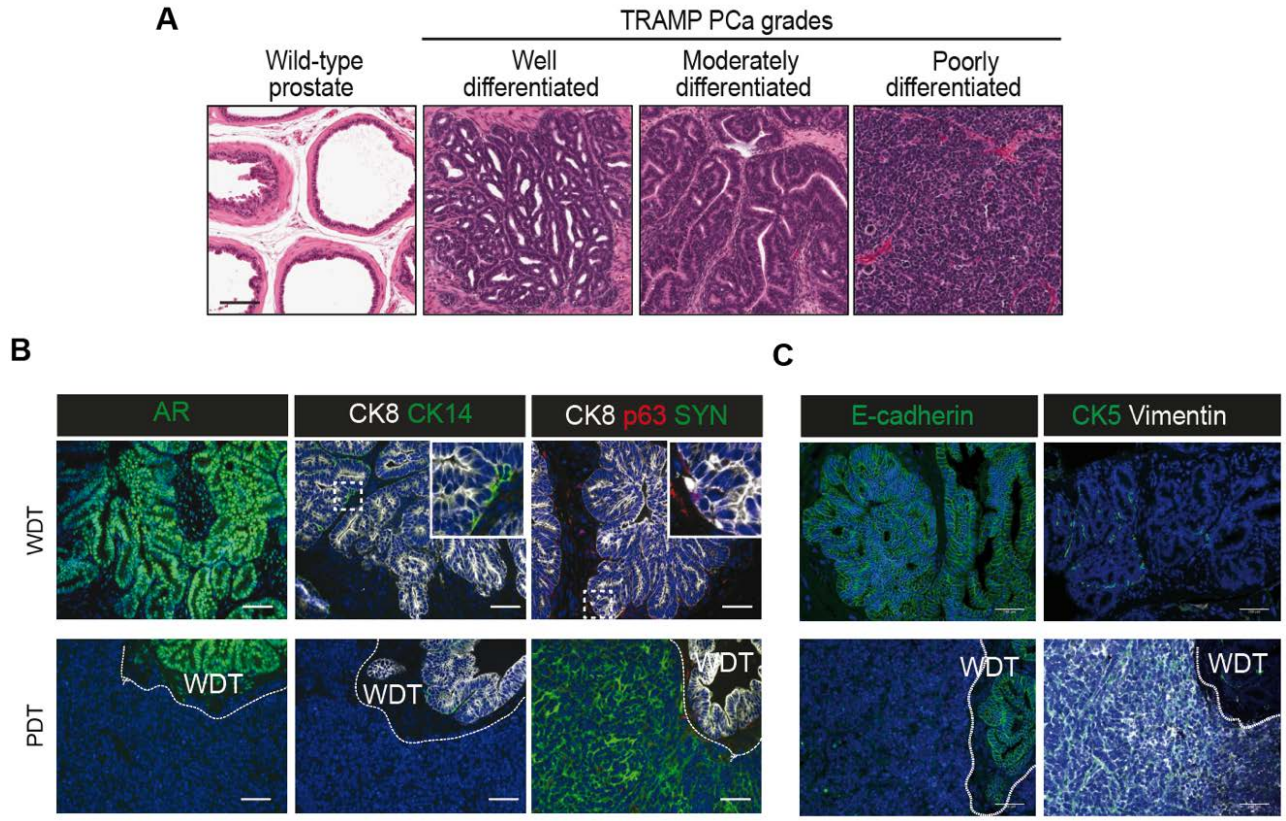

Figure 6. Characterization of the different stages of PCa development in the TRAMP mouse model. A) *Representative H&E staining of prostate tissue derive from TRAMP mice at different stages of PCa development. Scale bar=200 µm.* ***B-C)*** *Immunofluorescence characterization of a representative well-differentiated tumor (WDT) (upper panels) and a representative poorly-differentiated tumor (PDT) (lower panels) derived from the TRAMP mouse model. The expression of the luminal markers androgen receptor (AR) and cytokeratin-8 (CK8), the basal markers cytokeratin-14 (CK14) and p63 and the neuroendocrine marker synaptophysin (SYN) are shown in "B". The expression of the epithelial marker E-cadherin, the mesenchymal marker vimentin and the basal marker cytokeratin-5 (CK5) are shown in "C". In the PDT, an area of WDT is indicated with the white dotted line and clearly shows the change in expression of the different markers during PCa development. Nuclei are stained with DAPI. Scale bar=200 µm. Magnification show the presence of CK14-positive cells and very few p63-positive cells in WDT.*

Then we checked the expression of NCAM1 in tumors (WDT and PDT) developed in TRAMP mice. We stained cross-sections of entire prostate glands for NCAM1 and NE marker expression, i.e., SYN, CHGA. We noticed that single scattered cells with an NE phenotype, i.e., with a neuronal-like morphology and expressing simultaneously SYN, CHGA and NCAM1, are present in the "normal-like" periurethral region **(Fig. 7A,B)**. Interestingly, in areas of WDT in the distant lobes of the prostate, we detected large clusters of cells that are positive only for NCAM1 expression **(Fig. 7A)**. In contrast, in areas of PDT in the distant lobes, the tumor cells expressed all three NE markers **(Fig. 7B)**. These results indicate that the upregulation of NCAM1 expression appears to be an early event

in PCa development (occurring in WDTs), while the acquisition of the full NE traits occurs at a later stage of PCa progression (alongside the acquisition of the mesenchymal phenotype, see **Fig. 6C**) in PDTs. Thus, the appearance of NCAM1 is an early event in the process of NED, while the expression of CHGA and SYN occur in late NCAM1^{+} progenitors.

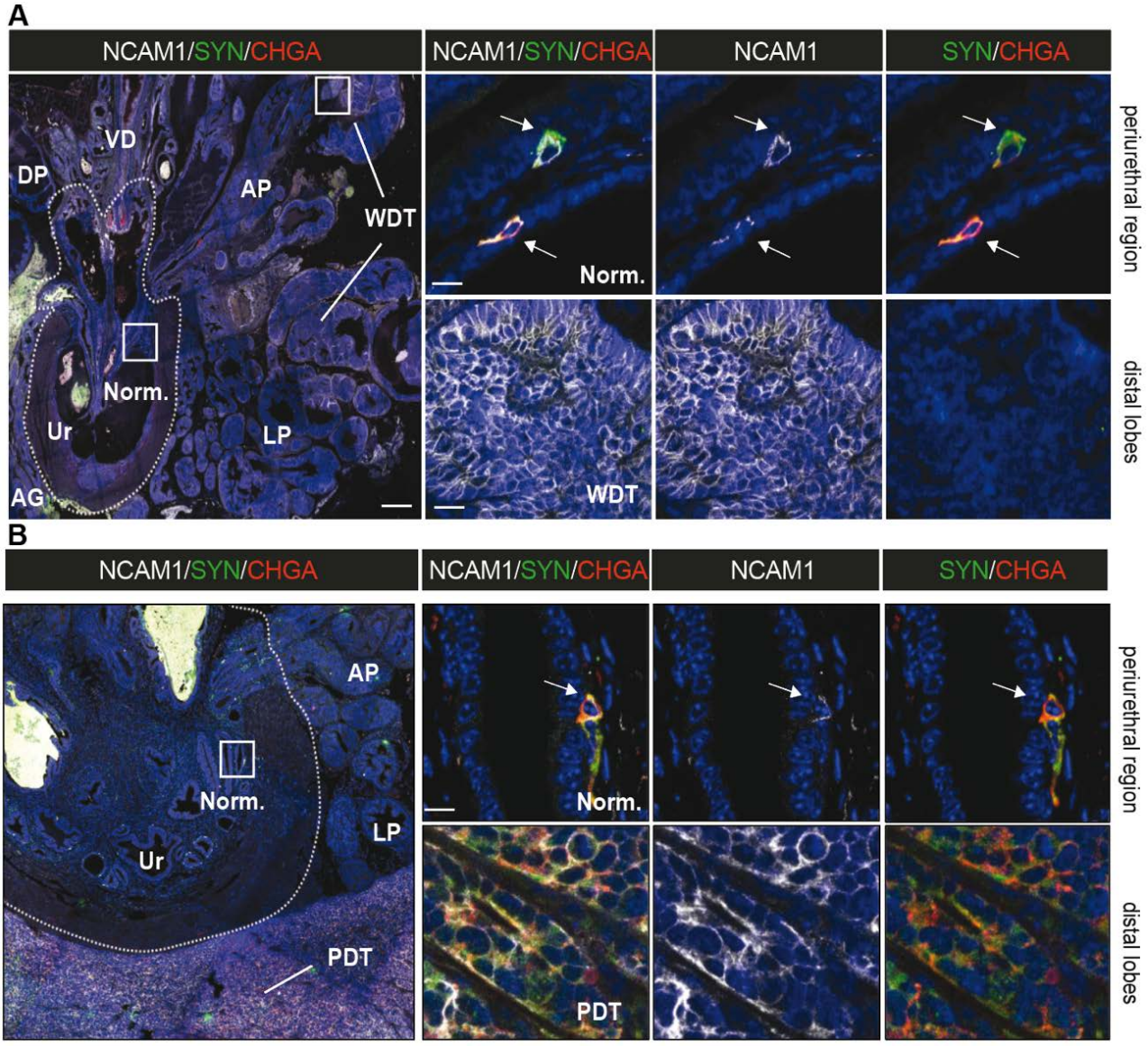

Figure 7. NE marker expression in TRAMP mouse PCa. **A-B)** *Representative immunofluorescence staining of cross-sectioned TRAMP prostate glands containing areas of well-differentiated tumor (WDT) (A) or poorly-differentiated tumor (PDT) (B) for the NE markers chromogranin-A (CHGA), synaptophysin (SYN) and NCAM1. Dashed line delimits the periurethral region containing the urethra (Ur) and the normal-area of tissue (Norm.). Outside this area, the anterior (AP) and lateral (LP) prostatic lobes are indicated, along with the tumor (WDT or PDT). For WDT in "A", the dorsal prostatic lobes (DP), the vas deferens (VD) and the ampullary gland (AG) are also indicated. Magnifications of the boxed areas within the periurethral region are shown in the upper panels on the right (Norm.) and indicate the presence of NE cells co-expressing NCAM1, SYN and CHGA (A-B). Magnifications of the boxed areas within the distal prostatic lobes containing areas of the WDT/PDT are shown in the lower panels on the right. Scale bars: entire cross-sections: 500 µm; magnifications: 50 µm.*

6.1.2 NCAM1 is fundamental for PCa progression to malignant lesions in the TRAMP PCa model

To understand better how NCAM1 expression changes during PCa progression, we analyzed prostate cells derived from TRAMP prostate glands at different stages of PCa development (normal, WDT, MDT, and PDT) by FACS analysis. Cells were analyzed for the expression of the epithelial marker EpCAM alongside NCAM1. In the normal prostate gland, we observed that ~10% of cells are NCAM1$^+$ **(Fig. 3A)**. This percentage increases gradually in correlation with the stage of the disease until ~100% of cells in PDT are NCAM1$^+$ **(Fig. 8A)**. Interestingly, we confirmed by IF that NCAM1$^+$ cells increased along PCa progression in TRAMP mice, in correlation with the alterations in the morphology of prostate glands **(Fig. 8B)**. Thus, suggesting that the NCAM1$^+$ cells are responsible for the appearance of most aggressive phenotype progression in TRAMP mouse PCa.

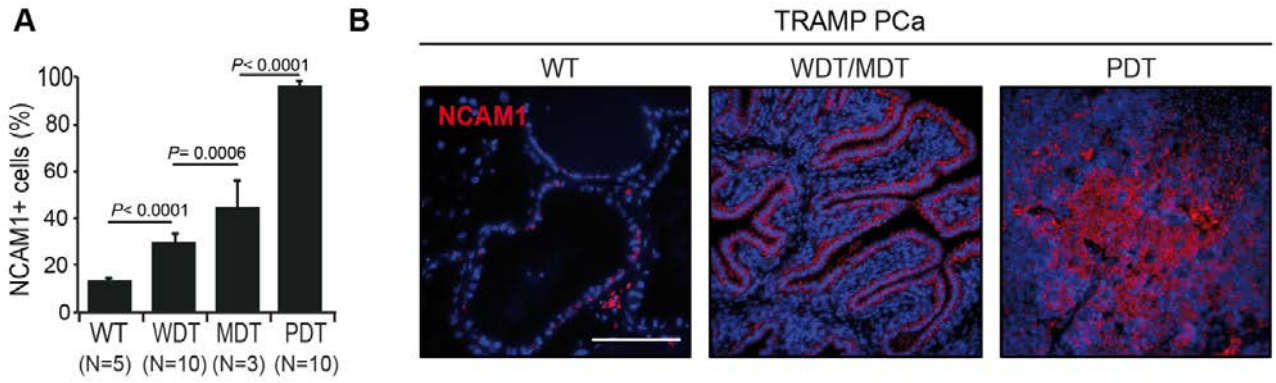

Figure 8. Estimation of NCAM1$^+$ cells during TRAMP mouse PCa progression. Entire prostate glands were collected from TRAMP mice with different stages of PCa development. Glands were mechanically dissociated, as indicated in the section 5.7, to yield prostate cell suspensions. Cell populations were analyzed for the expression of NCAM1 and EpCAM by FACS analysis. **A)** *Histogram representing data from FACS analysis of NCAM1$^+$ cells (expressed as % of all cells) in normal wild-type prostate tissue (WT; n=5), well-differentiated tumors (WDT; n=10), moderately-differentiated tumors (MDT; n=3) and poorly-differentiated tumors (PDT; n=10) from TRAMP mice. Data are reported as the mean ± SD. p-values were determined by Two-way ANOVA test.* **B)** *Immunofluorescence characterization of representative WDT and PDT compared to wild-type (WT) TRAMP-derived prostate for NCAM1 (red). Scale bar= 400 µm*

To provide direct genetic evidence that NCAM1 is a critical determinant for PCa development and progression, we crossed NCAM1$^{-/-}$ null mice with TRAMP mice. Two groups of mice TRAMP-NCAM1$^{+/+}$ (n=10) and TRAMP-NCAM1$^{-/-}$ (n=7) were monitored for up to 28 weeks and then analyzed for the presence of histological alterations in the prostate gland. As a control, SV40 large T-Ag immunostaining was performed to ensure maintenance of the TRAMP phenotype. No noticeable differences in large T-Ag expression between TRAMP-NCAM1$^{+/+}$ and TRAMP-NCAM1$^{-/-}$ mice were observed, demonstrating that NCAM1 ablation did not affect transgene expression **(Fig.**

9A). A qualitative analysis, based on pathological criteria, and a quantitative analysis of the extent of pathomorphological lesions in the prostate glands of TRAMP-NCAM1$^{+/+}$ and TRAMP-NCAM1$^{-/-}$ mice was performed. We found that in the TRAMP-NCAM1$^{+/+}$ mice, all of the animals had developed tumors, which were represented in 50% of the cases by massive PDT lesions that had completely subverted and replaced the prostate architecture and, in the remaining 50% of mice, by WDT lesions that typically infiltrated more than 70% of the gland **(Fig. 9B,D)**. Conversely, in the TRAMP-NCAM1$^{-/-}$ mice, we observed less severe lesions: the most predominant alteration observed in 5 mice and affecting ~20% of the gland was PIN (both high and low grade), with the presence of foci of WDT (in two of the 7 mice) which, however affected < 2% of entire prostate gland **(Fig. 9B,D)**. No progression towards MDT or PDT could be observed.

These data clearly indicate that NCAM1 is fundamental for the oncogene (large T-Ag)-driven formation and progression of PCa in the TRAMP mouse model.

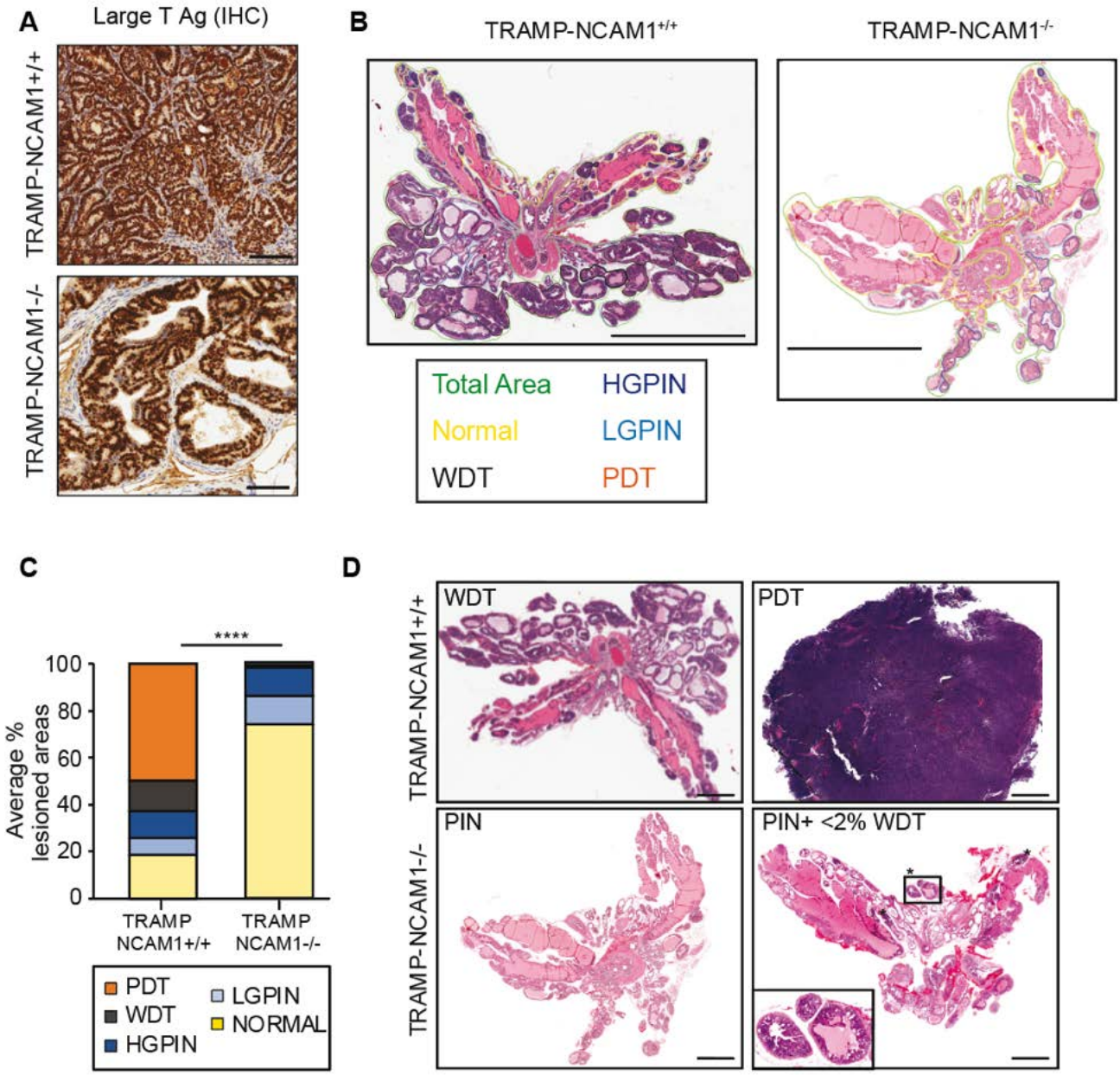

Figure 9. NCAM1 ablation inhibits PCa development and progression in the TRAMP mouse model. *The prostate glands of 28-week-old TRAMP-NCAM1$^{+/+}$ (n=10) and TRAMP-NCAM1$^{-/-}$ (n=7) mice were analyzed for the presence of histological alterations.* ***A)*** *Representative immunohistochemical (IHC) staining of the SV40 large T-antigen in prostate glands. Scale bar = 100 µm.* ***B)*** *Representative H&E staining of the prostate glands used to quantify the percentage of normal (yellow), hyperplastic low-grade prostate intraepithelial neoplasia (LG-PIN; pale blue), high-grade PIN (HGPIN; blue) and tumoral well-differentiated tumors (WDT; black) and poorly-differentiated tumors (PDT in orange) areas in relation to the total prostate area (green). Scale bars = 2 mm.* ***C)*** *Histogram showing the average area of normal tissue and of lesions, subdivided by type (LGPIN, HGPIN, WDT and PDT), as a % of the total prostate area. The color code is indicated below.* ***D)*** *Representative H&E staining of TRAMP-NCAM1$^{+/+}$ and TRAMP-NCAM1$^{-/-}$ prostate glands. Scale bar= 500 µm.*

6.1.3 NCAM1$^+$ PCa cells derived from TRAMP WDT have stem cell properties

CSCs are known to be responsible for tumor progression. Thus, to investigate the CSC properties of NCAM1$^+$ PCa cells, we isolated the subfraction of EpCAM$^+$/NCAM1$^+$ cells, and EpCAM$^+$/NCAM1$^-$ cells as controls, by FACS from bulk prostate cells derived from disaggregated TRAMP WDTs (see **Fig. 3**). We chose to isolate EpCAM$^+$ cells to ensure that we were examining the prostate epithelial cell population and to exclude NCAM1$^+$ cells belonging to the immune system or to the TME. The purified cells were assessed for their ability to form organoids *in vitro* by culturing in Matrigel (see section 5.7).

Organoids are clonally derived 3D cell structures shown to be derived from bipotent stem-like cells, thus the ability to form organoids can be used as an *in vitro* proxy for the stemness traits of asymmetric self-renewal and differentiation potential of a cell population (LeSavage *et al*., 2022) (see section 2.2.11.2).

The organoids generated from the isolated EpCAM$^+$/NCAM1$^+$ and EpCAM$^+$/NCAM1$^-$ cells were counted and assessed for morphological and molecular features by EVOS microscopy. NCAM1$^+$ organoids appeared as multilobular structures **(Fig. 10A)**. IF analysis of these organoids revealed basal CK5$^+$ cells on the border of the structure surrounding the luminal compartment (CK8$^+$ cells) **(Fig. 10B)**. The estimation of the OFE, i.e., the ratio between the number of obtained organoids and the number of plated cells, revealed that all NCAM1$^+$ cells exhibited an intrinsic ability to sustain the formation of organoids in 3D-Matrigel cultures **(Fig. 10C)**. In contrast, EpCAM$^+$/NCAM1$^-$ cells generated very few organoids **(Fig. 10A,C)**.

Since the ability to generate tumors *in vivo* is a defining characteristic of CSCs, we assessed the tumorigenic potential of the EpCAM$^+$/NCAM1$^+$ *vs.* EpCAM$^+$/NCAM1$^-$ WDT cells by the subcutaneous engraftment of 50,000 sorted cells, included in collagen type-I matrix, in immunodeficient NSG mice (see section 5.7). Tumor growth was periodically monitored, and mice were sacrificed when the outgrowth reached 0.8 cm of diameter measured by caliber (endpoint). We found that the ability to sustain tumorigenesis *in vivo* resided exclusively in the NCAM1$^+$ subpopulation (outgrowths/injection = 7/7) while the NCAM1$^-$ cells could not sustain tumor formation (outgrowths/injection = 0/7) **(Fig. 10D)**. The data obtained were presented as event-free survival in a Kaplan-Meier graph, which shows a clear difference in tumorigenicity of the two cell populations **(Fig. 10E)**. Together, these results demonstrate that cells functionally behaving as expected of CSCs (with self-renewal, differentiation and tumorigenic potential) reside in the subpopulation of NCAM1-expressing cells in the TRAMP PCa model.

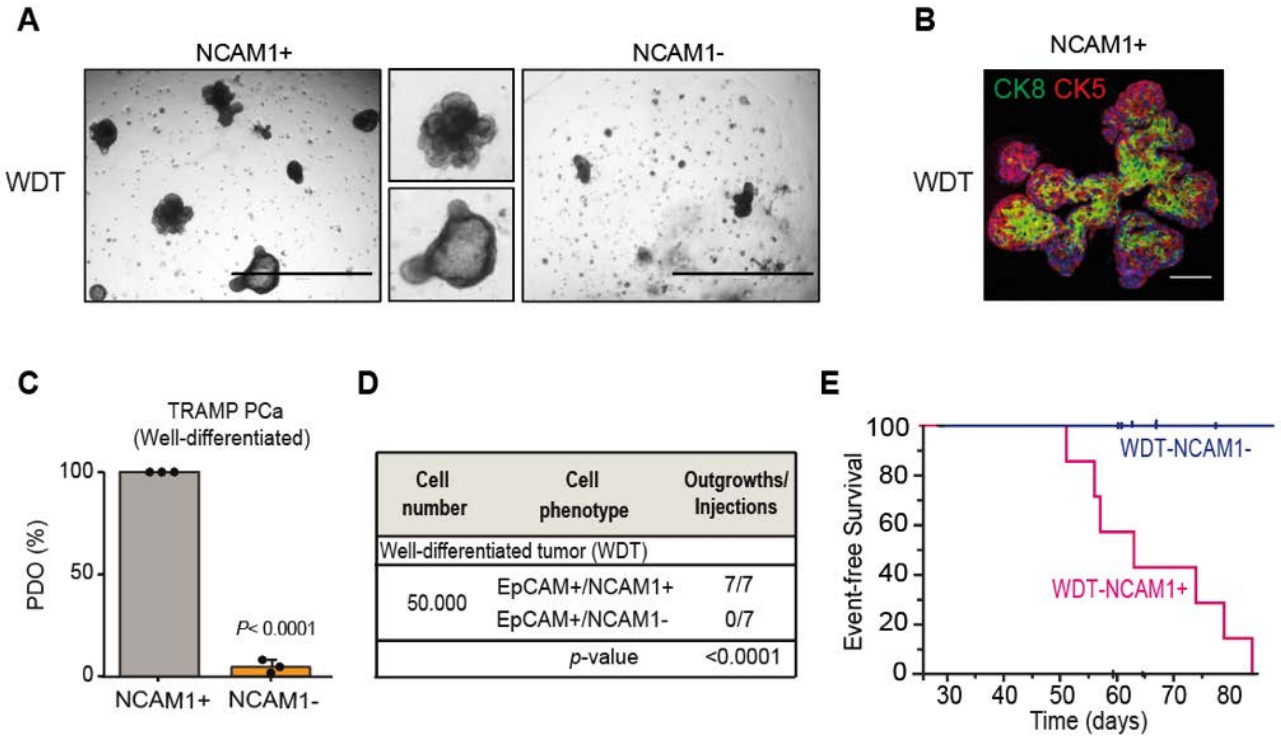

Figure 10. TRAMP mouse-derived EpCAM$^+$/NCAM1$^+$ cells display stem traits in vitro and in vivo. *EpCAM$^+$/NCAM1$^+$ and EpCAM$^+$/NCAM1$^-$ cells were isolated by FACS from well-differentiated tumors (WDTs) derived from TRAMP mice and assessed for CSC properties in the in vitro organoid assay (A-C) and by in vivo transplantation (D-E).* **A)** *Representative brightfield images of organoids generated by EpCAM$^+$/NCAM1$^+$and EpCAM$^+$/NCAM1$^-$ cells after 15 days in 3D-Matrigel culture. Scale bar= 1000 µm .* ***B)*** *Representative image of the immunofluorescence characterization of multilobular organoids generated from WDT EpCAM$^+$/NCAM1$^+$ cells. The expression of the epithelial luminal cytokeratin-8 (CK8, in green) and the basal cytokeratin-5 (CK5, in red) marker was assessed. DAPI was used to stain nuclei. Scale bar= 50 µm .* ***C)*** *OFE of EpCAM$^+$/NCAM1$^+$and EpCAM$^+$/NCAM1$^-$ cells. OFE (%) is shown as mean ± SD (n=5).* ***D)*** *Table reporting number of outgrowths obtained per subcutaneous injection of 5x10^5 EpCAM$^+$/NCAM1$^+$ and EpCAM$^+$/NCAM1$^-$ cells isolated from TRAMP-WDT in NSG mice. p-value was calculated Student's t test.* ***E)*** *Kaplan-Meier analysis of event-free survival in NSG mice injected as in (D).*

To investigate further the stem cell traits of NCAM1$^+$ TRAMP cells, we used two established TRAMP mouse-derived cell lines, TRAMP-C1 and -C2. These cells were derived from PDTs that formed in a 32-week-old TRAMP mouse and were characterized by total absence of P53 and tumorigenic ability when transplanted (Foster *et al.*, 1997). By FACS analysis, we revealed that ~100% of the TRAMP-C1 and -C2 cells are NCAM1$^+$ (*data not shown*). Therefore, we stably depleted NCAM1 expression in these cells by infection with a lentiviral vector expressing a shRNA against *Ncam1*. A scramble (Scr) lentiviral vector was used as a negative control. By western blot, we confirmed NCAM1 silencing at the protein level in both cell lines, although some detectable protein was still present **(Fig. 11A)**. Both TRAMP-C1-shNCAM1 and TRAMP-C2-shNCAM1 cells displayed a significantly reduced OFE (~50% lower) in the 3D-Matrigel organoid assay and impaired tumorigenicity *in vivo*

compared with the Scr control **(Fig. 11B,C).** Indeed, the subcutaneous injection of 500,000 TRAMP-C1 (T-C1) or -C2 (T-C2) shNCAM1 bulk cells in NSG mice resulted in significantly fewer outgrowths forming compared with Scr cells **(Fig. 11C)**. These observations further support the notion that NCAM1 is required for conferring stemness traits to PCa cells, such as organogenesis ability *in vitro* and tumorigenicity *in vivo*.

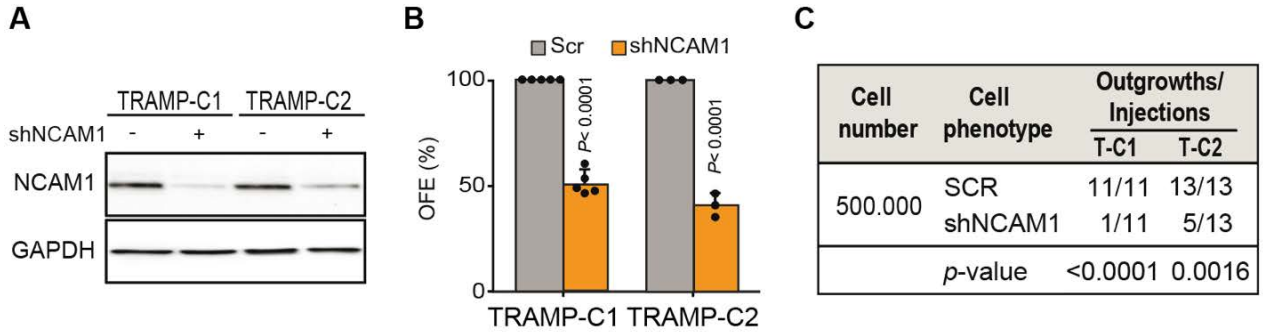

Cell number	Cell phenotype	Outgrowths/ Injections	
		T-C1	T-C2
500.000	SCR	11/11	13/13
	shNCAM1	1/11	5/13
	p-value	<0.0001	0.0016

Figure 11. NCAM1 is required for conferring stem cell traits to PCa cells. *TRAMP-C1 and -C2 cells were stably infected with a lentiviral vector expressing an shRNA against Ncam1 (shNCAM1).* **A)** *Immunoblot showing the efficiency of NCAM1 silencing. GAPDH, loading control.* ***B)*** *Organoid-forming efficiency (OFE %) of TRAMP-C1 and -C2 Scr control and shNCAM1 cells; OFE is reported as mean ± SD (n=3). P-values were calculated using Student's t test.* ***C)*** *Outgrowths generated upon subcutaneous injection of 5x10^5 TRAMP-C1 and -C2 (T-C1, T-C2) Scr control and shNCAM1 cells in NSG mice. Data are reported as number of outgrowths obtained per number of injections.* P-values were calculated using *Student's t test*.

6.1.4. EpCAM$^+$/NCAM1$^+$ cells isolated from human PCa are endowed with stem cell traits as assessed by the in vitro organoid assay

To investigate whether human NCAM1$^+$ PCa cells are endowed with stemness properties, as observed with TRAMP WDT cells, we first estimated by biparametric FACS analysis the amount of EpCAM$^+$/NCAM1$^+$ cells in four independent high-grade human PCa biopsies (Gleason Group 4-5). We found that these cells represent ~4% of the bulk EpCAM$^+$ population **(Fig. 12A,B)**. The EpCAM$^+$/NCAM1$^+$ and EpCAM$^+$/NCAM1$^-$ sorted cell fractions were assayed for their ability to sustain the formation of PDOs in a 3D-Matrigel culture. The EpCAM$^+$/NCAM1$^+$ cell fraction showed a significantly higher ability to form PDOs compared with EpCAM$^+$/NCAM1$^-$ cells **(Fig. 12C)** and the organoids appeared as filled structures with impaired hollow formation consistent with a transformed phenotype **(Fig. 12D)**. To further confirm the relevance of NCAM1 in the actuation of the CSC phenotype, we employed an α-NCAM1 monoclonal blocking antibody (123C3), which has been shown to inhibit NCAM1 downstream signaling in ovarian cancer in *in vitro* and *in vivo* models (Zecchini *et al*., 2011). We isolated EpCAM$^+$/NCAM1$^+$ and EpCAM$^+$/NCAM1$^-$ cells from high Gleason grade patients (Gleason Group 5) (n=5) by FACS and exposed them to the antibody for one

hour prior to culturing in 3D-Matrigel to form organoids. As observed, the treatment with the α-NCAM1 antibody completely abolished the ability of EpCAM$^+$/NCAM1$^+$ cells to form PDOs, confirming that NCAM1 function is absolutely required for this stemness trait **(Fig. 12E)**.

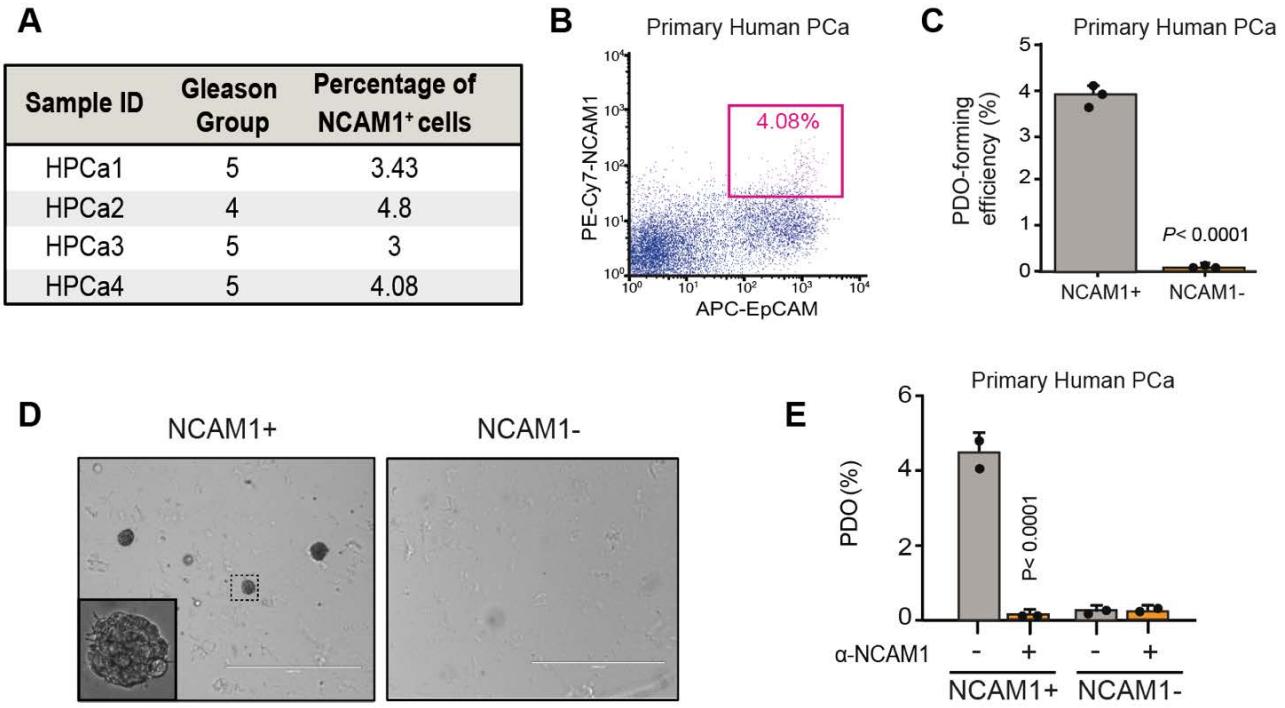

Sample ID	Gleason Group	Percentage of NCAM1$^+$ cells
HPCa1	5	3.43
HPCa2	4	4.8
HPCa3	5	3
HPCa4	5	4.08

Figure 12. NCAM1$^+$ cells isolated form human PCa display CSC traits in vitro. *EpCAM$^+$/NCAM1$^+$ and EpCAM$^+$/NCAM1$^-$ cell populations were isolated from bulk PCa cell populations derived from high-grade human PCa by FACS and analyzed for in vitro organoid-forming ability.* ***A)*** *Table reports the percentage of EpCAM$^+$/NCAM1$^+$ cells in human PCa (HPCa) biopsies (Gleason Group 4 or 5) revealed by FACS analysis.* ***B)*** *Representative biparametric FACS profile of a human PCa bulk cell population (Gleason group 5). The box identifies the EpCAM$^+$/NCAM1$^+$ cells.* ***C)*** *Patient-derived organoid (PDO)-forming ability of EpCAM$^+$/NCAM1$^+$ vs. EpCAM$^+$/NCAM1$^-$ cells derived from human high-grade PCa by FACS; PDO-forming efficiency (%) is reported as the mean ± SD (n=5).* ***D)*** *Representative images of PDOs generated by EpCAM$^+$/NCAM1$^+$ vs. EpCAM$^+$/NCAM1$^-$ cells, isolated by FACS from a PCa biopsy after 15 days in 3D-Matrigel culture. Scale bar= 1000 µm.* ***E)*** *PDO-forming efficiency (PDO %) by EpCAM$^+$/NCAM1$^+$and EpCAM$^+$/NCAM1$^-$ cells isolated by FACS from human PCa (High Gleason) biopsies and treated in vitro with the α-NCAM1 antibody [1:25] or vehicle control. Results are the mean ± SD (n=5). P-values were calculated using the Student's t test.*

6.1.5. The expression of NCAM1 and putative PCSC markers in primary human PCa

As previously observed, the NCAM1^{+}/NE^{-} cells are located mainly in the PIA regions in human PCa, which have been previously described as heterogeneously enriched in PCSCs (De Marzo *et al*., 1999). We therefore analyzed the expression of surface markers previously reported as associated with the PCSC phenotype (see section 2.3.4.1), such as CD117/c-kit, CD44, CD133/Prom1, CD166/ALCAM and CD38 (Jiao *et al*., 2012; Liu *et al*., 2016; Hurt *et al*., 2008; Collins *et al*., 2005; Leong *et al*., 2008) in PIA found in sections of high Gleason grade human PCa. PIA are wide areas (green lines) were located in the outer regions of the prostate gland next to tumor areas (black lines) **(Fig. 13A)**. We focused our attention on group of glands, indicated by the asterisk, within the PIA regions. By IHC, we detected that all the cells that make up the prostate glands are stained positive for CD166, suggesting that this marker cannot be a true markers of PCSCs. Interestingly, based on the knowledge on CD38 expression, we noticed that in the atrophic gland, indicated with black arrow, is not expressed, opposed to the neighboring gland that instead is positive for CD38 luminal staining, thus we considered this gland as "normal-like". Consistently, NCAM1 is expressed in "threads" just in the atrophic gland and not in the "normal-like", opposed to CHGA. In fact, the unique positive cells are located in the "normal-like" epithelium. We revealed also in the atrophic gland the unique expression of a very rare subpopulation of CD117^{+} cells and few CD133^{+} cells surrounding the lumen; instead CD44^{+} cells in the basal epithelium were detected in both atrophic and "normal-like" glands **(Fig. 13B)**.

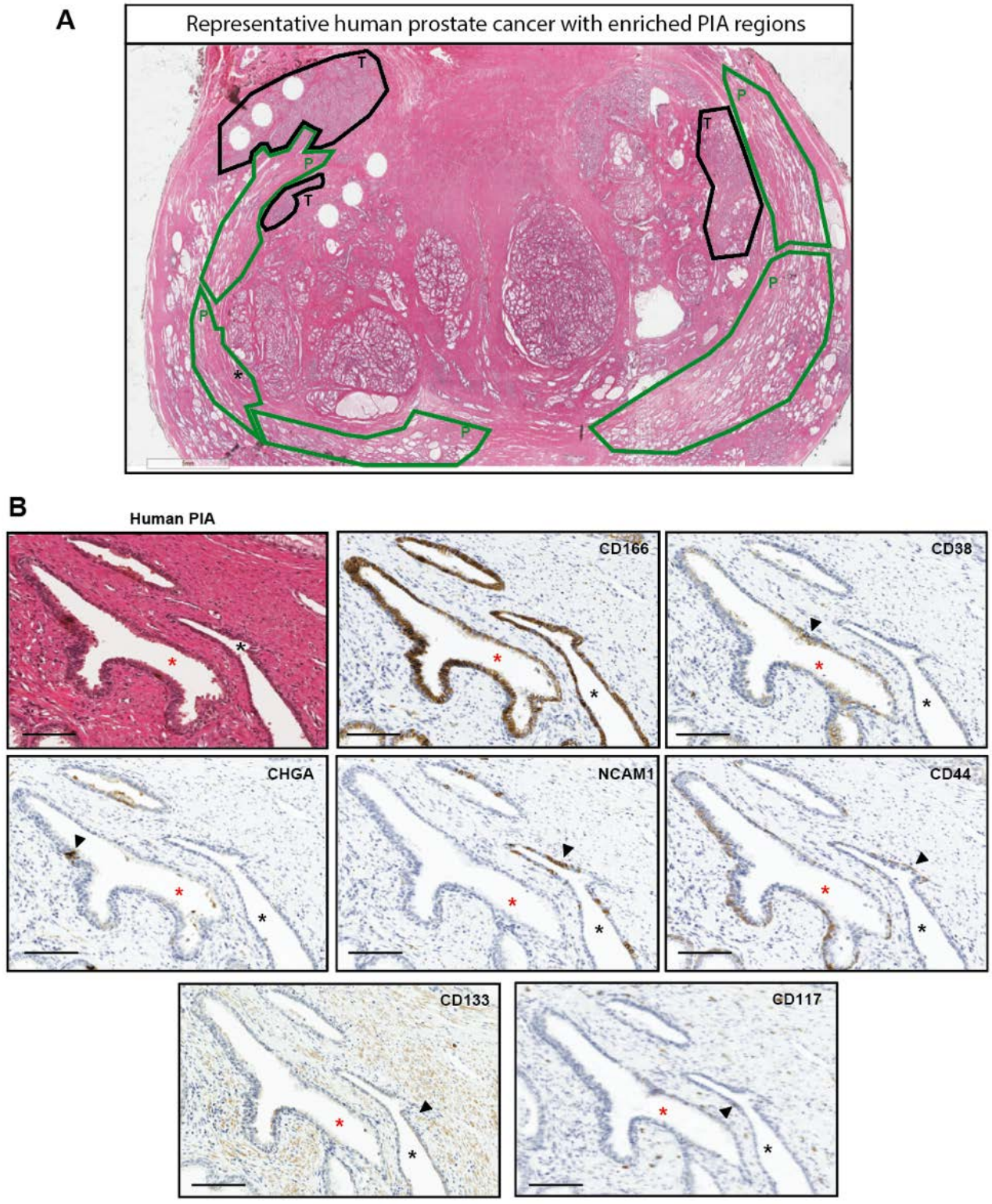

Figure 13. PIA glands are heterogeneously enriched in PCSCs. *Entire sections of a human tumoral prostate glands from patients with high Gleason grade PCa (n=3) were analyzed for the expression of putative PCSC markers in PIA by immunohistochemistry (IHC) on FFPE.* ***A)*** *Representative H&E staining of an entire section of a human PCa. The tumor (T) areas are encircled with black lines, while PIA regions (P) are indicated with green lines. Asterisk indicates the area magnified in the following panel "B". Scale bar = 5 mm.* ***B)*** *Representative IHC staining of CD117, CD133, CD44, CD38, CHGA and NCAM1 detected in PIA glands. Black arrows indicate glands positive for the related staining. Black asterisk indicates the atrophic gland, while the red asterisk the "normal-like" gland . Scale bar = 100 µm.*

By FACS analysis, we estimated the percentage of cells positive for the different markers in the bulk EpCAM$^+$ population obtained from a pool of three high Gleason grade (HG) or three low Gleason grade (LG) PCa patient biopsies. Interestingly, of all the markers tested, only NCAM1 expression correlated with tumor aggressiveness, showing a ~3-fold enrichment in HG *vs.* LG PCa, in line with the preliminary data showing that NCAM1 is a prognostic marker. In contrast, CD38 expression negatively correlated with tumor aggressiveness, consistent with the literature (Liu *et al*., 2016) **(Table 2)**. CD117 and CD133 were detected in relatively rare subpopulations of cells, while CD44 was more abundant, reflecting the IHC data.

Table 2. The expression of putative PCSC markers within the EpCAM$^+$ cell population of low and high Gleason grade PCa. *EpCAM+ cells from dissociated low Gleason grade (LG) vs. high Gleason grade (HG) PCa biopsies (n=3) were analyzed by FACS for the expression of the indicated PCSC-related biomarkers (EpCAM$^+$/Marker$^+$). Results are reported as the mean (%) ± SD. P-value was determined by Student's t test. NS, non-significant.*

Marker	Low Gleason (LG) (n=3)	High Gleason (HG) (n=3)	p-value (HG vs LG)
NCAM1	1.45% ± 0.2	4.5% ± 0.25	< 0.0001
CD133	0.75% ± 0.35	0.77% ± 0.32	NS
CD117	0.35% ± 0.28	0.42% ± 0.1	NS
CD38	1.5% ± 0.2	0.3% ± 0.12	0.019
CD44	17.5% ± 7.8	15% ± 3.38	NS

6.1.6. The expression of NCAM1 is determinant in conferring self-renewal ability compared to the other putative PCSC markers in established human PCa cell lines.

Next, we investigated the expression of putative PCSC markers in two established human cell lines commonly used for PCa studies: the LNCaP androgen-sensitive (AR$^+$) cell line and the DU145 androgen-insensitive (AR$^-$) cell line. Both cell lines were derived from lymph node metastases of adenocarcinoma of the prostate (Stone *et al.*, 1978; Horoszewicz *et al.*, 1983). By FACS analysis, we established that the putative PCSC biomarkers are variably expressed. CD166 was expressed by almost all cells in the two cell lines, whereas CD117, CD133, and NCAM1 were expressed by very few cells in both cell lines (~0.2% for CD117 and CD133; ~1-2% for NCAM1) **(Fig. 14)**. Instead, CD44, was expressed in 89% of the DU145 cell population and only ~1% of the LNCaP cell population, while CD38 was expressed on ~10% of DU145 cells and only 0.1% of LNCaP cells **(Fig. 14)**.

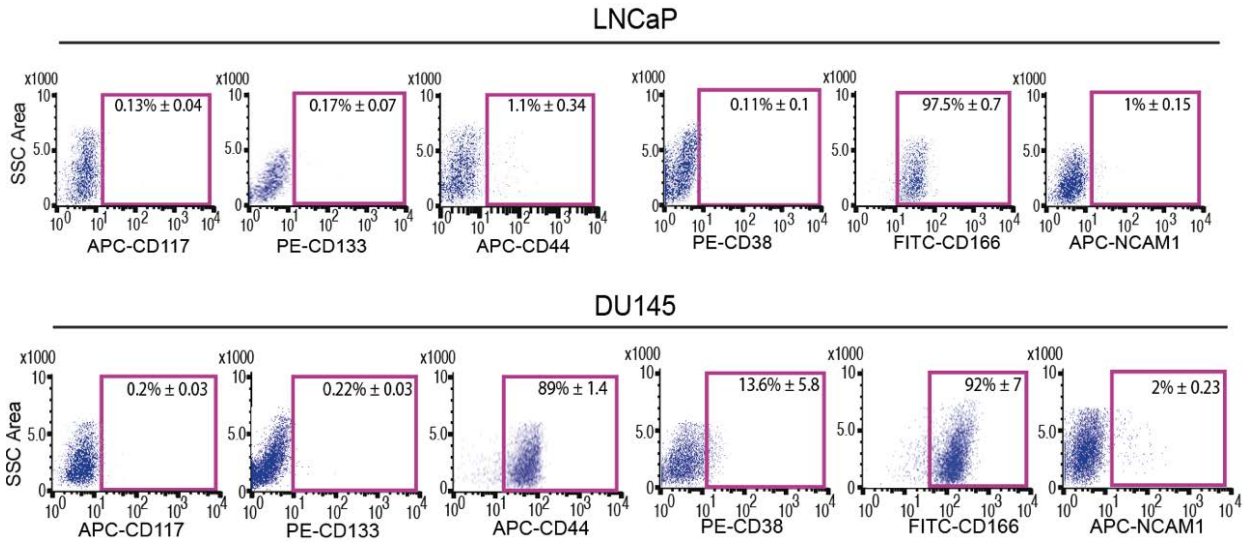

Figure 14. PCSC markers are differently expressed in both LNCaP and DU145 cells. *Representative FACS profiles of established human cells lines LNCaP (androgen-sensitive) (upper) and DU145 (androgen-insensitive) (lower) stained for the surface biomarkers CD117, CD133, CD44, CD38, CD166 and NCAM1. Data are represented as mean (%) ± SD (n = at least 3 independent experiments).*

To understand how stemness properties correlate with marker expression, we purified by FACS the different cellular subfractions, expressing or not the marker-of-interest, and then tested their ability to sustain the growth of successive generations organoids through the serial propagation assay in 3D-Matrigel; a well-established method to assess self-renewal ability of CSCs (Hofer and Lutolf, 2021). Strikingly, over three serial passages, only NCAM1^{+} cells, from both cell lines, maintained their original ability to form organoids as assessed by the OFE; all other cell populations displayed a progressive reduction of OFE **(Fig. 15)**. There were however some differences between cells expressing or not the different markers, with marker^{+} cells showing a higher OFE than marker^{-} cells in most cases.

These data corroborate our previous observation that NCAM1 identifies cells with stemness traits including that of self-renewal.

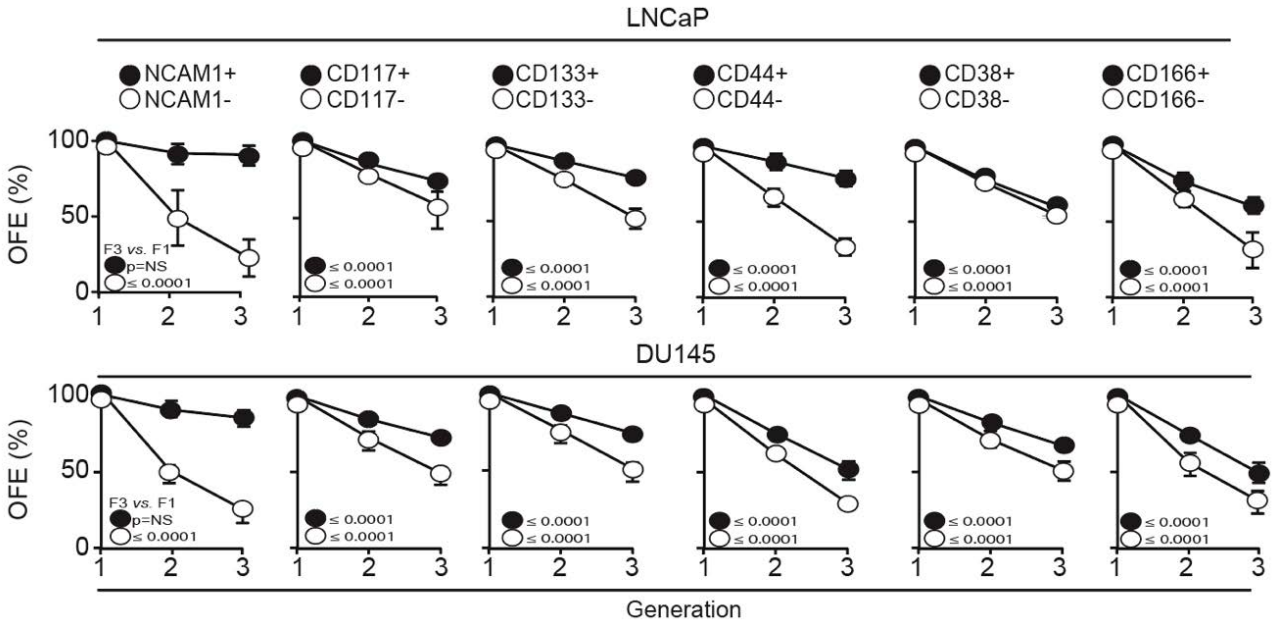

Figure 15. NCAM1$^+$ cells displayed a unique sustained self-renewal ability in vitro. **A)** *Serial organoid propagation ability in 3D-Matrigel of the indicated cell populations isolated from LNCaP and DU145 cell lines by FACS. Results are expressed as normalized organoid-forming efficiency (OFE) (n=3). P-values were calculated using the Two-way ANOVA test and are comparing the OFE of the first generation (F1) with the OFE of the third generation (F3). NS, non-significant.*

By bi-parametric FACS analysis, we analyzed the proportion of NCAM1+ cells in each of the isolated subfractions positive for one of the markers-of-interest. We found that NCAM1+ cells were enriched in the CD133$^+$ and CD117$^+$ populations (~20%) in both the LNCaP and DU145 cell lines **(Fig. 16A,B)**. For the CD44$^+$ population, NCAM1$^+$ cells were also enriched (~20%) in the LNCaP cells, but not in DU145 cells **(Fig. 16A,B)**, which unlike LNCaP are almost all positive for CD44 **(Fig. 16A)**. In all the other marker$^+$ populations, NCAM1$^+$ cells accounted for only a small proportion of the total (~2-8%) **(Fig. 16A)**.

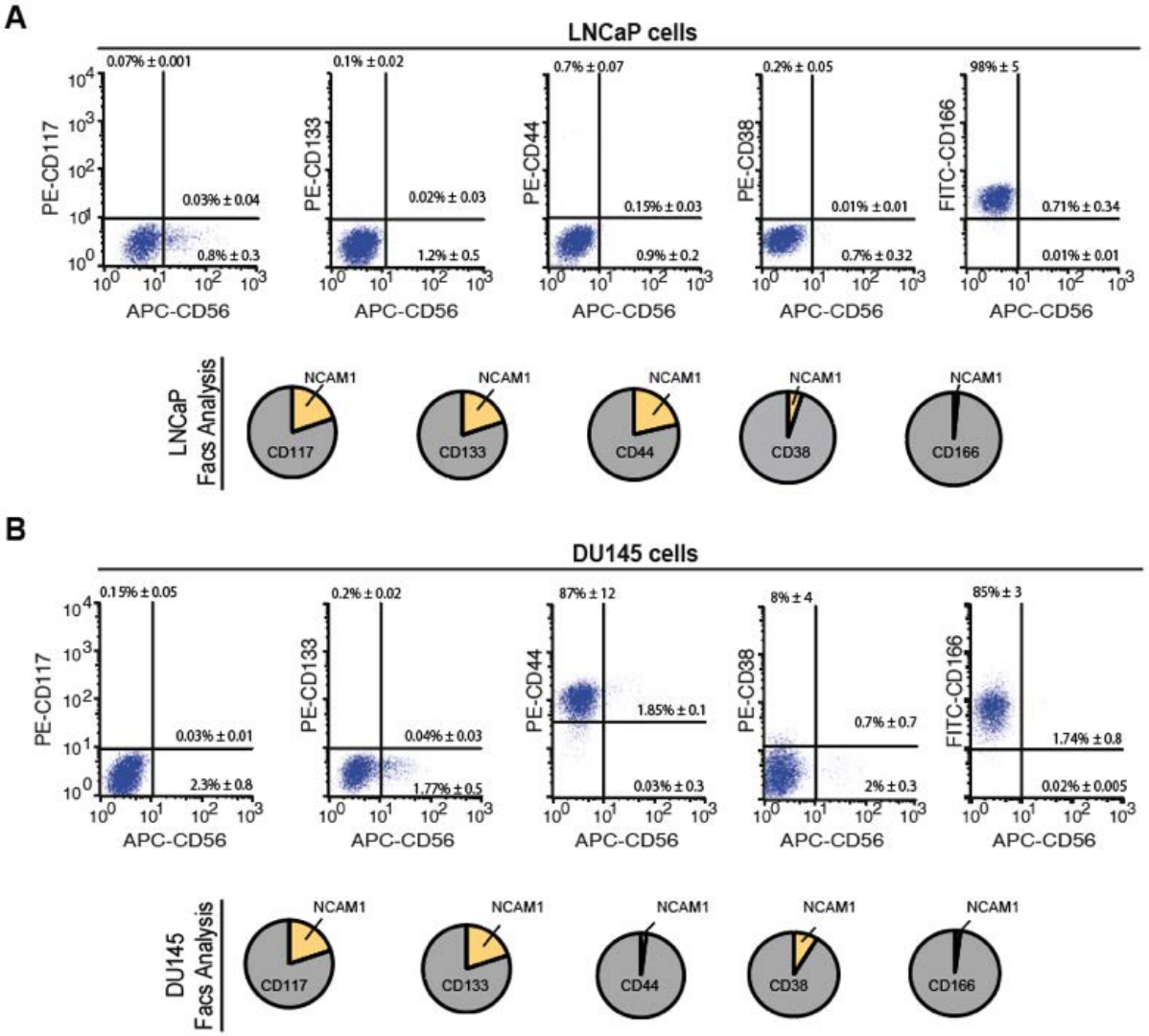

Figure 16. NCAM1 identifies a subfraction of positive cells in each Marker$^+$ population. A-B) *Representative FACS profiles of LNCaP (A) and DU145 (B) stained for NCAM1 in combination with CD117, CD133, CD44, CD38 or CD166. Data are presented as mean ± SD (n=3). Pie charts display the portion of the NCAM1$^+$ subfraction (yellow), quantified by FACS analysis, in each bulk marker$^+$ population (grey).*

Since NCAM1 expression correlated with self-renewal potential, we investigated whether the co-expression of any of the other putative markers was more efficient at isolating a PCSC population We sorted by FACS all the different subpopulations (NCAM1$^{+/-}$ and marker$^{+/-}$) from the two cell lines and assessed ability to maintain self-renewal potential in a 3D-Matrigel assay through the serial propagation assay. The CD133$^+$, CD177$^+$ and CD44$^+$ (LNCaP only) populations that were enriched in NCAM1$^+$ cells displayed a higher OFE at the first generation compared with the other cell populations indicative of an enrichment in CSCs in these populations **(Fig. 17)**. Moreover, regardless of the status of the other markers, only NCAM1$^+$ cells had a sustained OFE over serial passages **(Fig. 17A)**. These data demonstrate a strong correlation between NCAM1 expression and CSC self-renewal ability, supporting our previous findings indicating that NCAM1 is able to identify a subpopulation of PCa cells with stemness traits.

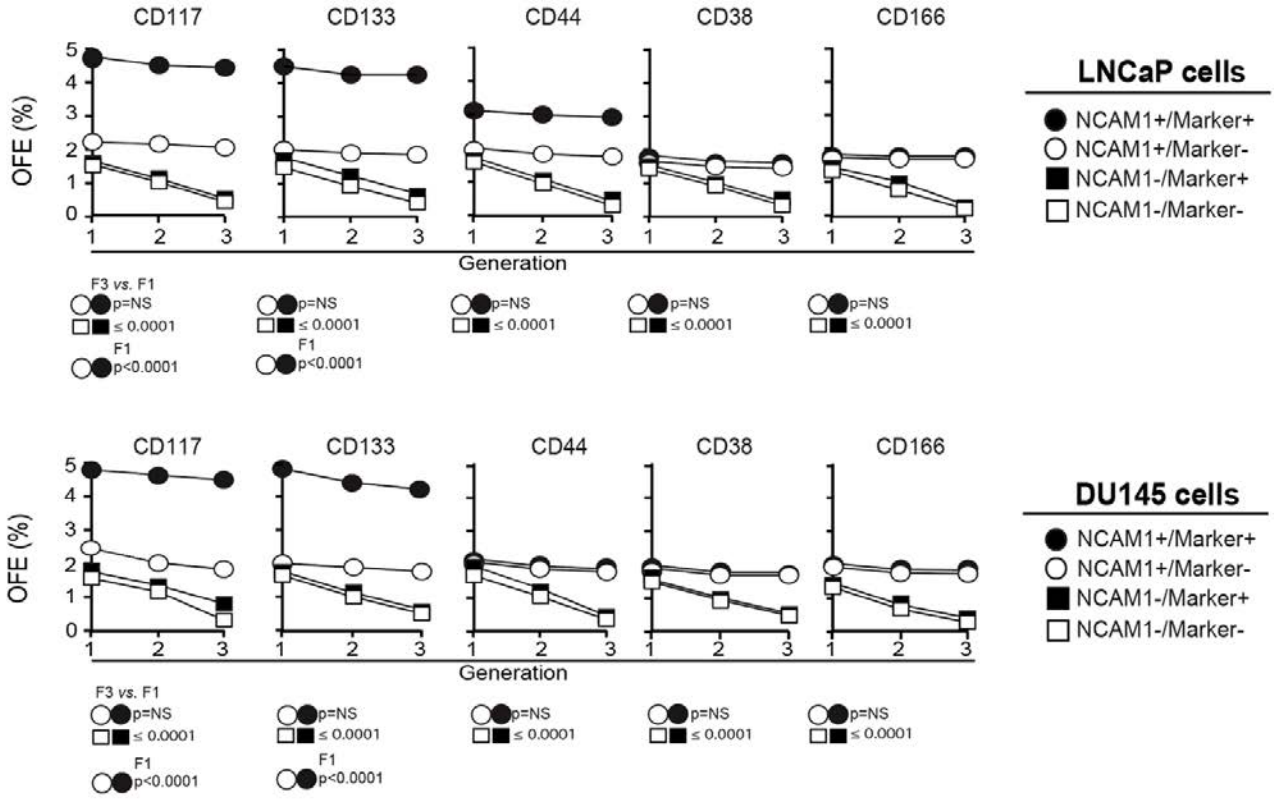

Figure 17. The enrichment of NCAM1$^+$ cells in other PCSC-marker$^+$ populations correlates with the CSC content of these populations. *Serial organoid propagation ability of NCAM1$^{+/-}$ and marker$^{+/-}$ cells (as indicated) isolated from the LNCaP and DU145 PCa cell lines. Organoid-forming efficiency (OFE%) over 3 serial passages is shown. Results are the mean ± SD (n=3). p-values were calculated using the Two-way ANOVA test and were used to compare the OFE in the first (F1) and third (F3) generations. NS, non-significant.*

Since the NCAM1$^+$ cell population in the two cell lines is enriched in stemness properties as assessed by the *in vitro* organoid assay, we investigated whether this population also has an increased ability to generate tumors *in vivo* – the gold standard for demonstrating the presence of CSCs. To this end, we performed the limiting dilution assay *in vivo* (see section 5.10), a well-established method for determining the number of TICs in a cell population (Hope and Bhatia, 2011). We isolated NCAM1$^+$, NCAM1$^-$ and bulk cells from both the LNCaP and DU145 cell lines and transplanted progressively decreasing numbers of these cells (10,000, 1000, 1000 and 10) subcutaneously in NSG mice. The formation of outgrowths was routinely monitored, and experiments were ended when outgrowths reached 0.8 cm in diameter.

We observed that NCAM1$^+$ cells from both cell lines were more efficient than NCAM1$^-$ and bulk cells at generating outgrowths **(Fig. 18)**. The frequency of TICs in the different cell populations was estimated using ELDA software (). NCAM1$^+$ cell populations from both cell line are enriched in TICs (1:203 cells in LNCaP and 1:43.6 cells in DU145) compared to NCAM1$^-$ (1:20.098 cells in

LNCaP and 1:17949 cells in DU145) or bulk cells (1:7609 cells in LNCaP and 1:4304 cells in DU145) **(Fig. 18)**.

Together, these results indicate that regardless of their AR status, NCAM1^{+} cells display tumorigenic ability *in vivo* and maintain their self-renewal ability in the organoid serial propagation assay *in vitro*, confirming that, as observed in primary PCa samples, NCAM1 identifies a subpopulation of PCa cells with CSC traits.

Cell number	Cell type	Outgrowths/Injections	
		LNCaP	DU145
10 000	NCAM1+	8/8	5/5
	NCAM1-	2/8	0/5
	BULK	1/4	2/5
1000	NCAM1+	10/11	3/3
	NCAM1-	1/11	2/3
	BULK	2/7	2/3
100	NCAM1+	5/7	4/5
	NCAM1-	1/7	1/5
	BULK	3/7	4/5
10	NCAM1+	2/7	2/4
	NCAM1-	0/7	0/4
	BULK	0/7	1/4

LNCaP Cell type	TRANSPLANTATION FREQUENCY			
	Predicted	Observed Range		p-value
NCAM1+	1:203 (0.49%)	1:84.4	1:489	4.11×10^{-18}
NCAM1-	1:20,098 (0.0049%)	1:7,199	1:56,110	
BULK	1:7,609 (0.013%)	1:2,513.8	1:23,035	

DU145 Cell type	TRANSPLANTATION FREQUENCY			
	Predicted	Observed Range		p-value
NCAM1+	1:43,6 (2.29%)	1:16,2	1:119	3.06×10^{-14}
NCAM1-	1:17,494 (0.0057%)	1:4,826.3	1:63,415	
BULK	1:4,304 (0.023%)	1:1,548.3	1:11,966	

***Figure 18*. NCAM1^{+} population is enriched in tumor-initiating cells.** *Limiting dilution transplantation assay to determine the frequency of tumor-initiating cells ("Predicted" column) in NCAM1^{+}, NCAM1^{-} and bulk cell populations isolated from LNCaP and DU145 by FACS and transplanted in immunocompromised NSG mice.*

6.1.7. NCAM1 is a molecular target for therapies to abrogate stem cell phenotypes

To understand the role of NCAM1 in determining the PCSC phenotype in the PCa cell lines, we knocked out the *NCAM1* gene in NCAM1$^+$ cells, isolated by FACS from the DU145 and LNCaP cell lines, using a CRISPR-CAS9 approach with reverse transfection in Matrigel. This technique efficiently abrogated the expression of NCAM1 mRNA **(Fig. 19A)**. The NCAM1-KO cells, when interrogated for organoid formation ability, displayed a strongly impaired OFE **(Fig. 19B)**, suggesting that NCAM1 expression is required for the maintenance of the PCSC population. To verify this finding, we treated NCAM1$^+$ cells, isolated from LNCaP and DU145 by FACS, with the α-NCAM1 blocking monoclonal antibody (123C3). The antibody strongly inhibited the OFE of NCAM1$^+$ cells in the 3D-Matrigel assay, while NCAM1$^-$ cells were unaffected by the 123C3 antibody **(Fig. 19C,D)**.

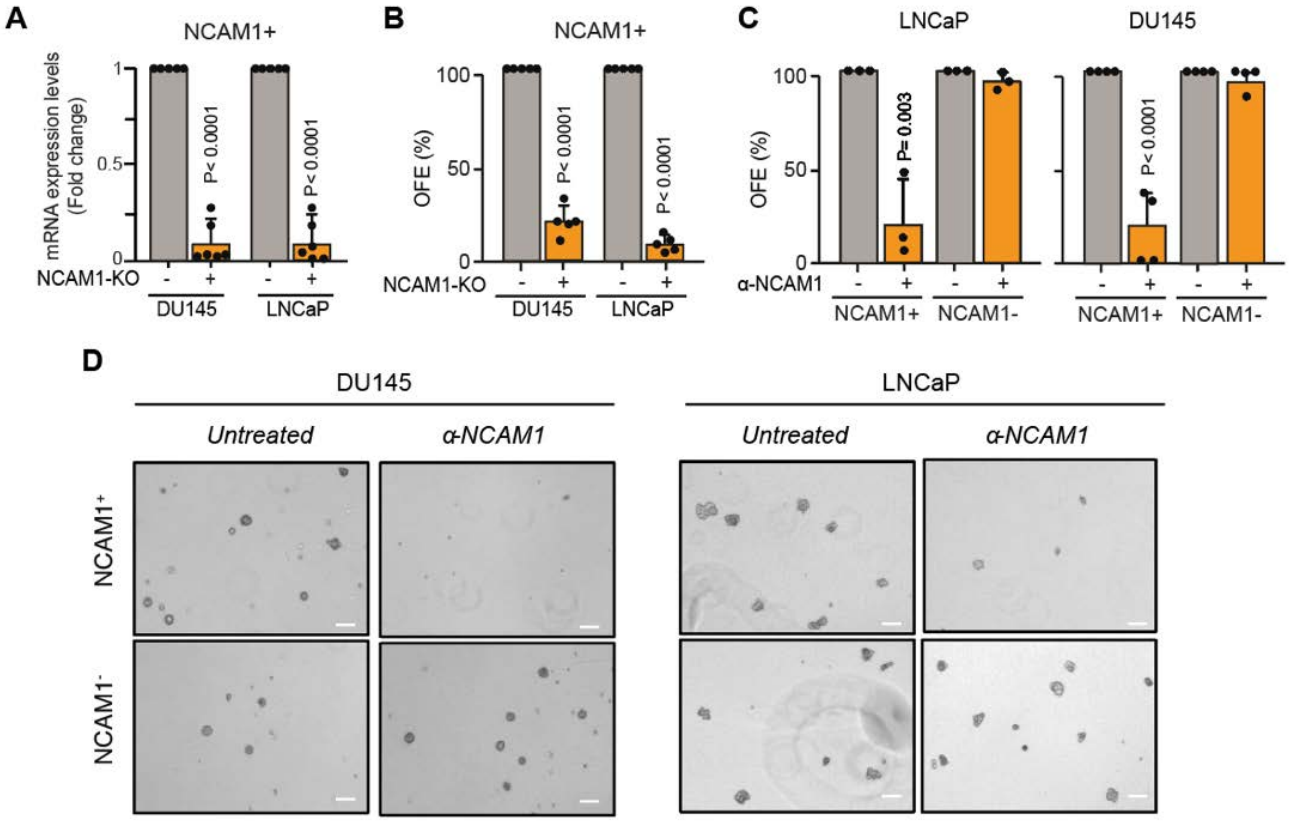

Figure 19. NCAM1 is essential for organoid formation in vitro. A) *RT-qPCR for NCAM1 detected in NCAM1$^+$cells isolated from bulk DU145 and LNCaP and reverse transfected with CRISPR-CAS9 for NCAM1 (-KO) in Matrigel, after 3 days from seeding (n=3).* ***B)*** *Organoid-forming efficiency (OFE%) of NCAM1 knockout (NCAM1-KO) and control NCAM1$^+$ cells isolated from DU145 and LNCaP (n=3).* ***C)*** *OFE (%) of NCAM1$^+$ and NCAM1$^-$ cells isolated from LNCaP and DU145 and treated with the α-NCAM1 123C3 antibody (1:25) for 1 hours post-sorting. Results are expressed as normalized to the OFE of corresponding untreated control (n=3).* ***D)*** *Representative images of organoids in Matrigel derived from NCAM1$^+$ and NCAM1$^-$ DU145 or LNCaP cells, untreated or treated with the 123C3 α-NCAM1 antibody. Scale bar= 400 µm. P-values were calculated using the Student's t test.*

Next, we tested the *in vivo* efficacy of the α-NCAM1 123C3 antibody in targeting the PCSC population in a serial xenotransplantation assay. The aggressive DU145 cells were transplanted into NSG mice and allowed to form palpable lesions. Mice were then injected intraperitoneally with the α-NCAM1 antibody (10 mg/kg), four times a week for two weeks as schematically represented **(Fig. 20A)**. The outgrowths obtained in the first-generation mice (X_n1) were digested and the resulting dissociated tumor cells were either tested for OFE *in vitro* or re-transplanted into second-generation (X_n2) mice, without any further treatment, to assess tumorigenicity.

The OFE of FACS-purified NCAM1$^+$ cells, derived from α-NCAM1 treated X_n1 mice, was significantly reduced compared to control treated X_n1 tumor cells, while no effect of the antibody treatment was observed in the NCAM1$^-$ population **(Fig. 20B)**, indicating the specificity of the treatment for the NCAM1$^+$ cells. Although antibody treatment did not affect the number of outgrowths generated upon re-transplantation in X_n2 mice **(Fig. 20C)**, it did inhibit their growth. Indeed, while treatment with the α-NCAM1 antibody did not affect tumor size in X_n1 mice **(Fig. 20D)**, it caused a significant reduction in tumor volume (~50%) in X_n2 mice, compared to cells derived from untreated mice **(Fig. 20E-G)**. These data suggest that NCAM1 is mandatory for determining/maintaining PCSC traits, such as self-renewal, differentiation and tumorigenicity.

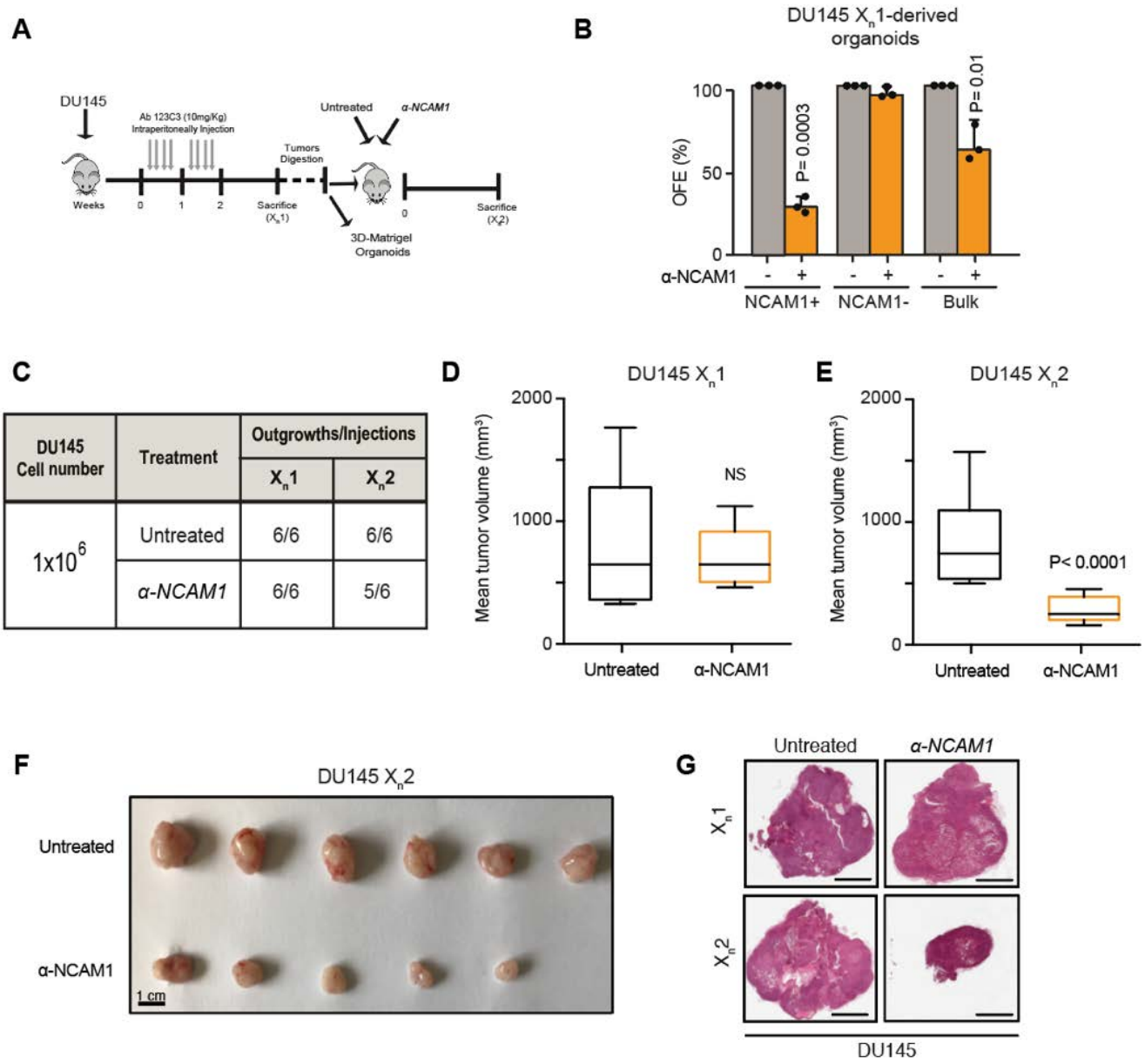

Figure 20. NCAM1 is a potential therapeutic target for anti-CSC therapies PCa. **A)** *Flowchart of the in vivo treatment of DU145 outgrowths with the α-NCAM1 antibody in NSG mice and the serial re-transplantation or OFE assay performed on cells derived from the first-generation (X_n1) tumors in the absence of further treatment. X_n2: second-generation.* ***B)*** *OFE (%) of FACS-purified $NCAM1^+$ and $NCAM1^-$ cells or bulk cells derived from X_n1 DU145 outgrowths obtained from α-NCAM1 treated mice or control untreated mice (n=5).* ***C)*** *Table reporting outgrowths obtained per injection of $1x10^6$ bulk DU145 cells in NSG mice at the first (X_n1) and second (X_n2) generation.* ***D-E)*** *Box plots of mean tumor volume (mm^3) of DU145 outgrowths in X_n1 (D; n=6) and X_n2 mice (E; n=5). Mean ± SD.* ***F)*** *Images of outgrowths obtained from X_n2 mice transplanted with X_n1-derived treated (α-NCAM1) or untreated cells. Scale bar = 1 cm.* ***G)*** *H&E staining of outgrowths obtained in control and α-NCAM1 treated X_n1 mice and in X_n2 mice serially transplanted (without further treatment) with tumor cells from control and α-NCAM1 treated X_n1 outgrowths. Scale bar= 400 µm. p-values were calculated using the Student's t test.*

All these previous results allow us to point out that the subpopulation of PCa cells isolated by the surface glycoprotein NCAM1, but lacking NED traits, can be considered to be as *bona fide* PCSCs with possessing unique sustained self-renewal ability, tumorigenicity and acquisition of EMT traits with invasive and migratory potential. Moreover, NCAM1$^+$ cells are necessary for PCa progression in TRAMP mouse to severe tumor lesions, and for maintaining stem traits *in vitro* and *in vivo.* Thus, NCAM1 is a valuable novel PCSCs biomarker with prognostic value in clinics.

6.2 The basal-like quiescent NCAM1$^+$/CD117$^+$ PCSCs are at the apex of the cellular hierarchy in the NCAM1$^+$ PCa cell population and display Hedgehog-sustained self-renewal ability

6.2.1. scRNA-Seq revealed a cluster of quiescent cells at the apex of cellular hierarchy in the bulk NCAM1$^+$ population

Our data indicate that NCAM1$^+$ PCa cells are a heterogenous subpopulation of cells which appear to comprise: i) NE *vs.* non-NE cells **(see Fig.1 and Fig. 7)**, ii) cells with variable expression of surface biomarkers associated with the luminal and basal compartment of prostate epithelium (i.e., CD44, CD133, CD117, CD38 and CD166) (**see Fig. 13 and Fig. 16**). Thus, we used the 10X Genome Chromium scRNA-Seq platform to determine whether the NCAM1$^+$ subfraction of PCa cells displays a hierarchal organization comprising true PCSCs and progenitors. We analyzed by scRNA-Seq NCAM1$^+$ cells isolated by FACS from the DU145 (n = 4122) and LNCaP (n = 3232) cell lines. AR and PSA (encoded by the *KLK3* gene) transcriptional expression levels were used as controls to confirm the origin of the sorted NCAM1$^+$ cells; DU145 are negative for these genes, while LNCaP are positive **(Fig. 21A)**. Cellular composition was investigated using the unbiased clustering base in the principal component analysis (PCA) and visualized by uniform manifold approximation and projection (UMAP) using a graph-based method. We grouped DU145 NCAM1$^+$ cells into 10 distinct cell clusters based on transcriptional similarities **(Fig. 21B,C)**; while LNCaP NCAM1$^+$ cells were divided into 6 cell clusters **(Fig. 21B,C)**. Interestingly, clusters 8, 9 and 10 in DU145 NCAM1$^+$ cells were uniquely characterized by the enhanced transcription of a gene that transcribes for the mucin-1 (MUC1), a membrane-bound protein. Of note, MUC1^{high} cells were identified only in DU145 and not LNCaP NCAM1$^+$ cells.

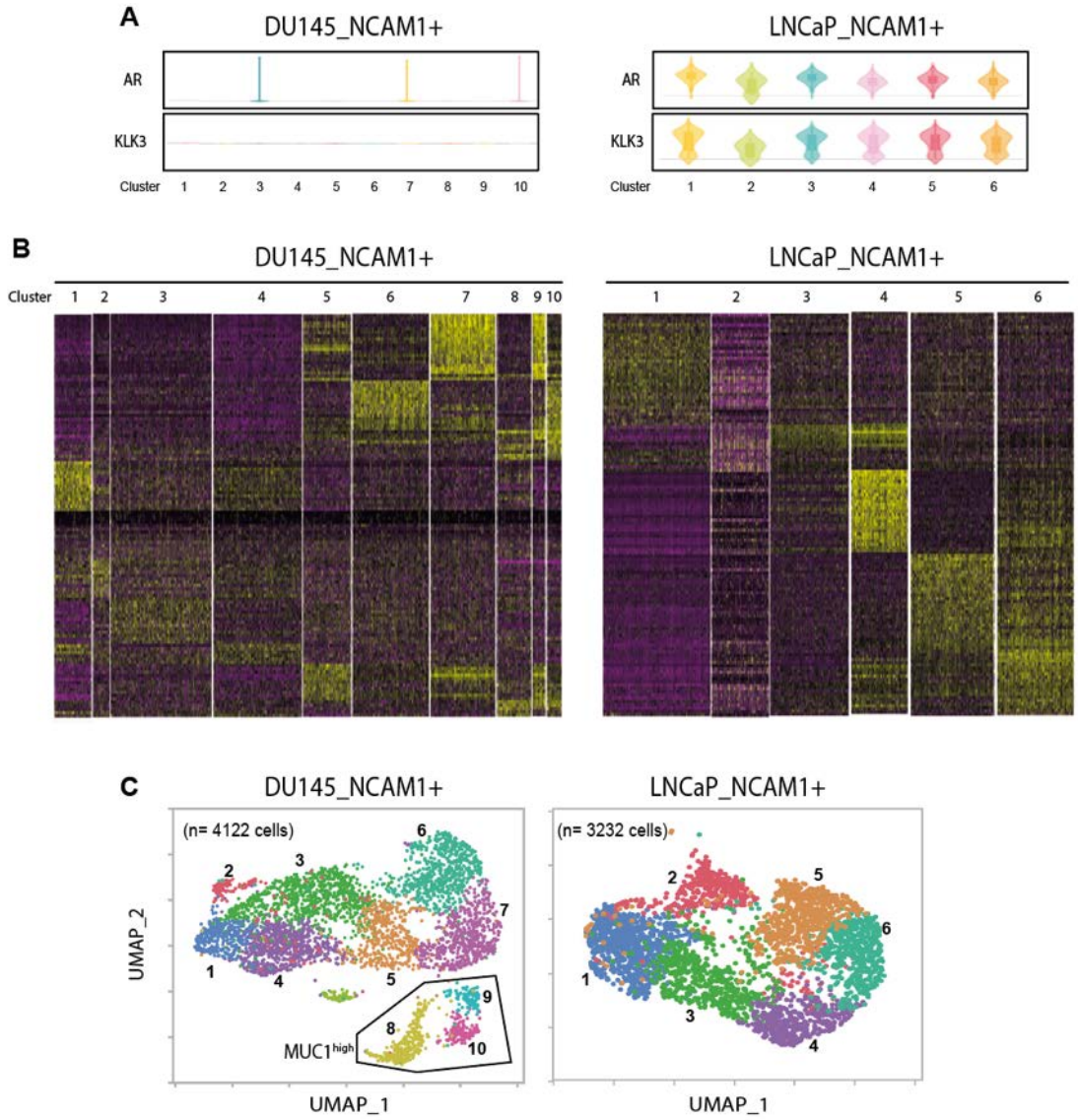

Figure 21. ScRNA-Seq reveals heterogeneity in the NCAM1$^+$ cell population. A) *Violin plot showing androgen receptor (AR) and KLK3 (PSA) expression, in each cluster revealed in the NCAM1$^+$ cells derived from DU145 (left) and LNCaP (right).* ***B)*** *List of top 15 (for DU145_NCAM1$^+$)(left) and top 30 (for LNCaP_NCAM1$^+$) (right) genes defining each cluster.* ***C)*** *UMAP representation of clustering analysis performed by Loupe software on NCAM1$^+$-derived from DU145 (left) (n= 4122 cells) and LNCaP (right) (n= 3232 cells). Each cluster is defined by a color. Clusters 8, 9 and 10 in DU145_NCAM1$^+$ are defined by high expression of the MUC1 gene (MUC1^{high}).*

To understand the contribution of proliferative genes to the observed cell heterogeneity, we analyzed the distribution of cell cycle phases in each cluster. Cells were assigned to G0/G1, S, and G2/M phases based on cell cycle-regulated gene signatures. We found that ~70% of cells in NCAM1$^+$_DU145 (in clusters 1 to 5) and ~20% of cells in NCAM1$^+$_LNCaP (in clusters 1 to 3) could be assigned to G0/G1, while the remaining cells were divided between S phase (cluster 6 in both NCAM1$^+$_DU145 and NCAM1$^+$_LNCaP) and G2/M phase (cluster 7 in NCAM1$^+$_DU145 and clusters 3 to 5 in NCAM1$^+$_LNCaP) **(Fig. 22A)**. Then, we investigated the expression of specific genes associated with cell cycle control such as marker of proliferation Ki-67 (*MKI67*), the cyclin-

dependent kinase inhibitor 1C (*CDKN1C/P57*) that controls the entering of cells into the G1 phase, cyclin-D1 (*CCND1*) that promotes the G1-S transition, the G2/mitotic-specific protein cyclin-B1 (*CCNB1*) that controls the G2/M transition, and the cell division cycle protein 20 (*CDC20*) that controls the M phase. Violin plots showed that *Ki67* defines the proliferating clusters 5 to 7 in NCAM1$^+$_DU145 cells and clusters 2 to 6 in NCAM1$^+$_LNCaP cells **(Fig. 22B)**. In the same clusters for both samples, the expression of *CCND1*, *CCNB1* and *CDC20* is enhanced, suggesting that cells in each of these clusters are cycling and distributed in all the different phases of cell cycle. In contrast, *Ki67* is less expressed in clusters 1 to 4 in NCAM1$^+$_DU145 cells and cluster 1 in NCAM1$^+$_LNCaP cells. In each of these clusters, the expression of the quiescent marker (*CDKN1C/P57*) is enhanced, in particular, in NCAM1$^+$_DU145 cells *P57* expression is highest in cluster 1 and progressively decreases in the successive clusters suggesting that these cells are blocked in G1/G0 phase **(Fig. 49B)**. These data reveal heterogeneity in the cell cycle status in NCAM1$^+$ cells, and that cluster 1 in both samples seems to be comprised of very slow proliferating/quiescent cells (enriched in P57 expression and low levels of Ki-67).

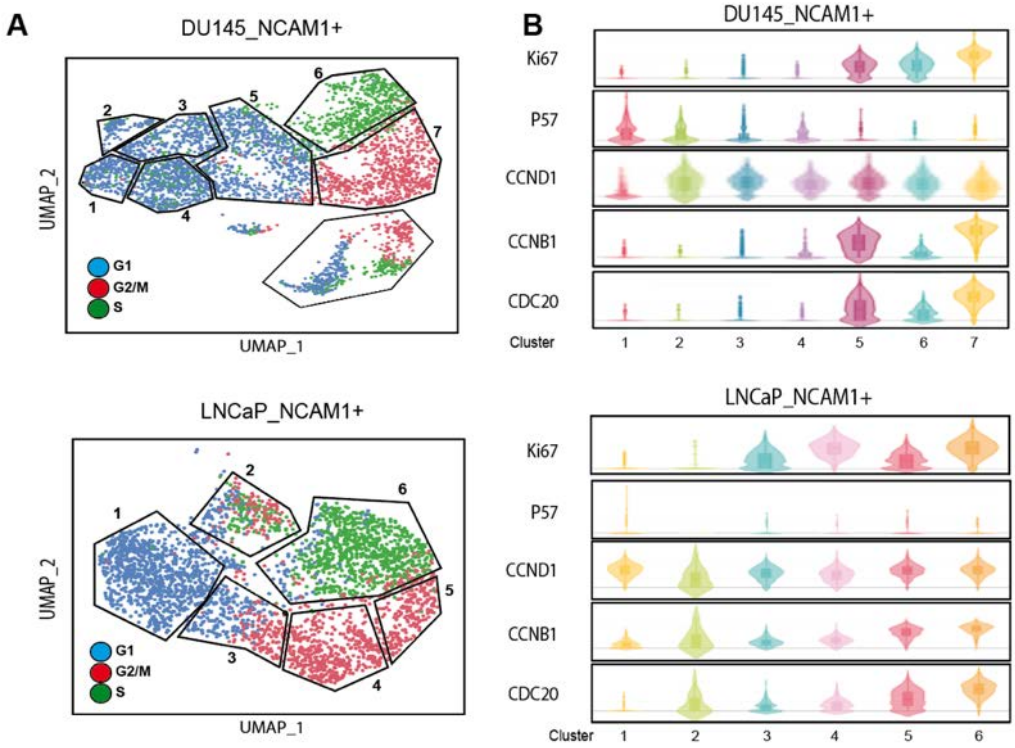

Figure 22. NCAM1$^+$ cell clusters are heterogeneously distributed in cell cycle stages. **A)** *UMAP representation of cell cycle stage signatures for G1 (blue), S (green), or G2/M (red) phase in the NCAM1$^+$ cells derived from DU145 (upper) and LNCaP (lower).* ***B)*** *Violin plots showing the expression of cell cycle-associated genes Ki67, P57, cyclin-D1 (CCND1), cyclin-B1 (CCNB1) and cell division cycle protein 20 (CDC20) in each cluster defined in the NCAM1$^+$ cells derived from DU145 (upper) and LNCaP (lower).*

In the literature, it is widely reported that the "true" CSCs are in a quiescent state (G0/G1 block) with the potential to originate CSC-like cells/progenitor with stem traits (reviewed in Chen W et al, Stem Cells Int 2016). To uncover whether an NCAM1$^+$ cell-of-origin exists in the NCAM1-expressing cell population, we performed a single cell a trajectory analysis using Monocle. As shown, we could place quiescent cells in G1-phase at the beginning of the trajectory, while those in the S- and G2/M-phases were at the end of the trajectories **(Fig. 23A, upper panels)**. Moreover, among all the G1-phase subfraction, only cells in cluster 1 were found at the origin of the trajectory from which all the branches (corresponding to different transcriptional states) originate, both in DU145_NCAM1$^+$ and in LNCaP_NCAM1$^+$ cells **(Fig. 23A, lower panels)**. These data indicate that quiescent cells in cluster 1 are at the apex of the cellular hierarchy in the NCAM1$^+$ cell population.

To verify this result, we performed an unsupervised phylogenetic analysis, shown as a dendrogram, to infer the evolutionary relationships among the different clusters. For both DU145_NCAM1$^+$ and LNCaP_NCAM1$^+$ cell populations, this analysis indicates that cluster 1 is the potential common "progenitor" of all other cell clusters, being in a branch from which all the others are derived **(Fig. 23B)**.

Together, these data suggest that the evolution of NCAM1$^+$ cells from the DU145 and LNCaP cell lines, starts from a quiescent cluster of cells that is at the apex of the hierarchy and which likely represents the *bona fide* PCSC population.

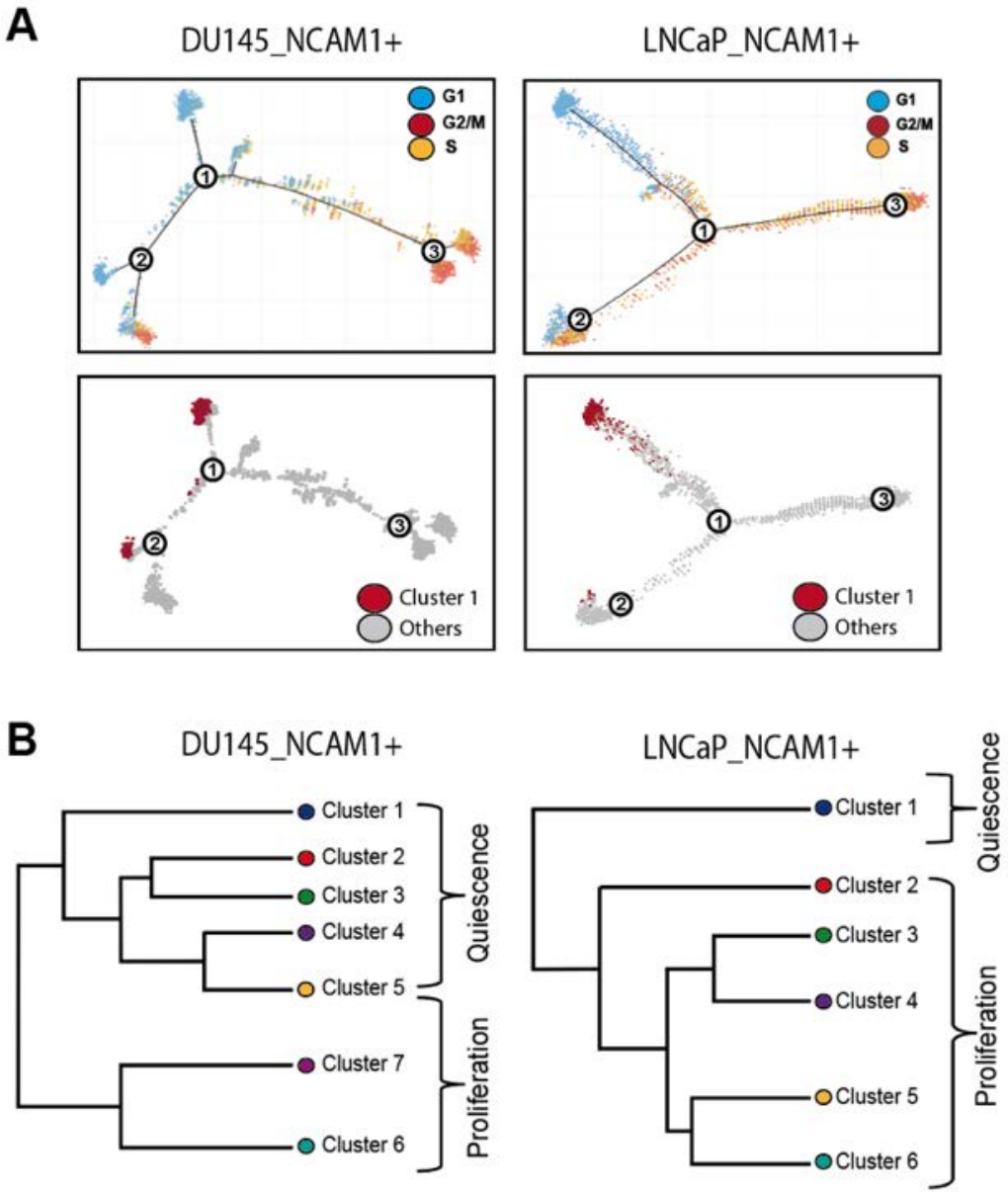

Figure 23. NCAM1$^+$ quiescent and proliferating clusters are hierarchically organized. A) *Evolutionary trajectory analysis of the clusters was analyzed in DU145_NCAM1$^+$ and LNCaP_NCAM1$^+$ cells using Monocle. The upper panel shows the evolution based on cell cycle phases with G1 as the apex of the trajectory. In the lower panel, the location of cluster 1 vs. other clusters is highlighted in the trajectory. Circled number indicates the branches.* ***B)*** *Dendrogram performed by Cerebro software showing the phylogenetic evolution of NCAM1$^+$ cells isolated form DU145 (left) and LNCaP (right) NCAM1$^+$ cells. Data are shown as phylogenetic trees in which each branch indicates a cluster of cells.*

Next, we sought to identify a common gene signature expressed by both DU145 and LNCaP cluster 1 cells which could be used as a molecular marker of quiescent "true" PCSCs. We identified significant genes (p-value < 0.005) defining each cluster 1: 367 genes for DU145-NCAM1$^+$ and 176 gens for LNCaP-NCAM1$^+$. The intersection of these two gene sets identified 40 common genes, which included transcription factors (*SOX4, ARID5B, MXD4, TSC22D1, KDM5B*), stress sensors (*TP53INP1, SESN3, NDRG1, DDIT4*), cell cycle regulators (*BTG1, CCNG2, TOB1*) and long non-

coding RNAs (*NEAT1, MALAT1*) **(Fig. 24A)**. Among the top ranked genes of cluster 1 for both cell lines, we found SOX4 **(Fig. 24A,B)**.

We therefore validated the role of SOX4 in stemness traits by silencing its expression with siRNA (siSOX4). NCAM1$^+$ cells were isolated by FACS sorting from DU145 and LNCaP cells and serially propagated to test the self-renewal ability in a 3D-Matrigel assay. As observed, the efficient silencing of SOX through reverse transfection in Matrigel, did not affect the initial OFE of sorted cells at the first generation, however it significantly impaired self-renewal ability in successive generations **(Fig. 24C)**.

Thus, we added to our cluster-1 common genes signature (n=40), the published Liu_SOX4_Target_up signature (n= 139 genes), obtained by the overexpression of SOX4 in LNCaP cells (Liu *et al.*, 2006). The new combined signature was defined as the "Stem Score" (n = 179 genes). We speculated that this "Stem Score" signature, which takes into account genes associated with quiescence (i.e., cluster 1 genes) and with the activity of SOX4 (i.e., SOX4 signature genes), could identify true NCAM1$^+$-PCSCs with high sensitivity. In both UMAP clustering graphs and trajectory analyses, the Stem Score signature was highly expressed, as expected, in cluster 1 of both the LNCaP and DU145 NCAM1$^+$ populations **(Fig. 24D)**.

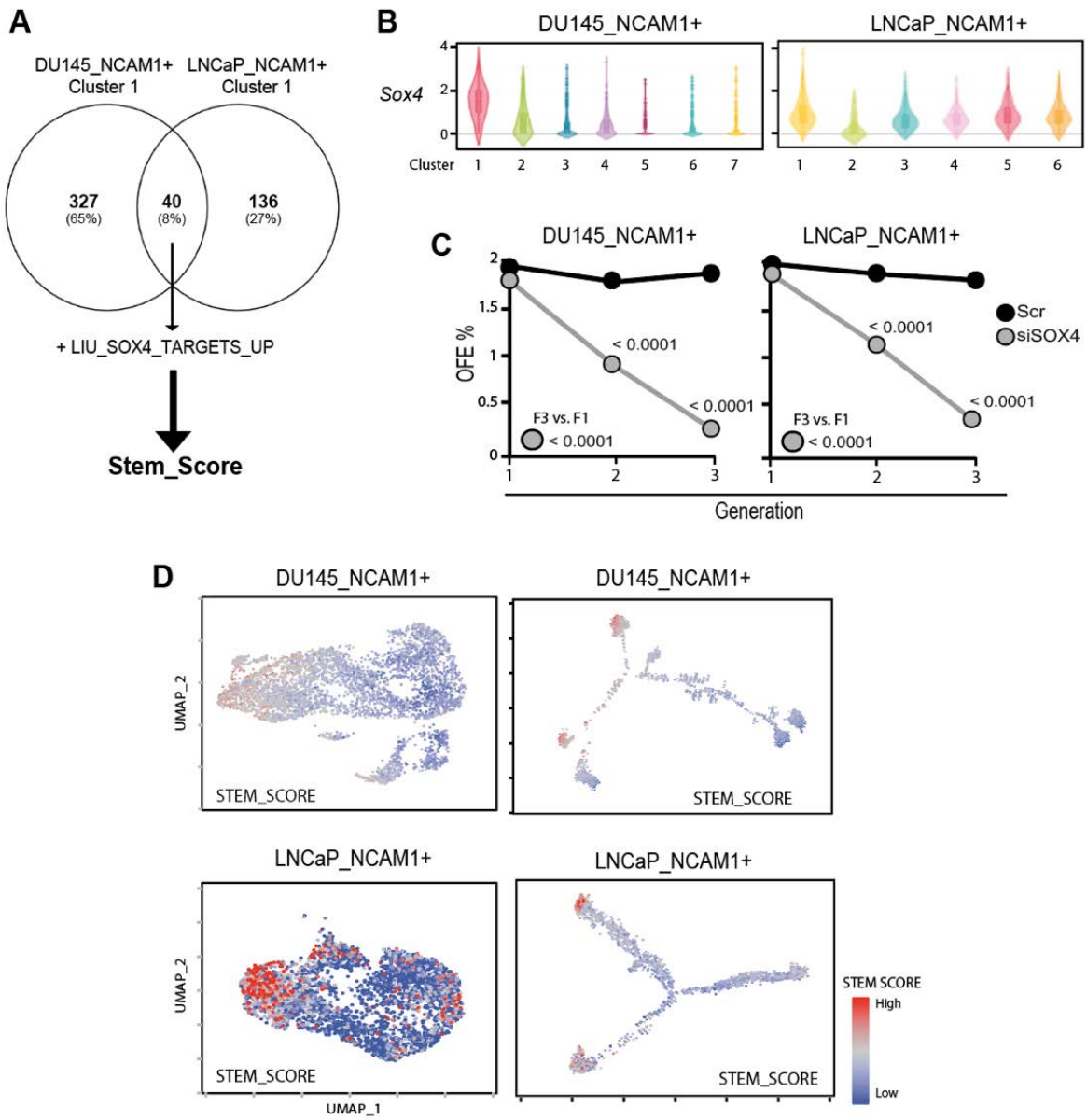

Figure 24. "Stem score" signature identifies cells at the apex of the NCAM1$^+$ cellular hierarchy. A) *Schematic showing the derivation of the Stem_Score signature. The Venn diagram shows overlapping genes (n=40) between cluster 1 of DU145_NCAM1$^+$ (n= 367 genes) and cluster 1 of LNCaP_NCAM1$^+$ (n = 176 genes). Genes upregulated by SOX4 in LNCaP cells (LIU_SOX4_TARGETS_UP is a published dataset (https://www.gsea-msigdb.org/gsea/msigdb/cards/LIU_SOX4_TARGETS_UP) containing n = 139 genes) were added to the 40 common cluster 1 genes to derive the Stem Score signature (n = 179).* ***B)*** *Violin plot showing the expression of Sox4 in DU145_NCAM1$^+$ (left) and in LNCaP_NCAM$^+$ (right) clusters.* ***C)*** *Serial organoid propagation ability in 3D-Matrigel of NCAM1$^+$ bulk cells isolated from DU145 (left) and LNCaP (right) and silenced with reverse transfection in Matrigel for SOX4 (siSOX4) (n=2). Results are expressed as organoid-forming efficiency (OFE %). P-values were calculated comparing the first (F1) and third (F3) generations using the two-way ANOVA test.* ***D)*** *The distribution of the expression of "Stem Score" genes in clusters in shown in UMAP representations (left) and in the evolutionary trajectories (right) for both samples (DU145_NCAM1$^+$ upper; LNCaP_NCAM1$^-$ lower). The color scale indicates the intensity of the "Stem Score".*

6.2.2. "Stem score" highlights a quiescent basal-like NCAM1$^+$CD117$^+$ cell population, with EMT traits, as the "true" PCSCs

To test whether the heterogeneity discovered in NCAM1$^+$ cells derived from cell lines reflects that occurring in human PCa biopsy samples, we performed a scRNA-Seq analysis of NCAM1$^+$ cells isolated by FACS from a pool of high Gleason grade primary frozen biopsy samples (n=10). Although we recovered only a few cells from these samples (n=285), the UMAP clusterization and visualization revealed four clusters **(Fig. 25A)**, with an equal distribution of the number of expressed genes **(Fig. 25 B,C)**. Of note, cluster 4 was characterized only by mitochondrial genes, therefore it was excluded from further analysis.

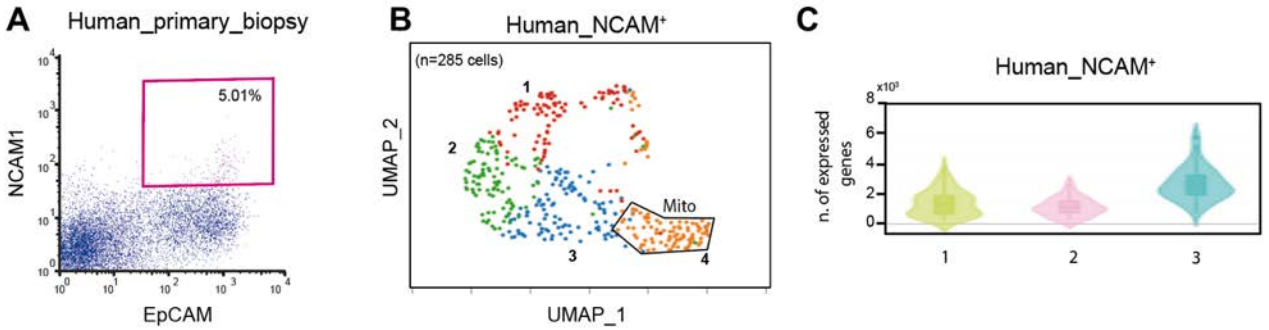

Figure 25. ScRNA-Seq deconvolutes the phenotypic heterogeneity in human PCa-derived NCAM1$^+$ cells. *A) FACS profile of human primary biopsy cells stained for NCAM1 and EpCAM1. The box indicates the percentage of EpCAM$^+$/NCAM1$^+$ cells in the bulk population.* ***B)*** *UMAP representation of the clustering analysis performed by Loupe software on NCAM1$^+$-derived cells from human primary PCa biopsies (n=10) pooled together (n=285 cells). Each cluster is defined by a color. Cluster 4 is characterized by mitochondrial-related genes only (Mito).* ***C)*** *Violin plot showing the number (n.) of expressed genes in each cluster (1-3).*

The primary human PCa NCAM1$^+$ population was interrogated with the Stem Score. As shown by the box plot, the expression of the Stem Score is enriched in cluster 1 of primary derived NCAM1$^+$ PCa cells, while it is very low in the other clusters **(Fig. 26A).** We determined that ~10% of the total NCAM1$^+$ PCa cells were highly expressing the Stem Score: intensity > 0.2 **(Fig. 26B)**. We characterized clusters for the expression of epithelial marker genes, such as the basal *P63, KRT5, KRT15,* and *KRT14* markers and the luminal *KRT8, KRT18, KRT19,* and *KRT7* markers, as well as the *AR*. Violin plots revealed that cluster 1 is enriched in all the basal-like markers, compared to clusters 2 and 3, although p63 and KRT14 are expressed at low frequency in the NCAM1$^+$ population **(Fig. 26C)**. Instead, luminal-like markers are expressed at higher levels in cluster 3 compared with clusters 1 and 2 **(Fig. 26C)**. Interestingly, we noted that AR is infrequently expressed in clusters 1 and 2 while in cluster 3 it is expressed more frequently at low levels **(Fig. 26C)**. This observation suggests that the "true" NCAM1$^+$-PCSCs are likely to be AR$^-$.

We also examined the expression, in the different clusters, of the putative PCSC biomarkers reported in the literature (*KIT/CD117, PROM1/CD133, CD44, CD38, ALCAM/CD166)* and the NE marker *CHGA,* which we previously investigated (see section 6.1.6). We found that cells in cluster 1 uniquely express CD117, high levels of CD44 ($CD44^{high}$) and low levels of CD133, while clusters 2 and 3 expressed higher levels of CD133 and lower levels of CD44 ($CD44^{low}$). CD38 was expressed at low levels only in cluster 2. Finally, CD166 was equally distributed in all the clusters, while the NE marker *CHGA* was not expressed in any cluster **(Fig. 26D)**.

Together, these data indicate that a subfraction of basal-like $AR^{-}/NCAM1^{+}/CD117^{+}$ cells expressing the Stem Score signature, sits at the apex of the hierarchical structure of the $NCAM1^{+}$ cells. By FACS analysis, we provided evidence to support the existence of this subfraction of cells in human PCa cells (low Gleason grade); we showed that rare $NCAM1^{+}/CD117^{+}$ cells exist and represent ∼10 % of the bulk $NCAM1^{+}$ population **(Fig. 26E)**

To further characterize this subfraction of cells and characterized the proliferative profile of these cells, we isolated by FACS sorting the $NCAM1^{+}/CD117^{+}$ and the $NCAM1^{+}/CD117^{-}$ cells from the LNCaP cell line. By IF, we revealed that less than 1% of $NCAM1^{+}CD117^{+}$ cells are $Ki67^{+}$ **(Fig. 26F,G; Fig. 27B)**. These data suggest that "true" PCSCs, sitting at the apex of the $NCAM1^{+}$ population in PCa, co-express CD117 and are phenotypically quiescent/slow-proliferating, compatible with the phenotype of stemness.

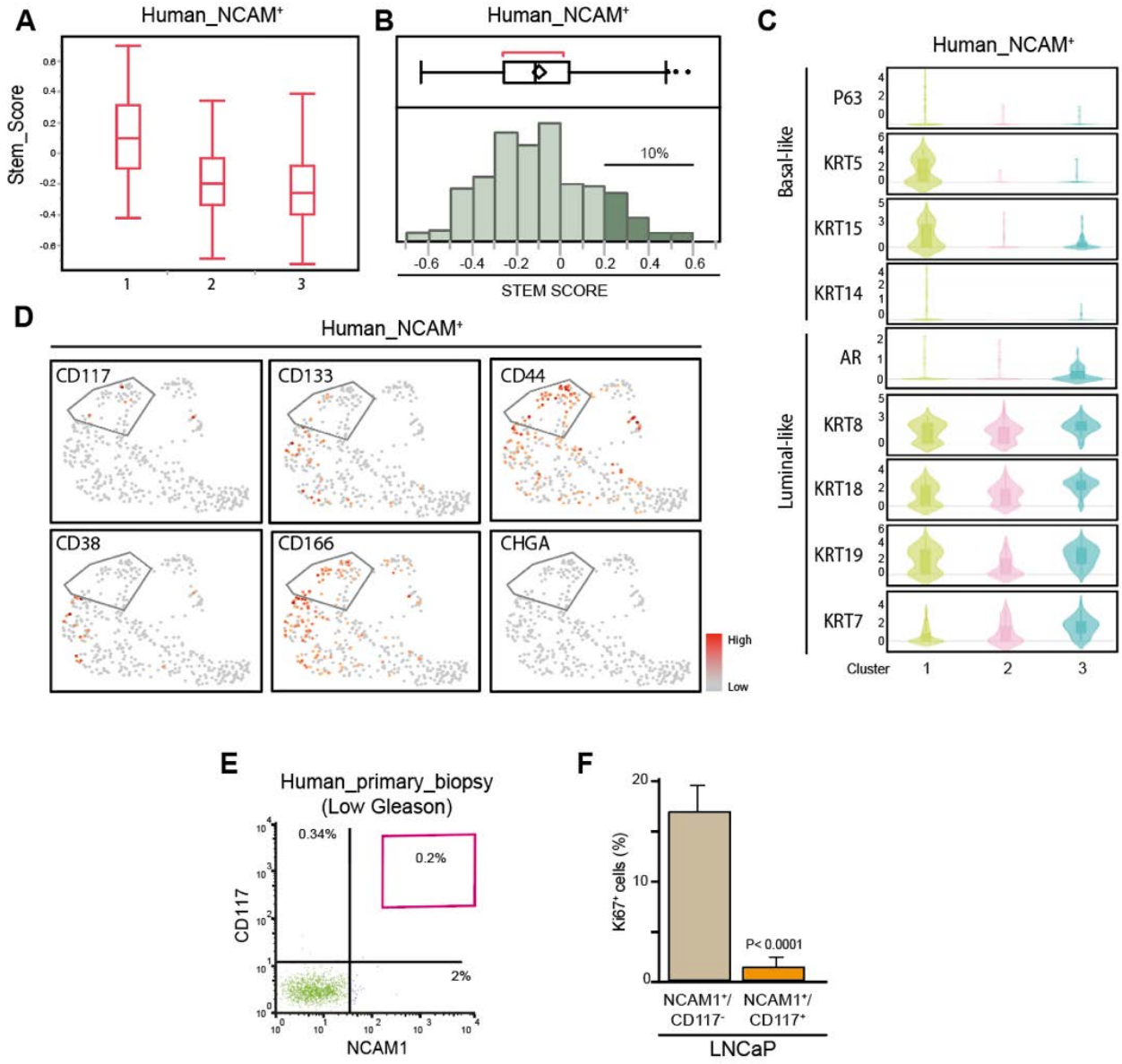

Figure 26. "Stem score" identifies basal-like quiescent NCAM1$^+$/CD117$^+$ cells. A) *Box plot showing the intensity of "Stem Score" in each cluster revealed in NCAM1$^+$ cells isolated from PCa biopsies.* ***B)*** *Bar chart depicting the percentage (%) of cells positive for the Stem Score (intensity > 0.2), as indicated.* ***C)*** *Violin plot for epithelial marker-related genes: basal-like (P63, KRT5/CK5, KRT15/CK15 and KRT14/CK14), and luminal-like (KRT8/CK8), KRT18/CK18, KRT19/CK19, and AR).* ***D)*** *UMAP representation of NCAM1$^+$ clusters interrogated for the distribution of our candidate PCSC-related biomarkers CD117, CD133, CD44, CD38, and CD166 and the NE marker CHGA. Color bar refers to intensity of expression.* ***E)*** *Representative FACS profile of cells derived from low Gleason grade PCa biopsy sample and stained for NCAM1 and CD117. The box shows the percentage of EpCAM$^+$/NCAM1$^+$/CD117$^+$ cells.* ***F)*** *Histogram showing the percentage of LNCaP-isolated NCAM1$^+$/CD117$^+$ and NCAM1$^+$/CD117$^-$ cells positive for the Ki-67 proliferation marker. Data are reported as a percentage. Mean ± SD* (n > 10 cells in at least 5 different fields). *P-values were calculated using the Student's t test.*

Cellular plasticity and the acquisition of EMT traits are intrinsic features of CSCs (see section 2.3.3.1). Since NCAM1 is widely associated with cell migration and the acquisition of metastatic potential in different cell types, which are features of cells that have undergone EMT (see section 2.2.10.5). Moreover, CD117 was found expressed by CTCs (Kerr *et al*., 2015) and quiescence is the main feature of DTCs, we investigated the distribution of EMT traits in each cluster of primary human-derived $NCAM1^+$ cells. Box plot shows that EMT hallmark is enriched in cluster 1 suggesting that the basal $NCAM1^+/CD117^+$ cells could have EMT traits **(Fig. 27A)**. Thus, we isolated both $NCAM1^+/CD117^+$ and $NCAM1^+/CD117^-$ cells from bulk LNCaP cell lines and we interrogated them for the expression of the epithelial marker E-Cadherin (ECAD) and the proliferative marker Ki67, by IF. Data revealed that the quiescent $NCAM1^+/CD117^+$ subfraction of cells expressed very low levels of ECAD opposed to the $NCAM1^+/CD117^-$ that appear to be more epithelial **(Fig. 27B)**. Furtherly we interrogated the $NCAM1^+$ clusters for the expression of EMT related transcription factors (ZEB1, SLUG, SNAIL and TWIST2) and the EMT-related proteins (VIMENTIN, VEGFA, MMP10 and MMP2) (see section 2.2.7.1.1). UMPA representation show that the $NCAM1^+/CD117^+$ subfraction of cells is enriched for the expression of ZEB1, SLUG and TWIST2, but not SNAIL **(Fig. 27C)**. Moreover, they positively express VIMENTIN and VEGFA, but exclusively MMP10, involved in invasion and angiogenesis, and MMP2, commonly associated to metastasis (Scheau C, 2019) **(Fig. 27C)**. Further studies will be necessary to validate the metastatic potential of these cells *in vitro* and *in vivo*.

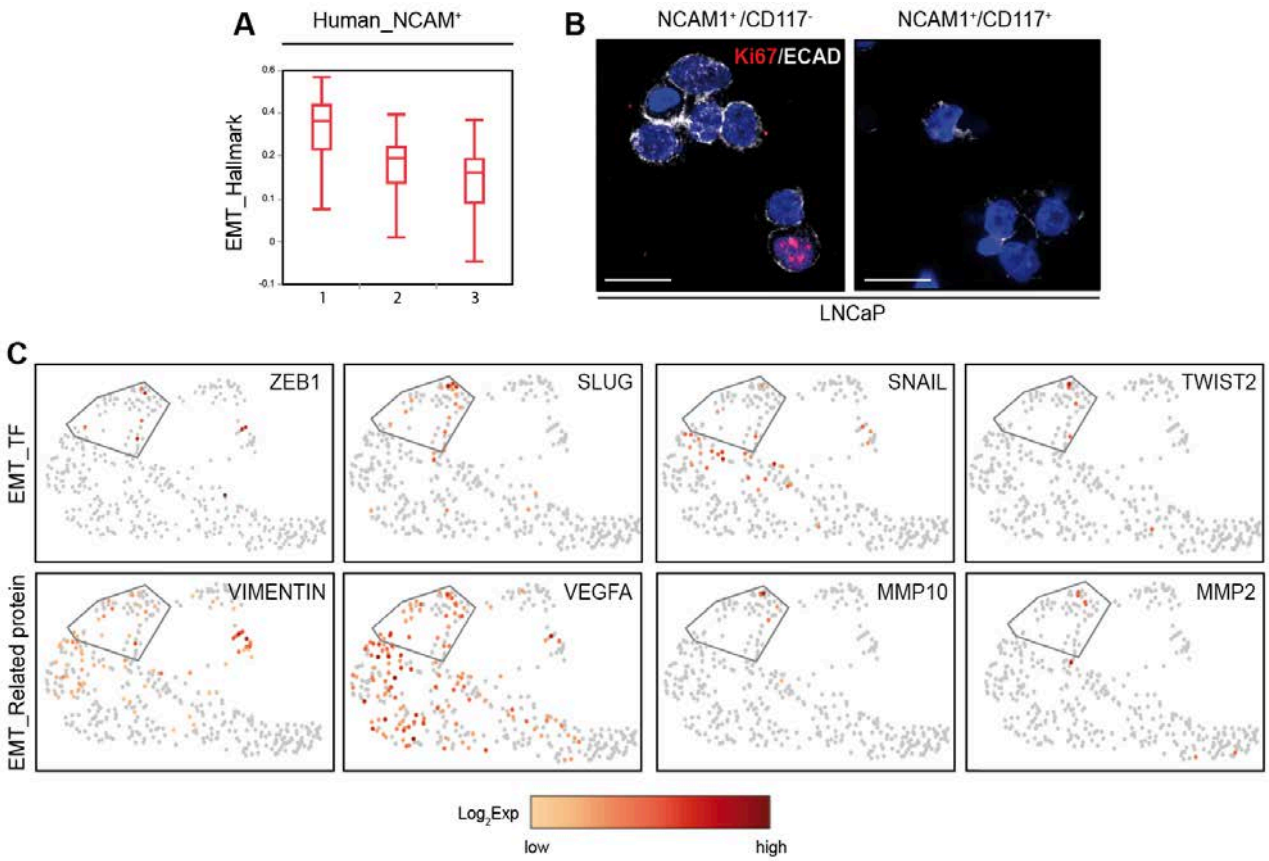

Figure 27. NCAM1$^+$/CD117$^+$ cells are enriched in EMT signature. A) *Box plot showing the distribution of published hallmarks for EMT and Hedgehog signaling in NCAM1$^+$ cells derived from human PCa biopsies (high Gleason grade).* ***B)*** *Representative immunofluorescence of LNCaP-isolated NCAM1$^+$/CD117$^+$ and NCAM1$^+$/CD117$^-$ cells stained for Ki67 (red) and E-Cadherin (ECAD) (white). DAPI was used to stain nuclei. Scale bar = 30 µm.* ***C)*** *UMAP representation of NCAM1$^+$ cluster interrogated for the distribution of the EMT-related transcription factor (TF) ZEB1, SLUG, SNAIL and TWIST2 (upper panels), and the EMT-related proteins VIMENTIN, VEGFA, MMP10 and MMP2 (lower panels). Color bar refers to intensity of expression (Exp).*

6.2.3. Hedgehog signaling controls the self-renewal ability of NCAM1$^+$/CD117$^+$ CSCs.

To gain insight the molecular mechanism relevant for self-renewal ability, we performed a pathway analysis using the upregulated genes (statistically significant p-value < 0.05) expressing in cluster 1 compared to all the other clusters defined in the NCAM1$^+$ population of cells derived from LNCaP and DU145. The analysis was performed with Molecular Signature Database (gsea.msigdb.org). We focused our attention on the obtained molecular signaling pathway, which are displayed based on enrichment score (the ratio between the number of pathway-associated genes in our dataset (k) and the number of genes reported in the hallmark (K) and statistical significance (-Log$_{10}$FDR > 2) **(Fig. 28A)**. Hedgehog pathway it is one of the most enriched pathways (k/K≥ 0.01 and FDR ≤ 0.0001) and uniquely expressed in both cluster 1 compared to the other clusters, in which is not present; and Hedgehog pathway has been widely associated in literature to stem traits and sustained self-renewal ability in PCa (Gonnissen *et al*., 2013) (see section 2.3.3) **(Fig. 28A)**. So, we investigated the distribution of the reported hallmarks of Hedgehog pathway in the dataset of human primary PCa-derived NCAM1$^+$ cells. Interestingly, we noticed that this hallmark is enriched in cluster 1 **(Fig. 28B)** compatible with the role of NCAM1$^+$/CD177$^+$ as "true" PCSCs with self-renewal ability.

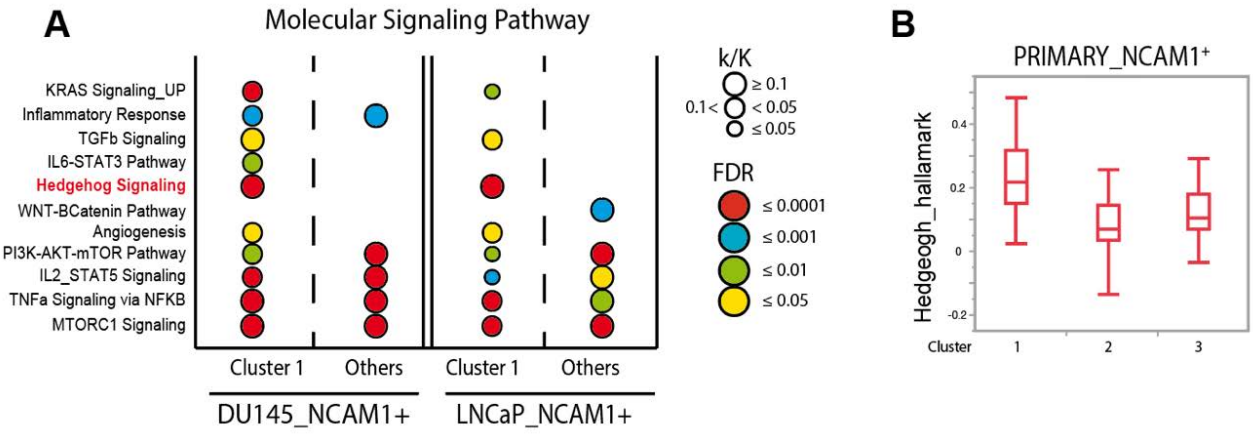

Figure 28. Hedgehogh signaling is enhanced in cluster of cells sitting at the apex of NCAM1$^+$ hierarchy. ***A)*** *Graphical representation of pathway analysis performed with upregulated genes of cluster 1 and others of DU145- and LNCaP-derived NCAM1$^+$ cells. Size dots refers to enrichment score, estimated as the ration between number of upregulated genes in the pathway and number of genes annotated in the pathway. Dots color refers to FDR adjusted p-value < 0.05.* ***B)*** *Box plot showing the distribution of published hallmarks for Hedgehog signaling in NCAM1$^+$ cells derived from human PCa biopsies (high Gleason grade).*

Thus, we tested whether the Hedgehog pathway is determinant for the self-renewal ability of NCAM1$^+$/CD117$^+$ cells. We isolated the NCAM1$^+$/CD117$^+$ and NCAM1$^+$/CD117$^-$ cell populations from the DU145 and LNCaP cell lines by FACS and tested their ability to sustain serial generations of organoids in the presence of the Hedgehog pathway inhibitor cyclopamine. Organoids were treated when they reached a minimum diameter of 30 μm in the first generation, and then serially propagated. Cyclopamine impaired the OFE of NCAM1$^+$/CD117$^+$ in the first generation and completely abrogated the self-renewal potential by the third generation **(Fig. 29)**. In contrast, no effects were observed on NCAM1$^+$/CD117$^-$ cells, which maintained an intact self-renewal ability even in presence of cyclopamine **(Fig. 29)**. This latter finding can be interpreted as evidence of heterogeneity in the PCSC compartment. Thus, we have identified a subfraction of NCAM1$^+$/CD117$^+$ cells with self-renewal ability controlled by the Hedgehog signaling.

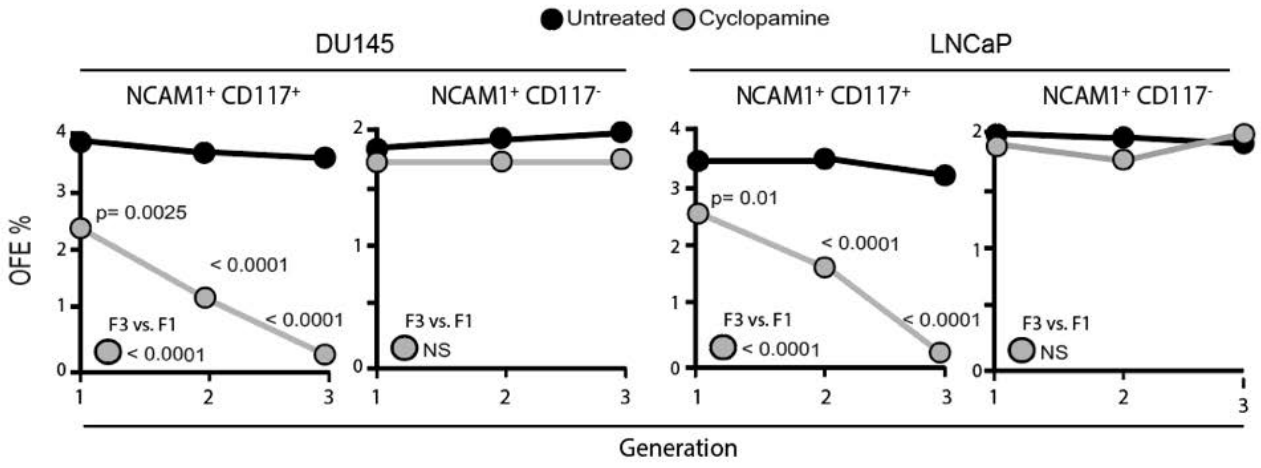

Figure 29. Hedgehog signaling controls self-renewal ability exclusively in NCAM1$^+$/CD117$^+$ cells. *Serial organoid propagation assay of NCAM1$^+$/CD117$^+$ and NCAM1$^+$/CD117$^-$ subfractions of cells, isolated form DU145 (left) and LNCaP (right) cells and treated in the first generation when organoids reached 30 µm of diameter with the Hedgehog pathway inhibitor cyclopamine [5µM] (grey dots). Data are represented as organoid-forming efficiency (OFE %) (n=3). P-values were calculated comparing the first (F1) and third (F3) generations using the two-way ANOVA test.*

In summary, scRNA-Seq analysis has allowed us to dissect he heterogeneity of the NCAM1$^+$ PCa cells revealing the existence of basal-like NCAM1$^+$/CD117$^+$ cells, whose self-renewal is sustained by Hedgehog signaling, at the apex of the hierarchy that could be the driver of NCAM1$^+$ heterogeneity. Thus, targeting this subfraction of cells with compound inhibiting Hedgehog signaling could be a valuable approach to target quiescent/slow-proliferating, AR$^-$/NCAM1$^+$/CD117$^+$-PCSCs to completely prevent tumor regrowth.

6.3 NCAM1$^+$ PCa cells are resistant to ADT and could be key players in the development of CRPC

6.3.1. NCAM1$^+$ cells resist the activation of an ADT-dependent senescence program

The presence in the bulk PCa population of a subset of PCSCs with intrinsic refractoriness to ADT has been postulated as a possible cause of PCa recurrence after treatment discontinuation and/or progression towards CRPC. Indeed, PCSCs appear to be able to survive in the absence of androgens and their number significantly increases after treatment (Germann *et al*., 2012; Lee *et al*., 2013; Qin *et al*., 2012; Shi *et al*., 2014). We therefore decided to test the effects of ADT on the androgen-sensitive LNCaP cells, compared to the androgen-insensitive DU145 cells, by growing them in an androgen-depleted medium (charcoal stripped medium) for 7 days. LNCaP cells exposed to ADT displayed a proliferative block as determined by a reduction in Ki67 expression at the protein and the transcriptional level **(Fig. 30A,B)**. Consistent with the strong downregulation of Ki67 in the presence of ADT, the transcription of the cell cycle inhibitors *P21* **(Fig. 30B)**, *P53* and *P27* **(Fig. 30C)** was enhanced (∼1.5-2-fold) compared to untreated cells. In addition, ADT induced senescence in the bulk LNCaP population, evidenced by positive beta-galactosidase (β-Gal) protein expression **(Fig. 30D)**, a well-established marker of senescence (Hernandez-Segura, Nehme and Demaria, 2018) , in more than 70% of cells **(Fig. 20E)**, and the induction of apoptosis, estimated by active caspase-3 staining, revealed in < 20% of cells **(Fig. 30E)**. At the mRNA level, we confirmed the upregulation of senescence marker genes such as *GLB1* (β-galactosidase) and the cyclin-dependent kinase inhibitor 2A (*CDKN2A/P16*) in ADT conditions in androgen-sensitive LNCaP cells **(Fig. 30F)**. As expected, no effects of ADT were observed in the androgen-insensitive DU145 cells **(Fig. 30E,F)**.

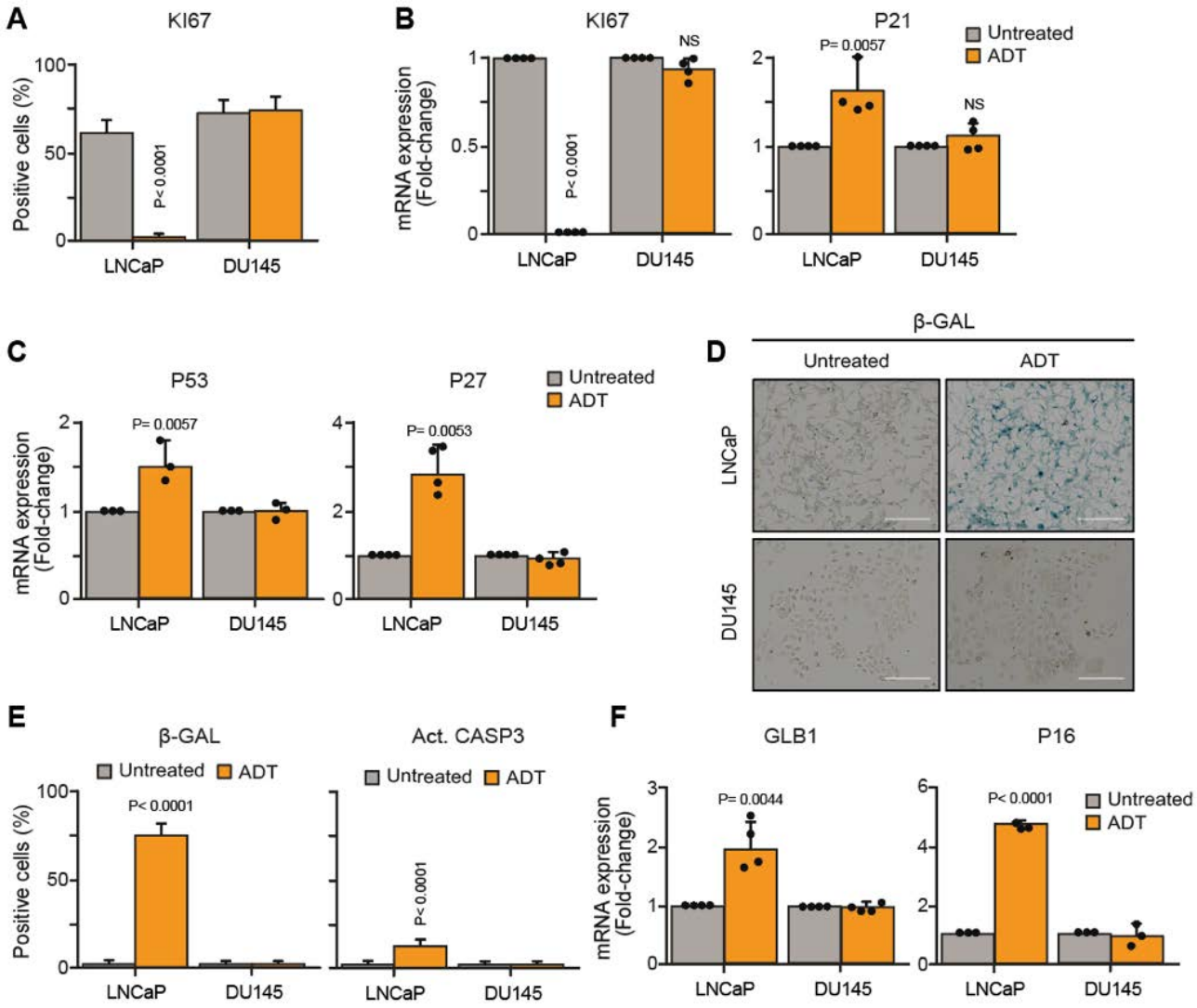

Figure 30. ADT promotes senescence in AR-expressing LNCaP cells. A) *Bulk LNCaP (androgen-sensitive) and DU145 (androgen-insensitive) cells were subjected to ADT (orange) for 7 days or left untreated (grey). Proliferation was assessed by measuring the percentage of Ki-67^{+} cells by immunofluorescence. Data are presented as the mean ± SD (n> 50 cells in at least 5 different fields).* ***B-C)*** *Cells as in "A" were assessed for the expression of proliferation markers Ki67, P21, P53 and P27 by RT-qPCR. Results are the mean ± SD (n=4 or n=3 for P53).* ***D)*** *Representative images of cell morphology and expression of the senescence marker beta-galactosidase (β-GAL in blue) in LNCaP and DU145 cells cultured in normal medium (control) and in ADT conditions for 7 days. Scale bar= 100 µm.* ***E)*** *Histogram showing percentage of cells positive for β-GAL and active caspase-3 revealed by immunofluorescence in bulk LNCaP and DU145 cells treated as in "A". Data are presented as mean ± SD (n> 50 cells in at least 5 different fields).* ***F)*** *RT-qPCR analysis of the expression of senescence genes GLB1 (β-galactosidase) and P16 in cells as in "A". Mean ± SD (n=4 for GLB1 and n=3 for p16). P-values were calculated using the Student's t test. NS: not significant.*

Since the PCSC pool has been shown to be enriched upon ADT exposure (Germann *et al*., 2012; Lee *et al*., 2013; Qin *et al*., 2012; Shi *et al*., 2014), we investigated how ADT affects the proportion of NCAM1-expressing cells. By FACS analysis, we observed that in untreated control conditions, NCAM1 identifies a small subfraction of cells (~1%) in the LNCaP cell line, which was however enriched (~5-fold) in bulk ADT-treated LNCaP cells **(Fig. 31A,B)**. In contrast, there was no variation in the percentage of NCAM1$^+$ cells in treated *vs.* untreated DU145 cells (2.2% untreated *vs.* 2.4% treated) **(Fig. 31A,B)**. We also checked for alterations in the transcription of NCAM1 in bulk cell populations by RT-qPCR and detected a ~6-fold increase in ADT treated LNCaP cells vs. untreated, in line with the increase in the number of NCAM1$^+$ cell, while no effect was observed in DU145 cells **(Fig. 31C)**. These results suggest the positive selection/clonal expansion of NCAM1$^+$ LNCaP cells following ADT.

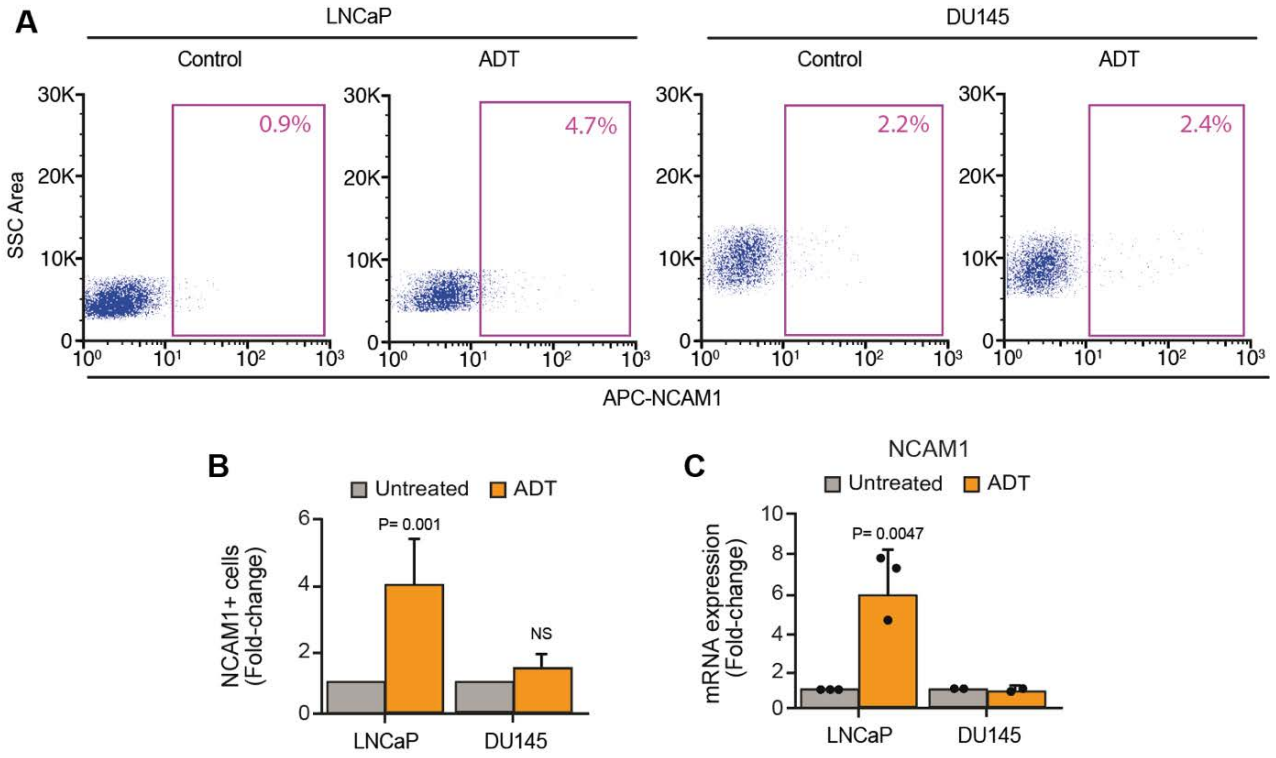

Figure 31. NCAM1$^+$ population is enriched in response to ADT. A) *LNCaP and DU145 cells were treated with ADT or left untreated (Control) for 7 days. The percentage of NCAM1$^+$ cells was determined by FACS using the anti-NCAM1-APC conjugated antibody Representative FACS profiles are shown.* ***B)*** *Quantification of the FACS analysis shown in "A". Results are presented as the fold-change in NCAM1$^+$ cells in treated samples relative to the untreated control. Mean ± SD (n=3).* ***C)*** *RT-qPCR analysis of NCAM1 expression in untreated or ADT-treated bulk LNCaP and DU145 cells as described in "A". Data are represented as fold-change relative to the untreated control. Mean ± SD (n=3 for LNCaP and n=2 for DU145). P-values were calculated using the Student's t test. NS: not significant.*

We next characterized untreated LNCaP-isolated NCAM1$^+$ cells for the expression of AR by RT-qPCR. DU145 cells were used as a negative control. Results revealed that NCAM1$^+$ cells isolated from LNCaP displayed lower levels of AR mRNA (~50%) compared to NCAM1$^-$ cells **(Fig. 32A)**. This reduction in mRNA was accompanied by a reduction in AR protein levels in NCAM1$^+$ LNCaP cells, revealed by western blot **(Fig. 32B)**. Interestingly, by IF staining for AR in LNCaP-purified NCAM1$^+$ and NCAM1$^-$, we revealed heterogeneity in the expression of AR in the NCAM1$^+$ subfraction. Indeed, ~50% of NCAM1$^+$ cells do not express AR compared to the other 50% that instead are AR$^+$ **(Fig. 32C,D)**.

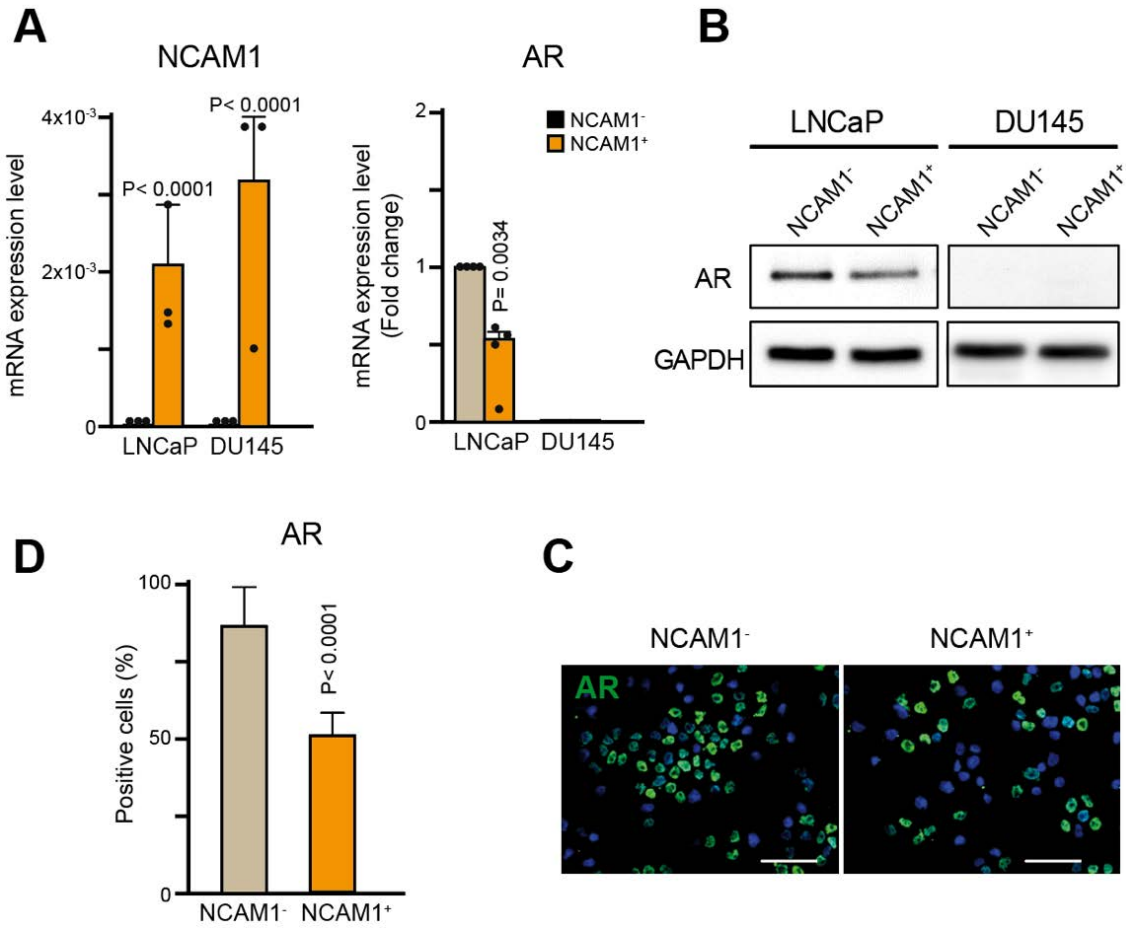

Figure 32. NCAM1$^+$ LNCaP cells display heterogeneous expression of AR. A) *RT-qPCR for NCAM1 and androgen receptor (AR) in NCAM1$^-$ (black) and NCAM1$^+$ (orange) cells isolated from bulk LNCaP and DU145. Results are the mean ± SD (n= 4)* ***B)*** *Quantification of the number of AR-positive cells (%) determined by immunofluorescence in NCAM1$^+$ and NCAM1$^-$ isolated from LNCaP cells. Mean ± SD (n>50 cells in at least five different fields).* ***C)*** *Representative images of the immunofluorescence analysis of AR expression in NCAM1$^+$ and NCAM1$^-$ isolated from LNCaP cells. Scale bar= 100 µm.* ***D)*** *Immunoblot analysis of AR expression in NCAM1$^+$ and NCAM1$^-$ isolated from LNCaP cells. DU145 were used as negative control and GAPDH as loading control. P-values were calculated using the Student's t test.*

To investigate at the molecular level the effects of ADT on the NCAM1$^+$ cells, we isolated both NCAM1$^+$ and NCAM1$^-$ cells from LNCaP by FACS sorting, and we interrogated them by RT-qPCR for proliferation (*KI67, CDKN1A/P21, CDKN1B/P27, P53*) and senescence-related genes (*CDKN2A/P16, GLB1*). In response to ADT, NCAM1$^-$ cells displayed a proliferative block, evidenced by the decreased expression of the proliferation marker Ki67 and the increased expression of the cell cycle inhibitors *P21, P27* and *P53* **(Fig. 33A)**. In contrast, NCAM1$^+$ cells, in response to ADT, displayed less pronounced effects on proliferation genes, with the decrease in Ki67 mRNA levels and the increase in *P53* and *P21* mRNA levels being less strong relative to that observed in NCAM1$^-$ cells, while *P27* showed a similar increase to NCAM1$^-$ cells **(Fig. 33A)**. This partial effect on proliferation genes is consistent with the heterogeneous expression of AR on NCAM1$^+$ cells, indicating that only some (~50%) of the NCAM1$^+$ cell population is likely responsive to the lack of androgens **(Fig. 33C)**. Interestingly, the activation of the senescence program, assessed by *GLB1* and *P16* mRNA levels, in response to ADT was observed exclusively in NCAM1$^-$ cells **(Fig. 33B)**. By IF analysis, we estimated that ~75% of NCAM1$^-$ cells are senescent, evidenced by the expression of β-Gal, while ~10% of them are positive for the apoptosis marker, activated caspase-3 **(Fig. 33C)**. These data demonstrate that in NCAM1$^+$ cells the induction of a proliferative block and the activation of senescence in response to ADT appear to be uncoupled, with NCAM1$^+$ cells appearing to be resistant to ADT-induced senescence, but not to inhibition of proliferation.

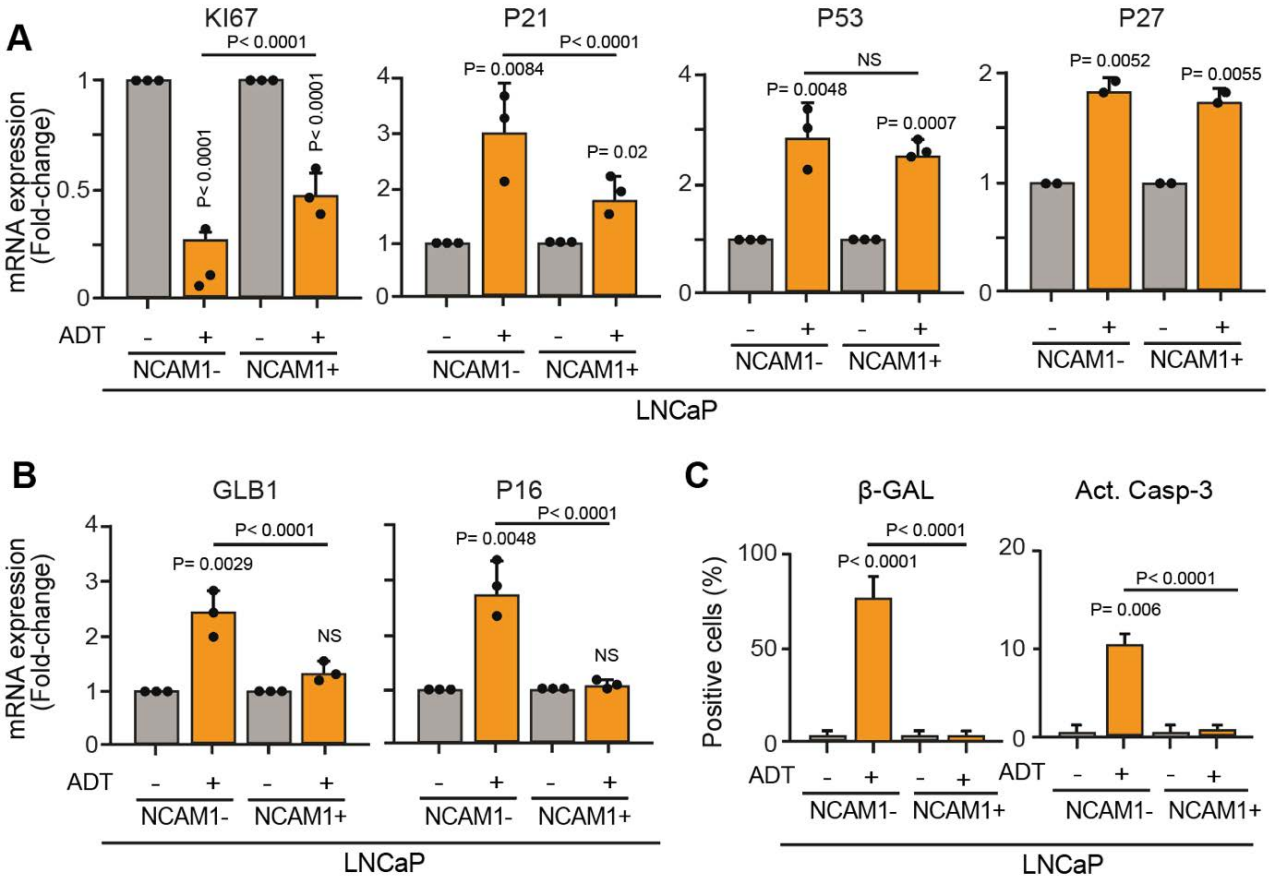

Figure 33. NCAM1$^+$ cells do not undergo ADT-induced senescence. A-B) *RT-qPCR analysis of the proliferation markers KI67, P21, P53 and P27 (A), and the senescence markers GLB1 and P16 (B) in NCAM1$^+$ and NCAM1$^-$ cells isolated from untreated and ADT-treated (7 days) bulk LNCaP. Mean ± SD (n=3 and n=2 for P27).* ***C)*** *NCAM1$^+$ and NCAM1$^-$ cells isolated from untreated and ADT-treated (7 days) bulk LNCaP cells were assessed for β-galactosidase (β-Gal) and active caspase-3 (Act. Casp-3) by immunofluorescence staining. Results are mean % positive cells ± SD (n > 50 cells in at least 5 different fields). P-values were calculated using the one-way ANOVA test. NS: not significant.*

To better understand the role of NCAM1 in determining ADT resistance, we developed stable LNCaP cell lines overexpressing NCAM1 (NCAM1-OE) though plasmid transfection and clonal selection. Empty vector (EV) was transfected to obtain a control cell line. The efficiency of transfection and the establishment of NCAM1-OE LNCaP cells was verified by western blot, RT-qPCR and IF **(Fig. 34A,C)**.

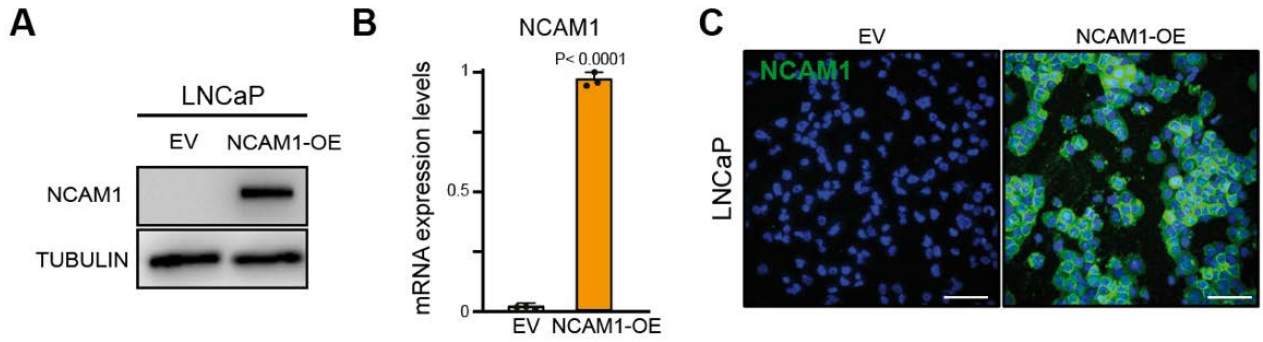

Figure 34. Establishment of the LNCaP NCAM1-overexpressing (-OE) cell line. *LNCaP cells were transfected with a plasmid pcDNA3.1 containing the human NCAM1 gene or empty vector (EV). Transfected clones were selected using FACS analysis for NCAM1 expression.* ***A)*** *Immunoblot for NCAM1 overexpression (NCAM1-OE) in LNCaP vs. LNCaP-EV. Tubulin was used as loading control. B) RT-qPCR for NCAM1 in EV and NCAM1-OE cells. Results are the mean ± SD (n=3). C) Immunofluorescence for NCAM1 (green) in EV and NCAM1-OE cells. Nuclei are stained with DAPI (blue). Scale bar= 100 µm.*

We assessed the sensitivity of our established LNCaP NCAM1-OE cells to ADT. As shown by RT-qPCR, the overexpression of NCAM1 did not prevent the effects of ADT on proliferation with the downregulation of *KI67* and the upregulation of *P21, P27* and *P53* in presence of ADT being similar in EV and NCAM1-OE cells **(Fig. 35A)**. However, NCAM1-OE was sufficient to prevent the upregulation of senescence markers (*P16, GLB1*) **(Fig. 35B).** IF analysis confirmed that the overexpression of NCAM1 inhibited the appearance of cells positive for β-Gal or active caspase-3 **(Fig. 35C)**. These results provide further evidence that NCAM1 expression is associated with resistance to ADT-induced senescence.

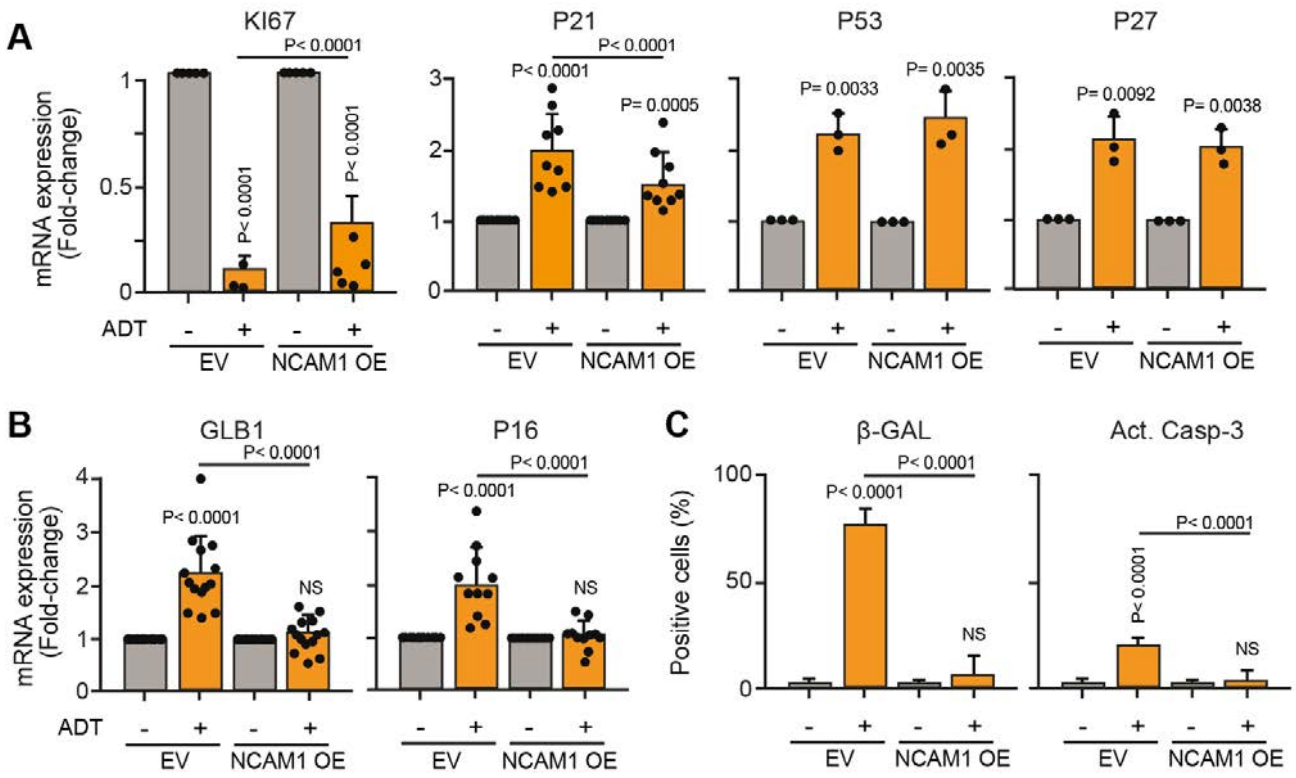

Figure 35. **NCAM1 overexpression is associated with resistance to ADT-induced senescence.** ***A-B)*** *RT-qPCR analysis of the proliferation markers KI67, P21, P53 and P27 (A), and the senescence markers GLB1 and P16 (B) in LNCaP-EV and -NCAM1-OE cells untreated and ADT-treated for 24 h. Mean ± SD (n. of replicates is indicated by black dots).* ***C)*** *Immunofluorescence analysis of β-galactosidase (β-Gal) and active caspase-3 (Act. Casp-3) in cells as described in "A-B". Results are the mean percentage of positive cells ± SD (n > 50 cells in at least 5 different fields). P-values were calculated using one-way ANOVA test. NS: not significant.*

6.3.2 NCAM1$^+$ cells retain proliferative potential and stem cell traits after exposure to ADT

In line with the postulated ability of PCSCs to promote PCa recurrence after ADT, we asked whether NCAM1$^+$ PCa cells retain stem cell traits after exposure to ADT. We isolated LNCaP NCAM1$^+$ and NCAM1$^-$ cells post-ADT and measured the OFE in a 3D-Matrigel assay. Only the NCAM1$^+$ subfraction of cells retained an intact OFE after ADT while NCAM1$^-$ cells were completely impaired in this readout **(Fig. 36A)**.

To understand whether NCAM1 expression could be associated with ADT-resistance also in human PCa, we treated *in vitro* EpCAM$^+$/NCAM1$^+$ cells isolated from primary human PCa biopsies (high Gleason grade) with Bicalutamide/Casodex, a clinically employed anti-androgen receptor drug. This subfraction of cells retained their PDO-forming ability following exposure to Bicalutamide in the 3D-Matrigel assay **(Fig. 36B)**, indicating that this stemness trait is unaffected by ADT in human PCa.

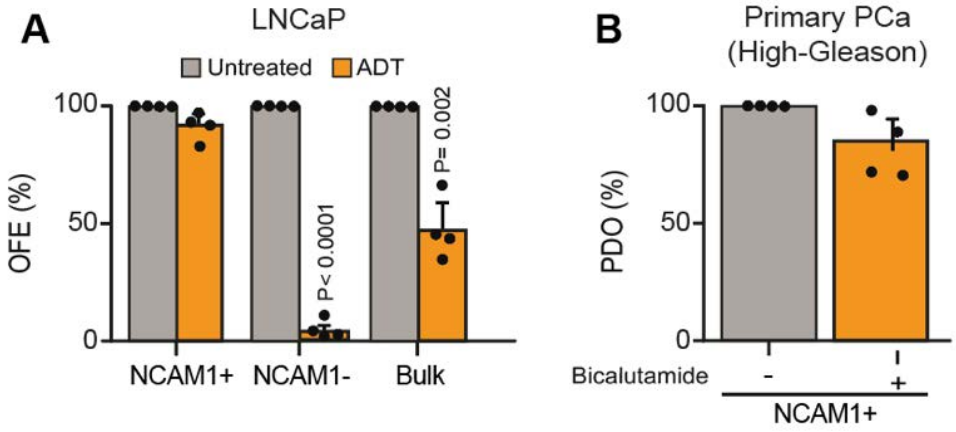

Figure 36. NCAM1$^+$ cells retain organoid-forming ability after exposure to ADT. A) *Organoid-forming efficiency (OFE%) in 3D-Matrigel of NCAM1$^+$, NCAM1$^-$ and bulk LNCaP cells treated with ADT for 7 days or left untreated in controls. Mean ± SD (n=4). B) Patient-derived organoid-forming efficiency (PDO %) in 3D-Matrigel of EpCAM$^+$/NCAM1$^+$ cells isolated from high-Gleason (Gleason Grade = 5) PCa biopsies by FACS and growth in presence of AR-inhibitor bicalutamide [5μM] in vitro. Mean ± SD (n= 4 independent biopsies). P-values were calculated using the Student's t test*

To confirm the relevance of NCAM1 in conferring this ADT resistant phenotype, LNCaP NCAM1-OE and -EV cells were compared for their sensitivity to ADT. Cells were exposed to ADT for 5 days. and then cultured in standard conditions for a further 48 h to assess whether the effects of ADT were long-lasting or reversible. Since we showed that NCAM1 expression correlates with resistance to ADT-induced senescence but not the proliferative block, we hypothesized that the NCAM1-OE cells would be more efficient in recovering their proliferative ability after the removal ADT. Indeed, while ADT inhibited proliferation in both NCAM1-OE and -EV cell lines **(Fig. 37A)**, also demonstrated by the strong reduction in cells positive for Ki67 after treatment (5 days) **(Fig. 37B)**, the re-exposure to normal culture conditions prompted the growth of only the NCAM1-OE cells **(Fig. 37A)**, accompanied by an increase in the number of Ki67$^+$ cells **(Fig. 37B)**. Furthermore, in the 3D-Matrigel organoid assay, the ADT-treated NCAM1-OE cells maintained an intact OFE while -EV cells displayed an impaired OFE **(Fig. 37C)**. Similarly, when transplanted (50,000 cells) in NSG mice, the NCAM1-OE cells showed an intact tumorigenic ability (outgrowths/injection = 8/8) while the tumorigenicity of EV cells was strongly inhibited (outgrowths/injection = 1/8) **(Fig. 37D)**. These results support the notion that NCAM1 expression is a determinant in ADT resistance and could therefore contribute to PCa relapse after ADT.

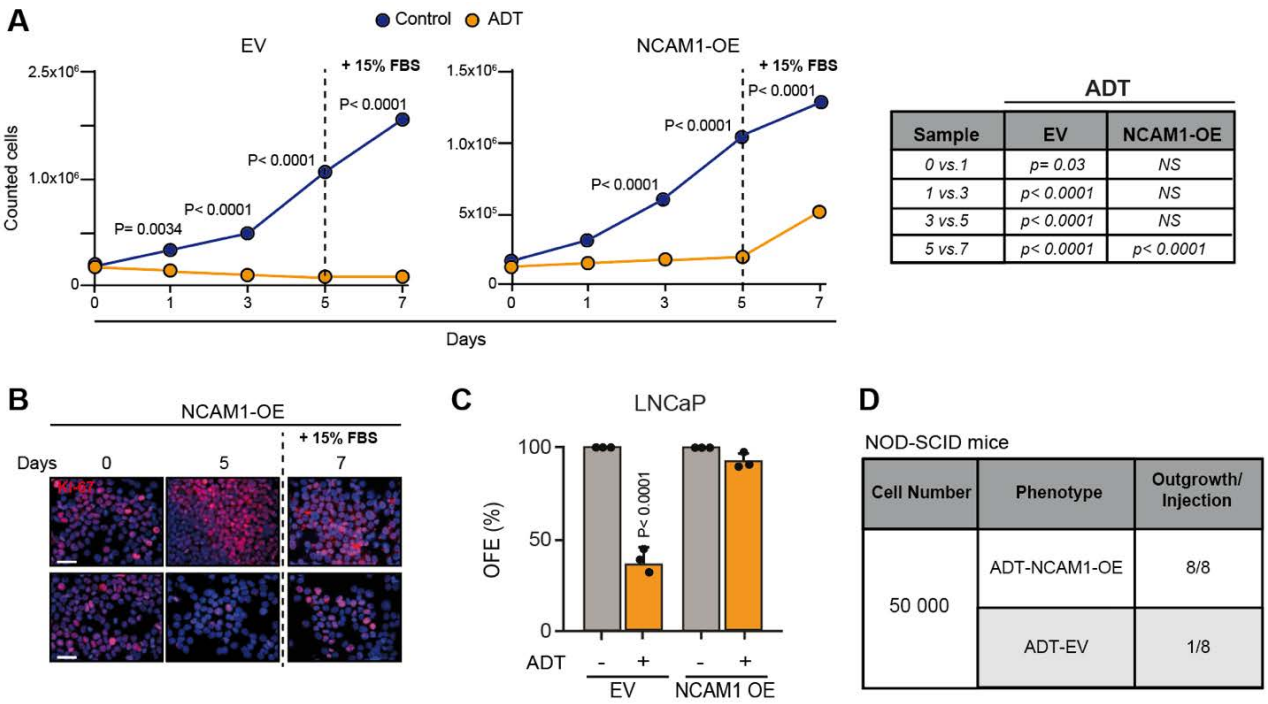

ADT

Sample	EV	NCAM1-OE
0 vs.1	*p= 0.03*	*NS*
1 vs.3	*p< 0.0001*	*NS*
3 vs.5	*p< 0.0001*	*NS*
5 vs.7	*p< 0.0001*	*p< 0.0001*

Cell Number	Phenotype	Outgrowth/ Injection
50 000	ADT-NCAM1-OE	8/8
	ADT-EV	1/8

Figure 37. LNCaP NCAM1-OE vs. -EV cells display resistance to ADT. A) *LNCaP-EV and -NCAM1-OE cells were exposed to ADT for 5 days and then re-cultured in complete media (15% FBS) for a further 48 h (indicated by the dashed line). Proliferation was assessed by counting cells at different time points (1, 3, 5 and 7 days). Growth curves of -EV and NCAM1-OE cells untreated (control) (blue line) or treated with ADT (orange line) are shown. Table aside reported the statistical analysis performed by the two-away ANOVA test, comparing mean data per each day in -EV and -NCAM1-OE cells treated with ADT.* ***B)*** *Immunofluorescence for Ki67 expression in NCAM1-OE cells treated as in "A". Dashed line indicates change from ADT to complete media (15% FBS).* ***C)*** *Organoid-forming ability of LNCaP-EV and -NCAM1-OE cells treated or not with ADT (n=3) for 5 days. Results are reported as percentage organoid-forming efficiency (OFE %). Mean ± SD (n=3).* ***D)*** *Transplantation efficiency of ADT-treated (5 days) NCAM1-OE or -EV cells (50,000 cells) injected subcutaneously into NSG mice. Data are reported as number of outgrowths obtained per number of injections. P-values were calculated using the Student's t test (C).*

6.3.3 NCAM1$^+$ cells retain tumorigenic and CSC potential after long-term exposure to ADT

Based on our findings that NCAM1 expression is associated with increased resistance to ADT, we investigated whether NCAM1 could be a determinant in the development of CRPC in an *in vivo* setting. We designed an experiment where purified NCAM1$^+$ and NCAM1$^-$ LNCaP cells that had been exposed to ADT *in vitro* for 6-8 weeks were transplanted subcutaneously into non-castrated (i.e., androgens present) and castrated (i.e., androgens absent) NSG mice, which resemble the cessation of ADT or continuous exposure ADT, respectively, as schematically represented **(Fig. 38A)**. The formation of outgrowths was monitored over several months and as expected, no outgrowths were generated from ADT-treated NCAM1$^-$ LNCaP cells in any of the mice **(Fig. 38B,C)**. In contrast, ADT-treated NCAM1$^+$ cells conserved their tumorigenic potential both in non-castrated (outgrowths/injection = 6/6) and in castrated (outgrowths/injection=2/3) mice. However, differences

in the time to appearance of outgrowths were observed. In non-castrated mice, outgrowths developed ~3 months post-transplantation, while in castrated mice no evidence of tumor formation was observed at 5 months post-transplantation. At this point, we wondered whether the absence of testosterone was directly affecting the tumorigenic potential of NCAM1$^+$ cells or whether it was preventing the expansion of the NCAM1$^-$ progeny required to generate a visible tumor mass. Therefore, three castrated mice that showed no evidence of tumor formation at 5 months were implanted with a testosterone osmotic pump. Testosterone supplementation resulted, in all three mice, in the appearance of tumor outgrowths in approximately ~1.8 months (~6.8 months from the start of the experiment) only at sites injected with ADT-NCAM1$^+$ cell, with no evidence of tumors at the sites injected ADT-NCAM1$^-$ cells. However, three mice that had not developed outgrowths at 5 months and had not been implanted with a testosterone pump eventually went on to develop outgrowths with a latency period of ~8.6 months **(Fig. 38B,C)**. These observations suggest that NCAM1$^+$ cells survive and retain an intact *in vivo* tumorigenic potential following ADT and even in the continuous presence of ADT, when NCAM1$^+$ cells can slowly proliferate and give rise to tumors after a prolonged latency.

To analyze the role of NCAM1 in sustaining cell growth during ADT, we used LNCaP NCAM1-OE cells that express AR **(Fig. 38D)**. We grew these cells for 10 days in the presence or absence of ADT (charcoal serum 15%) in 3D-Matrigel and monitored the growth of organoids by measuring their diameter. NCAM1-OE cells in standard culture conditions grew faster compared to ADT-treated cells, however, even in absence of androgens, NCAM1-OE cells were still able to form organoids with a diameter that reached ~50 μm at 10 days (**Fig. 38E)**. At this time point, replacing the charcoal serum with normal serum (15% FBS) induced a rapid increase in the dimension of NCAM1-OE organoids, while organoids maintained in charcoal serum grew more slowly **(Fig. 38E)**.

Together, these data suggest that even in the absence of androgens a subfraction of NCAM1$^+$ cells maintain the ability to proliferate and form tumors, suggesting the existence of dormant quiescent/slow-cycling cells in the NCAM1$^+$ population. Therefore, we propose that NCAM1$^+$ cells could be responsible for CRPC progression and tumor relapse even during continuous ADT administration.

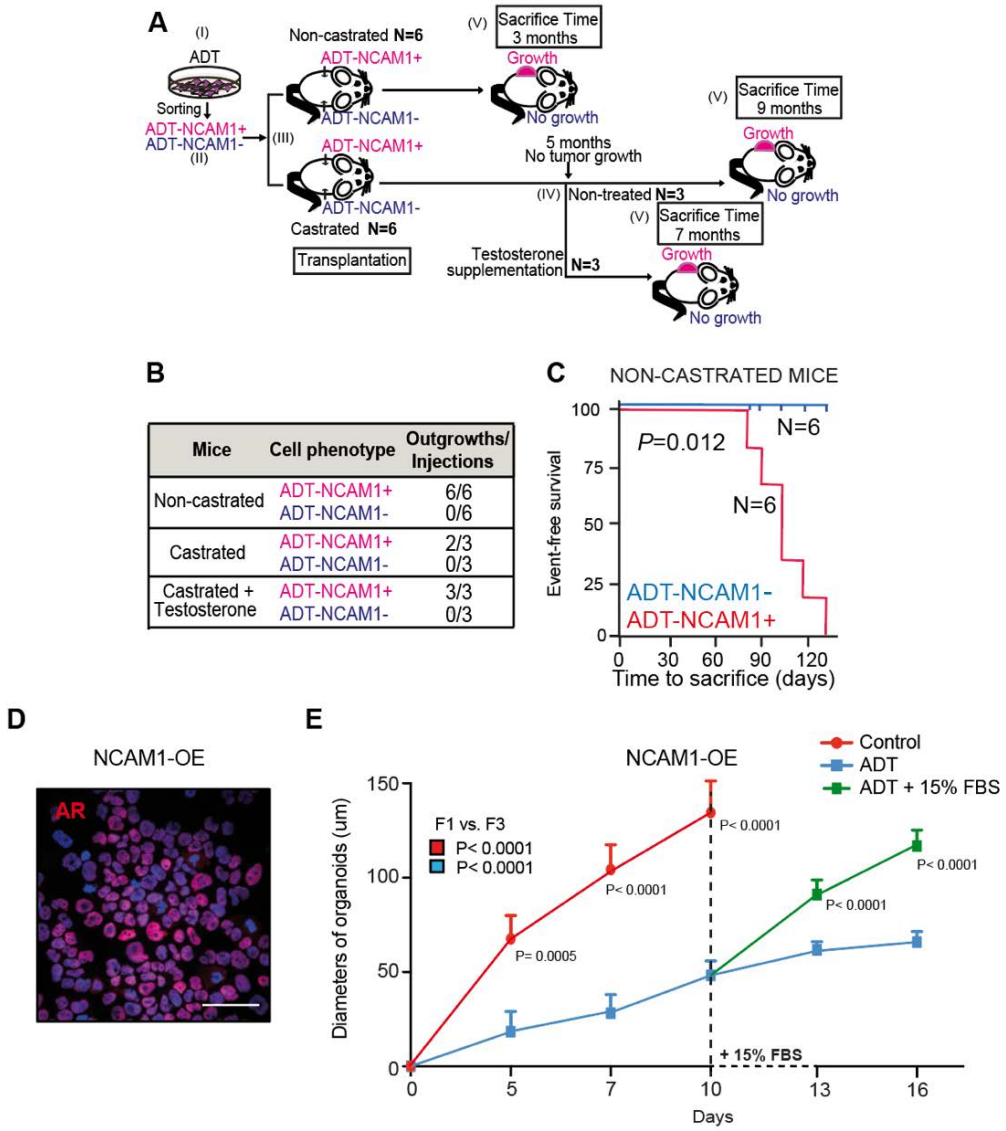

Figure 38. NCAM1-expressing cells maintain stem cell traits in vivo and in vitro even in under ADT conditions. ***A)*** *Schematic representation of the experimental design used for the assessment of the relevance of NCAM1 expression to the development of CRPC: I) LNCaP cells were cultured in hormone-depleted medium for 6-8 weeks. II) ADT-resistant NCAM1$^+$ and NCAM1$^-$ cells (~20,000) were isolated by FACS and embedded in a collagen gel for subsequent transplantation. III) ADT-NCAM1$^+$ and ADT-NCAM1$^-$ cells were transplanted in opposite flanks of non-castrated and castrated NSG mice and monitored for tumor development. IV) Castrated mice had not developed tumors at 5 months post-transplantation. At this time, half of the mice were supplemented with a testosterone osmotic pump and the other half was left untreated. V) Mice were sacrificed when tumors reached 0.8 cm of diameter. Mean time of sacrifice was: ~3 months for non-castrated mice, ~7 months for castrated mice supplemented with testosterone and ~9 months for untreated castrated mice.* ***B)*** *Summary of tumor formation by ADT-treated NCAM1$^+$ and NCAM1$^-$ cells in non-castrated and castrated mice. The tumorigenic potential of both cell subpopulations is also shown in castrated mice supplemented with a testosterone pump at 5.2 months post-transplantation.* ***C)*** *Survival analysis of non-castrated mice transplanted with ADT-NCAM1$^+$ and ADT-NCAM1$^-$ LNCaP cells.* ***D)*** *Immunofluorescence for androgen receptor (AR) in NCAM1-OE cells. DAPI was used to stain nuclei. Scale bar= 100 µm.* ***E)*** *Organoid diameter of NCAM1-OE cells untreated (red line) or treated with ADT (blue line) or treated with ADT for 10 days and then cultured in standard medium (15% FBS) (green line), measured in a 3D-Matrigel assay. P-values were calculated using the two-way ANOVA test.*

6.4 FGF-Notch-1 signaling underlies NCAM1-mediated ADT resistance of NCAM1$^+$ cells

6.4.1. Notch-1 signaling is upregulated upon NCAM1 overexpression

To gain insights into the molecular mechanism governing ADT resistance in NCAM1-expressing PCa cells, we performed a global transcriptomic profiling by RNA-Seq. For this purpose, we used the LNCaP NCAM1-OE cells to highlight the molecular pathways modulated directly by NCAM1, compared to the LNCaP-EV cells. Data analysis revealed 707 upregulated genes and 643 downregulated genes with a Log_2Fold change (Fc) $\geq$ 1 or $\leq$ -1 and statistical significance (FDR adjusted p-value $\leq$ 0.05) **(Fig. 39A)**. A pathway analysis was performed using the Molecular Signature Database (gsea.msigdb.org) with the R statistical package "msigdbr" on the upregulated transcripts. We focused our attention on the Top 10 pathways, ranked based on the enrichment score (K/k) and statistical significance (-Log_{10}FDR > 2). All the annotated pathways have more than 5% of the enrichment score.

This pathway analysis revealed that the overexpression of NCAM1 in LNCaP cells was associated with: i) the upregulation of pathways involved in cell adhesion and EMT; ii) the upregulation of the TNFα–NF- κB pathway, related to inflammation; iii) the downregulation of genes involved in DNA repair (UV-response); iv) the upregulation of Notch-1 signaling and the Hedgehog pathway, both with an enrichment score ∼10% **(Fig. 39B)**.

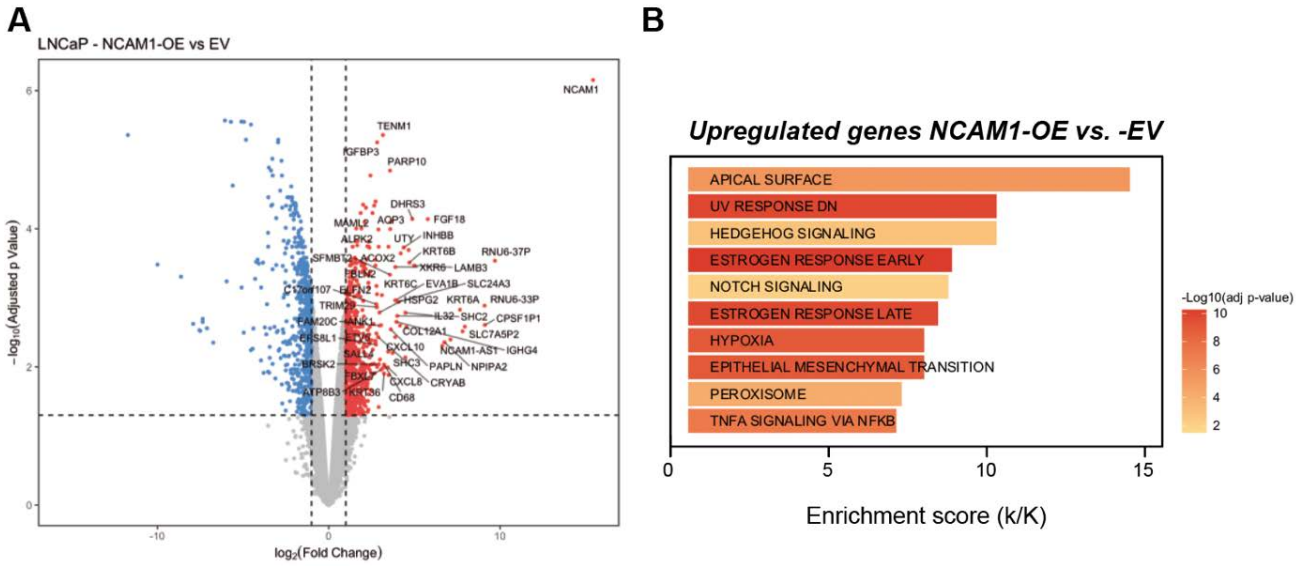

Figure 39. RNASeq revealed Hedgehog and Notch signaling are upregulated in LNCaP-NCAM1-OE cells. ***A)*** *Volcano plot of genes upregulated (red dots) and downregulated (blue dots) with Log_2(Fold change) ≤ -1 or >1 and FDR adjusted p-value < 0.05 in LNCaP-NCAM1-OE vs. -EV cells.* ***B)*** *Diagram displaying the pathway analysis performed with upregulated genes (red dots in panel A). Pathway with FDR adjusted p-value < 0.05 are ranked by their enrichment score (%), estimated as the ratio between number of upregulated genes in the pathway and number of genes annotated in the pathway.*

6.4.2. Hedgehog signaling does not mediate ADT-resistance in NCAM1-OE cells

We investigated whether the pathways identified by RNAseq are involved in ADT-resistance in NCAM1$^+$ cells. We started by analyzing the involvement of the Hedgehog pathway, which we previously demonstrated to be relevant for self-renewal ability (see section 6.2.3). Therefore, we tested the role of the Hedgehog pathway in ADT resistance. We exposed NCAM1-OE cells to ADT in the presence or absence of cyclopamine, a SMO inhibitor (Taipale *et al*., 2000), and GANT61, which specifically inhibits GLI-1/2 that are the transcription factors of this pathway (Lauth *et al*., 2007; Rubin and de Sauvage, 2006). First, we verified the efficacy of these compounds against their targets in our model system by measuring GLI-1 transcription levels using RT-qPCR; GLI-1 is a known target for Hedgehog pathway which is regulated through a feedback control (Katoh and Katoh, 2003). As shown, both compounds efficiently reduced the mRNA levels of GLI1 in NCAM1-OE cells confirming their efficacy in inhibiting the Hedgehog pathway **(Fig. 40A)**. By RT-qPCR, we then revealed that neither inhibitor influenced the mRNA levels of the senescence genes, GLB1 and P16, after ADT treatment suggesting that the suppression of ADT-induced senescence by NCAM1 was not overcome by the inhibitors. **(Fig. 40B)**. Finally, although both compounds partially impaired the OFE of NCAM1-OE cells, they did so in an ADT-independent manner indicating that the effect is not mediated through an NCAM1-ADT related mechanism **(Fig. 40C)**.

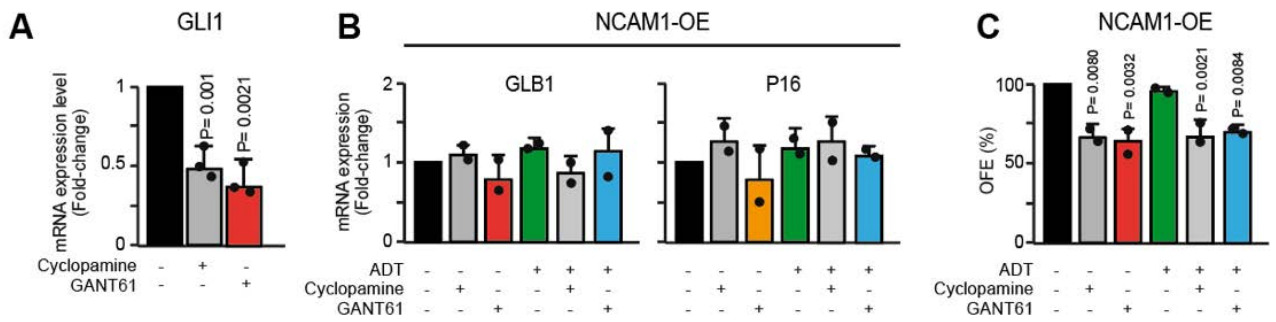

Figure 40. Hedgehog signaling is not involved in ADT-resistance in LNCaP-NCAM1-OE cells. ***A)*** *RT-qPCR analysis of GLI1 expression in LNCaP-NCAM1-OE cells treated with cyclopamine [5 µM] or GANT61 [20 µM] for 24 hours. Data are normalized to the untreated control (n=2).* ***B)*** *RT-qPCR for markers of senescence GLB1 and P16 in NCAM1-OE cells treated with cyclopamine and GANT61 (as in "C") alone or in combination with ADT. Data are normalized to the untreated control cells.* ***C)*** *Organoid-forming efficiency (OFE %) was estimated for NCAM1-OE treated as in "D" and plated in a 3D-Matrigel assay. P-values were calculated using the Student's t test. NS: not significant.*

6.4.3. Notch-1 pathway is necessary for ADT resistance in NCAM1$^+$ cells

Next, we investigated the role of Notch signaling in mediating ADT resistance in NCAM1-OE cells. First, we validated the RNASeq data showing Notch pathway modulation in LNCaP-NCAM1-OE *vs.* -EV cells, by RT-qPCR analysis of genes associated with the Notch pathway, such as Notch-1 (present in our dataset of genes), the Notch-related transcription factors and target genes (HES1 and HEY1), the transcriptional co-activators MAML2 and RBPJk, and the canonical ligand JAG-1. Data analysis revealed that the transcription of MAML2 is strongly enhanced in NCAM1-OE cells, while Notch-1 and HES1 are also significantly upregulated compared to NCAM1$^-$ cells **(Fig. 41A)**. Interestingly, the ligand JAG1 was found to be downregulated in NCAM1-OE cells **(Fig. 41A)**, suggesting that the Notch pathway could be activated through a non-canonical mechanism in these cells (see section 6.4.3). No substantial variations were observed for RBPJk mRNA levels **(Fig. 41A)**. We next investigated whether the modulation of Notch pathway genes was also observed in NCAM1$^+$ *vs.* NCAM1$^-$ cells isolated by FACS from the WT LNCaP cell line. Results revealed a very similar expression pattern of these genes, suggesting that the regulation of this pathway is associated with NCAM1 expression **(Fig. 41B)**. Finally, by western blot analysis, we revealed that Notch-1 is strongly activated by cleavage (cleaved-Notch-1) when NCAM1 is overexpressed **(Fig. 41C)**. Thus, Notch signaling appears to be activated downstream of NCAM1.

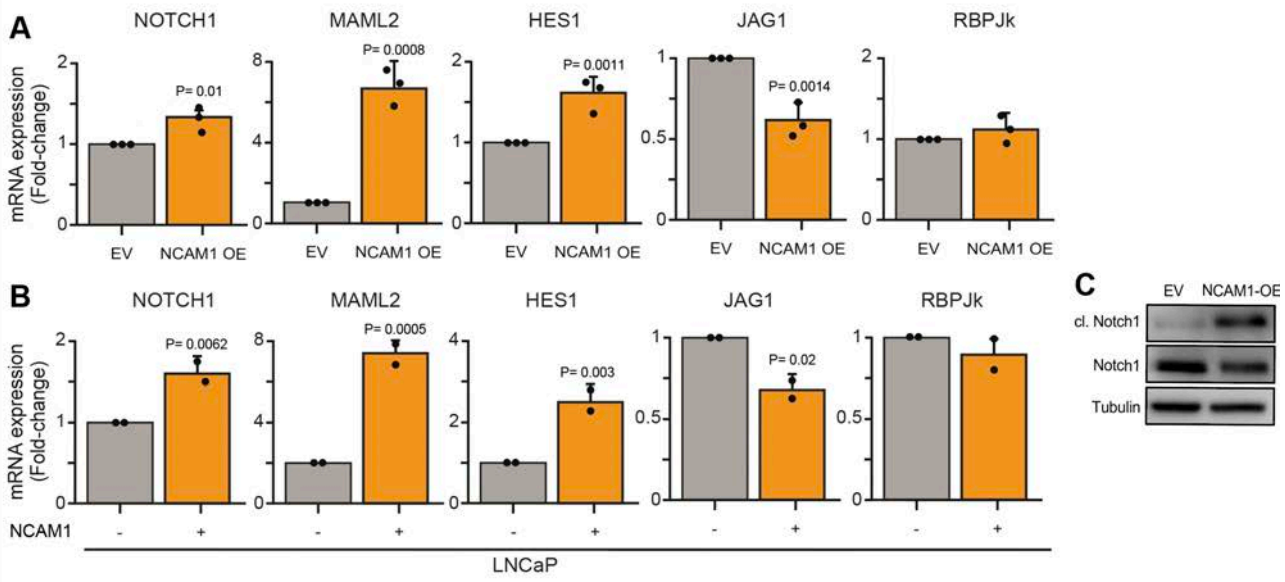

Figure 41. Validation of Notch signaling upregulation in NCAM1-expressing cells. A-B) *RT-qPCR analysis of genes involved in Notch signaling, Notch1, MAML2, HES1, JAG1 and RBPJk in LNCaP -EV and -NCAM1-OE cells (A), and in NCAM1$^+$ and NCAM1$^-$ cells isolated from the WT LNCaP cell line by FACS (B). Data are normalized to the control EV or NCAM1$^-$ cells and are presented as the mean ± SD (n= 3 for EV and -NCAM1-OE cells, and n=2 for sorted cells).* ***C)*** *Immunoblot for active cleaved Notch-1 (cl. Notch1) and total Notch-1, in LNCaP-EV and -NCAM1-OE cells. Tubulin was used as a loading control. P-values were calculated using the Student's t test.*

To investigate whether the Notch pathway has a role in conferring ADT resistance in the NCAM1-expressing PCa cells, we employed the γ-secretase inhibitor (GSI) DAPT; γ-secretase is a protein complex responsible for the cleavage of proteins including Notch-1 (Golde TE et al, 2014). As observed by western blot, the GSI compound DAPT efficiently abrogated the activation of Notch-1 by cleavage in both LNCaP-EV (1st *vs.* 3rd lane) and -NCAM1-OE cells (2nd *vs.*4th lane) **(Fig. 42A)**. RT-qPCR analysis revealed that GSI significantly reduced the mRNA levels of the Notch target gene HES1 in both EV and NCAM1-OE cells, confirming that DAPT is able to efficiently inhibit Notch signaling in our cell system **(Fig. 42B)**. Thus, bulk NCAM1-OE cells were treated with GSI and ADT alone or in combination for 24 h. Confirming our previous results, ADT alone was inefficient in inducing senescence in these cells as evidenced by GLB1 and P16 transcription and the percentage of β-Gal$^+$ cells **(Fig. 42C,D, see also Fig. 35)**. In contrast, treatment with GSI alone induced the activation of senescence which was however more pronounced in cells receiving the combined treatment **(Fig. 42C,D)**. Furthermore, treatment with GSI alone strongly inhibited proliferation, assessed by *KI67* mRNA levels, and induced the expression of the cell cycle inhibitor *P21*, while the combined treatment was even more effective at inducing a proliferative block (*KI67* mRNA levels) **(Fig. 42E)**. These results indicate that on the one hand Notch signaling is critical for maintaining the proliferation of LNCaP-NCAM1-OE cells and for preventing the activation of senescence programs, and on the other hand, the inhibition of Notch signaling sensitizes these cells to the ADT-induced

proliferative block and senescence. Thus, Notch signaling appears to be an important mediator of NCAM1 function in PCa cells.

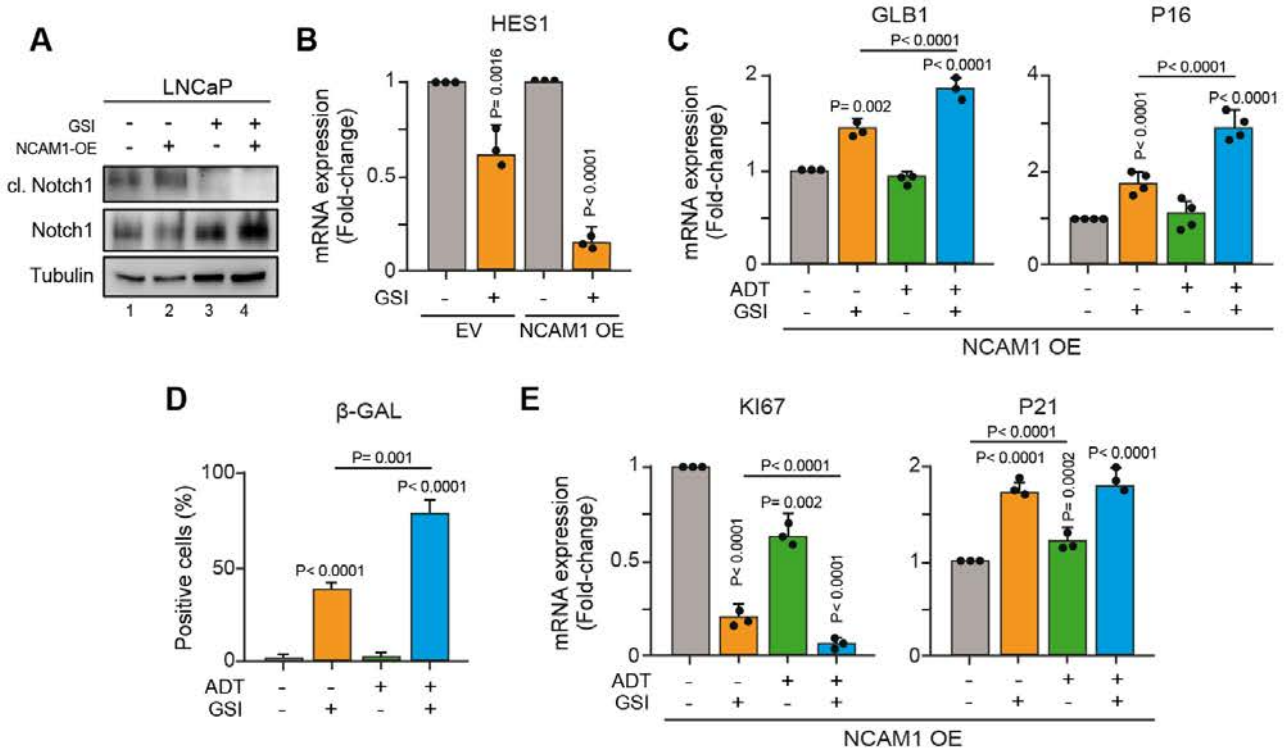

Figure 42*. Notch signaling inhibition reverts ADT-resistance in LNCaP-NCAM1-OE cells.** ***A-B) *LNCaP -EV and -NCAM1-OE cells were treated with the γ-secretase inhibitor (GSI) DAPT [30 μM] for 24 h. The efficacy of the inhibitor was assessed by measuring Notch activation by: (A) immunoblotting for active cleaved Notch-1 (cl. Notch1) and total Notch-1 in EV (1st and 3rd lane) and NCAM1-OE cells (2nd and 4th lane). Tubulin was used as loading control; (B) RT-qPCR for the Notch target gene HES1.* ***C-E)*** *LNCaP-NCAM1-OE cells were treated with GSI DAPT [30 μM] alone or in combination with ADT for 24 h. Activation of senescence was measured by RT-qPCR for the senescent markers GLB1 and P27 (C) and by the percentage of fluorescent β-GAL+ cells (D). Proliferation was assessed by RT-qPCR for the proliferative markers KI67 and P21. All data are normalized to the untreated control and reported the mean ± SD. The number of replicates is reported as black dots in each graph. P-values were calculated using the one-way ANOVA test.*

To genetically corroborate these results showing a critical role of Notch signaling in NCAM-OE cells, we transiently silenced the Notch-1 transcriptional co-activator RBPJk in NCAM1-OE cells using siRNA (siRBPJk) **(Fig. 43A).** Then we exposed cells to ADT for 24 h and measured the expression of senescence markers *GLB1* and *P16*. The results show that RBPJk KD synergized with ADT to increase the transcription of both *GLB1* and *P16* **(Fig. 43B)**, recapitulating our previous findings with GSI. These data provide further evidence for a functional involvement of Notch signaling in NCAM1-mediated ADT resistance.

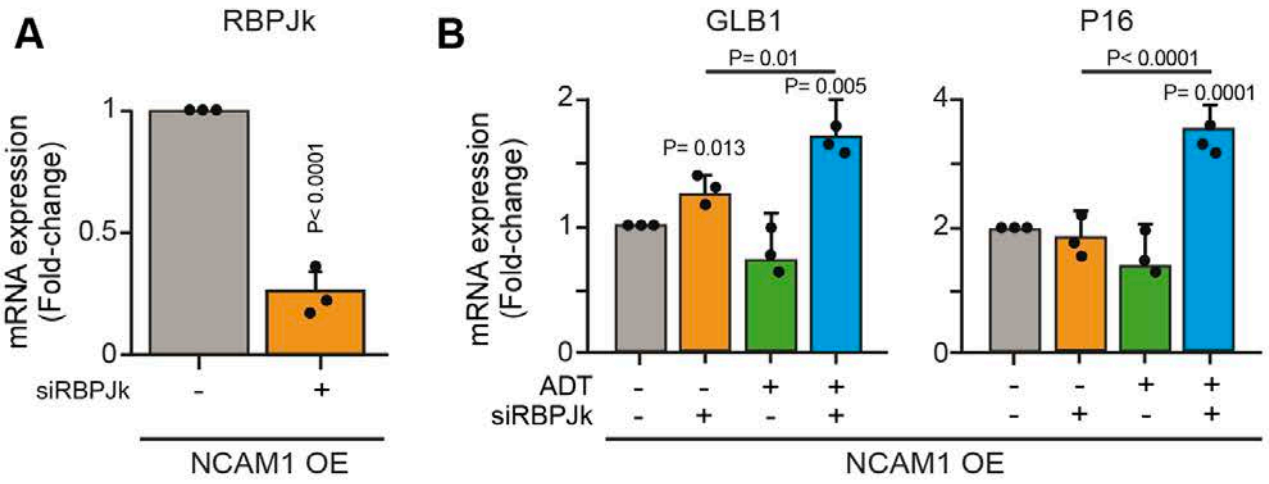

Figure 43. RBPJk silencing reverts ADT resistance in LNCaP NCAM1-OE cells. A) *The efficacy of transient silencing of RBPJk using siRNA (siRBPJk) in LNCaP NCAM1-OE cells was verified by RT-qPCR.* ***B)*** *LNCaP NCAM1-OE cells were treated with ADT in the presence or absence of siRBPJk and the expression of senescence markers GLB1 and P16 was assessed by RT-qPCR. Data are normalized to the untreated control and reported the mean ± SD (n=3). The number of replicates is reported as black dots in each graph. P-values were calculated using the one-way ANOVA test.*

We next asked whether Notch signaling, in addition to maintaining proliferation, is also important for the maintenance of stem cell traits in NCAM1-OE cells. In the 3D-Matrigel organoid assay, we observed that LNCaP-NCAM1-OE cells treated with GSI or silenced for RBPJk displayed a significantly impaired OFE **(Fig. 44A,B)**. Moreover, Notch signaling inhibition (GSI of siRBPJk) sensitized cells to ADT resulting in an almost complete inhibition of OFE in cells receiving the combined treatment **(Fig. 44A,B)**.

To extend the relevance of these findings to other cell systems, we first analyzed the effects of GSI, alone or in combination with ADT, on the OFE of $NCAM1^+$ cells isolated from the WT LNCaP cell line by FACS. In line with the results on LNCaP-NCAM1-OE cells, GSI alone significantly impaired the OFE of $NCAM1^+$ cells, while the combined treatment almost completely inhibited the OFE **(Fig. 44C)**. Similarly, in $NCAM1^+$ cells isolated from human PCa biopsy samples (high Gleason grade), the combined treatment of GSI and Bicalutamide (AR inhibitor) strongly inhibited the PDO-forming efficiency, while Bicalutamide treatment alone had little effect on these cells **(Fig. 44D)**. Together, these data suggest that Notch-1 signaling is critical for maintaining stem cell traits and for mediating ADT-resistance in NCAM1-expressing PCa cells. Thus, a combined therapeutic protocol involving Notch signaling inhibitors and ADT could be an effective strategy for the treatment of PCa.

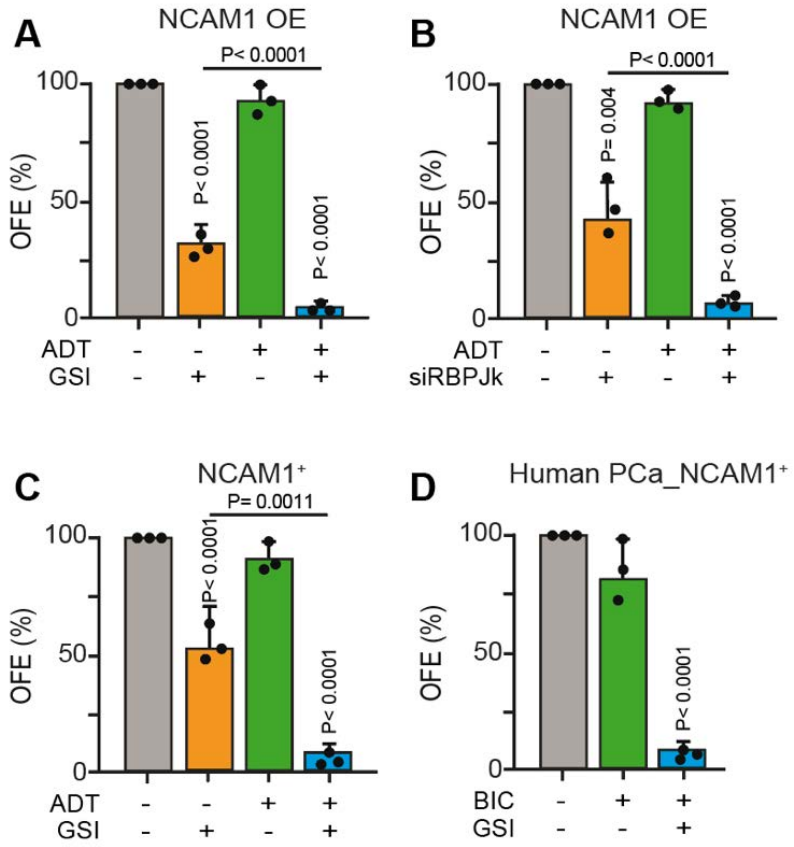

Figure 44*. Notch signaling inhibition impairs the OFE of NCAM1$^+$ PCa cells and sensitizes them to ADT. A-B)** *Organoid-forming efficiency (OFE %) of LNCaP-NCAM1-OE cells treated with ADT and GSI DAPT [30 μM] for 24 h (A) or siRNA against RBPJk (siRBPJK) (B), alone or in combination.* ***C) *NCAM1$^+$ cells were isolated by FACS from the WT LNCaP cell line and treated as in "A".* ***D)*** *NCAM1$^+$ cells were isolated by FACS from a high Gleason grade human PCa biopsy sample and treated in vitro with the anti-AR drug Bicalutamide (BIC) alone or in combination with the GDI DAPT [30 μM] for 24 h. All data were normalized to the untreated control and are reported as the mean ± SD (n=3). P-values were calculated using the one-way ANOVA test.*

6.4.4. DNER sustains the Notch-1-mediated ADT resistance in the NCAM1$^+$ cells

Since the canonical Notch-1 ligand JAG1 is transcriptionally downregulated in NCAM1-expressing PCa cells (**see Fig. 41**), we searched for other Notch-related regulators in the top upregulated genes (with a Fc ≥ 5) uncovered by RNASeq analysis of NCAM1-OE cells. We found that the Delta/Notch-like EGF-related receptor (DNER), which has been demonstrated to be a non-canonical transactivator of Notch-1 (Eiraku *et al*., 2005), was upregulated in NCAM1-OE cells **(Fig. 45A)**. We validated the upregulation of DNER by RT-qPCR in NCAM1-OE *vs.* EV cells and in FACS-isolated NCAM1$^+$ *vs.* NCAM1$^-$ cells from the WT LNCaP cell line **(Fig. 45B)**.

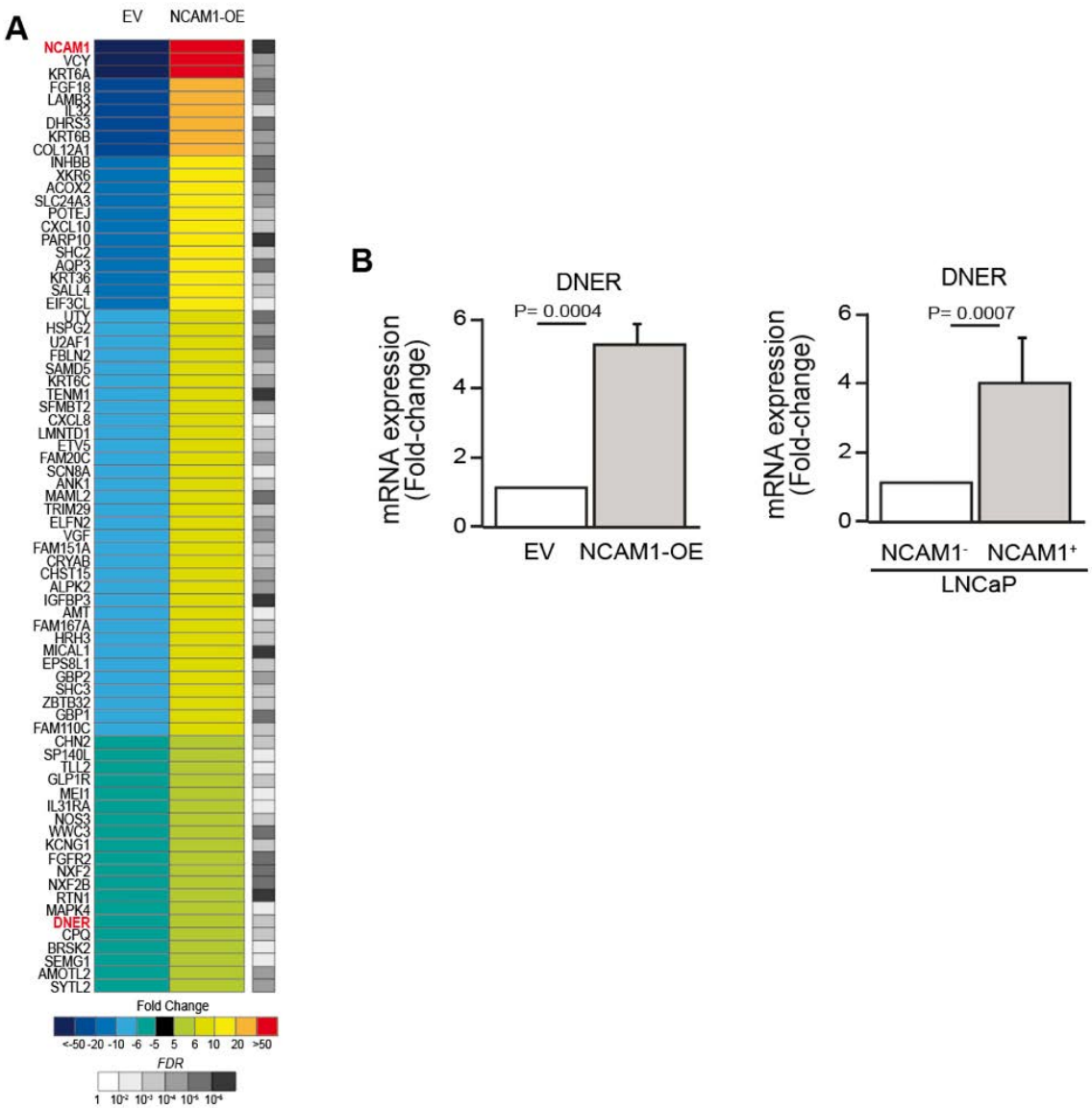

Figure 45. The atypical Notch signaling ligand DNER is upregulated in the presence of NCAM1. A) *Heatmap displaying top upregulated genes (Fc > 5) and statistically significant (FDR) upregulated genes in the RNAseq analysis of NCAM1-OE vs. EV cells. Color scale shows fold-change of the transcript; grey scale shows the false discovery rate (FDR) per each gene.* ***B)*** *RT-qPCR for DNER in LNCaP NCAM1-OE vs. EV cells (left), and in NCAM1^{+} vs. NCAM1^{-} cells isolated from WT LNCaP cells (right). Mean ± SD (n=3). P-values were calculated using the Student's t test.*

Next, we transiently silenced DNER with siRNA in LNCaP-NCAM1-OE and -EV cells. The efficient silencing of DNER in NCAM1-OE cells inhibited the transcription of both HES1 and Notch-1 **(Fig. 46A)** and the activation of Notch-1 by cleavage, as revealed by western blot (2nd *vs.* 4th lane) **(Fig. 46B),** indicating that DNER is directly involved in the Notch signaling in these cells. The LNCaP-EV cells which relatively low levels of DNER were used as a negative control. Interestingly, we observed that the inhibition of Notch signaling in NCAM1-OE cells by GSI treatment or RBPJk KD (siRBPJk), suppressed the transcription of DNER **(Fig. 46C**,**D)**, suggesting the existence of a positive

feedback loop where DNER activates Notch-1 which in turn promotes DNER transcription **(Fig. 46E)**.

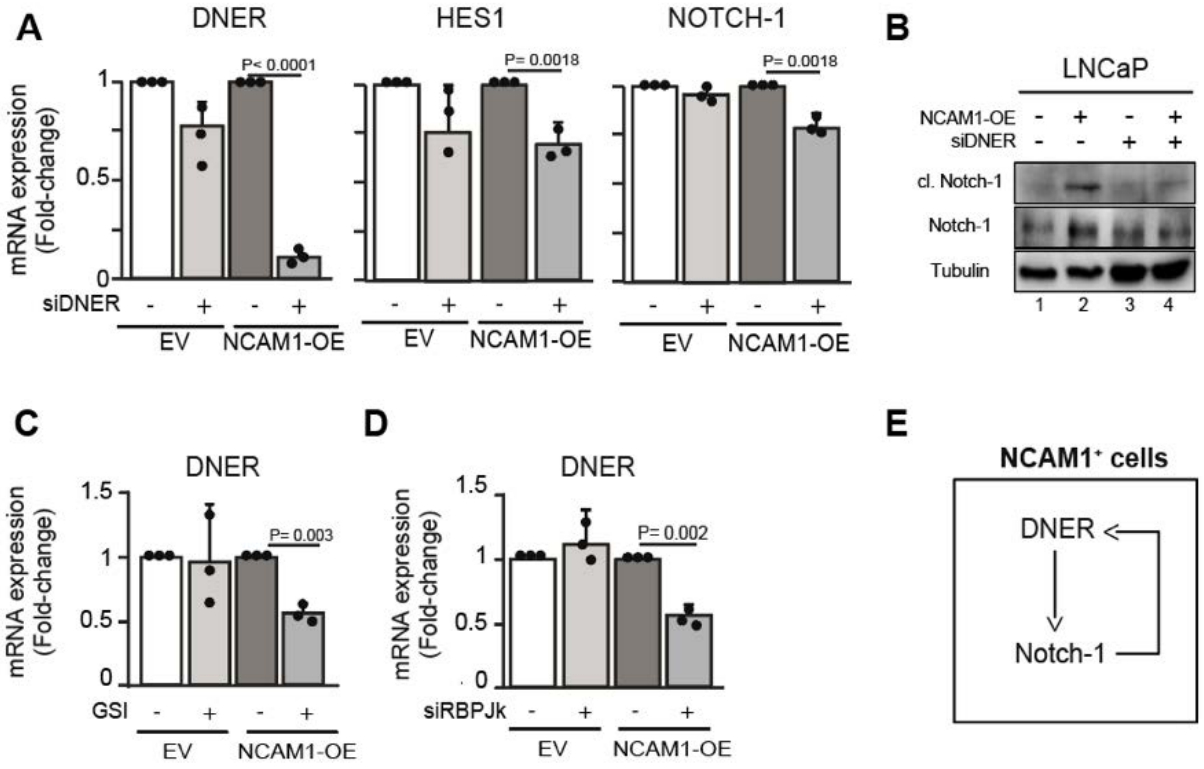

Figure 46. DNER controls Notch-1 activation in LNCaP-NCAM1-OE cells and Notch signaling upregulates DNER transcription. ***A)*** *LNCaP-EV and -NCAM1-OE cells were transiently silenced for DNER (siDNER) and the expression of DNER, HES1 and NOTCH-1 was assessed by RT-qPCR.* ***B)*** *Immunoblot of cleaved activated Notch-1 (cl. Notch-1) and total Notch-1 in EV (1st and 3rd lane) and NCAM1-OE (2nd and 4th lane) cells transiently transfected with siRNA for DNER (siDNER).* ***C-D)*** *RT-qPCR for DNER in -EV and -NCAM1-OE cells treated with GSI [30 μM] for 24 h (C) or transiently silenced for RBPJk (siRBPJk).* ***E)*** *Graphical representation of DNER-Notch-1 crosstalk in NCAM1+ cells. Data were normalized to the relevant untreated control and are reported as the mean ± SD (n= 3). P-values were calculated using the one-way ANOVA test.*

In line with our data showing that abrogation of Notch signaling sensitizes NCAM1-OE cells to ADT, we observed that the silencing of DNER sensitized NCAM1-OE cells to ADT-induced senescence, evidence by the increased transcription of the *GLB1* and *P16* genes **(Fig. 47A)**. Moreover, the silencing of DNER alone impaired the OFE of NCAM1-OE cells, while the combination of siDNER and ADT completely abrogated the OFE **(Fig. 47B)**. These data confirm a critical role of DNER in the maintenance of stem cell traits and ADT resistance in NCAM1-OE cells. Thus, considering all our data on the role of Notch signaling in NCAM1-expressing cells, we propose that DNER activates Notch-1 signaling in NCAM1-expressing cells which is required for maintaining the stem cell phenotype of these cells.

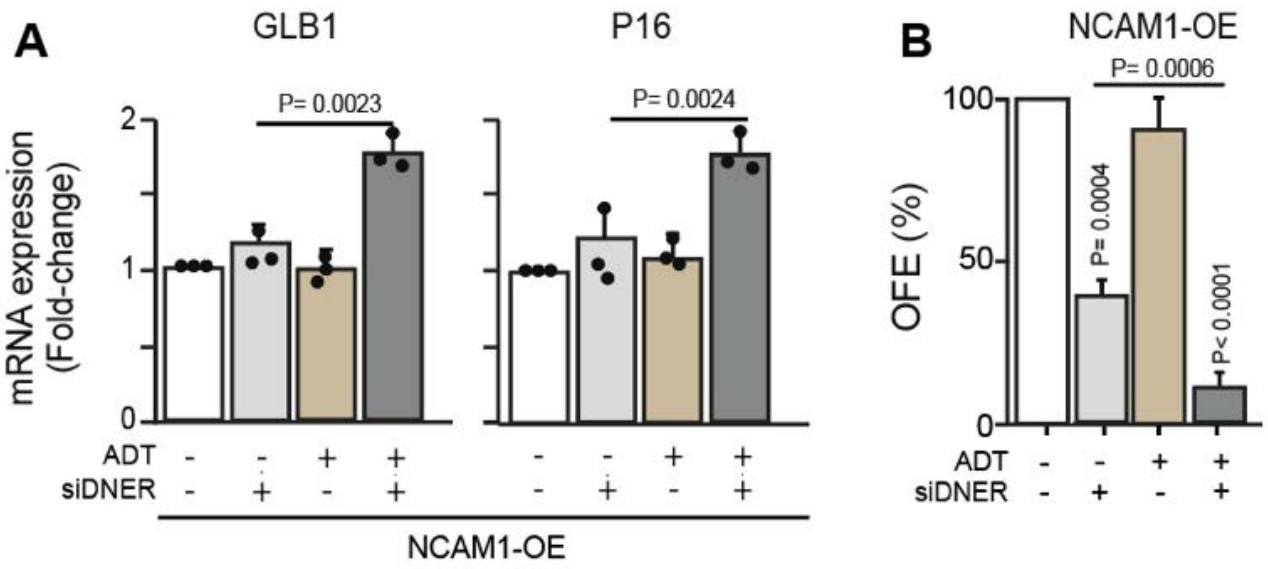

Figure 47. DNER mediates ADT resistance in LNCaP-NCAM1-OE cells. A) *LNCaP-NCAM1-OE cells were transiently silenced for DNER (siDNER) alone or in combination with ADT. The expression of the senescence markers GLB1 and P16 was assessed by RT-qPCR.* ***B)*** *Organoid-forming efficiency (OFE %) of NCAM1-OE cells treated as in "A" in the 3D-Matrigel assay. Data were normalized to the relevant untreated control and are reported as the mean ± SD (n= 3). P-values were calculated using the one-way ANOVA test.*

6.4.5. NCAM1 is a determinant in sustaining Notch-1 signaling in NCAM1-OE cells

We assessed whether the upregulation of Notch-1 and DNER in NCAM1-expressing cells is strictly dependent on NCAM1 itself. We exposed LNCaP-NCAM1-OE cells to the α-NCAM1 inhibitory antibody in a time course assay (1, 4 and 24 h). At the transcriptional level, the α-NCAM1 antibody reduced DNER and Notch-1 mRNA levels at 4 h post-treatment (~50%) and the levels remained similarly downregulated at 24 h, suggesting that Notch signaling is directly under the control of NCAM1 **(Fig. 48A)**. To investigate how NCAM1 sustains the activation of the Notch pathway, we first performed a co-immunoprecipitation (co-IP) assay against NCAM1 in NCAM1-OE cells and checked in the immunoprecipitate for the presence of Notch-1 or Nicastrin, a member of the γ-secretase complex. No physical interaction was observed **(Fig. 48B)**.

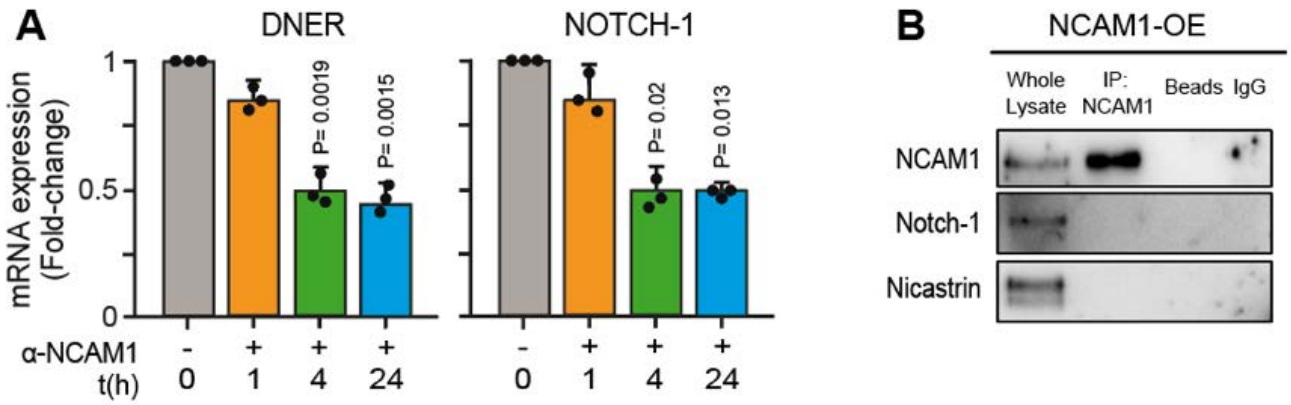

Figure 48. NCAM1 controls Notch signaling at the transcriptional level. A) *NCAM1-OE cells were treated with the α-NCAM1 monoclonal antibody (CONC?) for 1, 4 and 24 h and the expression of DNER and NOTCH-1 was assessed by RT-qPCR. Normalized data are presented as the mean ± SD (n= 3). P-values were calculated using the one-way ANOVA test comparing the mean of each column with the mean of a control column.* ***B)*** *Co-immunoprecipitation assay for NCAM1 in NCAM1-OE cells. The immunoprecipitate (IP) was tested for Notch-1 and the γ-secretase complex member Nicastrin by immunoblot. Beads only and immunoglobulin IgG were used as controls for non-specific binding.*

6.4.6. FGFR2 signaling is upregulated in NCAM1$^+$ cells

We looked for other mechanisms that might link NCAM1 expression with Notch-1 activation. NCAM1 is known to interact with FGFR family members, in particular, FGFR1 and FGFR2 (Francavilla *et al*., 2009; Christensen *et al*., 2006). In addition, FGF signaling has been reported in the literature to be associated with AR-independent PCa and its inhibition has antitumoral effects on bone metastasis in PCa patients (Bluemn *et al*., 2017; Wan *et al*., 2015).

We made a survey of the mRNA levels of FGFRs in our RNASeq database in NCAM1-OE *vs.* EV cells. The heatmap showed that all the FGFRs are upregulated in presence of NCAM1 and FGFR2 seems to be the most upregulated **(Fig. 49A)**. We validated the enhanced expression of FGFR2 by RT-qPCR in both NCAM1-OE cells and NCAM1$^+$ cells isolated from bulk LNCaP **(Fig. 49B).** At the protein level, FGFR2 was found to be highly expressed and also activated by phosphorylation (on the serine 782) in NCAM1-OE cells **(Fig. 49C)**. Finally, by co-IP we observed a physical interaction between NCAM1 and active phosphorylated FGFR2 in the NCAM1-OE cells **(Fig. 49D)**. Thus, we hypothesized that FGFR2 might be directly regulated by NCAM1.

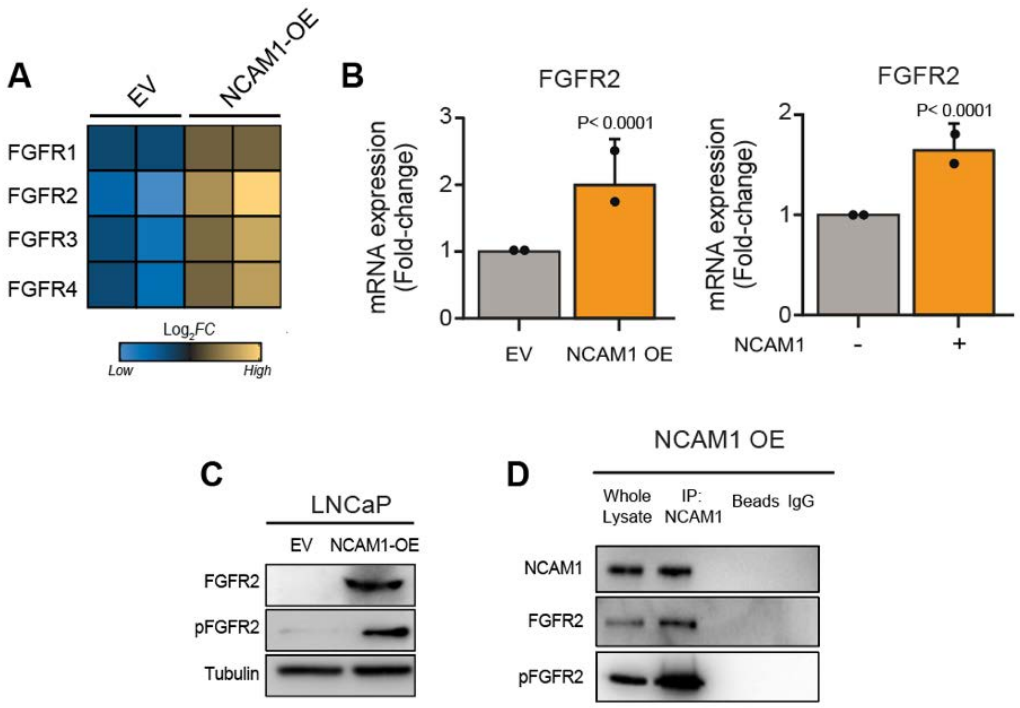

Figure 49. FGFR2 is upregulated in LNCaP-NCAM1-OE cells. A) *Heatmap representing mRNA levels of FGFR-1, -2, -3, and -4 in -NCAM1-OE vs. -EV cells from the RNASeq analysis. Data are represented as Log_2 fold-change (log2FC).* ***B)*** *RT-qPCR analysis of FGFR2 expression in -EV and -NCAM1-OE cells (left) and $NCAM1^+$ and $NCAM1^-$ cells isolated form WT LNCaP cells (right). Data are shown as the mean ± SD (n= 2). P-values were calculated using the Stundent's t test.* ***C)*** *Immunoblot (IB) of phospho-FGFR2 (pFGFR2) and total FGFR2 in LNCaP EV and NCAM-OE cells. Tubulin: loading control.* ***D)*** *Co-immunoprecipitation assay for NCAM1 in NCAM1-OE cells. The immunoprecipitate (IP) was tested for FGFR2 and pFGFR2 by IB. Beads alone and immunoglobulin G (IgG) were used as controls for non-specific binding.*

To test whether the FGFR2 pathway is involved in ADT resistance in NCAM1-OE cells, we employed two pharmacological inhibitors Dovitinib, which is pan-tyrosine kinase inhibitor (TKI), and AZD4547, which instead specifically target FGFRs, and both interfere with the signal transduction pathways (see section 2.2.10.4.3.1). After 24 h of treatment, both Dovitinib and AZD4547 appeared to downregulate the levels of total FGFR2 and phopho-FGFR2 in NCAM1-OE cells (**Fig. 50A,** respectively 2nd and 4th and 6th and 8th lanes) with minimal effects in EV cells **(Fig. 50A)**. The observation that Dovitinib and AZD4547 reduced total FGFR2 protein levels led us to investigate the effects of inhibitors on FGFR2 transcription. By RT-qPCR we observed that both inhibitors suppressed FGFR2 transcription **(Fig. 50B)** suggesting that FGFR2 is itself a target of FGF signaling in a positive feedback loop. Moreover, treatment of NCAM1-OE cells with the inhibitors alone decreased *Ki-67* levels and increased *P21* levels suggestive of inhibited proliferation. The inhibitors also synergized with ADT producing a stronger effect on the proliferation markers **(Fig. 50C)**. However, only the combined treatment was sufficient to induce the transcription of the senescence markers GLB1 and P16 and to promote the appearance of senescent cells (~70%), while

the single treatments were not **(Fig. 50D-E)**. Similar results were obtained when NCAM1-OE cells were transiently transfected with a siRNA for FGFR2 and treated with ADT **(Fig. 50F)**. Thus, these data indicate that FGFR2 is critical for maintaining proliferation and for mediating ADT resistance in NCAM1-OE cells.

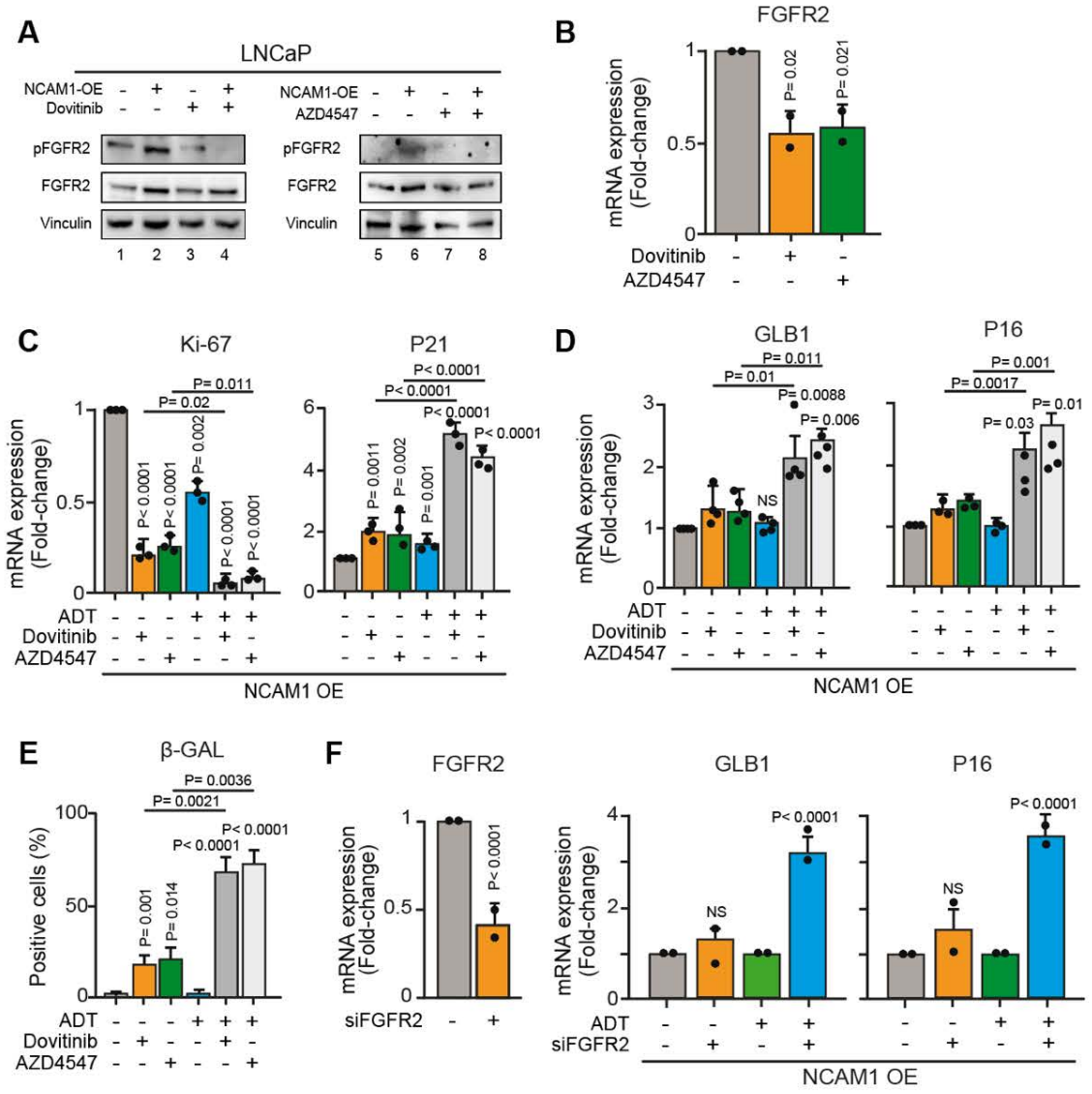

Figure 50. FGFR2 inhibition sensitizes LNCaP-NCAM1-OE cells to ADT-induced senescence. A) *Immunoblot for pFGFR2 and total FGFR2 in LNCaP-EV and -NCAM1-OE cells treated with Dovitinib (pan-tyrosine kinase inhibitor) [6 μM] or AZD4547 (FGFR2 inhibitor) [5 μM] for 24 h. Vinculin, loading control.* ***B)*** *RT-qPCR for FGFR2 in NCAM1-OE cells treated as in "A".* ***C-D)*** *RT-qPCR for KI67 and P21 proliferation markers (C) and GLB1 and P16 senescence markers (D) in NCAM1-OE treated with Dovitinib [6 μM] or AZD4547 [5 μM] alone or in combination with ADT for 24 h. Data are normalized on the untreated sample.* ***E)*** *Immunofluorescence analysis of β-galactosidase (β-GAL) positive NCAM1-OE cells treated as in "C-D". Mean ± SD (n > 50 cells in at least 5 different fields).* ***F)*** *Left, RT-qPCR to verify the efficacy of FGFR2 silencing in NCAM1-OE cells treated with siFGFR2. Right, RT-qPCR for GLB1 and P16 (markers of senescence) in NCAM1-OE cells treated with siFGFR2 alone or in combination with ADT for 24 h. Data are presented as the mean ± SD (no. of replicates is indicated as black dots in each histogram). P-values were calculated using the Student's t test and one-way ANOVA test. NS: not significant*

We next examined the effect of the Dovitinib and AZD4547 on the stemness traits of NCAM1-expressing PCa cells in the presence and absence of ADT. In the 3D-Matrigel assay, LNCaP-NCAM1-OE cells treated with Dovitinib or AZD4547 alone displayed a significantly reduced OFE, which was further decreased in the presence of ADT **(Fig. 51A)**. The same response was recapitulated by the silencing of FGFR2 (siFGFR2) in NCAM1-OE cells in the presence or absence of ADT **(Fig. 51B)**. Furthermore, while NCAM1-OE cells treated *in vitro* with ADT alone maintained their tumorigenic potential upon transplantation in NSG mice, cells treated with ADT in combination with Dovitinib or AZD4547 were almost completely devoid of this ability **(Fig. 51C)**. Since we showed that treatment with the FGFR inhibitors in combination with ADT induced senescence in NCAM1-OE cells **(Fig. 51D)**, it is possible that this combinatorial therapy is a good strategy to induce irreversible senescence in PCSCs and permanently inhibit their tumorigenic ability *in vivo*.

We extended these results to other cell systems and showed that $NCAM1^+$ cells isolated by FACS from WT LNCaP cells behaved similarly to NCAM1-OE cells in the organoid assay; while both kinase inhibitors strongly impaired OFE when used as a single treatment, the combination with ADT almost completely abrogated OFE **(Fig. 51D)**. To investigate the clinical relevance of these findings, we tested the efficacy of the kinase inhibitors in combination with Bicalutamide on primary PCa cells derived from a pool of biopsy specimens (high Gleason grade). While Bicalutamide treatment alone was ineffective in blocking the formation of PDOs in 3D-Matrigel *in vitro*, the combined treatments almost completely inhibited PDO formation, recapitulating the inhibitory effects observed upon direct targeting of NCAM1 with a specific blocking antibody **(Fig. 51E)**.

These data suggest that FGFR signaling is critical for maintaining stem cell traits in NCAM1-expressing PCa cells, similarly to DNER-Notch-1 signaling. Moreover, inhibition of the FGFR pathway with selective TKIs could be a valuable approach to restore ADT-sensitivity to $NCAM1^+$-PCSCs and to promote the induction of senescence to avoid tumor progression to CRPC.

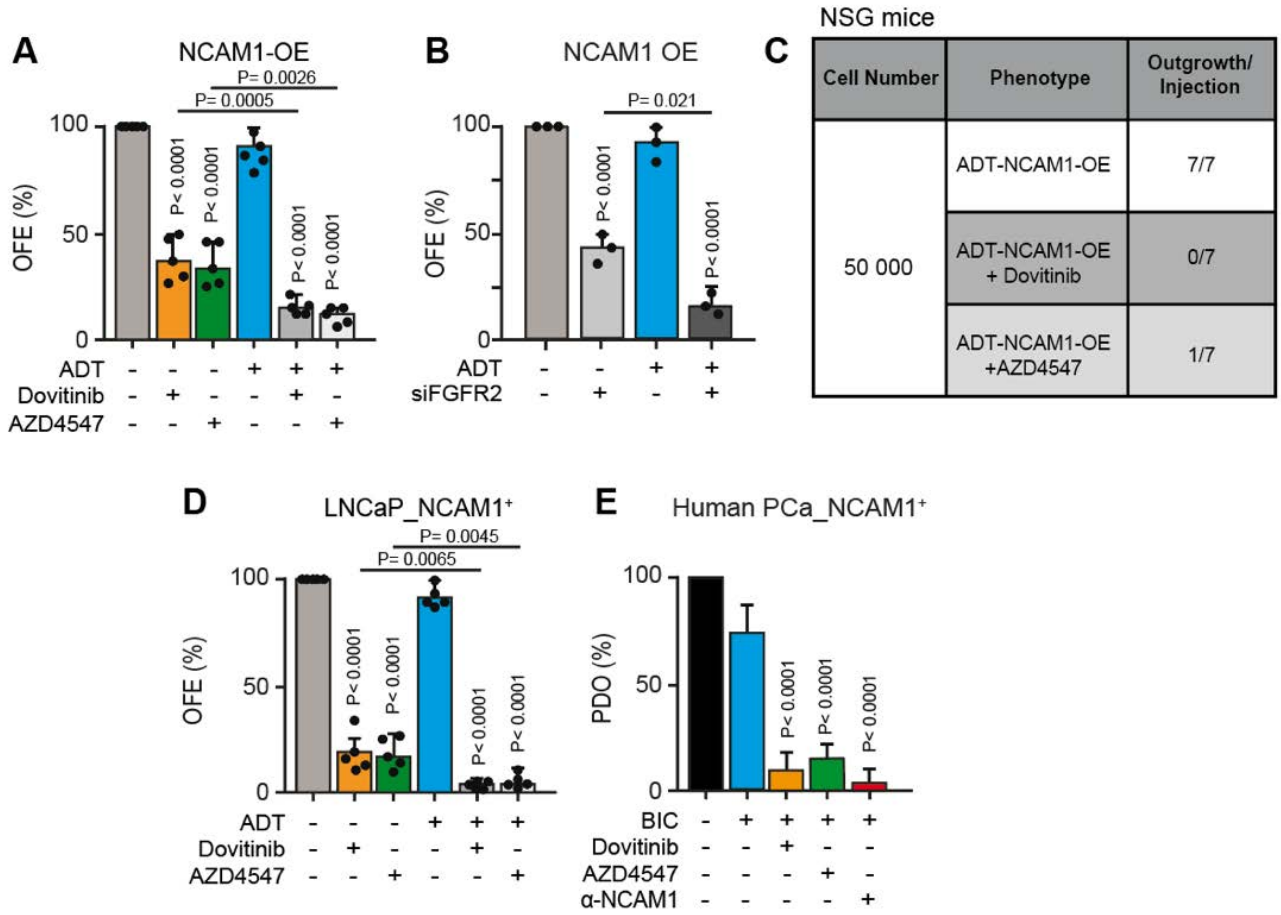

Figure 51. Drugs targeting FGFR2 inhibit stem cell properties of NCAM1-expressing PCa cells and sensitize them to ADT. A) *NCAM1-OE cells were treated with Dovitinib [6 µM] or AZD4547 [5 µM] alone or in combination with ADT for 24 h and assessed for organoid-forming efficiency (OFE %).* ***B)*** *OFE was assessed in NCAM1-OE cells silenced or not for FGFR2 (siFGFR2) in the presence or absence of ADT for 24 h.* ***C)*** *NCAM1-OE or EV cells were treated in vitro with ADT alone or in combination with Dovitinib [6 µM] or AZD4547 [5 µM] for 24 h, Cells (50,000) were then transplanted into NSG mice and tumor outgrowths were routinely monitored and sacrifice when outgrowths reached 0.8 cm. Data are reported as number of outgrowths obtained per number of injections.* ***D)*** *OFE of NCAM1$^+$ cells isolated by FACS from WT LNCaP cells and treated with Dovitinib or AZD4547, alone or in combination with ADT for 24 h as in "A".* ***E)*** *PDO-forming efficiency of NCAM1$^+$ cells isolated from human primary PCa biopsies and treated in vitro with the AR inhibitor Bicalutamide alone or in combination with Dovitinib [6 µM] or AZD4547 [5 µM]. The α-NCAM1 antibody was used as a positive control. Data are reported as mean ± SD (N = at least 3 replicates). P-values were calculated using the one-way ANOVA test.*

6.4.7. FGF18 is the ligand responsible for FGFR2 activation in NCAM1-expressing PCa cells

To better understand how the FGFR2 pathway is activated in NCAM-expressing cells, we attempted to identify the ligand responsible. Using our RNAseq data, we performed a receptor-ligand pair analysis in which the crosstalk between upregulated ligands and receptors is predicted. We found that FGF18 was ranked second among the upregulated ligands in NCAM1-OE *vs.* EV cells and was predicted to interact most strongly with FGFR2 **(Fig. 52A)**. Moreover, FGF18 was among the top 20 upregulated genes in NCAM1-OE *vs.* EV cells with a Fc $\geq$ 20 (**Fig. 52B**) and was the most upregulated member of the FGF family **(Fig. 52C)**. Interestingly, FGF18 is described in the literature to be associated with sustained proliferation in cancer tissue, to have a prognostic value in ovarian cancer, and to act as ligand of FGFR2 in gastric cancer (Wei *et al*., 2013). We therefore validated the upregulation of FGF18 expression by RT-qPCR in NCAM1-OE cells and NCAM1$^+$ cells isolated form bulk LNCaP **(Fig. 52D)**.

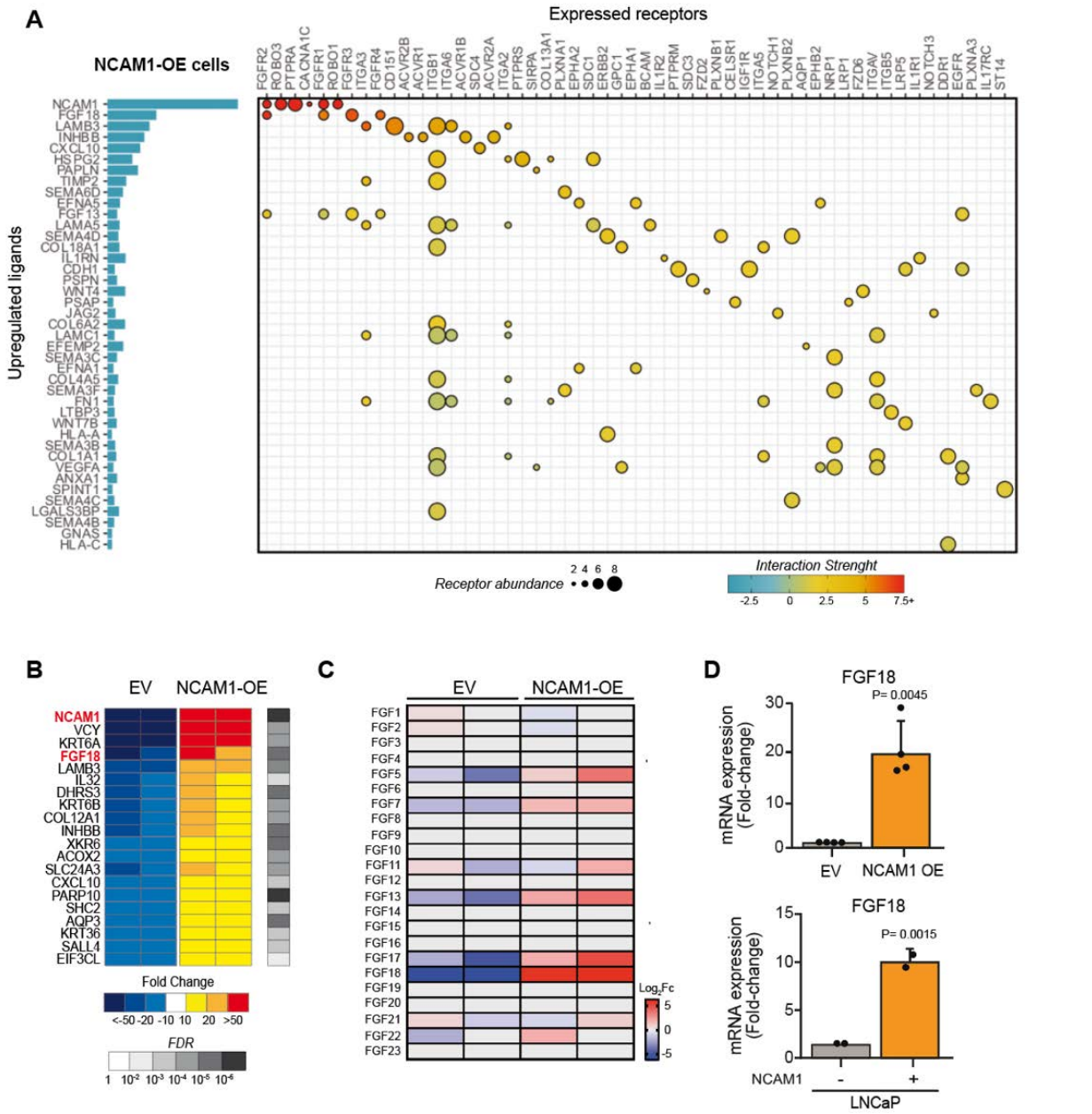

Figure 52. FGF18 is a FGFR2 ligand upregulated in LNCaP-NCAM1-OE cells. ***A)*** *Graphical representation of receptor-ligand analysis performed in NCAM1-OE cells genes annotated in our RNA-Seq-derived dataset. The blue bar indicates the amount of ligand mRNA reported in NCAM1-OE cells. Dots dimension referred to the receptor abundance (2, 4, 6 or 8 are arbitrary measure). Color scale shows the strength intensity between ligand and receptor.* ***B)*** *Heatmap displaying top 20 genes upregulated in LNCaP-NCAM1-OE vs. -EV cells, revealed by RNA-Seq analysis. Color scale shows fold-change of the transcript; grey scale shows the false discovery rate (FDR) per each gene. FDR is a p-value adjusted for multiple tests.* ***C)*** *Heatmap displaying the mRNA, revealed by RNASeq, of FGF family members. Data are represented as Log_2Fold change (Fc).* ***D)*** *RT-qPCR for FGF18 in LNCaP-EV and -NCAM1-OE cells (upper) (n=4) and $NCAM1^+$ and $NCAM1^-$ (lower) (n=2) cells isolated form WT LNCaP cells. Data are shown as mean ± SD. P-values were calculated using the Student's t test*

To elucidate the relevance of FGF18 in mediating NCAM1-associated effects in PCa cells, we transiently silenced its expression with siRNA in LNCaP NCAM1-OE cells and measured the effects on senescence and organoid formation. The efficiency of FGF18 silencing was first confirmed at the mRNA level by RT-qPCR **(Fig. 53A)**. While FGF18 silencing alone did not affect the expression of senescence genes P16 and GLB1, in presence of ADT it induced a senescent phenotype in the NCAM1-OE cells **(Fig. 53B)**. Moreover, FGF18 silencing significantly impaired the OFE of NCAM1-OE cells, which was further inhibited by co-treatment with ADT **(Fig. 53B)**, recapitulating the results observed for FGFR inhibitors **(Fig. 51A)** and the silencing of FGFR2 **(Fig. 51B)**. These results are consistent with FGF18 being a key component of a signaling axis in NCAM1-expressing PCa cells that is responsible for maintaining the PCSC phenotype and resistance to ADT.

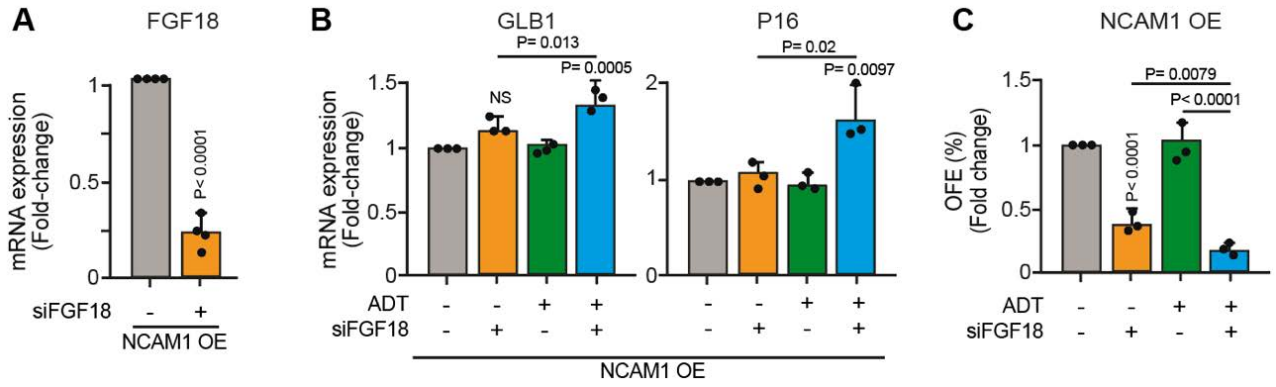

Figure 53*. FGF18 silencing sensitizes NCAM1-OE cells to ADT. A)** *RT-qPCR for FGF18 to control the efficacy of silencing with siFGF18 in NCAM1-OE cells.* ***B) *RT-qPCR for GLB1 and P16 in NCAM1-OE cells silenced or not for FGF18 (siFGF18) and treated or not with ADT for 24 h.* ***C)*** *Organoid-forming efficiency (OFE %) of NCAM-OE cells treated as panel B. Data are reported as mean ± SD (N = at least 3 replicates). P-values were calculated using the Student's t test (A) and one-way ANOVA test (B,C).*

To test the specificity of FGF18 as a ligand of FGFR2, we first silenced FGF18 and checked the phosphorylated status of both FGFR1 and FGFR2. Western blot analysis revealed that FGF18 KD efficiently reduced phospho-FGFR2 but not phospho-FGFR1 (Tyr653-654) levels in the NCAM1-OE cells (**Fig. 54A,** 2nd *vs.* 4th lane), while EV cells maintained the same levels of phosphorylation for both proteins **(Fig. 54A)**. Moreover, exposure of NCAM1-OE cells to a recombinant human FGF18 (rhFGF18) in a time course assay (5', 10' and 30'), resulted in the progressive increase of phospho-FGFR2 and also of phospho-ERK1/2, a downstream target of FGFR2 **(Fig. 54B)**. No effects of rhFGF18 on phospho-FGFR2 were seen in LNCaP-EV cells **(Fig. 54C)**. To test whether the downstream activation of the MAPK pathway in NCAM1-OE cells is dependent on FGF18 -FGFR2 signaling, we silenced FGFR2 in cells treated with rhFGF18 for 30'. By western blot, we uncovered that FGFR2 KD completely inhibited the phosphorylation of ERK1/2 induced by rhFGF18 **(Fig.**

54D). These data suggest that in NCAM1-OE but not EV cells an FGF18-FGFR2-ERK signaling cascade is activated.

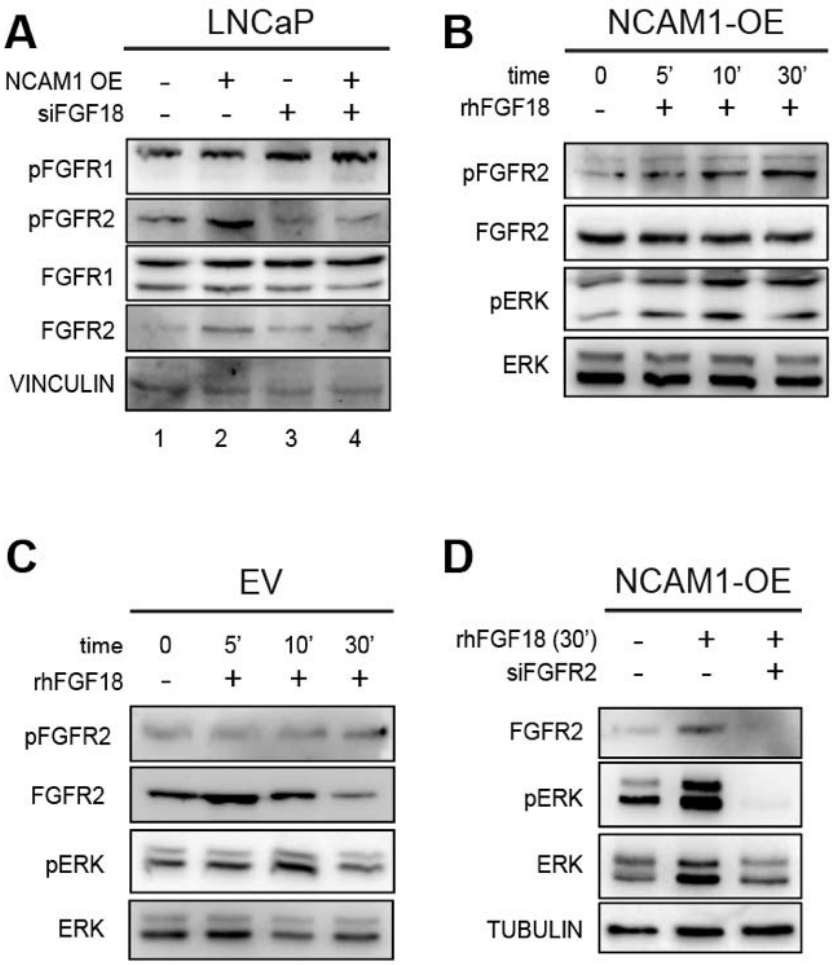

Figure 54*. FGF18 induces phosphorylation of FGFR2 and ERK1/2 in LNCaP-NCAM1-OE cells A)** *Immunoblot (IB) of phospho-FGFR1, total FGFR1, phospho-FGFR2 and total FGFR2 in EV (lane 1 and 3) and NCAM-OE cells (lane 2 and 4) silenced or not for FGF18 (siFGF18).* ***B-C) *IB of phospho-FGFR2, total FGFR2, phospho-p44/42 MAPK (pERK) and total p44/42 MAPK (ERK) in NCAM1-OE (B) and EV (C) cells stimulated with recombinant human FGF18 (rhFGF18) (50 nm) for 5', 10' and 30'.* ***D)*** *IB for total FGFR2, phospho-p44/42 MAPK (pERK) and total p44/42 MAPK (ERK) in NCAM1-OE cells treated with rhFGF18 for 30' in the presence or absence of siFGFR2. Vinculin and tubulin were used as loading controls. Blots of representative of 2 repeats.*

To further investigate the crosstalk between NCAM1, FGFR2 and FGF18, we treated NCAM1-OE cells and -EV cells with AZD4547 and Dovitinib and assessed effects on FGFR2 and FGF18 transcription by RT-qPCR. We found that FGFR2 and FGF18 transcription is downregulated when the FGFR axis is inhibited **(Fig. 55A)**. Similarly, these effects were recapitulated upon silencing of FGFR2 (siFGFR2) and *vice versa* the silencing of FGF18 (siFGF18) impaired the transcription of FGFR2 **(Fig. 55B)** indicating that the transcriptional regulation of FGF18 and FGFR2 is reciprocal

in a feedback loop that could act in autocrine/paracrine manner. In line with this idea, we demonstrated by an ELISA test that NCAM1-OE cells release significantly more FGF18 protein into the culture medium (∼15-fold) compared with EV cells **(Fig. 55C)** and that rhFGF18 administration to NCAM1-OE cells for different timepoints (1, 4 and 24 h) increases the transcription of FGFR2 and FGF18 itself, in a time-dependent fashion **(Fig. 55D)** confirming the existence of this regulatory axis. Finally, to demonstrate that the FGF18-FGFR2 axis depends on NCAM1, we employed the α-NCAM1 blocking antibody in a short time course assay (5', 10' and 30'). Data show that both FGFR2 and ERK are strongly dephosphorylated in a time-dependent fashion upon exposure to the antibody **(Fig. 55E)**. Thus, the inhibition of NCAM1 by the antibody is sufficient to prevent FGF18-FGFR2 induced activation of ERK, suggesting that NCAM1 could be acting as a co-receptor facilitating the interaction between FGF18 and FGFR2. At the transcriptional level, the α-NCAM1 antibody reduced FGF18 and FGFR2 mRNA levels with inhibitory effects observed after just 1 hour of treatment and by 24 h an ∼50% reduction was observed **(Fig. 55F)**.

In summary, these data point to a novel autocrine/paracrine loop circuitry that links together FGF18, NCAM1 and FGFR2. The presence of NCAM1 is necessary for efficient FGF18-FGFR2 signaling, which controls the ADT response by preventing the induction of irreversible senescence in NCAM1^{+}-PCSCs **(Fig. 55G)**.

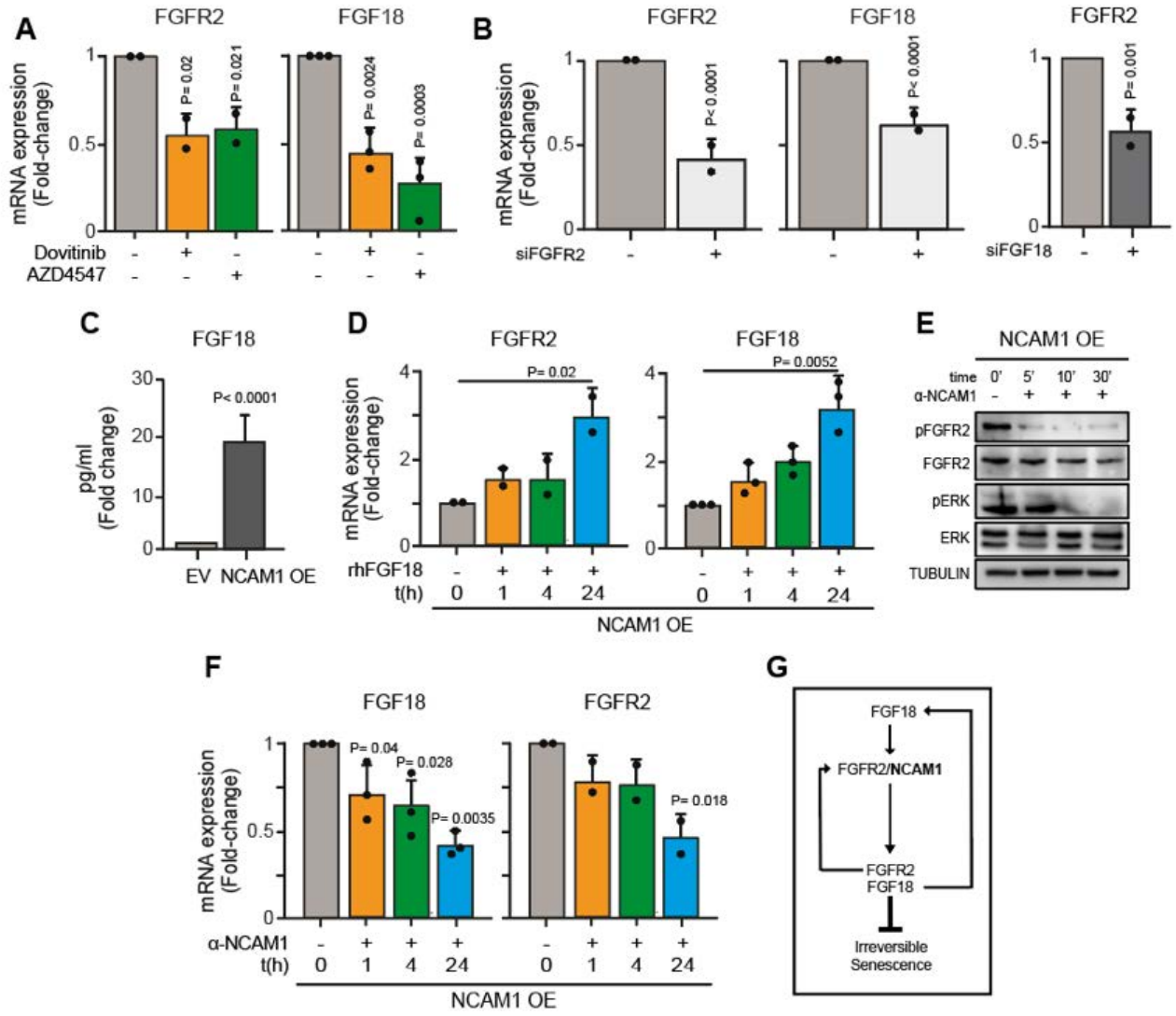

Figure 55. The existence of an FGF18-NCAM1-FGFR2 autocrine loop in LNCaP-NCAM1-OE cells. A-B) *RT-qPCR for FGF18 and FGFR2 in -EV and -NCAM1-OE cells treated with Dovitinib [6 μM] or AZD4547 [6 μM] for 24 h (A) and in NCAM1-OE cells silenced for FGFR2 (B, left) and FGF18 (B, right).* ***C)*** *ELISA assay measuring FGF18 levels (pg/ml) released by the LNCaP-EV and -NCAM1-OE cells into the culture medium. Data are presented as fold-change relative to EV cells.* ***D)*** *RT-qPCR for FGF18 and FGFR2 in NCAM1-OE cells stimulated with recombinant human FGF18 (rhFGF18) for 1, 4 and 24 h.* ***E)*** *Immunoblot with the indicated antibodies of lysate from NCAM1-OE cells treated with the α-NCAM1 123C3 antibody for 5',10' and 30'. Tubulin, loading control.* ***F)*** *RT-qPCR for FGF18 and FGFR2 in NCAM1-OE cells stimulated with α-NCAM1 antibody for 1, 4 and 24 h.* ***G)*** *Scheme representing the proposed FGF18-NCAM1-FGFR2 autocrine loop that prevents ADT-induced senescence. All data are presented as mean fold-change ± SD (n= at least 2). P-values were calculated using the Student's t test (A-C) and one-way ANOVA test comparing the mean of each column with the mean of control column (D,F).*

6.4.8. FGFR2-Notch-1 pathway crosstalk in NCAM1^{+} cells prevents ADT-induced senescence

The above described findings suggest that both the DNER-Notch-1 axis and the FGF18-FGFR axis are involved in mediating ADT-resistance in the NCAM1-expressing PCa cells. Thus, we examined the literature for evidence of a molecular circuitry involving these two axis and found that a crosstalk between these axes was discovered in pancreatic cancer (Li *et al*., 2015). Therefore, we first investigated whether inhibition of Notch signaling influences the FGF18-FGFR axis. Results revealed that GSI reduces FGFR2 protein levels **(Fig. 56A)** and the transcription of both FGFR2 and FGF18 **(Fig. 56B)** in the NCAM1-OE cells. Likewise, although less efficient but statistically significant, the silencing of DNER (siDNER) reduced the transcription of both FGFR2 and FGF18 **(Fig. 56C)**. We next asked whether FGFR pathway inhibition influences Notch. We treated NCAM1-OE cells with Dovitinib and AZD4547 **(Fig. 56D)**, and we silenced both FGF18 (siFGF18) **(Fig. 56E)** and FGFR2 (siFGFR2) **(Fig. 56F)**. As shown by RT-qPCR, all these approaches inhibited the transcription of both Notch-1 and DNER. These results reveal the existence of a molecular crosstalk between the DNER-Notch-1 and the FGF18-FGFR axes in NCAM1-OE cells which likely converge on preventing the induction of irreversible senescence in presence of androgen deprivation strategies, strictly under the control of NCAM1.

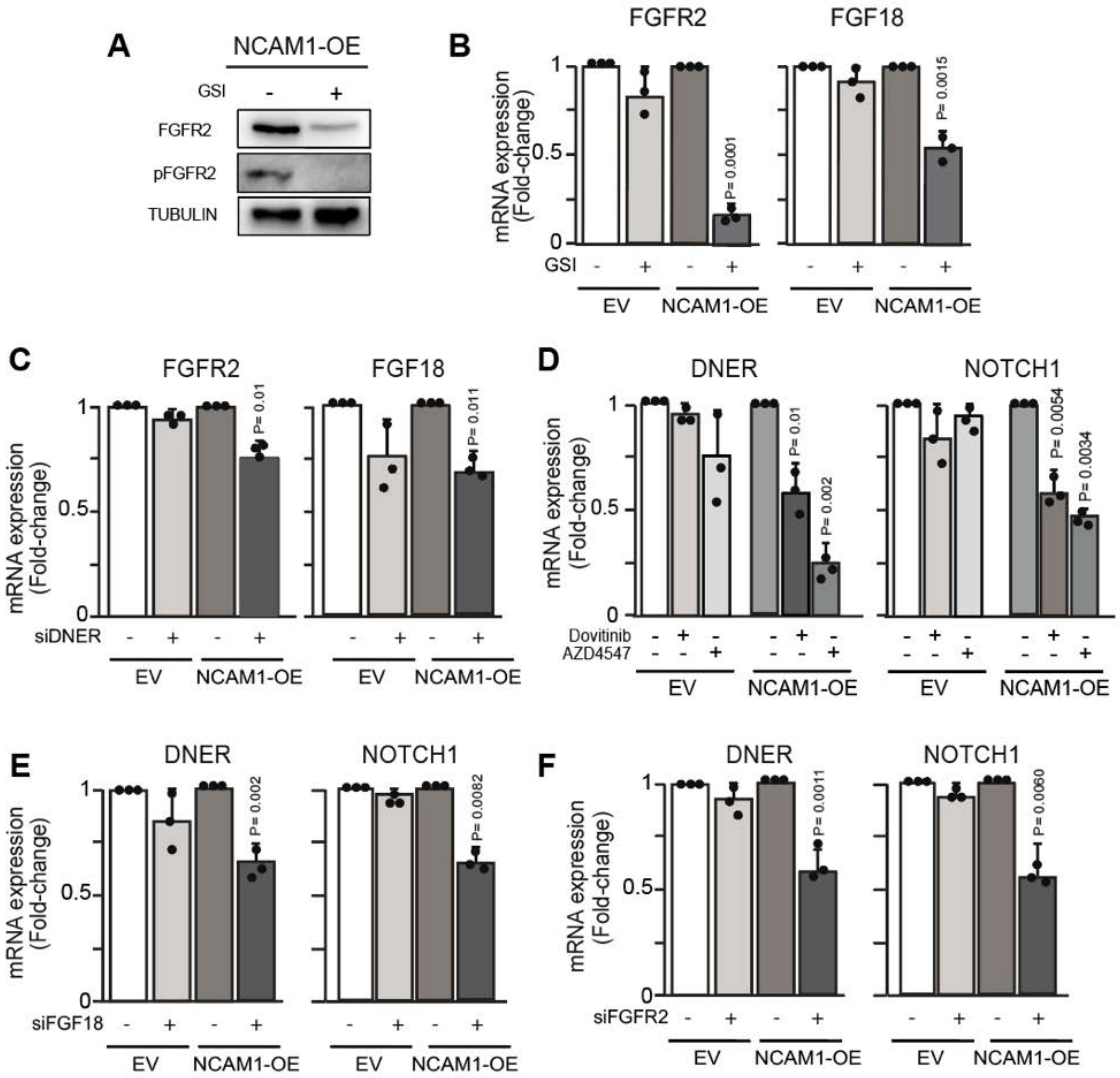

Figure 56. Crosstalk between FGFR and Notch signaling in LNCaP-NCAM1-OE cells. A) *Immunoblot for phospho-FGFR2 and total FGFR2 in NCAM1-OE cells treated with the GSI DAPT [30 μM] for 24 h. Tubulin, loading control.* ***B-C)*** *RT-qPCR for FGFR2 and FGF18 in EV and NCAM1-OE cells treated with GSI (B) or silenced for DNER (C).* ***D-F)*** *RT-qPCR for Notch-1 and DNER in EV and NCAM1-OE cells treated with Dovitinib [6 μM] or AZD4547 [6 μM] for 24 h (D) or silenced for FGF18 (siFGF18) (E) or FGFR2 (siFGFR2) (F). All data are shown as mean fold-change ± SD (n= 3). P-values were calculated using the Student's t test.*

In conclusion, these results revealed a novel molecular circuitry involving DNER-Notch-1 and FGF18-FGFR2 functioning in the presence of NCAM1 that is responsible for maintaining CSC traits and preventing the activation of the senescence program under androgen-deprivation conditions, mimicking the ADT used in clinics for the management of aggressive PCa **(Fig. 57)**. This novel circuitry highlights several druggable targets to potentially revert ADT resistance and eradicate NCAM1^{+}-PCSCs from the tumor that could prevent tumor relapse and the progression to CRPC.

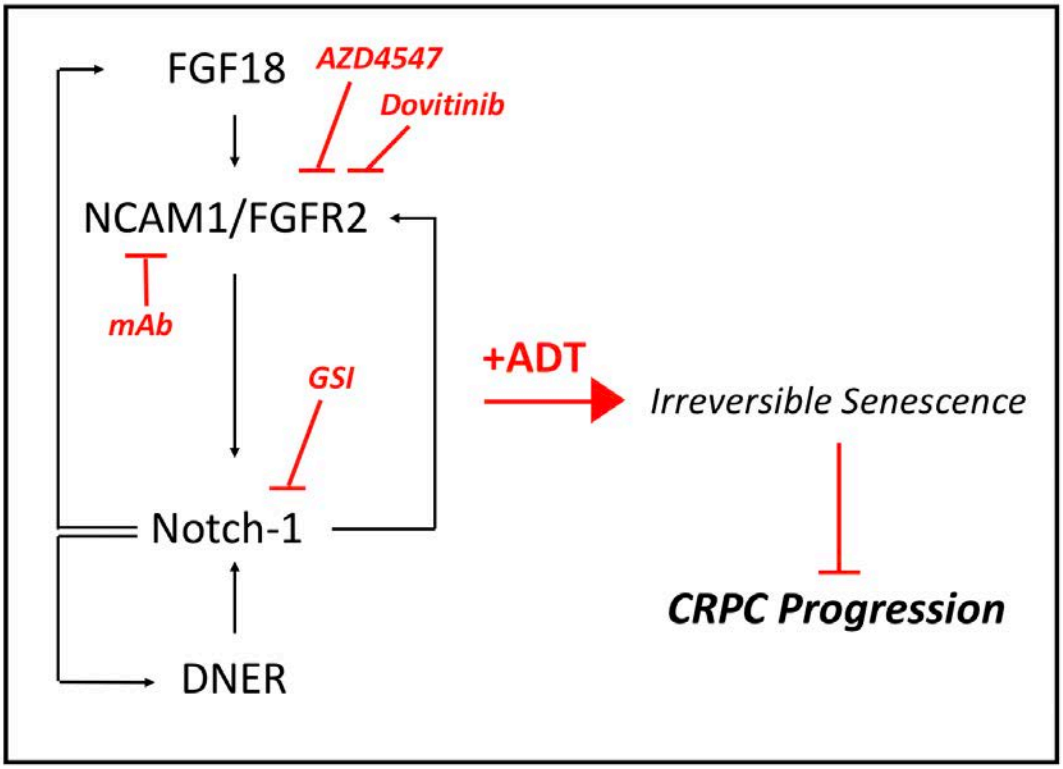

Figure 57. Molecular crosstalk between the FGF18-FGFR2 axis and DNER-Notch-1 axis in preventing ADT-induced senescence in NCAM1^{+} cells. *Scheme summarizing the transcriptional crosstalk occurring between FGF18-FGFR2, which requires the presence of NCAM1 to function, and DNER-Notch-1 to control senescence response to ADT.*

7. DISCUSSION

The precise identification of the CSC population in a tumor is critical for the development of targeted therapies to eradicate them and to improve the prognosis of patients by preventing therapy failure and disease relapse. However, intratumoral heterogeneity in tumor cell populations complicates the molecular characterization of these cells. PCa is characterized by a high level of spatial and temporal intratumoral heterogeneity and several markers have been proposed in the literature to identify putative PCSCs (see section 2.3.4.1). Other published studies have focused on identifying the cell-of-origin of PCa and shown that both luminal and basal epithelial prostate cells have the potential to regenerate tissue under physiological conditions of damage (Leong *et al.*, 2008; Liu *et al.*, 2016), and if forced to express oncogenes they can be transformed into potentially cancerous cells (Lawson *et al.*, 2007; Liu *et al.*, 2016). Thus, both the luminal and basal compartments of the prostate gland have been proposed to harbor the potential TICs, making the molecular identification of PCSCs more difficult.

NCAM1 is a membrane glycoprotein marker that has only been associated in the prostate with the identification and isolation of NE cells present in the prostatic epithelium (Parimi *et al.*, 2014). Of note, little is known about the physiological function of these cells or the biological function of NCAM1 in PCa. Nevertheless, NCAM1 has been shown to be relevant for tumorigenesis, resistance to therapy and disease progression in other types of cancer such as AML, ovarian cancer, multiple myeloma, and pancreatic cancer (Kameda *et al.*, 1999; Bataille *et al.*, 2006; Zecchini *et al.*, 2011; Sasca *et al.*, 2019).

Here, we have investigated the role of NCAM1 in PCa, in particular its connection to the PCSC compartment. This study stemmed from the unexpected observation that $NCAM1^+$ cells that appeared as cell clusters or "threads" associated with PIA in human PCa biopsy samples have prognostic significance. PIA are areas in human PCa characterized by high proliferation, strong inflammation and immune infiltrate, and are considered to be the initial site of tumor growth (De Marzo *et al.*, 2016) . However, when assessed for clinical relevance, the distribution of PIA *per se* showed no prognostic value (De Marzo *et al.*, 1999). In this study, we demonstrated that PIA expressing “threads” of $NCAM1^+$ cells, detected by IHC, are clinically relevant. In fact, these PIA-associated $NCAM1^+$ threads correlated with increased risk of BCR and DM after RP, while $NCAM1^-$ cancers have a significantly better prognosis. Thus, NCAM1 status could be used in the clinical practice as a biomarker to identify, on the one hand, patients at low risk of disease recurrence and relapse who might be eligible for AS, and on the other, patients at high risk of recurrence who should be treated aggressively.

We further showed that NCAM1$^+$ cells do not express canonical NE markers, such as CHGA and SYN, as shown in both human PCa and the TRAMP mouse PCa model and NCAM1 expression correlates with disease progression in the TRAMP model (comparing WDT and PDT) and in human PCa (comparing Low *vs.* High Gleason PCa biopsies). Moreover, we determined that NCAM1$^+$ PCa cells from the TRAMP model and patient samples harbored stemness traits, leading us to hypothesize that NCAM1 could be PCSC biomarker. In this thesis, we have performed an in-depth characterization of NCAM1$^+$ PCa cells investigating their molecular and functional traits, relevance to therapy resistance and evolutionary trajectories in attempt to isolate the PCa cell-of-origin. However, we do not demonstrate whether NCAM1 and the NCAM1$^+$/NE$^+$ cells have a common origin. A very recent paper (Chan, 2022) points out very relevant aspects of lineage plasticity and drgu resistance in PCa. They propose a subfraction of cells with mixed luminal and basal traits to be the origin of the plasticity and responsible for ADT-resistance in absence of two key oncosuppressors such as P53 and Rb, showing that only the treated-cells *in vivo* display a progression to NE tumors thus proposing a transdifferentiating mechanism. However, we could investigate whether this mechanism is strictly dependent on the presence of NCAM1 to clearly establish its role in the origin of NE tumors and highlight the grade of plasticity of the NCAM1$^+$ cells, which is necessary for the acquisition of invasive traits.

NCAM1 as a prognostic biomarker in PCa

One of the major clinical challenges in PCa research is to improve risk stratification in order to aid the selection of the best therapeutic options for patients. PCa diagnosis/prognosis currently relies on serum PSA levels and the histopathological evaluation of prostate biopsies, analyzing general clinicopathological parameters such as GG and TNM classification. The same unrefined parameters are used for the selection of AS *vs.* aggressive therapy and also for guiding the treatment of metastasized PCa and CRPC. These limited diagnostic and prognostic tools together with a high prevalence of indolent PCa have led to the overdiagnosis and overtreatment of PCa patients (Canfield *et al.*, 2014), unveiling the urgent need for novel molecular markers for the early detection and accurate clinical management of potential aggressive forms of PCa.

In this study, we have demonstrated that NCAM1 status identifies PCa patients at higher risk of disease progression. We observed increased risk of BCR and DM in NCAM1^{POS} patients independently of other well-known clinicopathological predictors of PCa, demonstrating the relevance of NCAM1 as a new independent prognostic marker. Interestingly, NCAM1 status also stratifies patients in low/intermediate and high/very high-risk tumor categories based on the NCCN

guidelines. We have identified NCAM1^{NEG} tumors as potentially indolent forms of PCa that would not likely experience disease recurrence and, hence, might benefit from AS protocols. Clinical studies to compare disease-specific survival of low-risk patients with NCAM1^{NEG} PCa treated with RP *vs.* AS would be useful to confirm our findings. As a result, the use of NCAM1 in IHC might reduce both overdiagnosis and overtreatment of PCa patients.

NCAM1 also exhibits strong predictive power in patients with positive surgical margins (PSM). Current treatment guidelines assert that pT2-3 tumors with PSM and no signs of lymph node invasion are suitable candidates for adjuvant radiation therapy after RP. PSM have been repeatedly demonstrated to be associated with an increased risk of BCR following RP and, usually, clinicians advocate immediate adjuvant radiation therapy; however, this may result in deterioration in quality-of-life and overtreatment for many patients (Silberstein and Eastham, 2014). In light of our results, it would be interesting to study, through a randomized clinical trial, whether NCAM1 might be helpful to spare unnecessary radiation therapy in PCa patients with pT2-3 tumors and PSM that showed no PIA-associated NCAM1 clusters. Conversely, NCAM1 status could guide the prescription of additional adjuvant treatment to patients with PSM and NCAM1^{POS} status.

Noteworthy, results obtained on a cohort of 75 PCa suggested that the analysis of NCAM1 status could be easily scored at the time of initial diagnosis to assess the risk of progression of PCa patients. Despite the detection of NCAM1 is efficient in 88% of cases, few patients could be mis-classified. Indeed, undetectability of NCAM1 in biopsy would direct these patients to active surveillance but with a primary tumor that is actually NCAM1-pos (16% of cases). Despite this, mis-classification would result in aggressive tumor diagnosis further down the line by continuous monitoring during AS but would avoid over-treatment of these patients. On the other hand, there is in 9% of cases the risk of detecting an NCAM1-POS biopsy but with negative primary tumor that would result, in this case, in over-diagnosis and over-treatment of the patient. In light of these borderline cases, the detection technique will have to be refined from a clinical point of view by minimizing especially the cases of positive biopsies and negative primaries for NCAM. Confirmation of these results in larger cohorts of needle-core biopsies and their respective RPs might allow a quick integration of NCAM1 into PCa diagnostic routines.

NCAM1 as a PCSC biomarker

The existence of PCSCs offers plausible explanations for many uncertainties regarding PCa development, progression, and therapy resistance. The identification of these cells is a crucial step for understanding the mechanisms of tumorigenesis and for developing new therapeutic approaches.

Given the prognostic value of NCAM1 in PCa and the emerging notion that the increase in the number of CSCs in a tumor correlates with aggressiveness (Pece *et al.*, 2010), we investigated whether NCAM1 could have a role in identifying cells with stem potential.

CSCs are the fuel of tumors, and key CSC hallmarks are relevant for driving tumor progression. We examined these hallmarks in NCAM1-expressing PCa cells:

1) Self-renewal and differentiation potential. CSCs can self-regenerate (self-renewal) which allows the tumor to maintain a constant pool of CSCs that can regenerate the heterogeneous tumor cell populations even after eradication by surgery or conventional therapies such as radiotherapy or chemotherapy that kill highly proliferating differentiated cells. By exploiting the 3D-Matrigel organoid model system, we have shown that primary NCAM1$^+$ cells isolated from well-differentiated TRAMP mouse tumors or from human prostate tumors (high Gleason) have a unique organogenic capacity *in vitro* that is not observed in the NCAM1$^-$ cells. This organogenesis ability was reversed by KD or inhibition of NCAM1. Moreover, by the serial propagation assay, we showed that only NCAM1$^+$, but not NCAM$^–$, cells isolated from established PCa cells lines, have the ability to sustain organoid formation at each passage, indicative of prolonged self-renewal potential, consistent with a CSC phenotype. At variance with NCAM1$^-$ cells from primary tissues, these cells derived from the cell lines did have organogenesis ability at the first generation, suggesting that they could represent early progenitor-like cells that retain some organoid formation potential, which however was quickly exhausted upon serial propagation.

2) Tumorigenic potential. CSCs are functionally defined by their ability to generate tumor outgrowths upon transplantation *in vivo.* We found that primary NCAM1$^+$ cells isolated from well-differentiated TRAMP mouse tumors or from human PCa cell lines were able to generate tumor outgrowths *in vivo* while NCAM$^–$ cells could not. This tumorigenic potential of NCAM1-expressing cells was abrogated by silencing NCAM1 (in TRAMP-C1, -C2 cell lines) or by *in vivo* inhibition of NCAM1 in DU145 tumor outgrowths. Moreover, we found that NCAM1 expression is mandatory for PCa progression. Indeed, we showed that genetic deletion of NCAM1 in the TRAMP mouse model prevents the expansion of pre-malignant lesions to an aggressive tumor phenotype characterized by loss of the AR and acquisition of NE traits. Thus, a subpopulation of PCa cells expressing NCAM1, but lacking NED traits, possesses self-renewal ability *in vitro* and tumorigenic ability *in vivo* consistent with a CSC phenotype.

3) Therapy resistance. A series of studies attempted to demonstrate the existence of a subpopulation PCa cells that are resistant to anti-androgen therapies and thus could reconstitute tumor heterogeneity after treatment cessation driving disease recurrence. Indeed, for the majority of PCa

patients with advanced cancer treated with conventional androgen ablation therapies or AR-inhibitors (e.g., Bicalutamide), the effectiveness of the therapy is transient, with patients typically developing CRPC within 2-3 years (Harris *et al.*, 2009; Jones *et al.*, 2011). Indeed, $PSA^{-/low}$ cells expressing low levels of AR and resistance to ADT have been identified in human PCa (Qin *et al.*, 2012). Also, in a study of 200 CRPC cores, three AR pattern subtypes were revealed, nuclear, nuclear/cytoplasm and low/no expression, of which the $AR^{-/low}$ cells were intrinsically resistant to enzalutamide (Li *et al.*, 2018). Through a series of approaches, we have shown that in the LNCaP androgen-sensitive PCa cell line, a subfraction of $NCAM1^+$ cells display reduced expression of the AR (~50%) compared with the negative counterparts, which prompted us to investigate therapy resistance in these cells.

In vitro assays showed that $NCAM^+$ cells treated with ADT or Bicalutamide retain the ability to form organoids and tumors when retransplanted post-treatment, and that NCAM1 is required to confer this resistance phenotype. These data are in line with the observation in patients showing a correlation between NCAM1 expression and the risk of developing BCR. At the mechanistic level, we showed that NCAM1 expression prevents the senescence phenotype induced by ADT, but it is not sufficient to prevent the reduction in proliferation. As demonstrated by the Ki67 proliferation marker and the cell cycle inhibitors p21, p27, and p53, cells expressing NCAM1 entered a state of proliferative quiescence when exposed to ADT therapy for even as little as 24 h. This observation suggests that the senescence phenotype is uncoupled from the proliferation mechanism in the presence of NCAM1 while it is linked in $NCAM1^-$ cells that respond to ADT by blocking proliferation and entering senescence. This finding could have profound implications in the clinic because it suggests that ADT treatment, by inducing a dormant/slow-proliferating state in NCAM1 cells, would make these cells impervious to standard chemotherapy and radiation therapy. Therefore, treatment with ADT in $NCAM1^+$ patients without targeted therapy to selectively hit these cells could worsen the patient's prognosis by selecting resistant clones responsible for CRPC progression, which is currently not effectively treated.

We performed an *in vivo* experiment in castrated immunocompromised mice that mimicked the condition of a patient receiving cycles of ADT. We reported how even in the continuous absence of androgen, the treated $NCAM1^+$ cells gave rise to tumors after about 9 months, suggesting that $NCAM1^+$ cells could continue to grow even in the absence of hormones. *In vitro,* we showed that cells overexpressing NCAM1, despite showing reduced organoid growth in the presence of ADT, were able to quickly recover after ADT treatment was stopped. These observations support the idea that both continuous and intermittent ADT treatment would be ineffective against $NCAM1^+$ PCa cells, which have the potential to drive disease recurrence even in the absence of androgens.

Moreover, ADT could promote the emergence of much more aggressive resistant tumors enriched in NCAM1$^+$ stem-like cells. In support of this notion, we showed that treatment of LNCaP PCa cells with ADT enriches the population of NCAM1$^+$ cells.

Thus, based on our evidence demonstrating NCAM1 as valid marker of a subfraction of cells involved in ADT resistance, tumor progression, and sustained self-renewal and tumorigenic ability, we hypothesized that NCAM1 could be exploited in the development of new strategies for targeted PCa therapy. In support of this notion, we showed that targeting NCAM1 directly with a blocking monoclonal antibody (123C3) proved to be an effective strategy to abate the stemness traits of NCAM1$^+$ cells, abrogating OFE *in vitro* and preventing tumor regrowth *in vivo* in the serial transplantation assay. Interestingly, α-NCAM1 therapy is currently available in the clinic in the form of a monoclonal antibody, Lorvotuzumab, conjugated with the drug mertansine, a potent microtubule-targeted cytotoxic agent (see section 2.2.10.6.1). Lorvotuzumab mertansine is proposed, in combination with first-line therapies, for the treatment of multiple myeloma, small-cell lung cancer, and ovarian cancer (McCann *et al.*, 2007; Chanan-Khan *et al.*, 2016). Despite some encouraging results, systemic α-NCAM1 therapy has been associated with diffuse cytotoxicity in clinical (Whiteman *et al.*, 2014; Shah *et al.*, 2016; Socinski *et al.*, 2021). Therefore, to test this drug, in combination with conventional therapies, in PCa clinical trials, it would be necessary to explore different administration modalities (e.g., local in the prostate cavity; dose) or second-generation drugs that might be associated with reduced cytotoxicity. An alternative approach to directly targeting NCAM1 could be to inhibit other players in the NCAM1 pathway, in the hope of improving the toxicity profile to avoid systemic damage.

Of note, we tested the stem potential of NCAM1$^+$ cells isolated from human normal prostate (*data not shown*) in 3D-Matrigel assay in which they demonstrated to also have a unique organoid forming ability and moreover, by scRNA-Seq we discovered that in normal prostate the majority of NCAM1$^+$ cells are NE$^-$ but exist a small subfraction (1%) of NCAM1$^+$/NE$^+$ cells, recapitulating what observed in tumors. Further experiments will be necessary to investigate the potential role of NCAM1 as cell-of-origin for PCa and understand whether the evolution of the NCAM1$^+$ population of tumors resemble the physiological evolution.

NCAM1 downstream signaling in PCa cells

Through the unbiased bulk sequencing technique RNASeq, we set out to identify molecular mechanisms, directly controlled by NCAM1, which are involved in the mechanism of therapy resistance and could represent therapeutic target. From the pathway analysis of upregulated genes,

we observed the upregulation of several signaling pathways linked to phenotypic traits typical of CSCs in PCa cells overexpressing NCAM1:

1) *The EMT pathway.* This pathway is characterized by:
    a. Upregulation of collagen genes (*COL1A1, COL6A2, COL12A1*) that are released from cells with mesenchymal traits into the surrounding tissue promoting the physiological process of repair, in healthy tissue, and that of invasion in cancer (Shintani *et al.*, 2008; Scott, Weinberg and Lemmon, 2019).
    b. Upregulation of interleukin-32 (*IL-32*) and chemokine ligand/interleukin-8 (*CXCL8/IL-8*). IL-32 has been described to promote EMT in the lung adenocarcinoma cell line (Gong *et al.*, 2020) through STAT3 signaling, NF-kB and the β-Catenin pathway resulting in production of MMP2 and MMP9, revealed in gastric cancer (Tsai *et al.*, 2014), and of MMP13 in osteosarcoma (Zhou *et al.*, 2015). Instead, IL-8 controls EMT in colon cancer by decreasing E-cadherin and upregulating N-cadherin and vimentin, as shown in established colon cancer cell lines and the BALB mouse model (Shen *et al.*, 2017). In PCa, IL-8 mediates EMT but also the progression to AR-independent tumors (Kim *et al.*, 2001; Araki *et al.*, 2007).

2) *The DNA damage response pathway (UV-Response).* This pathway modulates cell cycle-regulated genes such as *CDKN1C* (p57) and *CDKN2B* (p15), both of which are involved in keeping cells locked in G1 phase, avoiding the risk of accumulating DNA damage during the proliferation phase, and *RUNX1*, a transcription factor that through p53 repairs DNA damage through base excision, homologous recombination and interstrand DNA crosslink repair mechanisms in different tumor contexts (Bellissimo and Speck, 2017; Samarakkody, Shin and Cantor, 2020)

3) *The Hypoxia pathway.* This pathway is characterized by:
    a. *HOXB9*, an epigenetic mediator that enhances the transcription of VEGFA and neoangiogenesis to counteract the lack of oxygen (Contarelli, Fedele and Melisi, 2020)
    b. N-Myc downstream regulated 1 (*NDRG1*) that is a hypoxia-inducible protein with a role in tumor adaptation to oxygen levels, as shown in breast and PCa (Cangul, 2004).
    c. Insulin receptor substrate 2 (*IRS2*) that is a direct target of HIF factors, which control (among other functions) the switch from oxidative phosphorylation to anaerobic glycolysis for ATP generation and energy production (Mardilovich and Shaw, 2009; Robey and Hay, 2009)

4) *The estrogen pathway.* The response to estrogen has been shown in the literature to be relevant to PCa growth (Tan *et al.*, 1997; Yeh *et al.*, 1998). In NCAM1^{+} cells, we observed the upregulation of several estrogen targets such as glucocorticoid regulate kinase (*GSK*) and the enzyme Acyl-CoA oxidase 2 (*ACOX2*).

5) *The NF-kB inflammation pathway.* The upregulation of this pathway suggests that NCAM1 may have a key role in sustaining inflammation in the surrounding prostate tissue rather than being just regulated by it. This opens up the possibility of crosstalk between PCSCs and the TME mediated by inflammatory factors. NCAM1 overexpression is associated with upregulated transcription of:

a. *RELB*, the functional subunit of NFkB.
b. *IL-32* that we described earlier as associated with EMT but which is also related to chronic inflammation and has functions in mediating the release of factors, such as TNFα and IL-6 that regulate the recruitment of immune cells though the stimulation of STAT3 and NF-kB pathways in several cancers (Yun *et al.*, 2013)
c. *IL-8* that modulates the recruitment of neutrophils and macrophages to the peritumoral area in several tissues (Teijeira *et al.*, 2021) as well as EMT as described above.
d. *IL-10* that control T-cells thus modulating an immune suppressive environment favoring CSC immune escape (Dennis *et al.*, 2013; Mannino *et al.*, 2015)

6) *The Hedgehog pathway.* This pathway is involved in controlling SC self-renewal ability and therefore, we have investigated its role in NCAM1-expressing PCa cells with a view to highlighting potential anti-CSC therapies.

In the literature, this pathway has been described to have a key role in the physiological tissue repair mechanism in the prostate after castration in mouse models (Karhadkar *et al.*, 2004), a process blocked by the Hedgehog pathway inhibitor cyclopamine (Rubin and de Sauvage, 2006). This finding suggests a direct involvement of Hedgehog in SC activation. The physiological mechanism of repair correlates with the expression of self-renewal factors including Bmi-1, which if forced can promote malignant transformation, suggesting that trapping normal SCs in a continuous state of repair predisposes them to cancer initiation and the formation of aggressive tumors (Beachy, Karhadkar and Berman, 2004). Interestingly, Hedgehog signaling is typical observed in SCs devoted to tissue repair and with metastatic potential and invasive and migratory capacity (Cano *et al.*, 2000). In addition, Hedgehog is involved in the acquisition of mesenchymal traits and the EMT process, which are relevant to metastasis. Indeed, Hedgehog has been shown to be instrumental to metastasis in different cancers and Hedgehog pathway target genes, such as PTCH1 and GLI, have been shown to be

expressed in metastatic human PCa sections but not in healthy prostate sections (Karhadkar *et al.*, 2004).

In our study, we showed using pharmacological inhibitors (cyclopamine and GANT61) that Hedgehog signaling does not appear to mediate resistance to ADT in NCAM1-expressing cells. Indeed, while these inhibitors alone reduced slightly the organoid-forming ability of NCAM1-overexpressing cells, they did so in an ADT-independent manner. However, these Hedgehog inhibitors were able to inhibit the self-renewal of NCAM1$^+$ LNCaP cells as witnessed in the organoid serial propagation assay, indicating that Hedgehog could be important for the maintenance of the PCSC population.

7) *The Notch Pathway*. Notch signaling has been shown to have a role in ADT resistance, as demonstrated by a recent paper that revealed how enzalutamide-resistant C4-2R PCa cells became responsive to ADT when silenced for Notch1, undergoing a proliferative block and apoptosis (Farah *et al.*, 2019). A similar effect was observed in VCaP PCa cells positive for the TMPRSS2-ERG translocation, in which treatment with the Notch pathway inhibitor GSI sensitized cells to the AR inhibitors bicalutamide and enzalutamide or to the AR production inhibitor abiraterone, resulting in reduced cell growth and survival, and enhanced apoptosis (Mohamed *et al.*, 2017). Moreover, Notch acts in progression to CRPC, integrating several other pathways, such as AKT, Myc and MAPK, to promote EMT and tumor aggressiveness (Stoyanova *et al.*, 2016). Therefore, we decided to investigate the role of Notch in NCAM1-mediated resistance to ADT-induced senescence in our model systems.

Using several approaches, we established how administration of GSI to NCAM1-expressing cells confers sensitivity to ADT that results in a block in cell proliferation but more importantly allows NCAM1 cells to undergo ADT-mediated senescence. It has been reported that Notch can have a direct role in the regulation of AR expression. Indeed, treatment with the GSI DAPT not only increased AR mRNA levels but also its nuclear localization in the presence of testosterone by promoting the physiological AR-DNA interaction process, indicating that Notch signaling downregulates the AR. In addition, the Notch co-factors HEY and HEYL directly interact with AF1 region of AR and inhibit steroid receptor coactivator-1 (SRC1) of AR transcriptional activity (Belandia and Parker, 2006; Lavery *et al.*, 2011). Thus, Notch signaling appears to suppress AR transcription, which would confer resistance to ADT. In our study, we showed that inhibition of Notch signaling in human established and primary NCAM1-expressing PCa cells, either pharmacologically with GSI and/or genetically by RBPKk KD, reverses ADT resistance, witnessed by inhibition of proliferation, activation of the senescence program and reduction in organoid-forming ability. Of note, Notch inhibition alone

induced a proliferative block, senescence and inhibition of OFE in these cells, albeit less pronounced than the combined treatment with ADT, indicating an important role of Notch in maintaining the bulk NCAM1-expressing cell population. Importantly, Notch inhibition was effective at inhibiting the self-renewal potential of NCAM1$^+$ cells, as assessed in the organoid serial propagation assay, indicating that Notch signaling could be important for maintenance of the PCSC compartment. Further studies are required to determine whether the sensitization to ADT upon Notch inhibition is determined by modulation of the AR levels by Notch in NCAM1$^+$ cells.

To deepen our analysis of the upregulation of the Notch pathway in NCAM1-expressing PCa cells, we analyzed Notch1 ligand expression by RNASeq and uncovered DNER as a possible activator of this pathway. DNER is an "atypical" Notch ligand mainly studied in developing brain areas (Eiraku *et al.*, 2005). In PCa, DNER has been described to support the SC phenotype of CD44$^+$ cells isolated from PC-3 metastatic PCa cells by promoting tumor progression and growth *in vitro* and *in vivo* (Wang *et al.*, 2017). In our NCAM1$^+$ cell models, DNER mRNA is upregulated in NCAM1$^+$ cells (∼5-fold) compared to NCAM1$^-$. Moreover, we found that DNER is involved in the regulation of the Notch pathway and actively contributes, in an autocrine/paracrine manner, to ADT resistance. NCAM1 directly regulates the expression of DNER and Notch1, as shown by the anti-NCAM1 blocking antibody. Although we showed that NCAM1 does not appear to bind directly to Notch or members of the gamma-secretase complex (Nicastrin), we have yet to uncover the exact mechanism underlying NCAM1 regulation of Notch.

Together, our data indicate that the Notch pathway could be a relevant therapeutic target in PCa. However, although several GSI drugs have been developed and tested in clinical trials in different cancer types , they have not yet shown promising results in their ability to control tumor progression (Ran *et al.*, 2017; McCaw *et al.*, 2021).

8) *The FGFR pathway.* To uncover pathways that could link NCAM1 to Notch, we reanalyzed our RNAseq data and by ligand-receptor analysis revealed a possible NCAM1-FGFR2-FGF18 axis that all shared a high interaction affinity. The binding of NCAM1 to FGFRs is well known in the literature as described previously (see section 2.2.10.4.3) and FGF18 has been revealed in gastric cancer to be a ligand closely related to this receptor. Moreover, we discovered *FGF18* as one of the most highly upregulated genes in NCAM1$^+$ cells (∼20-fold) compared to NCAM1$^-$, together with structural genes (*KRT6A, KRT6B, KRT36, LAMB3, COL12A1, AQP3, SLC24A3)*, inflammation-related genes (*IL32, CXCL10)*, enzymes (*DHRS6, ACOX2),* transcription factors *(PARP10, SALL4)* and signal transducers (*SHC2, INHBB, EIF3CL).*

This FGFR signaling axis can be targeted by kinase inhibitors that have been widely tested in clinical trials (Konecny *et al.*, 2015; Musolino *et al.*, 2017; Katoh, 2019b), such as Dovitinib, a first-generation multi-kinase FGFR inhibitor that has been shown to promote disease regression in men with CRPC and bone metastases (Wan *et al.*, 2014b), or AZD4547, a second-generation and more selective FGFR inhibitor (Paik *et al.*, 2017). We found that FGF18 forms a novel NCAM1-FGFR2-FGF18 autocrine positive feedback loop in NCAM1$^+$ PCa cells that is critical in conferring resistance to ADT-induced senescence. The data confirmed the role of this pathway in synergizing with ADT to confer an irreversible senescence phenotype important for abrogating tumorigenic ability *in vivo*. Furthermore, an in-depth transcriptional analysis revealed that inhibition of this axis impacts the transcription of Notch and its ligand DNER and, conversely, regulation of Notch through DNER modulates the transcription of FGFR2 and its ligand FGF18. The crosstalk between FGFR2-FGFs and Notch1 had already been described in the literature regulating pancreatic homeostasis and development (Li, Zhai and Teng, 2015), but here we showed that this mechanism also exists in the NCAM1$^+$ PCa cells and that the loop is activated by FGF18 and DNER but only in the presence of NCAM1. Moreover, this mechanism plays a key role in the regulation of resistance to anti-androgen therapies, including the standard therapy used in the clinic Bicalutamide. We demonstrated that FGFR inhibitors were able to reverse Bicalutamide-resistance in human primary PCa cells. Therefore, we propose the use of anti-FGFR drugs, in addition to GSI, as potential adjuvant therapies, to use in combination with ADT, to curb tumor progression by sensitizing tumor cells to androgen deprivation, preventing the appearance of a dormancy phenotype (since sensitized NCAM1$^+$ cells appear to activate irreversible senescence), cancer relapse and CRPC progression.

Deconvolution of the heterogeneity of the NCAM1$^+$ PCa cell compartment

Prostate adenocarcinoma is described as having luminal traits, however both luminal and basal cells have been shown to be capable of initiating tumorigenesis if forced with oncogenic insults (Wang *et al.*, 2014; Choi *et al.*, 2012; Wang *et al.*, 2013; Goldstein AS *et al.*, 2010; Stoyanova *et al.*, 2013; Taylor *et al.*, 2012; Wang *et al.*, 2009). This suggests that PCSCs could have different cellular origins and/or that there is plasticity in progenitor cells allowing them to return to a CSC-like state in the presence of oncogenic insults. In the literature, several markers have been demonstrated to isolate prostate cells with stem traits, from both normal and cancer tissue, but none of these markers been shown to have clinical utility. Thus, we assessed the ability of some of these known markers to identify PCa cells with stem traits and compared them with NCAM1. We focused our analysis on cell surface biomarkers that permitted the isolation of expressing cells by FACS, such as the luminal

markers, CD166, CD38, CD133, and the basal markers, CD117 and CD44 (Leong *et al.*, 2008; Collins *et al.*, 2005; Hurt *et al.*, 2008; Jiao *et al.*, 2012; Liu *et al.*, 2016). We found that none of the markers alone were able to isolate a PCa cell population that could maintain self-renewal potential in the serial propagation assay. Indeed, only NCAM1$^+$ cells displayed this ability. However, the in-depth analysis of the NCAM1$^+$ population by FACS indicated heterogeneity in terms of co-expression of surface markers. Notably, NCAM1$^+$ cells co-expressing CD117, CD133 and to a lesser extent, CD44, were enriched in cells capable of forming organoids *in vitro* suggestive of an enrichment in CSC-like cells. This result suggests heterogeneity within the NCAM1$^+$ population, as observed with AR expression. Therefore, we conducted an in-depth analysis at the single cell level in order to deconvolute the heterogeneity in this cell population and hopefully identify the cell-of-origin that could represent the *bona fide* PCSC.

By scRNA-Seq analysis of NCAM1$^+$ DU145 and LNCaP cells, we confirmed the heterogeneity of the NCAM1$^+$ population at the transcriptional level and were able to define distinct clusters of cells (10 for DU145 cells and 6 for LNCaP) based on transcriptional similarities. By examining the distribution of proliferation genes in these different clusters, we showed that the clusters were associated different phases of the cell cycle. Notably, we demonstrated the existence of a subfraction of quiescent cells in the G0 cell cycle phase, as evidenced by the upregulation of the quiescence marker P57, among others, corresponding to cluster 1 in both cell lines. Quiescence is one of the hallmarks of CSCs, through which they avoid the effects of standard chemotherapy and radiation therapy (which target actively proliferation cells) and are therefore able to regrow when more favorable conditions occur resulting in disease relapse even after several years of remission (De Angelis *et al.*, 2019; Santos-de-Frutos and Djouder, 2021).

Using a single cell trajectory analysis and an unsupervised phylogenetic analysis, we established that the quiescent cluster 1 cells are positioned at the apex of the cellular hierarchy in the NCAM1$^+$ cell population, from which all other cells appear to be derived. Of note, our analysis placed G0/G1 cells at the beginning of the cell trajectories while cells in S and G2/M phase were at the end of the trajectories, consistent with the idea that CSCs derive a proliferating progeny of transit-amplifying cells. Thus, we concluded that cells within cluster 1 likely represent the *bona fide* PCSC population.

To characterize further the molecular features of the putative PCSC cluster 1 cells, we derived a transcriptional signature that uniquely identifies these cells. This signature, which we called "Stem Score", comprises genes upregulated in the quiescent cluster 1 cells and genes associated with the SOX4 transcription factor that is also upregulated in cluster 1. In patient-derived tumor samples, we identified a subfraction of basal-like AR$^-$/NCAM1$^+$/CD117$^+$ cells expressing the Stem Score

signature that sits at the apex of the hierarchical structure of the NCAM1+ cells. These cells possess phenotypic traits consistent with a CSC identity, i.e., they are quiescent (low Ki-67 levels) and display EMT traits (low E-cadherin levels). Moreover, NCAM1^{+}/CD117^{+} cells isolated from PCa cell lines were found to be enriched in organoid-forming capacity (4%) compared to other NCAM1^{+}/CD117^{-} cells (2%), suggesting an enriched CSC content.

CD117 as a PCSC marker

CD117 is known as the "KIT proto-oncogene receptor tyrosine kinase" and has been extensively studied in various cancers where it identifies cells with stem potential, such as: i) hematopoietic cancers (Sasaki *et al.*, 2003); ii) lung and ovarian cancer where it identifies a subpopulation of cells with self-renewal ability (Foster, Buckanovich and Rueda, 2013; Sakabe *et al.*, 2017), iii) osteosarcoma where it identifies a subpopulation of CSC-like cells with chemotherapy resistance (Adhikari *et al.*, 2010). Also in normal tissue, CD117 identifies cells with stem cell traits. In a murine model, single CD117^{+} cells isolated from normal prostate, which also co-expressed CD133 and CD44, were able to entirely regenerate prostate tissue when implanted with mesenchymal urogenital cells into the renal capsule (Leong *et al.*, 2008). In PCa, CD117^{+} cells are associated with the ability to metastasize to the bone and to originate more vascularized tumors compared with CD117$^{–}$ cells (Wiesner *et al.*, 2008; Kerr *et al.*, 2015). Furthermore, the presence of circulating CD117^{+} PCa cells is increased in the blood of patients with high Gleason grade (> 8) PCa, supporting their role in metastasis (Kyjacova *et al.*, 2015). At the molecular level, CD117 regulates several pathways including Notch (Foster *et al*., 2018), which is consistent with our observations showing a role of Notch signaling in maintaining stemness traits in PCa. Moreover, the fraction of CD117^{+} cells from PCa cancers has been shown to be resistant to targeted TKI therapies, such as imatinib and sunitinib (Harris *et al.*, 2021). These data support our findings pointing to CD117 as a biomarker of PCSCs.

Hedgehog signaling is critical for PCSCs

We demonstrated that cells at the hierarchical apex of patient-derived NCAM1^{+} PCa cells are enriched in Hedgehog signaling compared to cells further down the evolutionary trajectory. We also showed that Hedgehog signaling is crucial for maintaining the self-renewal potential of NCAM1^{+}/CD117^{+} cells in the serial organoid propagation assay. Thus, targeting Hedgehog signaling could be an effective strategy for eliminating NCAM1^{+}/CD177^{+} putative PCSCs.

Interestingly in the literature, a mouse model overexpressing the Hedgehog-related protein Shh (pCX-shh-IG mice) developed PIN that progressed to metastatic PCa in 90 days, and the potential cell-of-origin of these tumors was defined as $P63^+/AR^-$ basal cells with Hedgehog pathway activation (Chang *et al.*, 2011), consistent with our findings. This result suggests that the origin of more aggressive androgen-insensitive tumors after anti-hormonal therapy may depend on the clonal selection of resistant $P63^+/AR^-$ CSC-like cells that can regenerate the stem population and originate tumors with highly aggressive traits. These data, together with our results, point to the existence of a $NCAM1^+/CD177^+/AR^-$ dormant PCSC population that is intrinsically resistant to ADT but sensitive to Hedgehog pathway inhibitors, which could prove to be an effective therapeutic target for preventing disease recurrence. However, further studies are needed to understand the direct involvement of $NCAM1^+/CD117^+/AR^-$ PCa cells in tumor relapse and the occurrence of highly aggressive AR-negative tumors. In addition, studies in normal tissue could clarify whether this $NCAM1^+/CD117^+$ cell fraction exists under physiological conditions and whether, in the presence of an oncogenic insult, these cells could transform into PCSCs capable of originating a tumor.

Several therapies against the Hedgehog pathway have been developed and many are being assessed in clinical trials. Among these cyclopamine is highly used to inhibit this pathway (Rubin *et al*., 2006). We showed that treatment of $NCAM1^+/CD117^+$ LNCaP and DU145 cells with this inhibitor is highly effective and specific in abrogating the ability of these cells to sustain self-renewal ability, while having no effect on the $NCAM1^+/CD117^-$ fraction. Of note, $NCAM1^+/CD117^-$ cells also harbour sustained self-renewal potential *in vitro,* indicating possible heterogeneity in the PCSC population or the existence of early progenitors that retain some self-renewal capacity. Further investigations, including examining the *in vivo* serial transplantation ability of these cells, are required to understand better the potential heterogeneity in the PCSC compartment.

Considering the role of Hedgehog in conferring the EMT phenotype and the existence of $CD117^+$ circulating T cells in PCa patients (Katoh *et al.*, 2008; Kerr *et al.,* 2015), Hedgehog inhibitors could also prevent the acquisition of the invasive phenotype by blocking mesenchymal traits in PCSCs. Further studies are needed to understand the metastatic potential of $NCAM1^+/CD117^+$ cells and to investigate whether Hedgehog inhibition could keep these cells in a prolonged dormant state or send them into irreversible senescence, thereby preventing the distant metastasis. In addition, more studies are needed to understand the molecular mechanism by which NCAM1 activates the Hedgehog pathway by delving into the role of surface receptors capable of activating this pathway.

EMT and metastatic potential

Poor prognosis of PCa patients is often associated with the development of metastatic disease and as analyzed in our patient cohort, the risk of developing DM was 13% in $NCAM1^+$ patients compared to 2% in $NCAM1^-$ patients. Furthermore, in patients with positive surgical margins, NCAM1 status was strongly associated with risk of relapse: risk of BCR over 15 years was 63% in $NCAM1^{POS}$ patients compared with 15% in $NCAM1^{NEG}$ patients. In addition, one of the intrinsic characteristics of CSCs is the ability to acquire EMT traits, especially a partial EMT state. This partial EMT manifests itself by the simultaneous expression of epithelial and mesenchymal markers. Physiologically, partial EMT is required to regenerate damaged tissue while in cancer it confers the capacity of invasion and migration to the cells which are necessary for metastasis.

We therefore decided to investigate the relationship between NCAM1 expression and EMT state. Not all the CSCs have metastatic potential. Brabletz proposed that just a subfraction of these cells, the MCSCs, have intrinsically the capacity to migrate and promote metastasis (Brabletz *et al.*, 2005). The subfraction of primary human-derived $NCAM1^+/CD117^+$ cells is enriched in EMT hallmarks and EMT-related transcription factors, ZEB1, SLUG and TWIST2, but not SNAIL, and the MMPs family members MMP2 and MMP10, extensively associated with invasive potential (Scheau *et al.*, 2019) (see section 2.2.7.1.1). Moreover, the $NCAM1^+/CD117^+$ population displayed a dormant/slow-proliferating traits necessary for cell dissemination, and survival and drug escape in the secondary tissue as DTCs (Phan and Croucher, 2020) (see section 2.2.7.1.3). We also pointed out that the $NCAM1^+/CD117^+$ cells are characterized by the expression of VEGFA. VEGFA is strongly associated to metastasis and it acts in paracrine fashion to stimulate angiogenesis but also in autocrine fashion to sustain dormancy and self-renewal ability (Maxwell *et al.*, 1997; Hamerlik *et al.*, 2012; Goel and Mercurio, 2013). Of note, SOX4, which we demonstrated necessary fo self-renewal ability of the $NCAM1^+$ cells, is known to be master regulator of EMT in several cancers (Liao *et al.*, 2008; J. Zhang *et al.*, 2012; Tiwari *et al.*, 2013) including PCa (Wang *et al.*, 2014; Liu *et al.*, 2017). Thus, based on all these evidences we speculate that the $NCAM1^+/CD117^+$ fraction of cells is *bona fide* related with metastatic potential and can be defined as MCSCs. Thus, it would be interesting to identify $NCAM1^+$ cells circulating in the blood, as CTCs, or within the metastases, mainly to bone or in other secondary tissues, since NCAM1-POS patients have an increased risk of developing metastases. By doing so, developing anti-NCAM1 therapy could have an effect not only in preventing local recurrence but also preventing the occurrence of metastasis in dormant cells that have already disseminated and colonized the secondary site. *In vivo* and *in vitro* experiments will be necessary to corroborate this our hypothesis.

STEM SCORE: a prognostic signature for PCa

Given the rarity of NCAM1$^+$/CD117$^+$ cells in patient tumors (~0.2% of EpCAM$^+$ cells), these cells would be difficult to detect by direct visualization in tissue sections. Therefore, the use of molecular signatures, such as the "Stem Score" described here, which are able to measure the presence of these putative PCSCs in prostate tumors through a panel of genes, could have important implications for personalized clinical protocols. Such signatures could be used for a more precise stratification of patients for BCR/DM risk and the tailoring of therapies.

Our lab has recently demonstrated the clinical value of such prognostic signatures with StemPrinter, a molecular signature of 20 stem genes that enables the improved stratification of patients with luminal, ER-positive/HER-negative breast cancer in terms of risk of developing metastases (Pece *et al.*, 2019). Further studies are needed to better understand the applicability and clinical validity of our Stem Score signature in predicting prognosis and possibly determining patient eligibility for targeted therapies such as Hedgehog inhibitors.

7.1 CONCLUSIONS AND FUTURE PERSPECTIVES

In sum, with this work we have demonstrated that the protein NCAM1 is not uniquely associated with NE phenotype in PCa, but instead can be used for the isolation of a heterogenous population of CSC-like cells that are necessary for PCa progression in the TRAMP mouse model, and possess sustained self-renewal ability, EMT traits and resistance to ADT (both androgen depletion and the AR-inhibitor Bicalutamide). Moreover, our data strongly point to the clinical relevance of NCAM1 as a prognostic PCSC biomarker, which could be employed as a *low-cost* clinical tool to guide therapeutic decisions (*AS vs. RP*), and as a therapeutic target (together with its signaling effectors, e.g., Notch, FGFR, Hedgehog) for the development of anti-CSCs therapies. Finally, within the heterogeneous NCAM1$^+$ cell population, we have identified a rare population of cells characterized by quiescence, expression of CD117, basal markers and EMT markers, lack of AR, and upregulated Hedgehog signaling, sitting at the apex of the cellular hierarchy. We conclude that these cells represent *bona fide* PCSCs.

Several future goals stem from this project:

1. Further characterization of the NCAM1$^+$/CD117$^+$ PCSC compartment to investigate metastasis *in vivo* models.
2. Pre-clinical validation of the efficacy of drugs, such as cyclopamine and GSI, as anti-CSC therapies using *in vivo* studies.

3. Clinical validation of Stem Score in publicly available PCa datasets and eventually in the IEO PCa cohort.

Investigation of the role of NCAM1 in the normal prostate gland. Due to the expression of NCAM1 in high inflammatory regions, we are interested in investigating the role of NCAM1 in prostate physiology and its oncogenic role in presence of chronic inflammation, typical of prostate disease (de Bono *et al.*, 2020), and oncogenic insults. In addition, we will investigate the possible crosstalk between PCSCs and the tumor immune infiltrate to uncover mediators relevant to PCSC maintenance and PCa progression with the purpose of identifying potential immunotherapeutic strategies to target aggressive tumors and overcome intratumoral and intra-PCSC heterogeneity.

BIBLIOGRAPHY

Abrahamsson, P.A. (1999) 'Neuroendocrine cells in tumour growth of the prostate', *Endocrine-Related Cancer*, 6(4), pp. 503–519.

Aceto, N. *et al.* (2014) 'Circulating tumor cell clusters are oligoclonal precursors of breast cancer metastasis', *Cell*, 158(5), pp. 1110–1122.

Adhikari, A.S. *et al.* (2010) 'CD117 and Stro-1 identify osteosarcoma tumor-initiating cells associated with metastasis and drug resistance', *Cancer Research*, 70(11), pp. 4602–4612.

Aggarwal, C. *et al.* (2019) 'Clinical Implications of Plasma-Based Genotyping With the Delivery of Personalized Therapy in Metastatic Non-Small Cell Lung Cancer', *JAMA oncology*, 5(2), pp. 173–180.

Ahmadiyeh, N. *et al.* (2010) '8q24 prostate, breast, and colon cancer risk loci show tissue-specific long-range interaction with MYC', *Proceedings of the National Academy of Sciences of the United States of America*, 107(21), pp. 9742–9746.

Ahmed, H.U. *et al.* (2017) 'Diagnostic accuracy of multi-parametric MRI and TRUS biopsy in prostate cancer (PROMIS): a paired validating confirmatory study', *Lancet (London, England)*, 389(10071), pp. 815–822.

Airaksinen, M.S., Titievsky, A. and Saarma, M. (1999) 'GDNF family neurotrophic factor signaling: four masters, one servant?', *Molecular and Cellular Neurosciences*, 13(5), pp. 313–325.

Albertsen, P.C., Hanley, J.A. and Fine, J. (2005) '20-year outcomes following conservative management of clinically localized prostate cancer', *JAMA*, 293(17), pp. 2095–2101.

Alexander, D.D. *et al.* (2010) 'A review and meta-analysis of prospective studies of red and processed meat intake and prostate cancer', *Nutrition Journal*, 9, p. 50.
Ames, B.N., Gold, L.S. and Willett, W.C. (1995) 'The causes and prevention of cancer', *Proceedings of the National Academy of Sciences of the United States of America*, 92(12), pp. 5258–5265.
Ames, E. *et al.* (2015) 'NK Cells Preferentially Target Tumor Cells with a Cancer Stem Cell Phenotype', *Journal of Immunology (Baltimore, Md.: 1950)*, 195(8), pp. 4010–4019.
Ammirante, M. *et al.* (2010) 'B-cell-derived lymphotoxin promotes castration-resistant prostate cancer', *Nature*, 464(7286), pp. 302–305.
Amoureux, M.-C. *et al.* (2010) 'Polysialic acid neural cell adhesion molecule (PSA-NCAM) is an adverse prognosis factor in glioblastoma, and regulates olig2 expression in glioma cell lines', *BMC cancer*, 10, p. 91.
Anassi, E. and Ndefo, U.A. (2011) 'Sipuleucel-T (provenge) injection: the first immunotherapy agent (vaccine) for hormone-refractory prostate cancer', *P & T: A Peer-Reviewed Journal for Formulary Management*, 36(4), pp. 197–202.
Anderson, A.A. *et al.* (2005) 'A peptide from the first fibronectin domain of NCAM acts as an inverse agonist and stimulates FGF receptor activation, neurite outgrowth and survival', *Journal of Neurochemistry*, 95(2), pp. 570–583.
Anguille, S. *et al.* (2012) 'Interleukin-15-induced CD56(+) myeloid dendritic cells combine potent tumor antigen presentation with direct tumoricidal potential', *PloS One*, 7(12), p. e51851.
Araki, S. *et al.* (2007) 'Interleukin-8 is a molecular determinant of androgen independence and progression in prostate cancer', *Cancer Research*, 67(14), pp. 6854–6862.
Arlen, P.M. *et al.* (2008) 'Prostate Specific Antigen Working Group guidelines on prostate specific antigen doubling time', *The Journal of Urology*, 179(6), pp. 2181–2185; discussion 2185-2186.
Armenia, J. *et al.* (2018) 'The long tail of oncogenic drivers in prostate cancer', *Nature Genetics*, 50(5), pp. 645–651.
Armstrong, A.J. *et al.* (2019) 'ARCHES: A Randomized, Phase III Study of Androgen Deprivation Therapy With Enzalutamide or Placebo in Men With Metastatic Hormone-Sensitive Prostate Cancer', *Journal of Clinical Oncology: Official Journal of the American Society of Clinical Oncology*, 37(32), pp. 2974–2986.
Armstrong, A.J. *et al.* (2020) 'Prospective Multicenter Study of Circulating Tumor Cell AR-V7 and Taxane Versus Hormonal Treatment Outcomes in Metastatic Castration-Resistant Prostate Cancer', *JCO precision oncology*, 4, p. PO.20.00200.
Attard, G. *et al.* (2016) 'Prostate cancer', *Lancet (London, England)*, 387(10013), pp. 70–82.
Attard, G., Cooper, C.S. and de Bono, J.S. (2009) 'Steroid hormone receptors in prostate cancer: a hard habit to break?', *Cancer Cell*, 16(6), pp. 458–462.
Babina, I.S. and Turner, N.C. (2017) 'Advances and challenges in targeting FGFR signalling in cancer', *Nature Reviews. Cancer*, 17(5), pp. 318–332.
Baca, S.C. *et al.* (2013) 'Punctuated evolution of prostate cancer genomes', *Cell*, 153(3), pp. 666–677.
Baccelli, I. and Trumpp, A. (2012) 'The evolving concept of cancer and metastasis stem cells', *The Journal of Cell Biology*, 198(3), pp. 281–293.
Balbas, M.D. *et al.* (2013) 'Overcoming mutation-based resistance to antiandrogens with rational drug design', *eLife*, 2, p. e00499.
Balic, M. *et al.* (2006) 'Most early disseminated cancer cells detected in bone marrow of breast cancer patients have a putative breast cancer stem cell phenotype', *Clinical Cancer Research: An Official Journal of the American Association for Cancer Research*, 12(19), pp. 5615–5621.
Baloh, R.H. *et al.* (2000) 'The GDNF family ligands and receptors - implications for neural development', *Current Opinion in Neurobiology*, 10(1), pp. 103–110.

Barabé, F. *et al.* (2007) 'Modeling the initiation and progression of human acute leukemia in mice', *Science (New York, N.Y.)*, 316(5824), pp. 600–604.
Barrallo-Gimeno, A. and Nieto, M.A. (2005) 'The Snail genes as inducers of cell movement and survival: implications in development and cancer', *Development (Cambridge, England)*, 132(14), pp. 3151–3161.
Bartucci, M. *et al.* (2012) 'Therapeutic targeting of Chk1 in NSCLC stem cells during chemotherapy', *Cell Death and Differentiation*, 19(5), pp. 768–778.
Bataille, R. *et al.* (2006) 'The phenotype of normal, reactive and malignant plasma cells. Identification of "many and multiple myelomas" and of new targets for myeloma therapy', *Haematologica*, 91(9), pp. 1234–1240.
Batlle, E. and Clevers, H. (2017) 'Cancer stem cells revisited', *Nature Medicine*, 23(10), pp. 1124–1134.
Baylin, S.B. and Jones, P.A. (2011) 'A decade of exploring the cancer epigenome - biological and translational implications', *Nature Reviews. Cancer*, 11(10), pp. 726–734.
Beachy, P.A., Karhadkar, S.S. and Berman, D.M. (2004) 'Tissue repair and stem cell renewal in carcinogenesis', *Nature*, 432(7015), pp. 324–331.
Beer, T.M. *et al.* (2014) 'Enzalutamide in metastatic prostate cancer before chemotherapy', *The New England Journal of Medicine*, 371(5), pp. 424–433.
Beer, T.M. *et al.* (2017) 'Randomized, Double-Blind, Phase III Trial of Ipilimumab Versus Placebo in Asymptomatic or Minimally Symptomatic Patients With Metastatic Chemotherapy-Naive Castration-Resistant Prostate Cancer', *Journal of Clinical Oncology: Official Journal of the American Society of Clinical Oncology*, 35(1), pp. 40–47.
Beggs, H.E. *et al.* (1997) 'NCAM140 interacts with the focal adhesion kinase p125(fak) and the SRC-related tyrosine kinase p59(fyn)', *The Journal of Biological Chemistry*, 272(13), pp. 8310–8319.
Belandia, B. and Parker, M.G. (2006) 'Nuclear receptor regulation gears up another Notch', *Nuclear Receptor Signaling*, 4, p. e001.
Bellissimo, D.C. and Speck, N.A. (2017) 'RUNX1 Mutations in Inherited and Sporadic Leukemia', *Frontiers in Cell and Developmental Biology*, 5, p. 111.
Beltran, H. *et al.* (2014) 'Aggressive variants of castration-resistant prostate cancer', *Clinical Cancer Research: An Official Journal of the American Association for Cancer Research*, 20(11), pp. 2846–2850.
Berger, M.F. *et al.* (2011) 'The genomic complexity of primary human prostate cancer', *Nature*, 470(7333), pp. 214–220.
Berthold, D.R. *et al.* (2008) 'Treatment of hormone-refractory prostate cancer with docetaxel or mitoxantrone: relationships between prostate-specific antigen, pain, and quality of life response and survival in the TAX-327 study', *Clinical Cancer Research: An Official Journal of the American Association for Cancer Research*, 14(9), pp. 2763–2767.
Bethel, C.R. *et al.* (2006) 'Decreased NKX3.1 protein expression in focal prostatic atrophy, prostatic intraepithelial neoplasia, and adenocarcinoma: association with gleason score and chromosome 8p deletion', *Cancer Research*, 66(22), pp. 10683–10690.
Bettermann, A.S. *et al.* (2019) '[68Ga-]PSMA-11 PET/CT and multiparametric MRI for gross tumor volume delineation in a slice by slice analysis with whole mount histopathology as a reference standard - Implications for focal radiotherapy planning in primary prostate cancer', *Radiotherapy and Oncology: Journal of the European Society for Therapeutic Radiology and Oncology*, 141, pp. 214–219.
Bhattacharya, R. *et al.* (2009) 'MiR-15a and MiR-16 control Bmi-1 expression in ovarian cancer', *Cancer Research*, 69(23), pp. 9090–9095.
Birnie, R. *et al.* (2008) 'Gene expression profiling of human prostate cancer stem cells reveals a pro-inflammatory phenotype and the importance of extracellular matrix interactions',

Genome Biology, 9(5), p. R83.
Boehm, B.J. *et al.* (2012) 'Acute bacterial inflammation of the mouse prostate', *The Prostate*, 72(3), pp. 307–317.
Boggon, T.J. and Eck, M.J. (2004) 'Structure and regulation of Src family kinases', *Oncogene*, 23(48), pp. 7918–7927.
Bonkhoff, H. (2003) 'Morphogenetic Aspects of Prostate Cancer', in R. Hofmann, A. Heidenreich, and J.W. Moul (eds) *Prostate Cancer*. Berlin, Heidelberg: Springer Berlin Heidelberg, pp. 3–12.
de Bono, J. *et al.* (2020) 'Olaparib for Metastatic Castration-Resistant Prostate Cancer', *The New England Journal of Medicine*, 382(22), pp. 2091–2102.
de Bono, J.S. *et al.* (2010) 'Prednisone plus cabazitaxel or mitoxantrone for metastatic castration-resistant prostate cancer progressing after docetaxel treatment: a randomised open-label trial', *Lancet (London, England)*, 376(9747), pp. 1147–1154.
de Bono, J.S. *et al.* (2020) 'Prostate carcinogenesis: inflammatory storms', *Nature Reviews. Cancer*, 20(8), pp. 455–469.
Boorjian, S.A. *et al.* (2009) 'Radiation therapy after radical prostatectomy: impact on metastasis and survival', *The Journal of Urology*, 182(6), pp. 2708–2714.
Brabletz, T. *et al.* (2005) 'Opinion: migrating cancer stem cells - an integrated concept of malignant tumour progression', *Nature Reviews. Cancer*, 5(9), pp. 744–749.
Bray, F. *et al.* (2018) 'Global cancer statistics 2018: GLOBOCAN estimates of incidence and mortality worldwide for 36 cancers in 185 countries', *CA: a cancer journal for clinicians*, 68(6), pp. 394–424.
Bruinsma, S.M. *et al.* (2016) 'Active surveillance for prostate cancer: a narrative review of clinical guidelines', *Nature Reviews. Urology*, 13(3), pp. 151–167.
Bubendorf, L. *et al.* (1999) 'Survey of gene amplifications during prostate cancer progression by high-throughout fluorescence in situ hybridization on tissue microarrays', *Cancer Research*, 59(4), pp. 803–806.
Bubendorf, L. *et al.* (2000) 'Metastatic patterns of prostate cancer: an autopsy study of 1,589 patients', *Human Pathology*, 31(5), pp. 578–583.
Buchanan, G. *et al.* (2001) 'Collocation of androgen receptor gene mutations in prostate cancer', *Clinical Cancer Research: An Official Journal of the American Association for Cancer Research*, 7(5), pp. 1273–1281.
Bul, M. *et al.* (2013) 'Active surveillance for low-risk prostate cancer worldwide: the PRIAS study', *European Urology*, 63(4), pp. 597–603.
Bussemakers, M.J. *et al.* (1999) 'DD3: a new prostate-specific gene, highly overexpressed in prostate cancer', *Cancer Research*, 59(23), pp. 5975–5979.
Butler, W. and Huang, J. (2021) 'Neuroendocrine cells of the prostate: Histology, biological functions, and molecular mechanisms', *Precision Clinical Medicine*, 4(1), pp. 25–34.
Cai, C. *et al.* (2011) 'Intratumoral de novo steroid synthesis activates androgen receptor in castration-resistant prostate cancer and is upregulated by treatment with CYP17A1 inhibitors', *Cancer Research*, 71(20), pp. 6503–6513.
Caini, S. *et al.* (2014) 'Sexually transmitted infections and prostate cancer risk: a systematic review and meta-analysis', *Cancer Epidemiology*, 38(4), pp. 329–338.
Calcinotto, A. *et al.* (2018) 'IL-23 secreted by myeloid cells drives castration-resistant prostate cancer', *Nature*, 559(7714), pp. 363–369.
Calon, A. *et al.* (2012) 'Dependency of colorectal cancer on a TGF-β-driven program in stromal cells for metastasis initiation', *Cancer Cell*, 22(5), pp. 571–584.
Campbell, I.D. and Spitzfaden, C. (1994) 'Building proteins with fibronectin type III modules', *Structure (London, England: 1993)*, 2(5), pp. 333–337.
Canfield, S.E. *et al.* (2014) 'A guide for clinicians in the evaluation of emerging molecular diagnostics for newly diagnosed prostate cancer', *Reviews in Urology*, 16(4), pp. 172–180.

Cangul, H. (2004) 'Hypoxia upregulates the expression of the NDRG1 gene leading to its overexpression in various human cancers', *BMC genetics*, 5, p. 27.
Cano, A. *et al.* (2000) 'The transcription factor snail controls epithelial-mesenchymal transitions by repressing E-cadherin expression', *Nature Cell Biology*, 2(2), pp. 76–83.
Carlsson, S.V. and Vickers, A.J. (2020) 'Screening for Prostate Cancer', *Medical Clinics of North America*, 104(6), pp. 1051–1062.
Carroll, P.H. and Mohler, J.L. (2018) 'NCCN Guidelines Updates: Prostate Cancer and Prostate Cancer Early Detection', *Journal of the National Comprehensive Cancer Network: JNCCN*, 16(5S), pp. 620–623.
Carver, B.S. *et al.* (2009) 'ETS rearrangements and prostate cancer initiation', *Nature*, 457(7231), pp. E1; discussion E2-3.
Catalona, W.J. *et al.* (1991) 'Measurement of prostate-specific antigen in serum as a screening test for prostate cancer', *The New England Journal of Medicine*, 324(17), pp. 1156–1161.
Cavallaro, U. *et al.* (2001) 'N-CAM modulates tumour-cell adhesion to matrix by inducing FGF-receptor signalling', *Nature Cell Biology*, 3(7), pp. 650–657.
Chan, K.S. (2016) 'Molecular Pathways: Targeting Cancer Stem Cells Awakened by Chemotherapy to Abrogate Tumor Repopulation', *Clinical Cancer Research: An Official Journal of the American Association for Cancer Research*, 22(4), pp. 802–806.
Chanan-Khan, A. *et al.* (2016) 'Ibrutinib combined with bendamustine and rituximab compared with placebo, bendamustine, and rituximab for previously treated chronic lymphocytic leukaemia or small lymphocytic lymphoma (HELIOS): a randomised, double-blind, phase 3 study', *The Lancet. Oncology*, 17(2), pp. 200–211.
Chang, H.-H. *et al.* (2011) 'Hedgehog overexpression leads to the formation of prostate cancer stem cells with metastatic property irrespective of androgen receptor expression in the mouse model', *Journal of Biomedical Science*, 18, p. 6.
Charitou, P. *et al.* (2015) 'FOXOs support the metabolic requirements of normal and tumor cells by promoting IDH1 expression', *EMBO reports*, 16(4), pp. 456–466.
Chen, J. *et al.* (2011) 'Solving the puzzle of metastasis: the evolution of cell migration in neoplasms', *PloS One*, 6(4), p. e17933.
Chen, J. *et al.* (2012) 'A restricted cell population propagates glioblastoma growth after chemotherapy', *Nature*, 488(7412), pp. 522–526.
Chen, R.C. *et al.* (2016) 'Active Surveillance for the Management of Localized Prostate Cancer (Cancer Care Ontario Guideline): American Society of Clinical Oncology Clinical Practice Guideline Endorsement', *Journal of Clinical Oncology: Official Journal of the American Society of Clinical Oncology*, 34(18), pp. 2182–2190.
Chen, W. *et al.* (2016) 'Cancer Stem Cell Quiescence and Plasticity as Major Challenges in Cancer Therapy', *Stem Cells International*, 2016, p. 1740936.
Chiang, S.P.H., Cabrera, R.M. and Segall, J.E. (2016) 'Tumor cell intravasation', *American Journal of Physiology. Cell Physiology*, 311(1), pp. C1–C14.
Chikamatsu, K. *et al.* (2012) 'Resistance to apoptosis-inducing stimuli in CD44+ head and neck squamous cell carcinoma cells', *Head & Neck*, 34(3), pp. 336–343.
Cho, M.S. *et al.* (2012) 'Platelets increase the proliferation of ovarian cancer cells', *Blood*, 120(24), pp. 4869–4872.
Choi, N. *et al.* (2012) 'Adult murine prostate basal and luminal cells are self-sustained lineages that can both serve as targets for prostate cancer initiation', *Cancer Cell*, 21(2), pp. 253–265.
Chothia, C. and Jones, E.Y. (1997) 'The molecular structure of cell adhesion molecules', *Annual Review of Biochemistry*, 66, pp. 823–862.
Christensen, C. *et al.* (2006) 'The neural cell adhesion molecule binds to fibroblast growth factor receptor 2', *FEBS letters*, 580(14), pp. 3386–3390.
Chua, C.W. *et al.* (2014) 'Single luminal epithelial progenitors can generate prostate organoids in

culture', *Nature Cell Biology*, 16(10), pp. 951–961, 1–4.
Claessens, F. *et al.* (1996) 'The androgen-specific probasin response element 2 interacts differentially with androgen and glucocorticoid receptors', *The Journal of Biological Chemistry*, 271(32), pp. 19013–19016.
Clark, A. and Burleson, M. (2020) 'SPOP and cancer: a systematic review', *American Journal of Cancer Research*, 10(3), pp. 704–726.
Clarke, M.F. and Fuller, M. (2006) 'Stem cells and cancer: two faces of eve', *Cell*, 124(6), pp. 1111–1115.
Clevers, H. (2011) 'The cancer stem cell: premises, promises and challenges', *Nature Medicine*, 17(3), pp. 313–319.
Coffelt, S.B. *et al.* (2015) 'IL-17-producing γδ T cells and neutrophils conspire to promote breast cancer metastasis', *Nature*, 522(7556), pp. 345–348.
Coffey, K. and Robson, C.N. (2012) 'Regulation of the androgen receptor by post-translational modifications', *The Journal of Endocrinology*, 215(2), pp. 221–237.
Cole, G.J. and Glaser, L. (1986) 'A heparin-binding domain from N-CAM is involved in neural cell-substratum adhesion', *The Journal of Cell Biology*, 102(2), pp. 403–412.
Colotta, F. *et al.* (2009) 'Cancer-related inflammation, the seventh hallmark of cancer: links to genetic instability', *Carcinogenesis*, 30(7), pp. 1073–1081.
Contarelli, S., Fedele, V. and Melisi, D. (2020) 'HOX Genes Family and Cancer: A Novel Role for Homeobox B9 in the Resistance to Anti-Angiogenic Therapies', *Cancers*, 12(11), p. E3299.
Cookson, M.S. *et al.* (2013) 'Castration-resistant prostate cancer: AUA Guideline', *The Journal of Urology*, 190(2), pp. 429–438. Available at: https://doi.org/10.1016/j.juro.2013.05.005.
Coppé, J.-P. *et al.* (2010) 'The senescence-associated secretory phenotype: the dark side of tumor suppression', *Annual Review of Pathology*, 5, pp. 99–118.
Coussens, L.M. and Werb, Z. (2002) 'Inflammation and cancer', *Nature*, 420(6917), pp. 860–867.
Cozzio, A. *et al.* (2003) 'Similar MLL-associated leukemias arising from self-renewing stem cells and short-lived myeloid progenitors', *Genes & Development*, 17(24), pp. 3029–3035.
Crawford, E.D. (2003) 'Epidemiology of prostate cancer', *Urology*, 62(6 Suppl 1), pp. 3–12.
Crawford, E.D. *et al.* (2019) 'Androgen-targeted therapy in men with prostate cancer: evolving practice and future considerations', *Prostate Cancer and Prostatic Diseases*, 22(1), pp. 24–38.
Cross, A.J. *et al.* (2005) 'A prospective study of meat and meat mutagens and prostate cancer risk', *Cancer Research*, 65(24), pp. 11779–11784.
Cui, D. *et al.* (2015) 'Notch Pathway Inhibition Using PF-03084014, a γ-Secretase Inhibitor (GSI), Enhances the Antitumor Effect of Docetaxel in Prostate Cancer', *Clinical Cancer Research: An Official Journal of the American Association for Cancer Research*, 21(20), pp. 4619–4629.
Dai, B. *et al.* (2010) 'Compensatory upregulation of tyrosine kinase Etk/BMX in response to androgen deprivation promotes castration-resistant growth of prostate cancer cells', *Cancer Research*, 70(13), pp. 5587–5596.
Dalerba, P. *et al.* (2007) 'Phenotypic characterization of human colorectal cancer stem cells', *Proceedings of the National Academy of Sciences of the United States of America*, 104(24), pp. 10158–10163.
D'Amico, A.V. *et al.* (1998) 'Biochemical outcome after radical prostatectomy, external beam radiation therapy, or interstitial radiation therapy for clinically localized prostate cancer', *JAMA*, 280(11), pp. 969–974.
D'amico, M.A. *et al.* (2014) 'Biological function and clinical relevance of chromogranin A and derived peptides', *Endocrine Connections*, 3(2), pp. R45-54.
Davidsson, S. *et al.* (2013) 'CD4 helper T cells, CD8 cytotoxic T cells, and FOXP3(+) regulatory T cells with respect to lethal prostate cancer', *Modern Pathology: An Official Journal of*

the United States and Canadian Academy of Pathology, Inc, 26(3), pp. 448–455.
Davies, P. *et al.* (2008) 'Consequences of poly-glutamine repeat length for the conformation and folding of the androgen receptor amino-terminal domain', *Journal of Molecular Endocrinology*, 41(5), pp. 301–314.
Dawson, M.A. and Kouzarides, T. (2012) 'Cancer epigenetics: from mechanism to therapy', *Cell*, 150(1), pp. 12–27.
De Angelis, M.L. *et al.* (2019) 'Stem Cell Plasticity and Dormancy in the Development of Cancer Therapy Resistance', *Frontiers in Oncology*, 9, p. 626.
De Marzo, A.M. *et al.* (1999) 'Proliferative inflammatory atrophy of the prostate: implications for prostatic carcinogenesis', *The American Journal of Pathology*, 155(6), pp. 1985–1992.
De Marzo, A.M. *et al.* (2007) 'Inflammation in prostate carcinogenesis', *Nature Reviews. Cancer*, 7(4), pp. 256–269.
De Marzo, A.M. *et al.* (2016) 'Premalignancy in Prostate Cancer: Rethinking What we Know', *Cancer Prevention Research (Philadelphia, Pa.)*, 9(8), pp. 648–656.
De Talhouet, S. *et al.* (2020) 'Clinical outcome of breast cancer in carriers of BRCA1 and BRCA2 mutations according to molecular subtypes', *Scientific Reports*, 10(1), p. 7073.
Dehm, S.M. *et al.* (2008) 'Splicing of a novel androgen receptor exon generates a constitutively active androgen receptor that mediates prostate cancer therapy resistance', *Cancer Research*, 68(13), pp. 5469–5477.
Delongchamps, N.B. *et al.* (2008) 'Evaluation of prostatitis in autopsied prostates--is chronic inflammation more associated with benign prostatic hyperplasia or cancer?', *The Journal of Urology*, 179(5), pp. 1736–1740.
Dennis, K.L. *et al.* (2013) 'Current status of interleukin-10 and regulatory T-cells in cancer', *Current Opinion in Oncology*, 25(6), pp. 637–645.
DePaolo, J.S. *et al.* (2016) 'Acetylation of androgen receptor by ARD1 promotes dissociation from HSP90 complex and prostate tumorigenesis', *Oncotarget*, 7(44), pp. 71417–71428.
Di Tomaso, T. *et al.* (2010) 'Immunobiological characterization of cancer stem cells isolated from glioblastoma patients', *Clinical Cancer Research: An Official Journal of the American Association for Cancer Research*, 16(3), pp. 800–813.
Dias Silva, É. *et al.* (2012) 'Goserelin versus leuprolide in the chemical castration of patients with prostate cancer', *International Urology and Nephrology*, 44(4), pp. 1039–1044.
Diehn, M. *et al.* (2009) 'Association of reactive oxygen species levels and radioresistance in cancer stem cells', *Nature*, 458(7239), pp. 780–783.
Dong, C. *et al.* (2013) 'Loss of FBP1 by Snail-mediated repression provides metabolic advantages in basal-like breast cancer', *Cancer Cell*, 23(3), pp. 316–331.
Dougan, M. and Dranoff, G. (2009) 'Immune therapy for cancer', *Annual Review of Immunology*, 27, pp. 83–117.
Driessens, G. *et al.* (2012) 'Defining the mode of tumour growth by clonal analysis', *Nature*, 488(7412), pp. 527–530.
Drost, F.-J.H. *et al.* (2019) 'Prostate MRI, with or without MRI-targeted biopsy, and systematic biopsy for detecting prostate cancer', *The Cochrane Database of Systematic Reviews*, 4, p. CD012663.
Du, W. *et al.* (2011) 'Overexpression of IL-3Rα on CD34+CD38- stem cells defines leukemia-initiating cells in Fanconi anemia AML', *Blood*, 117(16), pp. 4243–4252.
Eiraku, M. *et al.* (2005) 'DNER acts as a neuron-specific Notch ligand during Bergmann glial development', *Nature Neuroscience*, 8(7), pp. 873–880.
El-Alfy, M. *et al.* (1999) 'Localization of type 5 17beta-hydroxysteroid dehydrogenase, 3beta-hydroxysteroid dehydrogenase, and androgen receptor in the human prostate by in situ hybridization and immunocytochemistry', *Endocrinology*, 140(3), pp. 1481–1491.
Enderling, H. and Rejniak, K.A. (2013) 'Simulating cancer: computational models in oncology', *Frontiers in Oncology*, 3, p. 233.

Eramo, A. *et al.* (2008) 'Identification and expansion of the tumorigenic lung cancer stem cell population', *Cell Death and Differentiation*, 15(3), pp. 504–514.
Escamilla, A. *et al.* (2016) 'Distribution of Foxp3+ T cells in the liver and hepatic lymph nodes of goats and sheep experimentally infected with Fasciola hepatica', *Veterinary Parasitology*, 230, pp. 14–19.
Ewing, C.M. *et al.* (2012) 'Germline mutations in HOXB13 and prostate-cancer risk', *The New England Journal of Medicine*, 366(2), pp. 141–149.
Farah, E. *et al.* (2019) 'NOTCH signaling is activated in and contributes to resistance in enzalutamide-resistant prostate cancer cells', *The Journal of Biological Chemistry*, 294(21), pp. 8543–8554.
Fenton, J.J. *et al.* (2018) 'Prostate-Specific Antigen-Based Screening for Prostate Cancer: Evidence Report and Systematic Review for the US Preventive Services Task Force', *JAMA*, 319(18), pp. 1914–1931.
Ferraro, D.A. *et al.* (2020) 'Immunohistochemical PSMA expression patterns of primary prostate cancer tissue are associated with the detection rate of biochemical recurrence with 68Ga-PSMA-11-PET', *Theranostics*, 10(14), pp. 6082–6094.
Fichtner, J. *et al.* (1996) 'Prostate specific antigen releases a kinin-like substance on proteolysis of seminal vesicle fluid that stimulates smooth muscle contraction', *The Journal of Urology*, 155(2), pp. 738–742.
Figarella-Branger, D. *et al.* (1996) 'Correlation between polysialic-neural cell adhesion molecule levels in CSF and medulloblastoma outcomes.', *Journal of Clinical Oncology*, 14(7), pp. 2066–2072.
Flavin, R. *et al.* (2014) 'SPINK1 protein expression and prostate cancer progression', *Clinical Cancer Research: An Official Journal of the American Association for Cancer Research*, 20(18), pp. 4904–4911.
Foreman, K.J. *et al.* (2018) 'Forecasting life expectancy, years of life lost, and all-cause and cause-specific mortality for 250 causes of death: reference and alternative scenarios for 2016-40 for 195 countries and territories', *Lancet (London, England)*, 392(10159), pp. 2052–2090.
Foster, R., Buckanovich, R.J. and Rueda, B.R. (2013) 'Ovarian cancer stem cells: working towards the root of stemness', *Cancer Letters*, 338(1), pp. 147–157.
Francart, M.-E. *et al.* (2018) 'Epithelial-mesenchymal plasticity and circulating tumor cells: Travel companions to metastases', *Developmental Dynamics: An Official Publication of the American Association of Anatomists*, 247(3), pp. 432–450.
Francavilla, C. *et al.* (2007) 'Neural cell adhesion molecule regulates the cellular response to fibroblast growth factor', *Journal of Cell Science*, 120(Pt 24), pp. 4388–4394.
Francini, E. *et al.* (2018) 'Time of metastatic disease presentation and volume of disease are prognostic for metastatic hormone sensitive prostate cancer (mHSPC)', *The Prostate*, 78(12), pp. 889–895.
Franke, R.M. *et al.* (2010) 'Castration-dependent pharmacokinetics of docetaxel in patients with prostate cancer', *Journal of Clinical Oncology: Official Journal of the American Society of Clinical Oncology*, 28(30), pp. 4562–4567.
Fraser, M. *et al.* (2017) 'Genomic hallmarks of localized, non-indolent prostate cancer', *Nature*, 541(7637), pp. 359–364.
Friedlander, D.R. *et al.* (1994) 'The neuronal chondroitin sulfate proteoglycan neurocan binds to the neural cell adhesion molecules Ng-CAM/L1/NILE and N-CAM, and inhibits neuronal adhesion and neurite outgrowth', *The Journal of Cell Biology*, 125(3), pp. 669–680.
Fu, M. *et al.* (2006) 'Hormonal control of androgen receptor function through SIRT1', *Molecular and Cellular Biology*, 26(21), pp. 8122–8135.
Fujita, K. and Nonomura, N. (2019) 'Role of Androgen Receptor in Prostate Cancer: A Review', *The World Journal of Men's Health*, 37(3), pp. 288–295.
Gaddipati, J.P. *et al.* (1994) 'Frequent detection of codon 877 mutation in the androgen receptor

gene in advanced prostate cancers', *Cancer Research*, 54(11), pp. 2861–2864.
Gao, X. *et al.* (2021) 'Phosphorylation of the androgen receptor at Ser81 is co-sustained by CDK1 and CDK9 and leads to AR-mediated transactivation in prostate cancer', *Molecular Oncology*, 15(7), pp. 1901–1920.
Gao, Y. *et al.* (2019) 'Metastasis Organotropism: Redefining the Congenial Soil', *Developmental Cell*, 49(3), pp. 375–391.
Gardner, W.A., Culberson, D.E. and Bennett, B.D. (1986) 'Trichomonas vaginalis in the prostate gland', *Archives of Pathology & Laboratory Medicine*, 110(5), pp. 430–432.
Gasi Tandefelt, D. *et al.* (2014) 'ETS fusion genes in prostate cancer', *Endocrine-Related Cancer*, 21(3), pp. R143-152.
Gates, T.J. (2001) 'Screening for cancer: evaluating the evidence', *American Family Physician*, 63(3), pp. 513–522.
Gavine, P.R. *et al.* (2012) 'AZD4547: an orally bioavailable, potent, and selective inhibitor of the fibroblast growth factor receptor tyrosine kinase family', *Cancer Research*, 72(8), pp. 2045–2056.
Gelmann, E.P. (2002) 'Molecular biology of the androgen receptor', *Journal of Clinical Oncology: Official Journal of the American Society of Clinical Oncology*, 20(13), pp. 3001–3015.
Gerardy-Schahn, R. and Eckhardt, M. (1994) 'Hot spots of antigenicity in the neural cell adhesion molecule NCAM', *International Journal of Cancer. Supplement = Journal International Du Cancer. Supplement*, 8, pp. 38–42.
Gerlinger, M. *et al.* (2012) 'Intratumor heterogeneity and branched evolution revealed by multiregion sequencing', *The New England Journal of Medicine*, 366(10), pp. 883–892.
Ghaemi-Oskouie, F. and Shi, Y. (2011) 'The role of uric acid as an endogenous danger signal in immunity and inflammation', *Current Rheumatology Reports*, 13(2), pp. 160–166.
Ginestier, C. *et al.* (2007) 'ALDH1 is a marker of normal and malignant human mammary stem cells and a predictor of poor clinical outcome', *Cell Stem Cell*, 1(5), pp. 555–567.
Gingrich, J.R. *et al.* (1996) 'Metastatic prostate cancer in a transgenic mouse', *Cancer Research*, 56(18), pp. 4096–4102.
Gingrich, J.R. *et al.* (1997) 'Androgen-independent prostate cancer progression in the TRAMP model', *Cancer Research*, 57(21), pp. 4687–4691.
Gingrich, J.R. *et al.* (1999) 'Pathologic progression of autochthonous prostate cancer in the TRAMP model', *Prostate Cancer and Prostatic Diseases*, 2(2), pp. 70–75.
Giovannucci, E. *et al.* (1993) 'A prospective study of dietary fat and risk of prostate cancer', *Journal of the National Cancer Institute*, 85(19), pp. 1571–1579.
Gleason, D.F. (1966) 'Classification of prostatic carcinomas', *Cancer Chemotherapy Reports*, 50(3), pp. 125–128.
Godlewski, J. *et al.* (2008) 'Targeting of the Bmi-1 oncogene/stem cell renewal factor by microRNA-128 inhibits glioma proliferation and self-renewal', *Cancer Research*, 68(22), pp. 9125–9130.
Goel, H.L. and Mercurio, A.M. (2013) 'VEGF targets the tumour cell', *Nature Reviews. Cancer*, 13(12), pp. 871–882.
Gohagan, J.K. *et al.* (2000) 'The Prostate, Lung, Colorectal and Ovarian (PLCO) Cancer Screening Trial of the National Cancer Institute: history, organization, and status', *Controlled Clinical Trials*, 21(6 Suppl), pp. 251S-272S.
Goldstein, A.S. *et al.* (2008) 'Trop2 identifies a subpopulation of murine and human prostate basal cells with stem cell characteristics', *Proceedings of the National Academy of Sciences of the United States of America*, 105(52), pp. 20882–20887.
Goldstein, A.S. *et al.* (2010) 'Identification of a cell of origin for human prostate cancer', *Science (New York, N.Y.)*, 329(5991), pp. 568–571.
Gong, L. *et al.* (2020) 'IL-32 induces epithelial-mesenchymal transition by triggering endoplasmic

reticulum stress in A549 cells', *BMC pulmonary medicine*, 20(1), p. 278.
Gorgoulis, V. *et al.* (2019) 'Cellular Senescence: Defining a Path Forward', *Cell*, 179(4), pp. 813–827.
Grasso, C.S. *et al.* (2012) 'The mutational landscape of lethal castration-resistant prostate cancer', *Nature*, 487(7406), pp. 239–243.
Gravis, G. *et al.* (2018) 'Burden of Metastatic Castrate Naive Prostate Cancer Patients, to Identify Men More Likely to Benefit from Early Docetaxel: Further Analyses of CHAARTED and GETUG-AFU15 Studies', *European Urology*, 73(6), pp. 847–855.
Greaves, M. and Maley, C.C. (2012) 'Clonal evolution in cancer', *Nature*, 481(7381), pp. 306–313.
Greenberg, N.M. *et al.* (1995) 'Prostate cancer in a transgenic mouse', *Proceedings of the National Academy of Sciences of the United States of America*, 92(8), pp. 3439–3443.
Grivennikov, S.I., Greten, F.R. and Karin, M. (2010) 'Immunity, inflammation, and cancer', *Cell*, 140(6), pp. 883–899.
Gruenbacher, G. *et al.* (2009) 'CD56+ human blood dendritic cells effectively promote TH1-type gammadelta T-cell responses', *Blood*, 114(20), pp. 4422–4431.
Guia, S. *et al.* (2008) 'A role for interleukin-12/23 in the maturation of human natural killer and CD56+ T cells in vivo', *Blood*, 111(10), pp. 5008–5016.
Guo, G., Xu, Y. and Zhang, X. (2017) 'TRUS-guided transperineal prostate 12+X core biopsy with template for the diagnosis of prostate cancer', *Oncology Letters*, 13(6), pp. 4863–4867.
Guo, Z. *et al.* (2006) 'Regulation of androgen receptor activity by tyrosine phosphorylation', *Cancer Cell*, 10(4), pp. 309–319.
Guo, Z. *et al.* (2009) 'A novel androgen receptor splice variant is up-regulated during prostate cancer progression and promotes androgen depletion-resistant growth', *Cancer Research*, 69(6), pp. 2305–2313.
Haffner, M.C. *et al.* (2013) 'Tracking the clonal origin of lethal prostate cancer', *The Journal of Clinical Investigation*, 123(11), pp. 4918–4922.
Hall, A. (2009) 'The cytoskeleton and cancer', *Cancer Metastasis Reviews*, 28(1–2), pp. 5–14.
Hamburger, A.W. and Salmon, S.E. (1977) 'Primary bioassay of human tumor stem cells', *Science (New York, N.Y.)*, 197(4302), pp. 461–463.
Hamdy, F.C. *et al.* (2016) '10-Year Outcomes after Monitoring, Surgery, or Radiotherapy for Localized Prostate Cancer', *The New England Journal of Medicine*, 375(15), pp. 1415–1424.
Hamerlik, P. *et al.* (2012) 'Autocrine VEGF-VEGFR2-Neuropilin-1 signaling promotes glioma stem-like cell viability and tumor growth', *The Journal of Experimental Medicine*, 209(3), pp. 507–520.
Hanahan, D. and Weinberg, R.A. (2011) 'Hallmarks of cancer: the next generation', *Cell*, 144(5), pp. 646–674.
Haque, A. *et al.* (2016) 'Neuron specific enolase: a promising therapeutic target in acute spinal cord injury', *Metabolic Brain Disease*, 31(3), pp. 487–495.
Harris, K.S. *et al.* (2021) 'CD117/c-kit defines a prostate CSC-like subpopulation driving progression and TKI resistance', *Scientific Reports*, 11(1), p. 1465.
Harris, W.P. *et al.* (2009) 'Androgen deprivation therapy: progress in understanding mechanisms of resistance and optimizing androgen depletion', *Nature Clinical Practice. Urology*, 6(2), pp. 76–85.
Heinlein, C.A. and Chang, C. (2004) 'Androgen receptor in prostate cancer', *Endocrine Reviews*, 25(2), pp. 276–308.
Helpap, B., Köllermann, J. and Oehler, U. (1999) 'Neuroendocrine differentiation in prostatic carcinomas: histogenesis, biology, clinical relevance, and future therapeutical perspectives', *Urologia Internationalis*, 62(3), pp. 133–138.

Hendriks, R.J. *et al.* (2021) 'Clinical use of the SelectMDx urinary-biomarker test with or without mpMRI in prostate cancer diagnosis: a prospective, multicenter study in biopsy-naïve men', *Prostate Cancer and Prostatic Diseases*, 24(4), pp. 1110–1119.
Hernandez-Segura, A., Nehme, J. and Demaria, M. (2018) 'Hallmarks of Cellular Senescence', *Trends in Cell Biology*, 28(6), pp. 436–453.
Herndon, M.E., Stipp, C.S. and Lander, A.D. (1999) 'Interactions of neural glycosaminoglycans and proteoglycans with protein ligands: assessment of selectivity, heterogeneity and the participation of core proteins in binding', *Glycobiology*, 9(2), pp. 143–155.
Heyns, C.F. *et al.* (2003) 'Comparative efficacy of triptorelin pamoate and leuprolide acetate in men with advanced prostate cancer', *BJU international*, 92(3), pp. 226–231.
Hillje, R., Pelicci, P.G. and Luzi, L. (2020) 'Cerebro: interactive visualization of scRNA-seq data', *Bioinformatics (Oxford, England)*, 36(7), pp. 2311–2313.
Hirano, D. *et al.* (2004) 'Neuroendocrine differentiation in hormone refractory prostate cancer following androgen deprivation therapy', *European Urology*, 45(5), pp. 586–592; discussion 592.
Hitchins, M.P. *et al.* (2011) 'Dominantly inherited constitutional epigenetic silencing of MLH1 in a cancer-affected family is linked to a single nucleotide variant within the 5'UTR', *Cancer Cell*, 20(2), pp. 200–213.
Hofer, M. and Lutolf, M.P. (2021) 'Engineering organoids', *Nature Reviews. Materials*, 6(5), pp. 402–420.
Hong, M.K.H. *et al.* (2015) 'Tracking the origins and drivers of subclonal metastatic expansion in prostate cancer', *Nature Communications*, 6, p. 6605.
Hope, K. and Bhatia, M. (2011) 'Clonal interrogation of stem cells', *Nature Methods*, 8(4 Suppl), pp. S36-40.
Horning, A.M. *et al.* (2018) 'Single-Cell RNA-seq Reveals a Subpopulation of Prostate Cancer Cells with Enhanced Cell-Cycle-Related Transcription and Attenuated Androgen Response', *Cancer Research*, 78(4), pp. 853–864.
Horoszewicz, J.S. *et al.* (1983) 'LNCaP model of human prostatic carcinoma', *Cancer Research*, 43(4), pp. 1809–1818.
Hovelson, D.H. *et al.* (2015) 'Development and validation of a scalable next-generation sequencing system for assessing relevant somatic variants in solid tumors', *Neoplasia (New York, N.Y.)*, 17(4), pp. 385–399.
Hsing, A.W. *et al.* (2000) 'Polymorphic CAG and GGN repeat lengths in the androgen receptor gene and prostate cancer risk: a population-based case-control study in China', *Cancer Research*, 60(18), pp. 5111–5116.
Hsing, A.W. (2001) 'Hormones and prostate cancer: what's next?', *Epidemiologic Reviews*, 23(1), pp. 42–58.
Hu, R. *et al.* (2009) 'Ligand-independent androgen receptor variants derived from splicing of cryptic exons signify hormone-refractory prostate cancer', *Cancer Research*, 69(1), pp. 16–22.
Huang, C.-Y. *et al.* (2011) 'Leptin increases motility and integrin up-regulation in human prostate cancer cells', *Journal of Cellular Physiology*, 226(5), pp. 1274–1282.
Huang, J. *et al.* (2005) 'Differential expression of interleukin-8 and its receptors in the neuroendocrine and non-neuroendocrine compartments of prostate cancer', *The American Journal of Pathology*, 166(6), pp. 1807–1815.
Huang, J. *et al.* (2006) 'Immunohistochemical characterization of neuroendocrine cells in prostate cancer', *The Prostate*, 66(13), pp. 1399–1406.
Hughes, C.S., Postovit, L.M. and Lajoie, G.A. (2010) 'Matrigel: a complex protein mixture required for optimal growth of cell culture', *Proteomics*, 10(9), pp. 1886–1890.
Hugosson, J. *et al.* (2019) 'A 16-yr Follow-up of the European Randomized study of Screening for Prostate Cancer', *European Urology*, 76(1), pp. 43–51.

Huncharek, M. *et al.* (2010) 'Smoking as a risk factor for prostate cancer: a meta-analysis of 24 prospective cohort studies', *American Journal of Public Health*, 100(4), pp. 693–701.
Huntly, B.J.P. *et al.* (2004) 'MOZ-TIF2, but not BCR-ABL, confers properties of leukemic stem cells to committed murine hematopoietic progenitors', *Cancer Cell*, 6(6), pp. 587–596.
Hurwitz, A.A. *et al.* (2001) 'The TRAMP mouse as a model for prostate cancer', *Current Protocols in Immunology*, Chapter 20, p. Unit 20.5.
Hussain, M. *et al.* (2018) 'Enzalutamide in Men with Nonmetastatic, Castration-Resistant Prostate Cancer', *The New England Journal of Medicine*, 378(26), pp. 2465–2474.
Hussain, S.P., Hofseth, L.J. and Harris, C.C. (2003) 'Radical causes of cancer', *Nature Reviews. Cancer*, 3(4), pp. 276–285.
Hwang, B., Lee, J.H. and Bang, D. (2018) 'Single-cell RNA sequencing technologies and bioinformatics pipelines', *Experimental & Molecular Medicine*, 50(8), pp. 1–14.
Imamura, Y. and Sadar, M.D. (2016) 'Androgen receptor targeted therapies in castration-resistant prostate cancer: Bench to clinic', *International Journal of Urology: Official Journal of the Japanese Urological Association*, 23(8), pp. 654–665.
Iovino, F. *et al.* (2011) 'Immunotherapy targeting colon cancer stem cells', *Immunotherapy*, 3(1), pp. 97–106.
Isaacs, J.T. and Coffey, D.S. (1981) 'Adaptation versus selection as the mechanism responsible for the relapse of prostatic cancer to androgen ablation therapy as studied in the Dunning R-3327-H adenocarcinoma', *Cancer Research*, 41(12 Pt 1), pp. 5070–5075.
Ishitsuka, K. and Tamura, K. (2008) 'Treatment of adult T-cell leukemia/lymphoma: past, present, and future', *European Journal of Haematology*, 80(3), pp. 185–196.
Ishizawa, K. *et al.* (2010) 'Tumor-initiating cells are rare in many human tumors', *Cell Stem Cell*, 7(3), pp. 279–282.
Islami, F. *et al.* (2014) 'A systematic review and meta-analysis of tobacco use and prostate cancer mortality and incidence in prospective cohort studies', *European Urology*, 66(6), pp. 1054–1064.
Israeli, R.S. *et al.* (1993) 'Molecular cloning of a complementary DNA encoding a prostate-specific membrane antigen', *Cancer Research*, 53(2), pp. 227–230.
Izawa, J.I. *et al.* (2006) 'Histological changes in prostate biopsies after salvage cryotherapy: effect of chronology and the method of biopsy', *BJU international*, 98(3), pp. 554–558.
Jahn, J.L., Giovannucci, E.L. and Stampfer, M.J. (2015) 'The high prevalence of undiagnosed prostate cancer at autopsy: implications for epidemiology and treatment of prostate cancer in the Prostate-specific Antigen-era', *International Journal of Cancer*, 137(12), pp. 2795–2802.
James, N.D. *et al.* (2015) 'Survival with Newly Diagnosed Metastatic Prostate Cancer in the "Docetaxel Era": Data from 917 Patients in the Control Arm of the STAMPEDE Trial (MRC PR08, CRUK/06/019)', *European Urology*, 67(6), pp. 1028–1038.
Janiszewska, M. *et al.* (2012) 'Imp2 controls oxidative phosphorylation and is crucial for preserving glioblastoma cancer stem cells', *Genes & Development*, 26(17), pp. 1926–1944.
Jewett, A. *et al.* (2012) 'Natural killer cells preferentially target cancer stem cells; role of monocytes in protection against NK cell mediated lysis of cancer stem cells', *Current Drug Delivery*, 9(1), pp. 5–16.
Jiao, J. *et al.* (2012) 'Identification of CD166 as a surface marker for enriching prostate stem/progenitor and cancer initiating cells', *PloS One*, 7(8), p. e42564.
Jiborn, T., Bjartell, A. and Abrahamsson, P.A. (1998) 'Neuroendocrine differentiation in prostatic carcinoma during hormonal treatment', *Urology*, 51(4), pp. 585–589.
Jinka, R. *et al.* (2012) 'Alterations in Cell-Extracellular Matrix Interactions during Progression of Cancers', *International Journal of Cell Biology*, 2012, p. 219196.
Jones, C.U. *et al.* (2011) 'Radiotherapy and short-term androgen deprivation for localized prostate cancer', *The New England Journal of Medicine*, 365(2), pp. 107–118.

Joseph, J.D. *et al.* (2013) 'A clinically relevant androgen receptor mutation confers resistance to second-generation antiandrogens enzalutamide and ARN-509', *Cancer Discovery*, 3(9), pp. 1020–1029.
Junttila, M.R. *et al.* (2015) 'Targeting LGR5+ cells with an antibody-drug conjugate for the treatment of colon cancer', *Science Translational Medicine*, 7(314), p. 314ra186.
Kameda, K. *et al.* (1999) 'Expression of highly polysialylated neural cell adhesion molecule in pancreatic cancer neural invasive lesion', *Cancer Letters*, 137(2), pp. 201–207.
Kantoff, P.W. *et al.* (2010) 'Sipuleucel-T immunotherapy for castration-resistant prostate cancer', *The New England Journal of Medicine*, 363(5), pp. 411–422.
Kao, C.-C. *et al.* (2012) 'Open, multi-center, phase IV study to assess the efficacy and tolerability of triptorelin in Taiwanese patients with advanced prostate cancer', *Journal of the Chinese Medical Association: JCMA*, 75(6), pp. 255–261.
Kaplan, R.N. *et al.* (2005) 'VEGFR1-positive haematopoietic bone marrow progenitors initiate the pre-metastatic niche', *Nature*, 438(7069), pp. 820–827.
Karantanos, T., Corn, P.G. and Thompson, T.C. (2013) 'Prostate cancer progression after androgen deprivation therapy: mechanisms of castrate resistance and novel therapeutic approaches', *Oncogene*, 32(49), pp. 5501–5511.
Karhadkar, S.S. *et al.* (2004) 'Hedgehog signalling in prostate regeneration, neoplasia and metastasis', *Nature*, 431(7009), pp. 707–712.
Karlsson, R. *et al.* (2014) 'A population-based assessment of germline HOXB13 G84E mutation and prostate cancer risk', *European Urology*, 65(1), pp. 169–176.
Karthaus, W.R. *et al.* (2014) 'Identification of multipotent luminal progenitor cells in human prostate organoid cultures', *Cell*, 159(1), pp. 163–175.
Karthikeyan, S. and Hoti, S.L. (2015) 'Development of Fourth Generation ABC Inhibitors from Natural Products: A Novel Approach to Overcome Cancer Multidrug Resistance', *Anti-Cancer Agents in Medicinal Chemistry*, 15(5), pp. 605–615.
Katoh, M. (2019a) 'Fibroblast growth factor receptors as treatment targets in clinical oncology', *Nature Reviews. Clinical Oncology*, 16(2), pp. 105–122.
Katoh, M. (2019b) 'Fibroblast growth factor receptors as treatment targets in clinical oncology', *Nature Reviews. Clinical Oncology*, 16(2), pp. 105–122.
Kelly, P.N. *et al.* (2007) 'Tumor growth need not be driven by rare cancer stem cells', *Science (New York, N.Y.)*, 317(5836), p. 337.
Kern, W.F. *et al.* (1993) 'NCAM (CD56)-positive malignant lymphoma', *Leukemia & Lymphoma*, 12(1–2), pp. 1–10.
Kerr, B.A. *et al.* (2015) 'CD117^{+} cells in the circulation are predictive of advanced prostate cancer', *Oncotarget*, 6(3), pp. 1889–1897.
Kessenbrock, K., Plaks, V. and Werb, Z. (2010) 'Matrix metalloproteinases: regulators of the tumor microenvironment', *Cell*, 141(1), pp. 52–67.
Khalili, M. *et al.* (2010) 'Loss of Nkx3.1 expression in bacterial prostatitis: a potential link between inflammation and neoplasia', *The American Journal of Pathology*, 176(5), pp. 2259–2268.
Kim, D.Y., Karam, J.A. and Wood, C.G. (2014) 'Role of metastasectomy for metastatic renal cell carcinoma in the era of targeted therapy', *World Journal of Urology*, 32(3), pp. 631–642.
Kim, H. *et al.* (2018) 'The hypoxic tumor microenvironment in vivo selects the cancer stem cell fate of breast cancer cells', *Breast cancer research: BCR*, 20(1), p. 16.
Kim, S.J. *et al.* (2001) 'Expression of interleukin-8 correlates with angiogenesis, tumorigenicity, and metastasis of human prostate cancer cells implanted orthotopically in nude mice', *Neoplasia (New York, N.Y.)*, 3(1), pp. 33–42.
Kirby, R.S. *et al.* (1982) 'Intra-prostatic urinary reflux: an aetiological factor in abacterial prostatitis', *British Journal of Urology*, 54(6), pp. 729–731.
Kirkegaard, P. *et al.* (2013) 'A cluster-randomised, parallel group, controlled intervention study

of genetic prostate cancer risk assessment and use of PSA tests in general practice--the ProCaRis study: study protocol', *BMJ open*, 3(3), p. e002452.
Kiselyov, V.V. *et al.* (1997) 'The first immunoglobulin-like neural cell adhesion molecule (NCAM) domain is involved in double-reciprocal interaction with the second immunoglobulin-like NCAM domain and in heparin binding', *The Journal of Biological Chemistry*, 272(15), pp. 10125–10134.
Kiselyov, V.V. *et al.* (2003) 'Structural basis for a direct interaction between FGFR1 and NCAM and evidence for a regulatory role of ATP', *Structure (London, England: 1993)*, 11(6), pp. 691–701.
Kiss, J.Z. and Rougon, G. (1997) 'Cell biology of polysialic acid', *Current Opinion in Neurobiology*, 7(5), pp. 640–646.
Klotz, L. *et al.* (2008) 'The efficacy and safety of degarelix: a 12-month, comparative, randomized, open-label, parallel-group phase III study in patients with prostate cancer', *BJU international*, 102(11), pp. 1531–1538.
Klotz, L. and Emberton, M. (2014) 'Management of low risk prostate cancer-active surveillance and focal therapy', *Nature Reviews. Clinical Oncology*, 11(6), pp. 324–334.
Kneebone, A. *et al.* (2020) 'Adjuvant radiotherapy versus early salvage radiotherapy following radical prostatectomy (TROG 08.03/ANZUP RAVES): a randomised, controlled, phase 3, non-inferiority trial', *The Lancet. Oncology*, 21(10), pp. 1331–1340.
Köllermann, J. *et al.* (2008) 'Prognostic significance of disseminated tumor cells in the bone marrow of prostate cancer patients treated with neoadjuvant hormone treatment', *Journal of Clinical Oncology: Official Journal of the American Society of Clinical Oncology*, 26(30), pp. 4928–4933.
Komiya, A. *et al.* (2009) 'Neuroendocrine differentiation in the progression of prostate cancer', *International Journal of Urology: Official Journal of the Japanese Urological Association*, 16(1), pp. 37–44.
Konecny, G.E. *et al.* (2015) 'Second-line dovitinib (TKI258) in patients with FGFR2-mutated or FGFR2-non-mutated advanced or metastatic endometrial cancer: a non-randomised, open-label, two-group, two-stage, phase 2 study', *The Lancet. Oncology*, 16(6), pp. 686–694.
Kos, F.J. and Chin, C.S. (2002) 'Costimulation of T cell receptor-triggered IL-2 production by Jurkat T cells via fibroblast growth factor receptor 1 upon its engagement by CD56', *Immunology and Cell Biology*, 80(4), pp. 364–369.
Kote-Jarai, Z. *et al.* (2011) 'Identification of a novel prostate cancer susceptibility variant in the KLK3 gene transcript', *Human Genetics*, 129(6), pp. 687–694.
Kröger, S. and Schröder, J.E. (2002) 'Agrin in the developing CNS: new roles for a synapse organizer', *News in Physiological Sciences: An International Journal of Physiology Produced Jointly by the International Union of Physiological Sciences and the American Physiological Society*, 17, pp. 207–212.
Kweldam, C.F., van Leenders, G.J. and van der Kwast, T. (2019) 'Grading of prostate cancer: a work in progress', *Histopathology*, 74(1), pp. 146–160.
Kwon, E.D. *et al.* (2014) 'Ipilimumab versus placebo after radiotherapy in patients with metastatic castration-resistant prostate cancer that had progressed after docetaxel chemotherapy (CA184-043): a multicentre, randomised, double-blind, phase 3 trial', *The Lancet. Oncology*, 15(7), pp. 700–712.
Kwon, O.-J. *et al.* (2014) 'Prostatic inflammation enhances basal-to-luminal differentiation and accelerates initiation of prostate cancer with a basal cell origin', *Proceedings of the National Academy of Sciences of the United States of America*, 111(5), pp. E592-600.
Kyjacova, L. *et al.* (2015) 'Radiotherapy-induced plasticity of prostate cancer mobilizes stem-like non-adherent, Erk signaling-dependent cells', *Cell Death and Differentiation*, 22(6), pp. 898–911. Available at: https://doi.org/10.1038/cdd.2014.97.
Lacroix, M. (2006) 'Significance, detection and markers of disseminated breast cancer cells',

Endocrine-Related Cancer, 13(4), pp. 1033–1067.
Lagadinou, E.D. *et al.* (2013) 'BCL-2 inhibition targets oxidative phosphorylation and selectively eradicates quiescent human leukemia stem cells', *Cell Stem Cell*, 12(3), pp. 329–341. Available at: https://doi.org/10.1016/j.stem.2012.12.013.
Lapidot, T. *et al.* (1994) 'A cell initiating human acute myeloid leukaemia after transplantation into SCID mice', *Nature*, 367(6464), pp. 645–648.
Lauth, M. *et al.* (2007) 'Inhibition of GLI-mediated transcription and tumor cell growth by small-molecule antagonists', *Proceedings of the National Academy of Sciences of the United States of America*, 104(20), pp. 8455–8460.
Lavery, D.N. *et al.* (2011) 'Repression of androgen receptor activity by HEYL, a third member of the Hairy/Enhancer-of-split-related family of Notch effectors', *The Journal of Biological Chemistry*, 286(20), pp. 17796–17808.
Lawson, D.A. *et al.* (2007) 'Isolation and functional characterization of murine prostate stem cells', *Proceedings of the National Academy of Sciences of the United States of America*, 104(1), pp. 181–186.
van Leenders, G.J. *et al.* (2001) 'Expression of basal cell keratins in human prostate cancer metastases and cell lines', *The Journal of Pathology*, 195(5), pp. 563–570.
Lehembre, F. *et al.* (2008) 'NCAM-induced focal adhesion assembly: a functional switch upon loss of E-cadherin', *The EMBO journal*, 27(19), pp. 2603–2615.
Leibowitz-Amit, R. *et al.* (2014) 'Clinical variables associated with PSA response to abiraterone acetate in patients with metastatic castration-resistant prostate cancer', *Annals of Oncology: Official Journal of the European Society for Medical Oncology*, 25(3), pp. 657–662.
Leong, K.G. *et al.* (2008) 'Generation of a prostate from a single adult stem cell', *Nature*, 456(7223), pp. 804–808.
LeSavage, B.L. *et al.* (2022) 'Next-generation cancer organoids', *Nature Materials*, 21(2), pp. 143–159.
Li, Q. *et al.* (2018) 'Linking prostate cancer cell AR heterogeneity to distinct castration and enzalutamide responses', *Nature Communications*, 9(1), p. 3600.
Li, X.-Y., Zhai, W.-J. and Teng, C.-B. (2015) 'Notch Signaling in Pancreatic Development', *International Journal of Molecular Sciences*, 17(1), p. E48.
Liao, T. *et al.* (2013) 'Susceptibility to cytotoxic T cell lysis of cancer stem cells derived from cervical and head and neck tumor cell lines', *Journal of Cancer Research and Clinical Oncology*, 139(1), pp. 159–170.
Liao, Y.-L. *et al.* (2008) 'Identification of SOX4 target genes using phylogenetic footprinting-based prediction from expression microarrays suggests that overexpression of SOX4 potentiates metastasis in hepatocellular carcinoma', *Oncogene*, 27(42), pp. 5578–5589.
Lilja, H. *et al.* (1987) 'Seminal vesicle-secreted proteins and their reactions during gelation and liquefaction of human semen', *The Journal of Clinical Investigation*, 80(2), pp. 281–285.
Lilja, H., Ulmert, D. and Vickers, A.J. (2008) 'Prostate-specific antigen and prostate cancer: prediction, detection and monitoring', *Nature Reviews. Cancer*, 8(4), pp. 268–278.
Lilleby, W. *et al.* (2013) 'Disseminated tumor cells and their prognostic significance in nonmetastatic prostate cancer patients', *International Journal of Cancer*, 133(1), pp. 149–155.
Linja, M.J. *et al.* (2001) 'Amplification and overexpression of androgen receptor gene in hormone-refractory prostate cancer', *Cancer Research*, 61(9), pp. 3550–3555.
Liss, M.A. *et al.* (2018) 'Metabolic Biosynthesis Pathways Identified from Fecal Microbiome Associated with Prostate Cancer', *European Urology*, 74(5), pp. 575–582.
Little, E.B., Edelman, G.M. and Cunningham, B.A. (1998) 'Palmitoylation of the cytoplasmic domain of the neural cell adhesion molecule N-CAM serves as an anchor to cellular membranes', *Cell Adhesion and Communication*, 6(5), pp. 415–430.

Liu, P. *et al.* (2006) 'Sex-determining region Y box 4 is a transforming oncogene in human prostate cancer cells', *Cancer Research*, 66(8), pp. 4011–4019.
Liu, X. *et al.* (2016) 'Low CD38 Identifies Progenitor-like Inflammation-Associated Luminal Cells that Can Initiate Human Prostate Cancer and Predict Poor Outcome', *Cell Reports*, 17(10), pp. 2596–2606.
Liu, Y. *et al.* (2017) 'SOX4 induces tumor invasion by targeting EMT-related pathway in prostate cancer', *Tumour Biology: The Journal of the International Society for Oncodevelopmental Biology and Medicine*, 39(5), p. 1010428317694539.
Lobo, N.A. *et al.* (2007) 'The biology of cancer stem cells', *Annual Review of Cell and Developmental Biology*, 23, pp. 675–699.
Locke, J.A. *et al.* (2012) 'NKX3.1 haploinsufficiency is prognostic for prostate cancer relapse following surgery or image-guided radiotherapy', *Clinical Cancer Research: An Official Journal of the American Association for Cancer Research*, 18(1), pp. 308–316.
Lorente, D. *et al.* (2015) 'Baseline neutrophil-lymphocyte ratio (NLR) is associated with survival and response to treatment with second-line chemotherapy for advanced prostate cancer independent of baseline steroid use', *Annals of Oncology: Official Journal of the European Society for Medical Oncology*, 26(4), pp. 750–755.
Magee, J.A., Piskounova, E. and Morrison, S.J. (2012) 'Cancer stem cells: impact, heterogeneity, and uncertainty', *Cancer Cell*, 21(3), pp. 283–296.
Mahajan, K. *et al.* (2017) 'ACK1/TNK2 Regulates Histone H4 Tyr88-phosphorylation and AR Gene Expression in Castration-Resistant Prostate Cancer', *Cancer Cell*, 31(6), pp. 790-803.e8.
Mangelsdorf, D.J. *et al.* (1995) 'The nuclear receptor superfamily: the second decade', *Cell*, 83(6), pp. 835–839.
Mangiola, S. *et al.* (2019) 'Androgen deprivation therapy promotes an obesity-like microenvironment in periprostatic fat', *Endocrine Connections*, 8(5), pp. 547–558.
Mannino, M.H. *et al.* (2015) 'The paradoxical role of IL-10 in immunity and cancer', *Cancer Letters*, 367(2), pp. 103–107.
Mantovani, A. *et al.* (2008) 'Cancer-related inflammation', *Nature*, 454(7203), pp. 436–444.
Marcelli, M. *et al.* (2000) 'Androgen receptor mutations in prostate cancer', *Cancer Research*, 60(4), pp. 944–949.
Mardilovich, K. and Shaw, L.M. (2009) 'Hypoxia regulates insulin receptor substrate-2 expression to promote breast carcinoma cell survival and invasion', *Cancer Research*, 69(23), pp. 8894–8901.
Marhold, M. *et al.* (2015) 'HIF1α Regulates mTOR Signaling and Viability of Prostate Cancer Stem Cells', *Molecular cancer research: MCR*, 13(3), pp. 556–564.
Marker, P.C. *et al.* (2003) 'Hormonal, cellular, and molecular control of prostatic development', *Developmental Biology*, 253(2), pp. 165–174.
Martinon, F. *et al.* (2006) 'Gout-associated uric acid crystals activate the NALP3 inflammasome', *Nature*, 440(7081), pp. 237–241.
Marusyk, A. *et al.* (2014) 'Non-cell-autonomous driving of tumour growth supports sub-clonal heterogeneity', *Nature*, 514(7520), pp. 54–58.
Massagué, J. and Obenauf, A.C. (2016) 'Metastatic colonization by circulating tumour cells', *Nature*, 529(7586), pp. 298–306.
Matias, P.M. *et al.* (2000) 'Structural evidence for ligand specificity in the binding domain of the human androgen receptor. Implications for pathogenic gene mutations', *The Journal of Biological Chemistry*, 275(34), pp. 26164–26171.
Maxwell, P.H. *et al.* (1997) 'Hypoxia-inducible factor-1 modulates gene expression in solid tumors and influences both angiogenesis and tumor growth', *Proceedings of the National Academy of Sciences of the United States of America*, 94(15), pp. 8104–8109.
McCall, P. *et al.* (2013) 'Androgen receptor phosphorylation at serine 308 and serine 791 predicts

enhanced survival in castrate resistant prostate cancer patients', *International Journal of Molecular Sciences*, 14(8), pp. 16656–16671.
McCann, J. *et al.* (2007) 'Phase II trial of huN901-DM1 in patients with relapsed small cell lung cancer (SCLC) and CD56-positive small cell carcinoma', *Journal of Clinical Oncology*, 25(18_suppl), pp. 18084–18084.
McCaw, T.R. *et al.* (2021) 'Gamma Secretase Inhibitors in Cancer: A Current Perspective on Clinical Performance', *The Oncologist*, 26(4), pp. e608–e621.
McLeod, D. *et al.* (2001) 'A phase 3, multicenter, open-label, randomized study of abarelix versus leuprolide acetate in men with prostate cancer', *Urology*, 58(5), pp. 756–761.
McNeal, J.E. (1981) 'The zonal anatomy of the prostate', *The Prostate*, 2(1), pp. 35–49.
Meacham, C.E. and Morrison, S.J. (2013) 'Tumour heterogeneity and cancer cell plasticity', *Nature*, 501(7467), pp. 328–337.
Medema, J.P. (2013) 'Cancer stem cells: the challenges ahead', *Nature Cell Biology*, 15(4), pp. 338–344.
Meizlish, M.L. *et al.* (2021) 'Tissue Homeostasis and Inflammation', *Annual Review of Immunology*, 39, pp. 557–581.
Meng, S. *et al.* (2004) 'Circulating tumor cells in patients with breast cancer dormancy', *Clinical Cancer Research: An Official Journal of the American Association for Cancer Research*, 10(24), pp. 8152–8162.
Mercader, M. *et al.* (2001) 'T cell infiltration of the prostate induced by androgen withdrawal in patients with prostate cancer', *Proceedings of the National Academy of Sciences of the United States of America*, 98(25), pp. 14565–14570.
Merlo, L.M.F. *et al.* (2006) 'Cancer as an evolutionary and ecological process', *Nature Reviews. Cancer*, 6(12), pp. 924–935.
Michaud, D.S. *et al.* (2001) 'A prospective study on intake of animal products and risk of prostate cancer', *Cancer causes & control: CCC*, 12(6), pp. 557–567.
Milev, P. *et al.* (1994) 'Interactions of the chondroitin sulfate proteoglycan phosphacan, the extracellular domain of a receptor-type protein tyrosine phosphatase, with neurons, glia, and neural cell adhesion molecules', *The Journal of Cell Biology*, 127(6 Pt 1), pp. 1703–1715.
Mitsumori, K. *et al.* (1999) 'Virulence characteristics of Escherichia coli in acute bacterial prostatitis', *The Journal of Infectious Diseases*, 180(4), pp. 1378–1381.
Miyamoto, H. *et al.* (1998) 'Delta5-androstenediol is a natural hormone with androgenic activity in human prostate cancer cells', *Proceedings of the National Academy of Sciences of the United States of America*, 95(19), pp. 11083–11088.
Mohamed, A.A. *et al.* (2017) 'Synergistic Activity with NOTCH Inhibition and Androgen Ablation in ERG-Positive Prostate Cancer Cells', *Molecular cancer research: MCR*, 15(10), pp. 1308–1317.
Mohler, J. *et al.* (2010) 'NCCN clinical practice guidelines in oncology: prostate cancer', *Journal of the National Comprehensive Cancer Network: JNCCN*, 8(2), pp. 162–200.
Moldovan, P.C. *et al.* (2017) 'What Is the Negative Predictive Value of Multiparametric Magnetic Resonance Imaging in Excluding Prostate Cancer at Biopsy? A Systematic Review and Meta-analysis from the European Association of Urology Prostate Cancer Guidelines Panel', *European Urology*, 72(2), pp. 250–266.
Moretta, A. *et al.* (1989) 'Surface molecules involved in CD3-negative NK cell function. A novel molecule which regulates the activation of a subset of human NK cells', *International Journal of Cancer. Supplement = Journal International Du Cancer. Supplement*, 4, pp. 48–52.
Morote, J. *et al.* (2022) 'Definition of Castrate Resistant Prostate Cancer: New Insights', *Biomedicines*, 10(3), p. 689.
Morrison, S.J. and Kimble, J. (2006) 'Asymmetric and symmetric stem-cell divisions in

development and cancer', *Nature*, 441(7097), pp. 1068–1074.
Mottet, N. *et al.* (2017) 'EAU-ESTRO-SIOG Guidelines on Prostate Cancer. Part 1: Screening, Diagnosis, and Local Treatment with Curative Intent', *European Urology*, 71(4), pp. 618–629.
Mounir, Z. *et al.* (2016) 'ERG signaling in prostate cancer is driven through PRMT5-dependent methylation of the Androgen Receptor', *eLife*, 5, p. e13964.
Moussa, A.S. *et al.* (2010) 'Importance of additional "extreme" anterior apical needle biopsies in the initial detection of prostate cancer', *Urology*, 75(5), pp. 1034–1039.
Mulholland, D.J. *et al.* (2009) 'Lin-Sca-1+CD49fhigh stem/progenitors are tumor-initiating cells in the Pten-null prostate cancer model', *Cancer Research*, 69(22), pp. 8555–8562.
Musolino, A. *et al.* (2017) 'Phase II, randomized, placebo-controlled study of dovitinib in combination with fulvestrant in postmenopausal patients with HR+, HER2- breast cancer that had progressed during or after prior endocrine therapy', *Breast cancer research: BCR*, 19(1), p. 18.
Nadal, M. *et al.* (2017) 'Structure of the homodimeric androgen receptor ligand-binding domain', *Nature Communications*, 8(1), p. 14388.
Naito, Y. *et al.* (2006) 'CD56 (NCAM) expression in pancreatic carcinoma and the surrounding pancreatic tissue', *The Kurume Medical Journal*, 53(3–4), pp. 59–62.
Nakada, S.Y. *et al.* (1993) 'The androgen receptor status of neuroendocrine cells in human benign and malignant prostatic tissue', *Cancer Research*, 53(9), pp. 1967–1970.
Nakano, M. *et al.* (2019) 'Dedifferentiation process driven by TGF-beta signaling enhances stem cell properties in human colorectal cancer', *Oncogene*, 38(6), pp. 780–793.
Namekawa, T. *et al.* (2019) 'Application of Prostate Cancer Models for Preclinical Study: Advantages and Limitations of Cell Lines, Patient-Derived Xenografts, and Three-Dimensional Culture of Patient-Derived Cells', *Cells*, 8(1), p. E74.
Nanta, R. *et al.* (2013) 'NVP-LDE-225 (Erismodegib) inhibits epithelial-mesenchymal transition and human prostate cancer stem cell growth in NOD/SCID IL2Rγ null mice by regulating Bmi-1 and microRNA-128', *Oncogenesis*, 2, p. e42.
Nattinger, A.B. and Mitchell, J.L. (2016) 'Breast Cancer Screening and Prevention', *Annals of Internal Medicine*, 164(11), pp. ITC81–ITC96.
Navin, N. *et al.* (2011) 'Tumour evolution inferred by single-cell sequencing', *Nature*, 472(7341), pp. 90–94.
Nguyen, L.V. *et al.* (2012) 'Cancer stem cells: an evolving concept', *Nature Reviews. Cancer*, 12(2), pp. 133–143.
Noguera-Troise, I. *et al.* (2006) 'Blockade of Dll4 inhibits tumour growth by promoting non-productive angiogenesis', *Nature*, 444(7122), pp. 1032–1037.
Nouri, M. *et al.* (2017) 'Therapy-induced developmental reprogramming of prostate cancer cells and acquired therapy resistance', *Oncotarget*, 8(12), pp. 18949–18967.
Nouri-Majd, S. *et al.* (2022) 'Association Between Red and Processed Meat Consumption and Risk of Prostate Cancer: A Systematic Review and Meta-Analysis', *Frontiers in Nutrition*, 9, p. 801722.
Nowell, P.C. (1976) 'The clonal evolution of tumor cell populations', *Science (New York, N.Y.)*, 194(4260), pp. 23–28.
Nyquist, M.D. *et al.* (2013) 'TALEN-engineered AR gene rearrangements reveal endocrine uncoupling of androgen receptor in prostate cancer', *Proceedings of the National Academy of Sciences of the United States of America*, 110(43), pp. 17492–17497.
Otto, S.J. *et al.* (2003) 'Effective PSA contamination in the Rotterdam section of the European Randomized Study of Screening for Prostate Cancer', *International Journal of Cancer*, 105(3), pp. 394–399.
Oudard, S. *et al.* (2017) 'Cabazitaxel Versus Docetaxel As First-Line Therapy for Patients With Metastatic Castration-Resistant Prostate Cancer: A Randomized Phase III Trial-

FIRSTANA', *Journal of Clinical Oncology: Official Journal of the American Society of Clinical Oncology*, 35(28), pp. 3189–3197.
Ousset, M. *et al.* (2012) 'Multipotent and unipotent progenitors contribute to prostate postnatal development', *Nature Cell Biology*, 14(11), pp. 1131–1138.
Paget, S. (1989) 'The distribution of secondary growths in cancer of the breast. 1889', *Cancer Metastasis Reviews*, 8(2), pp. 98–101.
Paik, P.K. *et al.* (2017) 'A Phase Ib Open-Label Multicenter Study of AZD4547 in Patients with Advanced Squamous Cell Lung Cancers', *Clinical Cancer Research: An Official Journal of the American Association for Cancer Research*, 23(18), pp. 5366–5373.
Palapattu, G.S. *et al.* (2005) 'Prostate carcinogenesis and inflammation: emerging insights', *Carcinogenesis*, 26(7), pp. 1170–1181.
Paratcha, G., Ledda, F. and Ibáñez, C.F. (2003) 'The neural cell adhesion molecule NCAM is an alternative signaling receptor for GDNF family ligands', *Cell*, 113(7), pp. 867–879.
Parimi, V. *et al.* (2014) 'Neuroendocrine differentiation of prostate cancer: a review', *American Journal of Clinical and Experimental Urology*, 2(4), pp. 273–285.
Parker, C. (2004) 'Active surveillance: towards a new paradigm in the management of early prostate cancer', *The Lancet. Oncology*, 5(2), pp. 101–106.
Parker, C. *et al.* (2020) 'Prostate cancer: ESMO Clinical Practice Guidelines for diagnosis, treatment and follow-up', *Annals of Oncology: Official Journal of the European Society for Medical Oncology*, 31(9), pp. 1119–1134.
Patrikidou, A. *et al.* (2015) 'Locoregional symptoms in patients with de novo metastatic prostate cancer: Morbidity, management, and disease outcome', *Urologic Oncology*, 33(5), p. 202.e9–17.
Pece, S. *et al.* (2010) 'Biological and molecular heterogeneity of breast cancers correlates with their cancer stem cell content', *Cell*, 140(1), pp. 62–73.
Pece, S. *et al.* (2019) 'Identification and clinical validation of a multigene assay that interrogates the biology of cancer stem cells and predicts metastasis in breast cancer: A retrospective consecutive study', *EBioMedicine*, 42, pp. 352–362.
Petrylak, D.P. *et al.* (2021) 'KEYNOTE-921: Phase III study of pembrolizumab plus docetaxel for metastatic castration-resistant prostate cancer', *Future Oncology (London, England)*, 17(25), pp. 3291–3299.
Phan, T.G. and Croucher, P.I. (2020) 'The dormant cancer cell life cycle', *Nature Reviews. Cancer*, 20(7), pp. 398–411.
Poletti, F. *et al.* (1985) 'Isolation of Chlamydia trachomatis from the prostatic cells in patients affected by nonacute abacterial prostatitis', *The Journal of Urology*, 134(4), pp. 691–693.
Pollerberg, G.E. *et al.* (1987) 'The 180-kD component of the neural cell adhesion molecule N-CAM is involved in cell-cell contacts and cytoskeleton-membrane interactions', *Cell and Tissue Research*, 250(1), pp. 227–236. Available at: https://doi.org/10.1007/BF00214676.
Pritchard, C.C. *et al.* (2016) 'Inherited DNA-Repair Gene Mutations in Men with Metastatic Prostate Cancer', *The New England Journal of Medicine*, 375(5), pp. 443–453.
Probstmeier, R., Kühn, K. and Schachner, M. (1989) 'Binding properties of the neural cell adhesion molecule to different components of the extracellular matrix', *Journal of Neurochemistry*, 53(6), pp. 1794–1801.
Punnen, S., Pavan, N. and Parekh, D.J. (2015) 'Finding the Wolf in Sheep's Clothing: The 4Kscore Is a Novel Blood Test That Can Accurately Identify the Risk of Aggressive Prostate Cancer', *Reviews in Urology*, 17(1), pp. 3–13.
Qi, J. *et al.* (2013) 'The E3 Ubiquitin Ligase Siah2 Contributes to Castration-Resistant Prostate Cancer by Regulation of Androgen Receptor Transcriptional Activity', *Cancer Cell*, 23(3), pp. 332–346.
Qin, J. *et al.* (2012) 'The PSA(-/lo) prostate cancer cell population harbors self-renewing long-term tumor-propagating cells that resist castration', *Cell Stem Cell*, 10(5), pp. 556–569.

Radziwon-Balicka, A. *et al.* (2012) 'Platelets increase survival of adenocarcinoma cells challenged with anticancer drugs: mechanisms and implications for chemoresistance', *British Journal of Pharmacology*, 167(4), pp. 787–804.
Ramilowski, J.A. *et al.* (2015) 'A draft network of ligand-receptor-mediated multicellular signalling in human', *Nature Communications*, 6, p. 7866.
Ran, Y. *et al.* (2017) 'γ-Secretase inhibitors in cancer clinical trials are pharmacologically and functionally distinct', *EMBO molecular medicine*, 9(7), pp. 950–966.
Rans, K. *et al.* (2020) 'Salvage Radiotherapy for Prostate Cancer', *Clinical Oncology (Royal College of Radiologists (Great Britain))*, 32(3), pp. 156–162.
Rebello, R.J. *et al.* (2021) 'Prostate cancer', *Nature Reviews. Disease Primers*, 7(1), p. 9.
Ribas, A. (2015) 'Releasing the Brakes on Cancer Immunotherapy', *New England Journal of Medicine*, 373(16), pp. 1490–1492. Available at: https://doi.org/10.1056/NEJMp1510079.
Ricci-Vitiani, L. *et al.* (2007) 'Identification and expansion of human colon-cancer-initiating cells', *Nature*, 445(7123), pp. 111–115. Available at: https://doi.org/10.1038/nature05384.
Richards, Z. *et al.* (2019) 'Prostate Stroma Increases the Viability and Maintains the Branching Phenotype of Human Prostate Organoids', *iScience*, 12, pp. 304–317.
Roach, P.J. *et al.* (2018) 'The Impact of 68Ga-PSMA PET/CT on Management Intent in Prostate Cancer: Results of an Australian Prospective Multicenter Study', *Journal of Nuclear Medicine: Official Publication, Society of Nuclear Medicine*, 59(1), pp. 82–88.
Robbiani, D.F. *et al.* (2009) 'AID produces DNA double-strand breaks in non-Ig genes and mature B cell lymphomas with reciprocal chromosome translocations', *Molecular Cell*, 36(4), pp. 631–641.
Robey, R.B. and Hay, N. (2009) 'Is Akt the "Warburg kinase"?-Akt-energy metabolism interactions and oncogenesis', *Seminars in Cancer Biology*, 19(1), pp. 25–31.
Robinson, D. *et al.* (2015) 'Integrative clinical genomics of advanced prostate cancer', *Cell*, 161(5), pp. 1215–1228.
Rodrigues, G. *et al.* (2012) 'Pre-treatment risk stratification of prostate cancer patients: A critical review', *Canadian Urological Association Journal = Journal De l'Association Des Urologues Du Canada*, 6(2), pp. 121–127.
Ross, A.E. *et al.* (2017) 'Pharmacodynamic and pharmacokinetic neoadjuvant study of hedgehog pathway inhibitor Sonidegib (LDE-225) in men with high-risk localized prostate cancer undergoing prostatectomy', *Oncotarget*, 8(61), pp. 104182–104192.
Rubin, L.L. and de Sauvage, F.J. (2006) 'Targeting the Hedgehog pathway in cancer', *Nature Reviews. Drug Discovery*, 5(12), pp. 1026–1033.
Rutishauser, U. *et al.* (1978) 'Adhesion among neural cells of the chick embryo. III. Relationship of the surface molecule CAM to cell adhesion and the development of histotypic patterns', *The Journal of Cell Biology*, 79(2 Pt 1), pp. 371–381.
Saad, F. and Hotte, S.J. (2010) 'Guidelines for the management of castrate-resistant prostate cancer', *Canadian Urological Association Journal = Journal De l'Association Des Urologues Du Canada*, 4(6), pp. 380–384.
Safa, A.R. (2016) 'Resistance to Cell Death and Its Modulation in Cancer Stem Cells', *Critical Reviews in Oncogenesis*, 21(3–4), pp. 203–219.
Sahu, B. *et al.* (2011) 'Dual role of FoxA1 in androgen receptor binding to chromatin, androgen signalling and prostate cancer', *The EMBO journal*, 30(19), pp. 3962–3976.
Sakabe, T. *et al.* (2017) 'CD117 expression is a predictive marker for poor prognosis in patients with non-small cell lung cancer', *Oncology Letters*, 13(5), pp. 3703–3708.
Sakr, W.A. *et al.* (1994) 'High grade prostatic intraepithelial neoplasia (HGPIN) and prostatic adenocarcinoma between the ages of 20-69: an autopsy study of 249 cases', *In Vivo (Athens, Greece)*, 8(3), pp. 439–443.
Samanta, M. *et al.* (2003) 'High Prevalence of Human Cytomegalovirus in Prostatic Intraepithelial Neoplasia and Prostatic Carcinoma', *Journal of Urology*, 170(3), pp. 998–1002.

Samarakkody, A.S., Shin, N.-Y. and Cantor, A.B. (2020) 'Role of RUNX Family Transcription Factors in DNA Damage Response', *Molecules and Cells*, 43(2), pp. 99–106.
Sandhu, S. *et al.* (2021) 'Prostate cancer', *Lancet (London, England)*, 398(10305), pp. 1075–1090. Available at: https://doi.org/10.1016/S0140-6736(21)00950-8.
Santos-de-Frutos, K. and Djouder, N. (2021) 'When dormancy fuels tumour relapse', *Communications Biology*, 4(1), p. 747.
Sari Motlagh, R. *et al.* (2022) 'The Efficacy and Safety of Relugolix Compared with Degarelix in Advanced Prostate Cancer Patients: A Network Meta-analysis of Randomized Trials', *European Urology Oncology*, 5(2), pp. 138–145.
Sarosdy, M.F. *et al.* (1998) 'Comparison of goserelin and leuprolide in combined androgen blockade therapy', *Urology*, 52(1), pp. 82–88.
Sasaki, M. *et al.* (2003) 'The polyglycine and polyglutamine repeats in the androgen receptor gene in Japanese and Caucasian populations', *Biochemical and Biophysical Research Communications*, 312(4), pp. 1244–1247.
Sasca, D. *et al.* (2019) 'NCAM1 (CD56) promotes leukemogenesis and confers drug resistance in AML', *Blood*, 133(21), pp. 2305–2319.
Sceneay, J., Smyth, M.J. and Möller, A. (2013) 'The pre-metastatic niche: finding common ground', *Cancer Metastasis Reviews*, 32(3–4), pp. 449–464.
Scheau, C. *et al.* (2019) 'The Role of Matrix Metalloproteinases in the Epithelial-Mesenchymal Transition of Hepatocellular Carcinoma', *Analytical Cellular Pathology (Amsterdam)*, 2019, p. 9423907.
Schepers, A.G. *et al.* (2012) 'Lineage tracing reveals Lgr5+ stem cell activity in mouse intestinal adenomas', *Science (New York, N.Y.)*, 337(6095), pp. 730–735.
Schieferstein, G. (1999) 'Prostate-specific antigen (PSA) in human seminal plasma', *Archives of Andrology*, 42(3), pp. 193–197. Available at: https://doi.org/10.1080/014850199262850.
Scosyrev, E. *et al.* (2012) 'Prostate cancer in the elderly: frequency of advanced disease at presentation and disease-specific mortality', *Cancer*, 118(12), pp. 3062–3070.
Scott, L.E., Weinberg, S.H. and Lemmon, C.A. (2019) 'Mechanochemical Signaling of the Extracellular Matrix in Epithelial-Mesenchymal Transition', *Frontiers in Cell and Developmental Biology*, 7, p. 135.
Seo, J. *et al.* (2021) 'The role of epithelial-mesenchymal transition-regulating transcription factors in anti-cancer drug resistance', *Archives of Pharmacal Research*, 44(3), pp. 281–292.
Servant, R. *et al.* (2021) 'Prostate cancer patient-derived organoids: detailed outcome from a prospective cohort of 81 clinical specimens', *The Journal of Pathology*, 254(5), pp. 543–555.
Seyfried, T.N. and Huysentruyt, L.C. (2013) 'On the origin of cancer metastasis', *Critical Reviews in Oncogenesis*, 18(1–2), pp. 43–73.
Sfanos, K.S. *et al.* (2018) 'The inflammatory microenvironment and microbiome in prostate cancer development', *Nature Reviews. Urology*, 15(1), pp. 11–24.
Shaffer, P.L. *et al.* (2004) 'Structural basis of androgen receptor binding to selective androgen response elements', *Proceedings of the National Academy of Sciences of the United States of America*, 101(14), pp. 4758–4763.
Shah, M.H. *et al.* (2016) 'Phase I study of IMGN901, a CD56-targeting antibody-drug conjugate, in patients with CD56-positive solid tumors', *Investigational New Drugs*, 34(3), pp. 290–299.
Shah, N.P. *et al.* (2007) 'Sequential ABL kinase inhibitor therapy selects for compound drug-resistant BCR-ABL mutations with altered oncogenic potency', *The Journal of Clinical Investigation*, 117(9), pp. 2562–2569.
Sharp, A. *et al.* (2019) 'Androgen receptor splice variant-7 expression emerges with castration resistance in prostate cancer', *The Journal of Clinical Investigation*, 129(1), pp. 192–208.
Shen, R. *et al.* (1997) 'Transdifferentiation of cultured human prostate cancer cells to a

neuroendocrine cell phenotype in a hormone-depleted medium', *Urologic Oncology*, 3(2), pp. 67–75.
Shen, T. *et al.* (2017) 'CXCL8 induces epithelial-mesenchymal transition in colon cancer cells via the PI3K/Akt/NF-κB signaling pathway', *Oncology Reports*, 37(4), pp. 2095–2100.
Shen, Y.-A. *et al.* (2015) 'Metabolic reprogramming orchestrates cancer stem cell properties in nasopharyngeal carcinoma', *Cell Cycle (Georgetown, Tex.)*, 14(1), pp. 86–98.
Shi, X.-B. *et al.* (2002) 'Functional analysis of 44 mutant androgen receptors from human prostate cancer', *Cancer Research*, 62(5), pp. 1496–1502.
Shi, Y. *et al.* (2011) 'Neural cell adhesion molecule potentiates invasion and metastasis of melanoma cells through CAMP-dependent protein kinase and phosphatidylinositol 3-kinase pathways', *The International Journal of Biochemistry & Cell Biology*, 43(4), pp. 682–690.
Shibue, T. and Weinberg, R.A. (2017) 'EMT, CSCs, and drug resistance: the mechanistic link and clinical implications', *Nature Reviews. Clinical Oncology*, 14(10), pp. 611–629.
Shien, K. *et al.* (2013) 'Acquired resistance to EGFR inhibitors is associated with a manifestation of stem cell-like properties in cancer cells', *Cancer Research*, 73(10), pp. 3051–3061.
Shim, M. *et al.* (2019) 'Effectiveness of three different luteinizing hormone-releasing hormone agonists in the chemical castration of patients with prostate cancer: Goserelin versus triptorelin versus leuprolide', *Investigative and Clinical Urology*, 60(4), pp. 244–250.
Shintani, Y. *et al.* (2008) 'Collagen I promotes epithelial-to-mesenchymal transition in lung cancer cells via transforming growth factor-beta signaling', *American Journal of Respiratory Cell and Molecular Biology*, 38(1), pp. 95–104.
Shore, N.D. *et al.* (2017) 'Polymer-delivered subcutaneous leuprolide acetate formulations achieve and maintain castrate concentrations of testosterone in four open-label studies in patients with advanced prostate cancer', *BJU international*, 119(2), pp. 239–244.
Shore, N.D. *et al.* (2020) 'Oral Relugolix for Androgen-Deprivation Therapy in Advanced Prostate Cancer', *The New England Journal of Medicine*, 382(23), pp. 2187–2196.
Shrestha, E. *et al.* (2018) 'Profiling the Urinary Microbiome in Men with Positive versus Negative Biopsies for Prostate Cancer', *The Journal of Urology*, 199(1), pp. 161–171.
Sierra-Honigmann, M.R. *et al.* (1998) 'Biological action of leptin as an angiogenic factor', *Science (New York, N.Y.)*, 281(5383), pp. 1683–1686.
Silberstein, J.L. and Eastham, J.A. (2014) 'Significance and management of positive surgical margins at the time of radical prostatectomy', *Indian journal of urology: IJU: journal of the Urological Society of India*, 30(4), pp. 423–428.
Simental, J.A. *et al.* (1991) 'Transcriptional activation and nuclear targeting signals of the human androgen receptor', *The Journal of Biological Chemistry*, 266(1), pp. 510–518.
Singh, M. *et al.* (2014) 'Stromal androgen receptor in prostate development and cancer', *The American Journal of Pathology*, 184(10), pp. 2598–2607.
Singh, S.K. *et al.* (2003) 'Identification of a cancer stem cell in human brain tumors', *Cancer Research*, 63(18), pp. 5821–5828.
Sinha, R. *et al.* (2009) 'Meat and meat-related compounds and risk of prostate cancer in a large prospective cohort study in the United States', *American Journal of Epidemiology*, 170(9), pp. 1165–1177.
Smith, M.R. *et al.* (2018) 'Apalutamide Treatment and Metastasis-free Survival in Prostate Cancer', *The New England Journal of Medicine*, 378(15), pp. 1408–1418.
Socinski, M.A. *et al.* (2021) 'Durvalumab After Concurrent Chemoradiotherapy in Elderly Patients With Unresectable Stage III Non-Small-Cell Lung Cancer (PACIFIC)', *Clinical Lung Cancer*, 22(6), pp. 549–561. Available at: https://doi.org/10.1016/j.cllc.2021.05.009.
Somasundar, P. *et al.* (2004) 'Prostate cancer cell proliferation is influenced by leptin', *The Journal of Surgical Research*, 118(1), pp. 71–82.
Spitz, A. *et al.* (2016) 'Intramuscular depot formulations of leuprolide acetate suppress

testosterone levels below a 20 ng/dL threshold: a retrospective analysis of two Phase III studies', *Research and Reports in Urology*, 8, pp. 159–164.
Steiner, G.E. *et al.* (2003) 'Cytokine expression pattern in benign prostatic hyperplasia infiltrating T cells and impact of lymphocytic infiltration on cytokine mRNA profile in prostatic tissue', *Laboratory Investigation; a Journal of Technical Methods and Pathology*, 83(8), pp. 1131–1146.
Stone, K.R. *et al.* (1978) 'Isolation of a human prostate carcinoma cell line (DU 145)', *International Journal of Cancer*, 21(3), pp. 274–281. Available at: https://doi.org/10.1002/ijc.2910210305.
Stoyanova, T. *et al.* (2016) 'Activation of Notch1 synergizes with multiple pathways in promoting castration-resistant prostate cancer', *Proceedings of the National Academy of Sciences of the United States of America*, 113(42), pp. E6457–E6466.
Strickler, H.D. and Goedert, J.J. (2001) 'Sexual behavior and evidence for an infectious cause of prostate cancer', *Epidemiologic Reviews*, 23(1), pp. 144–151.
Stuart, T. *et al.* (2019) 'Comprehensive Integration of Single-Cell Data', *Cell*, 177(7), pp. 1888-1902.e21.
Suarez-Carmona, M. *et al.* (2017) 'EMT and inflammation: inseparable actors of cancer progression', *Molecular Oncology*, 11(7), pp. 805–823.
Sun, S. *et al.* (2010) 'Castration resistance in human prostate cancer is conferred by a frequently occurring androgen receptor splice variant', *The Journal of Clinical Investigation*, 120(8), pp. 2715–2730.
Suzuki, H. *et al.* (1993) 'Androgen receptor gene mutations in human prostate cancer', *The Journal of Steroid Biochemistry and Molecular Biology*, 46(6), pp. 759–765.
Takagi, S. *et al.* (2014) 'Platelets promote osteosarcoma cell growth through activation of the platelet-derived growth factor receptor-Akt signaling axis', *Cancer Science*, 105(8), pp. 983–988.
Takayama, K. and Inoue, S. (2013) 'Transcriptional network of androgen receptor in prostate cancer progression', *International Journal of Urology: Official Journal of the Japanese Urological Association*, 20(8), pp. 756–768.
Tan, J. *et al.* (1997) 'Dehydroepiandrosterone activates mutant androgen receptors expressed in the androgen-dependent human prostate cancer xenograft CWR22 and LNCaP cells', *Molecular Endocrinology (Baltimore, Md.)*, 11(4), pp. 450–459.
Tang, F. and Zheng, P. (2018) 'Tumor cells versus host immune cells: whose PD-L1 contributes to PD-1/PD-L1 blockade mediated cancer immunotherapy?', *Cell & Bioscience*, 8, p. 34.
Tannock, I.F. *et al.* (2004) 'Docetaxel plus prednisone or mitoxantrone plus prednisone for advanced prostate cancer', *The New England Journal of Medicine*, 351(15), pp. 1502–1512.
Taouk, G. *et al.* (2019) 'CD56 expression in breast cancer induces sensitivity to natural killer-mediated cytotoxicity by enhancing the formation of cytotoxic immunological synapse', *Scientific Reports*, 9(1), p. 8756.
Taplin, M.E. *et al.* (1999) 'Selection for androgen receptor mutations in prostate cancers treated with androgen antagonist', *Cancer Research*, 59(11), pp. 2511–2515.
Taylor, B.S. *et al.* (2010) 'Integrative genomic profiling of human prostate cancer', *Cancer Cell*, 18(1), pp. 11–22. Available at: https://doi.org/10.1016/j.ccr.2010.05.026.
Teijeira, A. *et al.* (2021) 'IL8, Neutrophils, and NETs in a Collusion against Cancer Immunity and Immunotherapy', *Clinical Cancer Research: An Official Journal of the American Association for Cancer Research*, 27(9), pp. 2383–2393.
Terry, S. and Beltran, H. (2014) 'The many faces of neuroendocrine differentiation in prostate cancer progression', *Frontiers in Oncology*, 4, p. 60.
Tezel, E. *et al.* (2001) 'Expression of Neural Cell Adhesion Molecule in Pancreatic Cancer':, *Pancreas*, 22(2), pp. 122–125.

Theodoropoulos, P.A. *et al.* (2010) 'Circulating tumor cells with a putative stem cell phenotype in peripheral blood of patients with breast cancer', *Cancer Letters*, 288(1), pp. 99–106.
Thiery, J.P. *et al.* (2009) 'Epithelial-mesenchymal transitions in development and disease', *Cell*, 139(5), pp. 871–890.
Thompson, I.M. *et al.* (2006) 'Effect of finasteride on the sensitivity of PSA for detecting prostate cancer', *Journal of the National Cancer Institute*, 98(16), pp. 1128–1133.
Till, J.E. and McCULLOCH, E.A. (1961) 'A direct measurement of the radiation sensitivity of normal mouse bone marrow cells', *Radiation Research*, 14, pp. 213–222.
Tilley, W.D. *et al.* (1996) 'Mutations in the androgen receptor gene are associated with progression of human prostate cancer to androgen independence', *Clinical Cancer Research: An Official Journal of the American Association for Cancer Research*, 2(2), pp. 277–285.
Timms, B.G. (2008) 'Prostate development: a historical perspective', *Differentiation; Research in Biological Diversity*, 76(6), pp. 565–577.
Tinzl, M. *et al.* (2004) 'DD3PCA3 RNA analysis in urine--a new perspective for detecting prostate cancer', *European Urology*, 46(2), pp. 182–186; discussion 187.
Tirino, V. *et al.* (2013) 'TGF-β1 exposure induces epithelial to mesenchymal transition both in CSCs and non-CSCs of the A549 cell line, leading to an increase of migration ability in the CD133+ A549 cell fraction', *Cell Death & Disease*, 4, p. e620.
Tirosh, I. *et al.* (2016) 'Dissecting the multicellular ecosystem of metastatic melanoma by single-cell RNA-seq', *Science (New York, N.Y.)*, 352(6282), pp. 189–196.
Tiwari, N. *et al.* (2013) 'Sox4 is a master regulator of epithelial-mesenchymal transition by controlling Ezh2 expression and epigenetic reprogramming', *Cancer Cell*, 23(6), pp. 768–783.
Todaro, M. *et al.* (2014) 'CD44v6 is a marker of constitutive and reprogrammed cancer stem cells driving colon cancer metastasis', *Cell Stem Cell*, 14(3), pp. 342–356.
Tomlins, S.A. *et al.* (2005) 'Recurrent fusion of TMPRSS2 and ETS transcription factor genes in prostate cancer', *Science (New York, N.Y.)*, 310(5748), pp. 644–648.
Tomlins, S.A. *et al.* (2008) 'Role of the TMPRSS2-ERG gene fusion in prostate cancer', *Neoplasia (New York, N.Y.)*, 10(2), pp. 177–188.
Trapnell, C. *et al.* (2014) 'The dynamics and regulators of cell fate decisions are revealed by pseudotemporal ordering of single cells', *Nature Biotechnology*, 32(4), pp. 381–386.
Trewartha, D. and Carter, K. (2013) 'Advances in prostate cancer treatment', *Nature Reviews. Drug Discovery*, 12(11), pp. 823–824.
Tsai, C.-Y. *et al.* (2014) 'Interleukin-32 increases human gastric cancer cell invasion associated with tumor progression and metastasis', *Clinical Cancer Research: An Official Journal of the American Association for Cancer Research*, 20(9), pp. 2276–2288.
Tsechelidis, I. and Vrachimis, A. (2022) 'PSMA PET in Imaging Prostate Cancer', *Frontiers in Oncology*, 12, p. 831429.
Turajlic, S. and Swanton, C. (2016) 'Metastasis as an evolutionary process', *Science (New York, N.Y.)*, 352(6282), pp. 169–175.
Turkalp, Z., Karamchandani, J. and Das, S. (2014) 'IDH mutation in glioma: new insights and promises for the future', *JAMA neurology*, 71(10), pp. 1319–1325.
Tutrone, R. *et al.* (2020) 'Clinical utility of the exosome based ExoDx Prostate(IntelliScore) EPI test in men presenting for initial Biopsy with a PSA 2-10 ng/mL', *Prostate Cancer and Prostatic Diseases*, 23(4), pp. 607–614.
Ung, J.O. *et al.* (2002) 'Evolution of the presentation and pathologic and biochemical outcomes after radical prostatectomy for patients with clinically localized prostate cancer diagnosed during the PSA era', *Urology*, 60(3), pp. 458–463.
Unterrainer, M. *et al.* (2020) 'Recent advances of PET imaging in clinical radiation oncology', *Radiation Oncology (London, England)*, 15(1), p. 88.
US Preventive Services Task Force *et al.* (2018) 'Screening for Cervical Cancer: US Preventive

Services Task Force Recommendation Statement', *JAMA*, 320(7), p. 674.
US Preventive Services Task Force *et al.* (2021) 'Screening for Colorectal Cancer: US Preventive Services Task Force Recommendation Statement', *JAMA*, 325(19), p. 1965.
Vale, C.L. *et al.* (2020) 'Adjuvant or early salvage radiotherapy for the treatment of localised and locally advanced prostate cancer: a prospectively planned systematic review and meta-analysis of aggregate data', *Lancet (London, England)*, 396(10260), pp. 1422–1431.
Valerio, M. *et al.* (2015) 'Detection of Clinically Significant Prostate Cancer Using Magnetic Resonance Imaging-Ultrasound Fusion Targeted Biopsy: A Systematic Review', *European Urology*, 68(1), pp. 8–19.
Valgardsdottir, R. *et al.* (2014) 'Direct involvement of CD56 in cytokine-induced killer-mediated lysis of CD56+ hematopoietic target cells', *Experimental Hematology*, 42(12), pp. 1013-1021.e1.
Van Acker, H.H. *et al.* (2017) 'CD56 in the Immune System: More Than a Marker for Cytotoxicity?', *Frontiers in Immunology*, 8, p. 892.
Van den Broeck, T. *et al.* (2019) 'Prognostic Value of Biochemical Recurrence Following Treatment with Curative Intent for Prostate Cancer: A Systematic Review', *European Urology*, 75(6), pp. 967–987.
Van den Broeck, T. *et al.* (2020) 'Biochemical Recurrence in Prostate Cancer: The European Association of Urology Prostate Cancer Guidelines Panel Recommendations', *European Urology Focus*, 6(2), pp. 231–234.
Vanneste, B.G.L. *et al.* (2016) 'Prostate Cancer Radiation Therapy: What Do Clinicians Have to Know?', *BioMed Research International*, 2016, p. 6829875.
Vassalli, G. (2019) 'Aldehyde Dehydrogenases: Not Just Markers, but Functional Regulators of Stem Cells', *Stem Cells International*, 2019, p. 3904645.
Veldscholte, J. *et al.* (1990) 'A mutation in the ligand binding domain of the androgen receptor of human LNCaP cells affects steroid binding characteristics and response to anti-androgens', *Biochemical and Biophysical Research Communications*, 173(2), pp. 534–540.
Verze, P., Cai, T. and Lorenzetti, S. (2016) 'The role of the prostate in male fertility, health and disease', *Nature Reviews. Urology*, 13(7), pp. 379–386. Available at: https://doi.org/10.1038/nrurol.2016.89.
Visakorpi, T. *et al.* (1995) 'In vivo amplification of the androgen receptor gene and progression of human prostate cancer', *Nature Genetics*, 9(4), pp. 401–406.
Vitale, I. *et al.* (2017) 'DNA Damage in Stem Cells', *Molecular Cell*, 66(3), pp. 306–319.
Vukojevic, V. *et al.* (2020) 'Evolutionary conserved role of neural cell adhesion molecule-1 in memory', *Translational Psychiatry*, 10(1), p. 217.
Wadosky, K.M. and Koochekpour, S. (2016) 'Molecular mechanisms underlying resistance to androgen deprivation therapy in prostate cancer', *Oncotarget*, 7(39), pp. 64447–64470.
Walmod, P.S. *et al.* (2004) 'Zippers make signals: NCAM-mediated molecular interactions and signal transduction', *Neurochemical Research*, 29(11), pp. 2015–2035.
Wan, X. *et al.* (2014a) 'Prostate cancer cell-stromal cell crosstalk via FGFR1 mediates antitumor activity of dovitinib in bone metastases', *Science Translational Medicine*, 6(252), p. 252ra122.
Wan, X. *et al.* (2014b) 'Prostate cancer cell-stromal cell crosstalk via FGFR1 mediates antitumor activity of dovitinib in bone metastases', *Science Translational Medicine*, 6(252), p. 252ra122.
Wang, L. *et al.* (2014) 'ERG-SOX4 interaction promotes epithelial-mesenchymal transition in prostate cancer cells', *The Prostate*, 74(6), pp. 647–658.
Wang, L. *et al.* (2017) 'Delta/notch-like epidermal growth factor-related receptor (DNER) orchestrates stemness and cancer progression in prostate cancer', *American Journal of Translational Research*, 9(11), pp. 5031–5039.
Wang, L., Lankhorst, L. and Bernards, R. (2022) 'Exploiting senescence for the treatment of

cancer', *Nature Reviews. Cancer*, 22(6), pp. 340–355.
Wang, W. and Epstein, J.I. (2008) 'Small cell carcinoma of the prostate. A morphologic and immunohistochemical study of 95 cases', *The American Journal of Surgical Pathology*, 32(1), pp. 65–71.
Wang, X. *et al.* (2009) 'A luminal epithelial stem cell that is a cell of origin for prostate cancer', *Nature*, 461(7263), pp. 495–500.
Wang, Y.A. *et al.* (2020) 'Molecular tracing of prostate cancer lethality', *Oncogene*, 39(50), pp. 7225–7238.
Watson, P.A., Arora, V.K. and Sawyers, C.L. (2015) 'Emerging mechanisms of resistance to androgen receptor inhibitors in prostate cancer', *Nature Reviews. Cancer*, 15(12), pp. 701–711.
Weckermann, D. *et al.* (2001) 'Biochemical course after radical retropubic prostatectomy: preliminary results', *European Urology*, 39(4), pp. 418–424.
Wen, S., Niu, Y. and Huang, H. (2020) 'Posttranslational regulation of androgen dependent and independent androgen receptor activities in prostate cancer', *Asian Journal of Urology*, 7(3), pp. 203–218.
Werner, R. *et al.* (2006) 'The A645D mutation in the hinge region of the human androgen receptor (AR) gene modulates AR activity, depending on the context of the polymorphic glutamine and glycine repeats', *The Journal of Clinical Endocrinology and Metabolism*, 91(9), pp. 3515–3520.
Whiteman, K.R. *et al.* (2014) 'Lorvotuzumab mertansine, a CD56-targeting antibody-drug conjugate with potent antitumor activity against small cell lung cancer in human xenograft models', *mAbs*, 6(2), pp. 556–566.
Wiedenmann, B. *et al.* (1986) 'Synaptophysin: a marker protein for neuroendocrine cells and neoplasms', *Proceedings of the National Academy of Sciences of the United States of America*, 83(10), pp. 3500–3504.
Wiesner, C. *et al.* (2008) 'C-kit and its ligand stem cell factor: potential contribution to prostate cancer bone metastasis', *Neoplasia (New York, N.Y.)*, 10(9), pp. 996–1003.
van de Wijngaart, D.J. *et al.* (2010) 'Systematic structure-function analysis of androgen receptor Leu701 mutants explains the properties of the prostate cancer mutant L701H', *The Journal of Biological Chemistry*, 285(7), pp. 5097–5105.
Williams, E.J. *et al.* (1994) 'Activation of the FGF receptor underlies neurite outgrowth stimulated by L1, N-CAM, and N-cadherin', *Neuron*, 13(3), pp. 583–594.
Wilson, R.L. *et al.* (2022) 'Obesity and prostate cancer: A narrative review', *Critical Reviews in Oncology/Hematology*, 169, p. 103543.
Wong, Y.N.S. *et al.* (2019) 'Nivolumab and ipilimumab treatment in prostate cancer with an immunogenic signature (NEPTUNES).', *Journal of Clinical Oncology*, 37(15_suppl), pp. TPS5090–TPS5090.
Wu, Y. *et al.* (2010) 'Therapeutic antibody targeting of individual Notch receptors', *Nature*, 464(7291), pp. 1052–1057.
Xin, L. *et al.* (2007) 'Self-renewal and multilineage differentiation in vitro from murine prostate stem cells', *Stem Cells (Dayton, Ohio)*, 25(11), pp. 2760–2769.
Ye, X.-Q. *et al.* (2011) 'Mitochondrial and energy metabolism-related properties as novel indicators of lung cancer stem cells', *International Journal of Cancer*, 129(4), pp. 820–831.
Yeh, S. *et al.* (1998) 'From estrogen to androgen receptor: a new pathway for sex hormones in prostate', *Proceedings of the National Academy of Sciences of the United States of America*, 95(10), pp. 5527–5532.
Yonover, P. *et al.* (2019) 'Clinical utility study of confirms mdx for prostate cancer in a community urology practice.', *Journal of Clinical Oncology*, 37(7_suppl), pp. 94–94.
Yu, S. *et al.* (2012) 'Altered prostate epithelial development in mice lacking the androgen receptor

in stromal fibroblasts', *The Prostate*, 72(4), pp. 437–449.
Yuan, S., Norgard, R.J. and Stanger, B.Z. (2019) 'Cellular Plasticity in Cancer', *Cancer Discovery*, 9(7), pp. 837–851.
Yun, H.-M. *et al.* (2013) 'Antitumor activity of IL-32β through the activation of lymphocytes, and the inactivation of NF-κB and STAT3 signals', *Cell Death & Disease*, 4, p. e640.
Zafarana, G. *et al.* (2012) 'Copy number alterations of c-MYC and PTEN are prognostic factors for relapse after prostate cancer radiotherapy', *Cancer*, 118(16), pp. 4053–4062.
Zaffuto, E. *et al.* (2017) 'Early Postoperative Radiotherapy is Associated with Worse Functional Outcomes in Patients with Prostate Cancer', *The Journal of Urology*, 197(3 Pt 1), pp. 669–675.
Zambrano, A. *et al.* (2002) 'Detection of human polyomaviruses and papillomaviruses in prostatic tissue reveals the prostate as a habitat for multiple viral infections', *The Prostate*, 53(4), pp. 263–276.
Zecchini, S. *et al.* (2011) 'The adhesion molecule NCAM promotes ovarian cancer progression via FGFR signalling', *EMBO molecular medicine*, 3(8), pp. 480–494.
Zecchini, S. and Cavallaro, U. (2010) 'Neural cell adhesion molecule in cancer: expression and mechanisms', *Advances in Experimental Medicine and Biology*, 663, pp. 319–333.
Zhang, J. *et al.* (2012) 'SOX4 induces epithelial-mesenchymal transition and contributes to breast cancer progression', *Cancer Research*, 72(17), pp. 4597–4608.
Zhang, T. *et al.* (2020) 'Androgen Receptor Splice Variant, AR-V7, as a Biomarker of Resistance to Androgen Axis-Targeted Therapies in Advanced Prostate Cancer', *Clinical Genitourinary Cancer*, 18(1), pp. 1–10.
Zhang, W.C. *et al.* (2012) 'Glycine decarboxylase activity drives non-small cell lung cancer tumor-initiating cells and tumorigenesis', *Cell*, 148(1–2), pp. 259–272.
Zhou, B.-B.S. *et al.* (2006) 'Targeting ADAM-mediated ligand cleavage to inhibit HER3 and EGFR pathways in non-small cell lung cancer', *Cancer Cell*, 10(1), pp. 39–50.
Zhou, L. *et al.* (2022) 'Lineage tracing and single-cell analysis reveal proliferative Prom1+ tumour-propagating cells and their dynamic cellular transition during liver cancer progression', *Gut*, 71(8), pp. 1656–1668.
Zhou, Y. *et al.* (2015) 'Interleukin-32 stimulates osteosarcoma cell invasion and motility via AKT pathway-mediated MMP-13 expression', *International Journal of Molecular Medicine*, 35(6), pp. 1729–1733.
Zhou, Z., Cong, L. and Cong, X. (2021) 'Patient-Derived Organoids in Precision Medicine: Drug Screening, Organoid-on-a-Chip and Living Organoid Biobank', *Frontiers in Oncology*, 11, p. 762184.
Zong, Y. and Goldstein, A.S. (2013) 'Adaptation or selection--mechanisms of castration-resistant prostate cancer', *Nature Reviews. Urology*, 10(2), pp. 90–98.